

# **Fluxes and mixing ratios of biogenic volatile organic compounds in temperate plant canopies**



**Nichola Copeland**

Doctor of Philosophy

The University of Edinburgh

2013



## **Declaration**

I declare that this written thesis is all my own work except where explicitly indicated otherwise by proper use of references. The work has not been submitted for any other degree or professional qualification.

Nichola Copeland

July 2013

<b>List of Figures</b> .....	<b>vii</b>
<b>List of Tables</b> .....	<b>xv</b>
<b>Acknowledgements</b> .....	<b>xvii</b>
<b>Abstract</b> .....	<b>xix</b>
<b>List of acronyms and abbreviations</b> .....	<b>xxi</b>
<b>Chapter 1: Introduction</b> .....	<b>1</b>
1.1    What are volatile organic compounds? .....	1
1.2    How are BVOCs emitted to the atmosphere? .....	3
1.3    Effects of VOCs on atmospheric chemistry .....	4
1.3.1    Tropospheric ozone .....	4
1.3.2    Secondary organic aerosol .....	5
1.4    VOC analytical measurement techniques .....	7
1.5    Flux methods .....	8
1.5.1    Leaf and branch enclosures .....	8
1.5.2    Eddy covariance .....	9
1.5.3    Proton transfer reaction mass spectrometry (PTR-MS).....	10
1.6    Research aims.....	15
1.7    Thesis structure .....	15
<b>Chapter 2: VOC mixing ratios and fluxes above a Douglas fir forest</b> .....	<b>17</b>
2.1    Introduction .....	17
2.2    Methods.....	20
2.2.1    Sampling site.....	20
2.2.2    PTR-MS set-up .....	23
2.2.3    Determination of VOC mixing ratios and fluxes .....	23
2.2.4    In-canopy gradient measurements .....	27
2.2.5    Chromatographic analysis of ambient air samples .....	27
2.3    Results .....	28
2.3.1    Above canopy fluxes.....	28

2.3.2	Above-canopy mixing ratios .....	35
2.3.3	In-canopy mixing ratios .....	51
2.4	Discussion .....	59
2.4.1	Terpenoids.....	59
2.4.2	Non-terpenoids.....	64
2.5	Conclusions .....	66
<b>Chapter 3: VOC emissions from <i>Miscanthus</i> and short rotation coppice willow bioenergy crops .....</b>		<b>67</b>
3.1	Introduction .....	67
3.2	Methods.....	69
3.2.1	Sampling site.....	69
3.2.2	PTR-MS set-up .....	72
3.2.3	Determination of VOC mixing ratios and fluxes .....	72
3.2.4	Chromatographic analysis of ambient air samples .....	76
3.2.5	Meteorological measurements .....	77
3.3	Results .....	77
3.3.1	<i>Miscanthus</i> .....	77
3.3.2	Short rotation coppice willow .....	82
3.3.3	Standardised isoprene emission .....	87
3.4	Discussion .....	90
3.5	Conclusions .....	92
<b>Chapter 4: VOC emissions from a temperate peat bog.....</b>		<b>93</b>
4.1	Introduction .....	93
4.2	Methods.....	95
4.2.1	Site location and description .....	95
4.2.2	N-treatment plots.....	96
4.2.3	Plot sampling.....	98
4.2.4	Chamber sampling .....	99
4.2.5	Sample analysis and flux calculations .....	103
4.3	Results .....	106
4.3.1	VOC fluxes from control plots.....	106

4.3.2	Effects of N-treatment on VOC emissions .....	121
4.4	Discussion .....	129
4.5	Conclusions .....	130
<b>Chapter 5: Effect of isoprene on the gas-phase oxidation of monoterpenes.....</b>		<b>131</b>
5.1	Introduction .....	131
5.2	Methods.....	132
5.2.1	PTR-MS set-up and measurements .....	136
5.2.2	Experiments with a monoterpenes and isoprene .....	138
5.2.3	MCM simulations .....	138
5.3	Results .....	139
5.3.1	Experimental chamber results .....	139
5.3.2	Simulated MCM results .....	144
5.4	Discussion .....	148
5.5	Conclusions .....	152
<b>Chapter 6: Final conclusions.....</b>		<b>153</b>
<b>References .....</b>		<b>156</b>
<b>Appendix I: Publication.....</b>		<b>174</b>
<b>Appendix II: MCM programs .....</b>		<b>184</b>
<b>Appendix III: Raw PTR-MS chamber data .....</b>		<b>185</b>

## List of Figures

- Figure 1-1 Chemical structures of isoprene and some monoterpenes (Finlayson-Pitts and Pitts Jr, 2000)..... 2
- Figure 1-2 Comparison of (A) NO-NO<sub>2</sub>-O<sub>3</sub> cycle in the absence of VOCs with (B) in the presence of VOCs. In scheme A there is a balance between destruction and formation of O<sub>3</sub>. Scheme B results in net production of O<sub>3</sub> (Atkinson, 2000). ... 5
- Figure 1-3 Contributions of atmospheric gases and particles on radiative forcing of the climate. Note the effects of tropospheric ozone and both direct and cloud albedo (indirect) effects of aerosol particles. VOC emissions contribute to all of these factors. (Solomon et al., 2007)..... 6
- Figure 1-4 Schematic diagram of a PTR-MS (Miszta, 2010). The instrument is comprised of 3 main sections: the ion source (H<sub>3</sub>O<sup>+</sup> ions are formed); the drift region (H<sub>3</sub>O<sup>+</sup> ions undergo proton-transfer reactions with trace components of air); and the detection region (protonated analyte molecules are detected by a secondary electron multiplier (SEM)). TM refers to turbo molecular pumps used to sustain a constant pressure of ~2 mbar in the drift tube and ~1 × 10<sup>-5</sup> mbar in the quadrupole mass analyser. Sample air inlet flow rate is also used to maintain drift tube pressure..... 11
- Figure 2-1 Location of the Speulderbos measurement site in The Netherlands. .... 20
- Figure 2-2 Aerial view of the Speuld measurement site. Grey lines show footpaths through the forest. The location of the sampling tower is indicated by the white marker. (Map attributable to ©2012 Aerodata International Surveys, Geoeye (Imagery) and ©2012 Google (map data))..... 21
- Figure 2-3 Modelled flux footprints for Speuld measurements. The following parameters were used: measurement height  $z_m$  45 m; roughness length  $z_0$  3.2 m (estimated as 1/10th of the canopy height, 32 m); boundary layer height  $h$  1000 m. Crosswind integrated footprint functions ( $f_y$ ) were calculated for minimum, median and maximum values of  $u^*$  (1 sd of the vertical wind speed,  $\sigma_w$ , shown in brackets) as indicated on the graph. The distance at which maximum contribution can be expected, and at which 80% of the flux is contained, are given as  $X_{max}$  and  $X_r$ , respectively. .... 22
- Figure 2-4 Map showing the predicted radius of the maximum 80% flux footprint using a simple parameterisation model (Kljun et al., 2004). The blue marker indicates the location of the sampling tower within Speuld forest. (Map data ©2012 Google Imagery ©2012 TerraMetrics. Radius plotted using [www.freemaptools.com](http://www.freemaptools.com)). .... 22
- Figure 2-5 Time series of VOC fluxes measured above Douglas fir. Dashed gridlines denote midnight. Note the variable flux scales. .... 29

Figure 2-6 Average diurnal profiles of VOC fluxes above Douglas fir and of sensible heat flux, prior to 20:00 on 29th June 2009. Data points are the mean of median values for a $\pm 1.5$ hour time window. Note the variable scales. Grey areas show variability calculated as $\pm 1$ sd. ....	32
Figure 2-7 Average diurnal profiles of VOC fluxes above Douglas fir and of sensible heat flux, after 20:00 on 29 June 2009. Data points are the mean of median values for a $\pm 1.5$ hour time window. Note the variable scales. Grey areas show variability calculated as $\pm 1$ sd. ....	34
Figure 2-8 Time series of VOC mixing ratios, and of temperature, measured above Douglas fir. Dashed gridlines denote midnight. Note the variable mixing ratio scales. ....	36
Figure 2-9 Average diurnal profiles of VOC mixing ratios above Douglas fir, and of temperature, before 20:00 on 29 June 2009. Note the variable scales. Dashed lines denote LOD. Grey areas show variability calculated as $\pm 1$ sd of the averaged half-hourly values of all measurements. ....	38
Figure 2-10 Average diurnal profiles of VOC mixing ratios above Douglas fir, and of temperature, after 20:00 on 29th June 2009. Note the variable scales. Dashed lines denote LOD. Grey areas show variability calculated as $\pm 1$ sd of the averaged half-hourly values of all measurements. ....	41
Figure 2-11 Diurnal variation in monoterpene mixing ratios above the Douglas fir canopy (40m). Samples were collected using adsorption tubes on 6 July 2009. ....	42
Figure 2-12 Annuli of diurnal variation in VOC mixing ratio as a function of wind direction for all campaign data. Colour corresponds to mixing ratio according to the scale for each individual plot. Temperature ( $^{\circ}\text{C}$ ) is shown for comparison. (White space indicates insufficient data.) ....	45
Figure 2-13 Bivariate plots showing how VOC mixing ratio varies by wind speed and wind direction. Polar coordinates correspond to wind direction, radial distance indicates wind speed ( $\text{m s}^{-1}$ ) and colour denotes VOC mixing ratio according to the key for each individual plot. Temperature ( $^{\circ}\text{C}$ ) is shown for comparison. ....	49
Figure 2-14 Land use map of The Netherlands. Adapted from Figure 7 in Clevers et al. (2007). ....	50
Figure 2-15 In-canopy mixing ratios (ppbv, denoted by colour) as a function of time of day (hour, x-axis) and canopy height above ground (m, y-axis). Note the variable mixing ratio scales. ....	55
Figure 2-16 Average total monoterpene mixing ratios within the Douglas fir canopy. Samples were taken at three heights (4, 18 and 32 m) and at three times during the day (morning, afternoon, evening). Results shown are the averages of two	

sampling days (1 and 6 July) except for 40 m samples which were only taken on 6 July 2009.....	57
Figure 2-17 Monoterpene composition as a function of height above ground within the Douglas fir canopy. Each data point is a mean of 6 repeat measurements. Canopy top is at 32 m. ....	58
Figure 2-18 Relationship between the half-hour averaged mixing ratios of $m/z$ 137 against those of $m/z$ 81. The black line shows the linear regression (equation shown inset). ....	59
Figure 2-19 Time series of wind speed measured above the Douglas fir canopy. Grey gridlines denote midnight.....	65
Figure 3-1 Aerial view of the <i>Miscanthus</i> and willow plantations. The white dots denote the measurement locations at the NE corner of the <i>Miscanthus</i> field and the N edge of the SRC willow field. (Map attributable to: ©2001 DigitalGlobe, GeoEye, Getmapping plc, Infoterra Ltd & Bluesky, TerraMetrics. Map data ©2011 Google).....	69
Figure 3-2 Modelled flux footprints for <i>Miscanthus</i> and SRC willow measurements. The following parameters were used. <i>Miscanthus</i> : measurement height $z_m$ 4 m; roughness length $z_0$ 0.25 m (estimated as 1/10th of the canopy height, 2.5 m); boundary layer height $h$ 1000 m. SRC willow: $z_m$ 6.7 m; $z_0$ 0.4m; $h$ 1000 m. Footprints were calculated for 90th percentile (P90), median and minimum values of $u^*$ (1 sd of the vertical wind speed, $\sigma_w$ , shown in brackets) as indicated on the graphs. The distance at which maximum contribution can be expected, and at which 80% of the flux is contained, are given as $X_{max}$ and $X_r$ , respectively. ....	71
Figure 3-3 Time series of VOC fluxes measured above <i>Miscanthus</i> . Dashed gridlines denote midnight. Note the variable flux scales. Note, spikes in data have been removed to allow day-to-day variation in fluxes to be seen more clearly. Data removed from this figure were still included in diurnal averaging (Figure 3-4). ....	78
Figure 3-4 Average diurnal profiles of VOC fluxes above <i>Miscanthus</i> when wind direction was between 180 and 270° (i.e. from over the <i>Miscanthus</i> field). Note the variable scales. Grey areas represent variability calculated as $\pm 1$ sd of the averaged half-hourly values of all measurements. A profile for MVK+MACR is not included due to insufficient data. ....	79
Figure 3-5 Time series of VOC mixing ratios, and of temperature, measured above <i>Miscanthus</i> . Dashed gridlines denote midnight. Note the variable mixing ratio scales. ....	80
Figure 3-6 Average diurnal profiles of VOC mixing ratios above <i>Miscanthus</i> , and of temperature, when wind direction was between 180 and 270° (i.e. from over the	

<p><i>Miscanthus</i> field). Note the variable scales. Dashed lines denote LOD. Grey areas represent variability calculated as <math>\pm 1</math> sd of the averaged half-hourly values of all measurements. ....</p>	81
<p>Figure 3-7 Time series of VOC fluxes measured above willow canopy. Dashed gridlines denote midnight. Note the variable scales. ....</p>	82
<p>Figure 3-8 Average diurnal profiles of VOC fluxes above willow, and of sensible heat flux, when wind direction was between 90 and 270° (i.e. from over the willow field). Note the variable scales. Grey areas show variability calculated as <math>\pm 1</math> sd of the averaged half-hourly values of all measurements.....</p>	83
<p>Figure 3-9 Time series of VOC mixing ratios, and of temperature, measured above willow. Dashed gridlines denote midnight. Note the variable mixing ratio scales. ....</p>	84
<p>Figure 3-10 Average diurnal profiles of VOC mixing ratios above willow, and of temperature, when wind direction was between 90 and 270° (i.e. from over the willow field). Note the variable scales. Dashed lines denote LOD. Grey areas represent variability calculated as <math>\pm 1</math> sd of the averaged half-hourly values of all measurements.....</p>	85
<p>Figure 3-11 Average diurnal profile of [MVK+MACR]:[isoprene] ratio above the willow canopy. Grey areas represent variability calculated as <math>\pm 1</math> sd of the averaged half-hourly values of all measurements.....</p>	86
<p>Figure 4-1 Location of Whim Moss experimental field site in relation to Edinburgh. (Attributable to ©2012 Google).....</p>	95
<p>Figure 4-2 Aerial view of Whim Moss field site, showing the boardwalk layout, within which 44 sampling plots are arranged. (Map attributable to ©2013 DigitalGlobe, Getmapping plc. Map data ©2013 Google).....</p>	96
<p>Figure 4-3 Schematic diagram showing treatment plots at Whim Moss. Plots are numbered 1 to 44, and are arranged in 4 replicate blocks. Numbers inside the circles indicate the deposition treatment received (<math>\text{kg N ha}^{-1} \text{y}^{-1}</math>) in addition to the <math>8 \text{ kg N ha}^{-1} \text{y}^{-1}</math> background deposition. The colour of the circle indicates whether N was in reduced <math>\text{NH}_4\text{Cl}</math> (turquoise) or oxidised <math>\text{NaNO}_3</math> (pale green) form, or were control plots (C) receiving no additional treatment other than background N (<math>8 \text{ kg N ha}^{-1} \text{y}^{-1}</math>). A purple/red outer circle shows plots which also received P and K. Plots circled pink indicate the plots used in this study..</p>	97
<p>Figure 4-4 Experimental set-up used during sampling of a chamber enclosure. A transparent, polystyrene chamber (33 L) was positioned onto a soil collar (which remains in the soil permanently). A mass-flow controlled pump was used to draw a 2 L air sample through an adsorbent tube, connected in-line to the sampling valve at the top of the chamber.....</p>	100

Figure 4-5 Absorption of radiation in the UV-visible range by the polystyrene chamber material. The grey region (400 - 700 nm) indicates the wavelengths of photosynthetically active radiation (PAR).....	101
Figure 4-6 VOC flux (from control plots 7, 16, 35 and 40) as a function of percentage vegetation cover for <i>Calluna vulgaris</i> . Error bars incorporate analytical and sampling uncertainties. ....	106
Figure 4-7 VOC flux (from control plots 7, 16, 35 and 40) as a function of percentage vegetation cover for <i>Eriophorum vaginatum</i> . Error bars incorporate analytical and sampling uncertainties. ....	107
Figure 4-8 VOC flux (from control plots 7, 16, 35 and 40) as a function of percentage vegetation cover for <i>Pleurozium</i> . Error bars incorporate analytical and sampling uncertainties.....	107
Figure 4-9 VOC flux (from control plots 7, 16, 35 and 40) as a function of percentage vegetation cover for <i>Sphagnum fallax</i> . Error bars incorporate analytical and sampling uncertainties. ....	108
Figure 4-10 VOC flux (from control plots 7, 16, 35 and 40) as a function of percentage vegetation cover for <i>Hypnum jutlandicum</i> . Error bars incorporate analytical and sampling uncertainties. ....	108
Figure 4-11 $\alpha$ -pinene flux (from control plots 7, 16, 35 and 40) as a function of ambient air temperature. The red line shows an exponential fit, $Flux = 0.170 e^{0.488 T}$ .....	110
Figure 4-12 $\beta$ -pinene flux (from control plots 7, 16, 35 and 40) as a function of ambient air temperature. The red line shows an exponential fit, $Flux = 1.69 e^{0.278 T}$ .....	110
Figure 4-13 3-carene flux (from control plots 7, 16, 35 and 40) as a function of ambient air temperature. The red line shows an exponential fit, $Flux = 4.51 \times 10^{-6} e^{1.14 T}$ .....	111
Figure 4-14 Limonene flux (from control plots 7, 16, 35 and 40) as a function of ambient air temperature. The red line shows an exponential fit, $Flux = 15.4 e^{0.186 T}$ .....	111
Figure 4-15 Isoprene flux (from control plots 7, 16, 35 and 40) as a function of ambient air temperature. The red line shows an exponential fit, $Flux = 5802 e^{0.213 T}$ .....	112
Figure 4-16 $\alpha$ -pinene flux (from control plots 7, 16, 35 and 40) as a function of PAR. The red line shows an exponential fit, $Flux = 6.83 \times 10^{-12} e^{0.0419 PAR}$ .....	114
Figure 4-17 $\beta$ -pinene flux (from control plots 7, 16, 35 and 40) as a function of PAR. The red line shows an exponential fit, $Flux = e^{0.00682 PAR}$ .....	114

Figure 4-18 3-carene flux (from control plots 7, 16, 35 and 40) as a function of PAR. The red line shows an exponential fit, $Flux = 2.02 \times 10^{-16} e^{0.0544 PAR}$ .....	115
Figure 4-19 Limonene flux (from control plots 7, 16, 35 and 40) as a function of PAR. The red line shows an exponential fit, $Flux = 8.93 e^{0.0053 PAR}$ .....	115
Figure 4-20 Isoprene flux (from control plots 7, 16, 35 and 40) as a function of PAR. The red line shows an exponential fit, $Flux = 29.2 e^{0.0121 PAR}$ .....	116
Figure 4-21 Graph of $\ln E_{meas}$ against $T - T_s$ (K). The red line shows a linear regression of the form $\ln E_{meas} = \beta (T - T_s) + \ln E_s$ , where $E_{meas}$ is the total monoterpene emission (in $\text{ng m}^{-2} \text{h}^{-1}$ ) at temperature, $T$ . $E_s$ is the basal emission rate at standard temperature $T_s$ (303 K). The temperature coefficient $\beta$ , was found to be $0.0951 (\pm 0.0088) \text{ K}^{-1}$ and $E_s$ was $1.54 (\pm 1.89) \mu\text{g m}^{-2} \text{h}^{-1}$ .....	119
Figure 4-22 Diurnal variation of $\alpha$ -pinene flux for control, nitrate and ammonium-treated plots. Each data point is the mean measurement from three replicate sample plots. Error bars denote 1 sd. ....	121
Figure 4-23 Diurnal variation of $\beta$ -pinene flux for control, nitrate and ammonium-treated plots. Each data point is the mean measurement from three replicate sample plots. Error bars denote 1 sd. ....	122
Figure 4-24 Diurnal variation of 3-carene flux for control, nitrate and ammonium-treated plots. Each data point is the mean measurement from three replicate sample plots. Error bars denote 1 sd. ....	122
Figure 4-25 Diurnal variation of limonene flux for control, nitrate and ammonium-treated plots. Each data point is the mean measurement from three replicate sample plots. Error bars denote 1 sd. ....	123
Figure 4-26 Diurnal variation of isoprene flux for control, nitrate and ammonium-treated plots. Each data point is the mean measurement from three replicate sample plots. Error bars denote 1 sd. ....	123
Figure 4-27 VOC fluxes of 4 monoterpenes and isoprene from duplicates of nitrate-treated (plots 11 and 26), control (16 and 7) and ammonium-treated (17 and 21) sample plots on 1 February 2012. Error bars incorporate analytical and sampling uncertainties. ....	126
Figure 4-28 VOC fluxes of 4 monoterpenes and isoprene from duplicates of nitrate-treated (plots 11 and 26), control (16 and 7) and ammonium-treated (17 and 21) sample plots on 6 February 2012. Error bars incorporate analytical and sampling uncertainties. ....	127
Figure 4-29 Percentage vegetation cover of the six plots sampled on 1 and 6 February 2012 and 22 July 2011. Blue bars denote those treated with nitrate, green denote control plots and red denote those treated with ammonium. ....	128

Figure 5-1 Schematic diagram of the Manchester University aerosol chamber filling system. Green lines show the path taken for air during flushing of the chamber. Red denotes path(s) taken while filling. Note that during filling the air intake always passes over the drier and filters. It may or may not pass through the ozone generator, humidifier or VOC injection bulb, depending on the stage in the fill cycle.....	134
Figure 5-2 Exponential fits to show rate of decrease of $\alpha$ -pinene with varying mixing ratios of isoprene. Initial mixing ratios of $\alpha$ -pinene used were 45, 43 and 40 ppbv for low, medium and high mixing ratios of isoprene respectively.....	140
Figure 5-3 Linear fits of the natural logarithm of $\alpha$ -pinene mixing ratio against time. Initial mixing ratios of $\alpha$ -pinene used were 45, 43 and 40 ppbv for low, medium and high mixing ratios of isoprene respectively. ....	141
Figure 5-4 Rate of decrease of limonene with varying mixing ratios of isoprene. Mixing ratios of limonene used were 15, 11 and 20 ppbv for low, medium and high mixing ratios of isoprene respectively. ....	143
Figure 5-5 Linear fits of the natural logarithm of limonene mixing ratio against time. Mixing ratios of limonene used were 15, 11 and 20 ppbv for low, medium and high mixing ratios of isoprene respectively. ....	144
Figure 5-6 Rate of decrease of $\alpha$ -pinene with varying mixing ratios of isoprene from MCM simulations. Mixing ratios of $\alpha$ -pinene used were 45, 43 and 40 ppbv for low, medium and high mixing ratios of isoprene respectively. Note that data output could not be calculated by the model for the full time course for 2 of the runs due to an instability in the model caused by low initial isoprene mixing ratio. ....	145
Figure 5-7 Linear fits of the natural logarithm of $\alpha$ -pinene mixing ratio against time for MCM simulations. Mixing ratios of $\alpha$ -pinene used were 45, 43 and 40 ppbv for low, medium and high mixing ratios of isoprene respectively.....	146
Figure 5-8 Rate of decrease of limonene with varying mixing ratios of isoprene from MCM simulations. Mixing ratios of limonene used were 15, 11 and 20 ppbv for low, medium and high mixing ratios of isoprene respectively. ....	147
Figure 5-9 Linear fits of the natural logarithm of limonene mixing ratio against time for MCM simulations. Mixing ratios of limonene used were 15, 11 and 20 ppbv for low, medium and high mixing ratios of isoprene respectively.....	148
Figure 5-10 Relationship between $k'$ values from MCM simulations with those measured from chamber experiments. Linear fit of limonene is $k'_{\text{MCM}} = 0.675 k'_{\text{experimental}} - 0.0227$ (errors: m 0.0673, c $4.65 \times 10^{-4}$ ). Linear fit of $\alpha$ -pinene is $k'_{\text{MCM}} = 3.68 k'_{\text{experimental}} - 0.0210$ (errors: m 2.82, c 0.0184). ....	149

Figure 5-11 Relationship between experimentally measured  $k'$  value and isoprene mixing ratio. A linear relationship was observed:  $k'_{\text{experimental}} = -1.95 \times 10^{-5}$  [isoprene] + 0.00680 (errors:  $m = 2.63 \times 10^{-6}$ ,  $c = 6.53 \times 10^{-5}$ ,  $R^2 = 0.964$ ).... 151

## List of Tables

Table 1-1 Global BVOC emissions estimates ( $\text{Tg C yr}^{-1}$ ) (Guenther et al., 1995).....	3
Table 1-2 List of proton affinities for common components of air and example VOCs. Data obtained from www.ionicon.com and Blake et al. (2009). .....	12
Table 2-1 Compounds measured during the Speuld field campaign including dwell times, sensitivities and limits of detection during the first (up to 20:00 on 29 <sup>th</sup> June) and second (from 20:00 on 29 <sup>th</sup> June) halves of the campaign. ....	25
Table 2-2 Typical atmospheric lifetimes of compounds investigated for the Speuld campaign. ....	46
Table 2-3 Comparison of standardised emission rates of monoterpenes and isoprene from Douglas fir. ....	63
Table 3-1 Compounds measured during the field campaign including dwell times, sensitivities and limits of detection. ....	75
Table 3-2 Comparison of standardised emission rates of isoprene from willow. REA = relaxed eddy accumulation. ....	89
Table 4-1 Sampling plan of $\text{NO}_3^-$ , $\text{NH}_4^+$ and control plot comparison study carried out at Whim Moss on 22 July 2011. Plots with $56 \text{ kg N ha}^{-1} \text{ y}^{-1}$ ammonium or nitrate treatment were investigated. Three replicates of each treatment type were used, and plots of the same treatment type were sampled simultaneously at the start (T1) and end (T2) of the enclosure time (mins from start of experiment). ....	98
Table 4-2 Fitting parameters for the relationship between VOC flux $F$ ( $\text{ng m}^{-2} \text{ h}^{-1}$ ), and temperature $T$ ( $^{\circ}\text{C}$ ), where $F = a e^{(b T)}$ . Standard errors are shown in parentheses. ....	113
Table 4-3 Fitting parameters for the relationship between VOC flux, $F$ ( $\text{ng m}^{-2} \text{ h}^{-1}$ ), and $PAR$ ( $\mu\text{mol m}^{-2} \text{ s}^{-1}$ ), where $F = a e^{(b PAR)}$ . Standard errors are shown in parentheses. ....	116
Table 4-4 Comparison of standardised monoterpene and isoprene emission rates for boreal wetland studies. ....	120
Table 5-1 Summary of instruments connected to the aerosol chamber with brief descriptions of the parameters measured. ....	135
Table 5-2 Compounds measured during the chamber experiments including dwell times and sensitivities. ....	137
Table 5-3 Summary of chamber experiments carried out. Mixing ratios at the start of the experiments are shown for VOCs (as measured by the calibrated PTR-MS), oxidant ( $\text{O}_3$ ) and $\text{NO}_x$ . ....	138

Table 5-4 Starting concentrations and conditions for each of the six MCM simulations. ....	139
Table 5-5 Linear fit parameters for the pseudo-first order decay of $\alpha$ -pinene, according to the equation $\ln[A]_t = \ln[A]_0 - k't$ . Numbers in parentheses denote standard errors. ....	142
Table 5-6 Linear fit parameters for the pseudo-first order decay of limonene, according to the equation $\ln[A]_t = \ln[A]_0 - k't$ . Numbers in parentheses denote standard errors. ....	144
Table 5-7 Linear fit parameters for the pseudo-first order decay of $\alpha$ -pinene from MCM simulations, according to the equation $\ln[A]_t = \ln[A]_0 - k't$ . Numbers in parentheses denote standard errors. ....	146
Table 5-8 Linear fit parameters for the pseudo-first order decay of limonene from MCM simulations, according to the equation $\ln[A]_t = \ln[A]_0 - k't$ . Numbers in parentheses denote standard errors. ....	148

## Acknowledgements

Throughout my PhD I have received help and support from a number of people who I would like to thank.

First and foremost, I would like to thank my supervisors Prof. Neil Cape and Dr. Mat Heal for the opportunity to undertake this PhD and for their invaluable advice, suggestions, encouragement and support. I appreciate the generosity in financially supporting my attendance at many interesting conferences and meetings in addition to carrying out field campaigns. Additionally, I owe a big thank you to Dr. Pawel Misztal for his excellent teaching and enthusiasm for all things PTR-MS and VOC-related and instilling confidence in me. I am also grateful to Dr. Susan Owen (CEH Edinburgh) for teaching me ATD-GC-MS and for interesting discussions and help with planning of fieldwork.

Much of the practical work undertaken during the project was carried out collaboratively. For fieldwork in Speuld, The Netherlands I would like to thank the following CEH Edinburgh colleagues: Dr. Eiko Nemitz, Dr. Gavin Phillips, Dr. Chiara di Marco and Dr. Mhairi Coyle. Also, Dr. Paul Williams, Dr. Max McGillan (Manchester University), Dr. Arnoud Frumau (ECN) and Hilbrand Weststrate (TNO) for practical help at the sampling site. Additionally I would like to thank Amy Tavendale for her help plotting in-canopy VOC data.

For fieldwork in Brattleby, Lincolnshire I would like to thank Jonathan Wright and Frank Wilson for site access, Eilidh Morrison (UoE and CEH), Dr. Julia Drewer (CEH Edinburgh) and Dr. Jon Finch (CEH Wallingford) for assistance with fieldwork set up, and Kirsti Ashworth (Lancaster University) and Dr. Catherine Hardacre (UoE, now Lancaster University) for discussion of standard emission factors.

Sampling at Whim Moss would not have been possible without the help of Eilidh Morrison, Dr. Sue Owen and project student Jennifer Heaney (UoE). I would also like to express my gratitude to Sarah Leeson (CEH Edinburgh) for sharing vegetation

cover and meteorology data for the site, and to Dr. Ian Leith and Dr. Lucy Sheppard (both CEH Edinburgh) for their advice and allowing access to the site.

Chamber experiments were carried out at Manchester University in collaboration with Dr. Rami Alfarra and Prof. Gordon McFiggans.

I am also grateful to fellow group members, students and post-docs in the chemistry department at Edinburgh University for their friendship and mutual support throughout my PhD. In particular: Kirsten Strain, Heather Johnston, Eilidh Morrison, Dr. Pawel Misztal, Dr. Mark Hammonds, Dr. Catherine Hardacre, Dr. Emanuel Blei, Dr. Chun Lin, the physical chemistry group and the Friday fika group, amongst many others.

Finally, I would like to thank my parents, Margaret and Paul, and brother Gary for their continuing support and encouragement throughout.

## Abstract

Biogenic volatile organic compounds (BVOC) are a wide-ranging group of trace gas components in the atmosphere which are emitted naturally from Earth's surface. It is now recognised that biogenically sourced VOCs are far more significant on a global scale than those from anthropogenic sources, with up to 10 times greater emissions. Very few field-based studies of fluxes from plant canopies have been undertaken, particularly for non-terpenoid compounds. This thesis presents mixing ratio and flux measurements of BVOC from a range of temperate plant canopies: Douglas fir, short-rotation coppice willow, *Miscanthus* and mixed peatland vegetation.

The virtual disjunct eddy covariance technique (vDEC) using a proton transfer reaction mass spectrometer (PTR-MS) as a fast VOC sensor was used for all measurements except for peatlands, where grab samples were collected on adsorbent sampling tubes for later chromatographic analysis. The PTR-MS was also utilised for measuring the rate of degradation of VOCs during laboratory chamber experiments.

Mixing ratios and fluxes of VOCs measured within and above a Douglas fir forest were the first canopy-scale measurements for this species. Fluxes of monoterpenes were comparable to previous studies while isoprene was also detected (standard emissions factors up to  $1.15 \mu\text{g g}_{\text{dw}}^{-1} \text{h}^{-1}$  and  $0.18 \mu\text{g g}_{\text{dw}}^{-1} \text{h}^{-1}$ , respectively). Emissions of oxygenated VOCs were also found to be significant, highlighting the importance of quantifying a wider variety of VOCs from biogenic sources, other than isoprene and monoterpenes.

Results for bioenergy crops *Miscanthus* and willow showed that willow was a high isoprene emitter ( $20 \mu\text{g g}_{\text{dw}}^{-1} \text{h}^{-1}$ ), but no measureable VOCs were detected from *Miscanthus*. This indicates that future expansion of bioenergy crops, and hence species selection, should take resultant air quality and human health impacts – due to changing VOC emissions – into account.

Fluxes of BVOC from a Scottish peatland are the first reported measurements for this ecosystem in a temperate climate. Additionally, to assess the impact of nitrogen deposition on VOC fluxes, BVOC measurements were taken from sample plots in a

pre-existing, long-term field manipulation study to assess impacts of wet nitrate or ammonium deposition on peatland. The peatland was found to be a significant source of isoprene and monoterpenes ( $590$  and  $1.5 \mu\text{g m}^{-2} \text{h}^{-1}$  respectively) and there was evidence that emissions were affected by wet nitrogen treatment. Isoprene emissions were reduced by both nitrate and ammonium treatment, while nitrate increased  $\beta$ -pinene fluxes. Increasing atmospheric nitrogen concentrations are therefore predicted to have an impact on VOC emission.

Chamber studies showed that the rate of loss of  $\alpha$ -pinene from the gas-phase during oxidation – and hence potential formation of secondary organic aerosol (SOA) – decreased with increasing isoprene mixing ratio. This was not observed for limonene. These results show that as isoprene mixing ratios increase with increasing global temperatures, negative feedback on radiative forcing from SOA particles may be suppressed.

Results from this thesis provide valuable experimental data for a range of temperate plant canopies, which will help constrain modelled predictions of future VOC emissions. Additionally, the importance of understanding the effects of land use and environmental change on VOC emissions was demonstrated.

## List of acronyms and abbreviations

AMS	Aerosol Mass Spectrometer
amsl	Above Mean Sea Level
amu	Atomic Mass Unit
ATD	Automated Thermal Desorption
ATD-GC-MS	Automated Thermal Desorption – Gas Chromatography – Mass Spectrometry
BER	Basal Emission Rate
BVOC	Biogenic Volatile Organic Compound
BSOA	Biogenic Secondary Organic Aerosol
CCN	Cloud Condensation Nuclei
CEH	Centre for Ecology and Hydrology
CPC	Condensation Particle Counter
cps	Counts Per Second
DEC	Disjunct Eddy Covariance
DEFRA	Department for Environment, Food and Rural Affairs
DMPS	Differential Mobility Particle Sizer
EC	Eddy Covariance
FID	Flame Ionisation Detector
G06	Guenther et al. (2006) algorithm
G95	Guenther et al. (1995) algorithm
G93	Guenther et al. (1993) algorithm
GC	Gas Chromatography
GC-MS	Gas Chromatography – Mass Spectrometry
HTDMA	Hygroscopicity Tandem Differential Mobility Analyser
ID	Inner Diameter
IPCC	Intergovernmental Panel on Climate Change
LAI	Leaf Area Index
LOD	Limit of Detection
MACR	Methacrolein
MBO	2-methyl-3-buten-2-ol
MCM	Master Chemical Mechanism

MEGAN	Model of Emissions of Gases and Aerosols from Nature
MEK	Methyl Ethyl Ketone
MID	Multiple Ion Detection
MS	Mass Spectrometry
MT	Monoterpene
MVK	Methyl Vinyl Ketone
$m/z$	Mass ( $m$ ) to charge ( $z$ ) ratio
ncps	Normalised Counts Per Second
NMHC	Non-Methane Hydrocarbon
OD	Outer Diameter
OVOC	Oxygenated Volatile Organic Compounds
PAR	Photosynthetically Active Radiation
ppbv	Parts Per Billion (by Volume)
ppmv	Parts Per Million (by Volume)
pptv	Parts Per Trillion (by Volume)
PTFE	Polytetrafluoroethylene
PTR-MS	Proton Transfer Reaction Mass Spectrometry
PTR-TOF-MS	Proton Transfer Reaction Time-of-Flight Mass Spectrometry
QMS	Quadrupole Mass Spectrometer
REA	Relaxed Eddy Accumulation
sd	Standard Deviation
SEM	Secondary Electron Multiplier
SOA	Secondary Organic Aerosol
SRC	Short Rotation Coppice
TD	Thermal Desorption
TOF	Time of Flight
TMA	Trimethylamine
$u^*$	Frictional velocity
UoE	University of Edinburgh
vDEC	Virtual Disjunct Eddy Covariance
VMR	Volumetric Mixing Ratio
VOC	Volatile Organic Compound

## Chapter 1: Introduction

This chapter introduces background contextual information on volatile organic compounds, their sources, atmospheric chemistry and techniques used for their analysis. The main aims of this thesis and its structure are also described. More specific introductory material is also presented at the start of each of Chapters 2 to 5.

### 1.1 What are volatile organic compounds?

Volatile organic compound (VOC) is the term used to describe a wide-ranging group of carbon-containing trace gases in the atmosphere. The term non-methane hydrocarbon (NMHC) has been used historically, since methane reacts slowly in the troposphere, unlike many other hydrocarbons. However, it is now recognised that a range of organic compounds, in addition to hydrocarbons, are important tropospheric constituents. The term VOC therefore includes alkanes, alkenes, carbonyls, alcohols, esters, acids and terpenoids (Kesselmeier and Staudt, 1999).

The importance of biogenic sources of VOCs in the atmosphere was first recognised in the late 1950s with the discovery that the terpenoid isoprene was a component of volatile emissions from plants (Sanadze, 2004), and formation of ‘blue haze’ over forests was due to terpene emissions (Went, 1960). Structures of isoprene and some monoterpenes are shown in Figure 1-1. More recently it has become apparent that natural sources of VOCs are far more significant on a global scale than anthropogenic sources, with emission rates up to ten times higher at  $\sim 1150 \text{ Tg Carbon yr}^{-1}$  (Guenther et al., 1995).

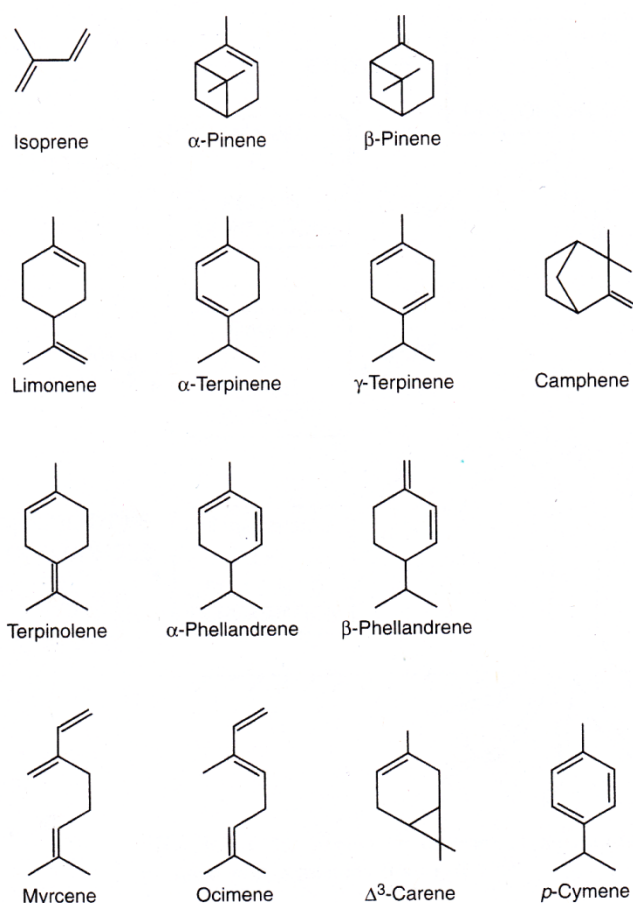


**Figure 1-1 Chemical structures of isoprene and some monoterpenes (Finlayson-Pitts and Pitts Jr, 2000).**

The most dominant biogenic VOC (BVOC) is isoprene, which accounts for 44 % of emissions, but other important groups of compounds include monoterpenes and oxygenated VOCs (OVOCs) which can be emitted directly or formed in-situ from oxidation of other VOCs.

The major source of biogenic VOC emissions is terrestrial vegetation (Steiner and Goldstein, 2007). Globally important sources of VOCs are dominated by tropical woodlands which contribute around half of global VOC emissions (Guenther et al., 1995) and in particular are a source of isoprene, monoterpenes and methanol (Taipale et al., 2008). Emissions from oceans and soil contribute as minor sources. Table 1-1 summarises current emissions estimates for BVOCs.

**Table 1-1 Global BVOC emissions estimates (Tg C yr<sup>-1</sup>) (Guenther et al., 1995).**

Source	Isoprene	Monoterpene	Other more reactive organics <sup>a</sup>	Other less reactive organics <sup>b</sup>	Total VOC
Woods	372	95	177	177	821
Crops	24	6	45	45	120
Shrubs	103	25	33	33	194
Ocean	0	0	2.5	2.5	5
Other	4	1	2	2	9
All	503	127	260	260	1150

<sup>a</sup> defined as VOCs with lifetimes < 1 day. <sup>b</sup> defined as VOCs with lifetimes > 1 day.

## 1.2 How are BVOCs emitted to the atmosphere?

Until the last decade there was little understanding about the mechanisms of BVOC emissions from plants. The ecological reasons for plant BVOC emission are still unclear, although some of the reasons cited include protection from thermal damage, attracting pollinators and deterring predators (Hanson et al., 1999; Sharkey and Yeh, 2001).

What is more clearly understood are the environmental conditions which drive emission. For example, the dependence of BVOC emission on temperature and light has been long known and is particularly well reported for isoprene and monoterpenes. Isoprene emission is very sensitive to photosynthetically active radiation (PAR) – the portion of the visible spectrum (400 – 700 nm) which activates photosynthesis – with emission almost instantaneous (Steiner and Goldstein, 2007).

Unlike isoprene, monoterpenes synthesised in plants are held in storage pools, therefore emission has been regarded as dependent only on temperature and not light (Guenther et al., 1993). There is now evidence however that monoterpene emissions also show light dependency (Staudt and Lhoutellier, 2011).

For this reason, results of flux studies are normally scaled to a standard or basal emission rate to allow comparison, taking standard conditions to be 303 K temperature and 1000  $\mu\text{mol m}^{-2} \text{s}^{-1}$  PAR. Methodology for standardisation of

emission rates has been explained elsewhere (Guenther et al., 1995; Guenther et al., 1993) and is covered in more detail in Chapters 2, 3 and 4.

### **1.3 Effects of VOCs on atmospheric chemistry**

VOCs are important for several reasons. Firstly, many may be harmful to human health, although many of their effects are as yet unknown. In addition, VOCs can rapidly oxidise in the atmosphere. For example, isoprene reacts in the troposphere with the hydroxyl radical (OH), nitrate radical (NO<sub>3</sub>) and ozone (O<sub>3</sub>) with a lifetime, under typical concentrations of these oxidants, of 1.4 h, 1.6 h and 1.3 days respectively (Steiner and Goldstein, 2007). This therefore affects the oxidative capacity of the atmosphere to ‘cleanse’ itself of other more long-lived pollutants such as methane, which has an OH lifetime of ~12 years. It is the high reactivity of VOCs in the troposphere which results in the formation of secondary pollutants, as outlined below.

#### **1.3.1 Tropospheric ozone**

Oxidation of VOCs can subsequently lead to the formation of tropospheric ozone through their interaction with the NO-NO<sub>2</sub>-O<sub>3</sub> system as shown in Figure 1-2 (Atkinson, 2000).

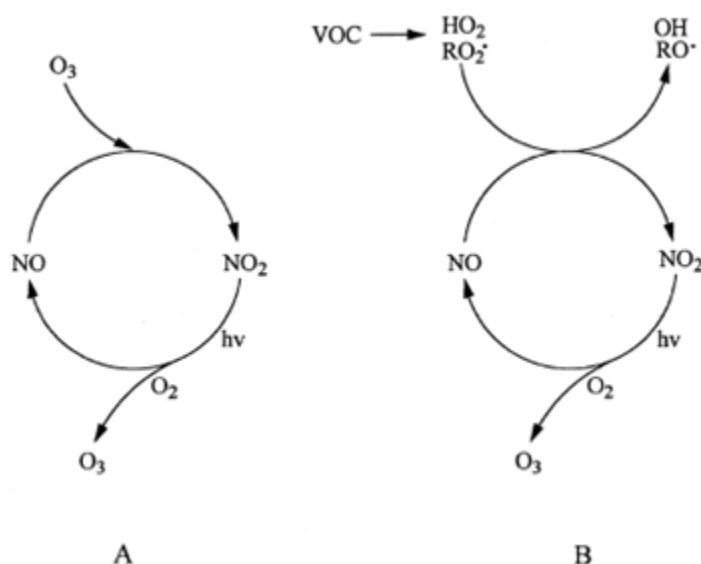


**Figure 1-2 Comparison of (A) NO-NO<sub>2</sub>-O<sub>3</sub> cycle in the absence of VOCs with (B) in the presence of VOCs. In scheme A there is a balance between destruction and formation of O<sub>3</sub>. Scheme B results in net production of O<sub>3</sub> (Atkinson, 2000).**

Although the ozone layer (at an altitude of ~25 km) is well-known for protecting the Earth's surface from harmful UV radiation, ozone is not desirable at tropospheric levels. Ozone is of concern to human health as it is a respiratory irritant, particularly to those with an existing respiratory condition such as asthma. In addition, it is toxic to plants and is a contributor to photochemical smog typical of many cities with long hours of intense sunshine.

### 1.3.2 Secondary organic aerosol

VOCs are also involved in the formation and growth of aerosol particles. As mentioned previously, Went first suggested in 1960 (Went, 1960) that VOCs were involved in the phenomenon of blue hazes above forest canopies, and that the particle size of these light-reflecting aerosol particles was indicative of formation by agglomeration from gas-phase volatiles. For these reasons, particles formed in this way are referred to as Secondary Organic Aerosol (SOA). This ability to form aerosol particles is important for human health as it has been shown there is a strong association between particulate matter concentration and mortality (Dockery et al., 1993). In addition, particles affect the radiative balance of the atmosphere and hence have an effect on climate as shown in Figure 1-3.

Figure 1-3 shows that aerosols can impact the climate in two ways: directly through absorption and scattering of solar radiation, or indirectly by acting as cloud condensation nuclei, thus changing the albedo of clouds. At present, the direct global mean radiative forcing is estimated at  $-0.5 \pm 0.4 \text{ W m}^{-2}$  with a low-medium level of scientific understanding (Solomon et al., 2007).

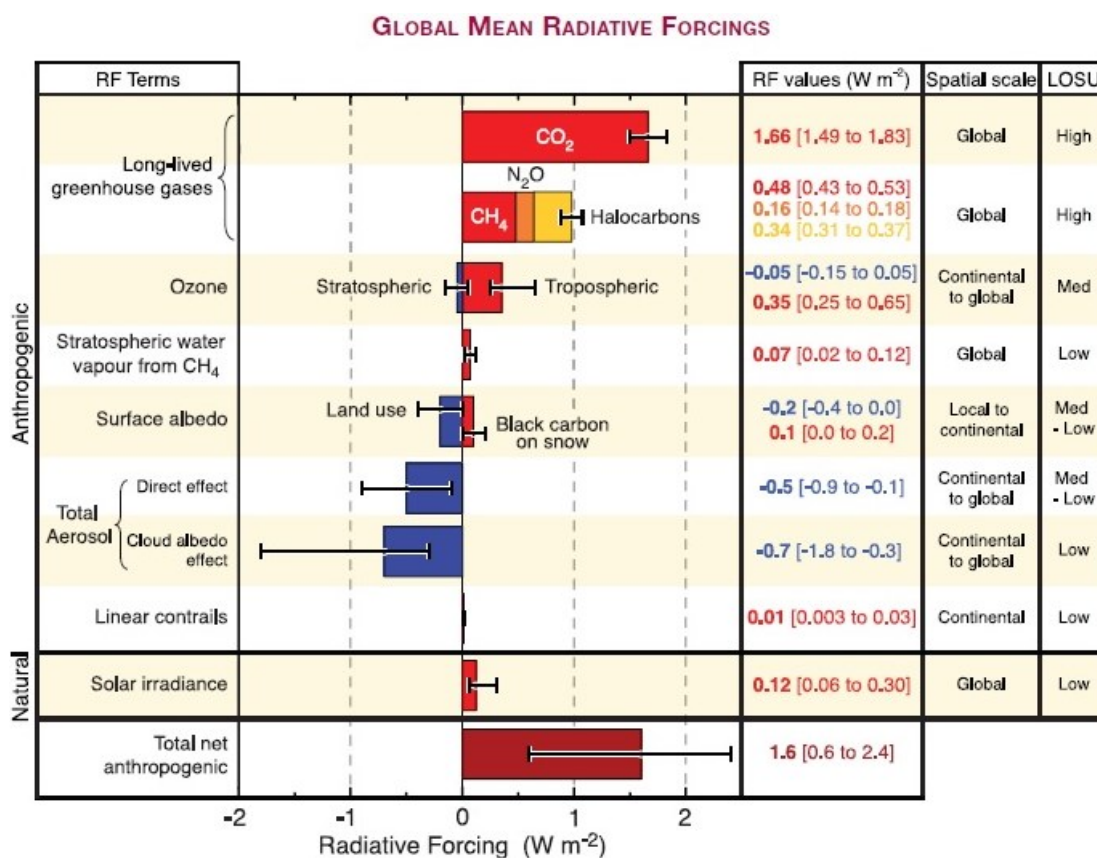


**Figure 1-3 Contributions of atmospheric gases and particles on radiative forcing of the climate. Note the effects of tropospheric ozone and both direct and cloud albedo (indirect) effects of aerosol particles. VOC emissions contribute to all of these factors. (Solomon et al., 2007).**

A study by Kulmala et al. (2004) investigated the feedback mechanisms which link CO<sub>2</sub> uptake and aerosol emissions of forests with climate. They attempted to quantify the expected increase in cloud condensation nuclei as a result of increased CO<sub>2</sub> concentrations, hence greater production of BVOCs. A doubling of CO<sub>2</sub> concentration was assumed to result in a 10% increase in BVOC emissions, due to radiative forcing effects and increased CO<sub>2</sub> fertilisation leading to increased forest biomass. It was then concluded that this would result in an increase of cloud optical

depth of 1-2%. Attention was also drawn to the point that in the extreme case that a doubling of CO<sub>2</sub> concentration resulted in doubling of BVOC emission rates, the increase in cloud optical depth could be as high as 20%. Nevertheless, it was also noted that the associated warming effect of a doubling in CO<sub>2</sub> concentration would outweigh any cooling effect produced by a comparatively small increase in cloud optical depth. Conversely, several studies (reviewed in Arneth et al., 2007) have observed that isoprene emission is suppressed by increased CO<sub>2</sub> mixing ratio through direct inhibition of metabolic pathways (Rosenstiel et al., 2003).

Although the importance of VOCs in SOA has been acknowledged for some time, very little is understood about the processes involved in the transition from the gas to aerosol phase. A recent study hypothesised that formation of new SOA particles from monoterpenes may be suppressed by the presence of isoprene, owing to its high reactivity towards the OH radical (Kiendler-Scharr et al., 2009). As isoprene emissions increase with temperature (Guenther et al., 1995), future climate changes could result in suppressed aerosol formation, thereby reducing the negative radiative forcing effects which may then amplify global temperature increase. The implications of suppressed isoprene emission as a result of increased CO<sub>2</sub> emission associated with temperature rise were not considered however.

## **1.4 VOC analytical measurement techniques**

The most common method of identifying and quantifying VOCs is gas chromatography (GC) to separate components in a gaseous sample, coupled with flame ionisation detection (FID) and/or mass spectrometry (MS) for quantification of components. Because of the low mixing ratios of VOCs in air, pre-concentration of the sample is normally required using an adsorbent material or cryogenic focussing. Detection limits as low as parts per trillion by volume (pptv) can be achieved, although the time resolution is slow (~30 min) despite developments in automated systems (Goldan et al., 1995). This makes the method unsuitable for on-line analysis of compounds which change on a relatively short timescale (less than 15 minutes). In addition, the need for pre-concentration can be particularly problematic for oxygenated VOCs which can irreversibly adsorb to surfaces.

Another method which has become a useful tool in atmospheric VOC measurements is proton transfer reaction mass spectrometry (PTR-MS), which provides fast online measurements with sensitivity in the order of ppt (Hansel et al., 1995; Lindinger et al., 1998). One disadvantage of PTR-MS however, is the inability to resolve isobaric compounds (i.e. those with identical nominal mass but differing exact mass), such as monoterpenes. PTR-MS is discussed in more detail in Section 1.5.3.

## 1.5 Flux methods

In addition to understanding the identities and concentrations of VOCs in an air sample, it is also important to understand biosphere-atmosphere exchange processes by quantifying the rate at which BVOCs are emitted to the atmosphere or taken up by plants.

### 1.5.1 Leaf and branch enclosures

Many early investigations of plant emissions were undertaken using branch or leaf enclosures, the most direct way to measure BVOCs from an individual species (Evans et al., 1982; Lamb et al., 1985; Zimmerman, 1979). A branch or leaf is placed inside a Teflon (Polytetrafluoroethylene, PTFE) or Tedlar (Polyvinyl fluoride, PVF) enclosure. In a dynamic system, air is pumped through the enclosure (at a known flow rate) and the flux is calculated using the difference between inlet ( $c_{in}$ ) and outlet ( $c_{out}$ ) mixing ratios using Equation 1-1.

$$Emission\ rate = \frac{flow\ rate}{mass\ of\ vegetation} (c_{in} - c_{out}) \quad (1-1)$$

In a static system, air is not pumped through the enclosure, so a sample is collected before and after a known enclosure time and subsequently analysed, normally using GC-MS. It is important not to damage the plant in enclosure experiments, as this may induce the release of BVOCs, while in static systems there is the additional concern of maintaining ambient temperature and humidity within the chamber, to avoid affecting BVOC emissions. Although enclosure sampling is direct, relatively simple and cheap, the method tends to result in overestimation of light-dependent VOC emissions, since average plant canopies will have some leaves in direct light and

some which are shaded (Guenther et al., 1996; Steiner and Goldstein, 2007). Static chamber measurements were used in Chapter 4 of this work.

## 1.5.2 Eddy covariance

Micrometeorology techniques require the simultaneous, fast measurement of VOC concentration and vertical wind speed to determine an up or downwards flux. Eddy covariance is one of the more direct methods of measuring trace gas fluxes, with several variants on the method (Hörtnagl et al., 2010) explained here.

### 1.5.2.1 Direct eddy covariance (EC)

The eddy covariance (EC) method is the most direct way of measuring trace gas fluxes. It requires the direct correlation of vertical wind-speed data,  $w$  (using a sonic anemometer) with comparatively fast concentration measurements,  $s$ , in order to capture as much of the small, fast, turbulent fluctuations as possible. The mean of  $w$  and  $s$  ( $\bar{w}$  and  $\bar{s}$  respectively) are determined over a suitable time period (usually 0.5 to 2 h), and fluctuations about the mean are denoted as  $w'$  and  $s'$ , where:

$$w = \bar{w} + w' \quad \text{and} \quad s = \bar{s} + s' \quad (1-2)$$

The flux is then calculated as the covariance of instantaneous deviations in vertical wind speed and VOC concentration according to Equation 1-3.

$$F_s = \overline{w's'} = \frac{1}{t_B - t_A} \int_{t_A}^{t_B} w'(t) s'(t) dt \quad (1-3)$$

Both instruments need to be able to sample at a frequency of  $\sim 10$  Hz. Few suitably fast sensors exist for measurement of VOCs using EC except for the fast isoprene sensor (Guenther and Hills, 1998) or proton transfer reaction mass spectrometry (PTR-MS) where only one compound is monitored (instrument detailed in Section 1.5.3).

### 1.5.2.2 Disjunct eddy covariance (DEC)

By relaxing the requirements for a fast trace gas sensor, it is possible to take fast grab samples followed by slow analysis of the sample. This method is termed Disjunct EC (DEC) and has been used in several campaigns (Davison et al., 2009; Grabmer et al., 2004; Langford et al., 2009; Rinne et al., 2001). Sample windows of  $\sim 0.1$  s are grabbed at relatively long intervals of up to 30 s ( $\Delta t$ ), during which time the sample is analysed. The number of samples,  $N$ , needed to calculate a flux is therefore reduced and the flux is calculated as:

$$F_s = \langle w's' \rangle = \frac{1}{N} \sum_{i=1}^N w'(i\Delta t)s'(i\Delta t) \quad (1-4)$$

This method therefore allows for the use of slower sensors, but at the expense of increased uncertainty and limit of detection for a given time period of measurement.

### 1.5.2.3 Virtual disjunct eddy covariance (vDEC)

A modification on the DEC technique has been introduced, termed virtual disjunct EC (vDEC) (Karl et al., 2002). Instead of having a slow analysis time between short grab samples, fast response measurements of several different compounds are taken in a sequential manner. This method allows for the quantification of a wide range of atmospheric compounds and is particularly suited to the PTR-MS, as described in the next section (1.5.3).

### 1.5.3 Proton transfer reaction mass spectrometry (PTR-MS)

The vDEC method is well-suited to PTR-MS which can be used as an appropriately fast sensor (order of 0.1 s) for a wide range of organic compounds, since the quadrupole mass filter scans masses in a sequential manner. The use of PTR-MS for trace gas flux measurements was first introduced in 2001 (Rinne et al., 2001) and has since been used in a wide range of field campaigns, for example in urban environments (Langford et al., 2009) as well as forest canopies (Grabmer et al., 2004; Holzinger et al., 2005; Karl et al., 2002).

### 1.5.3.1 Theoretical principle of operation

Proton transfer reaction mass spectrometry (PTR-MS) is a useful tool in the online measurement of volatile organic compounds (VOCs). Details of the instrument were first described in 1995 (Hansel et al., 1995) and it has since found wide-ranging applications in fields such as medical diagnosis and food science (Blake et al., 2009; Lindinger et al., 1998) as well as analysis of trace atmospheric components (Hewitt et al., 2003).

PTR-MS analysis is based on a ‘soft’ chemical ionisation method whereby analyte molecules undergo proton-transfer reactions. The instrument is comprised of three main components: an ion source, a drift tube and a quadrupole mass analyser. A diagram of the instrument is shown in Figure 1-4.

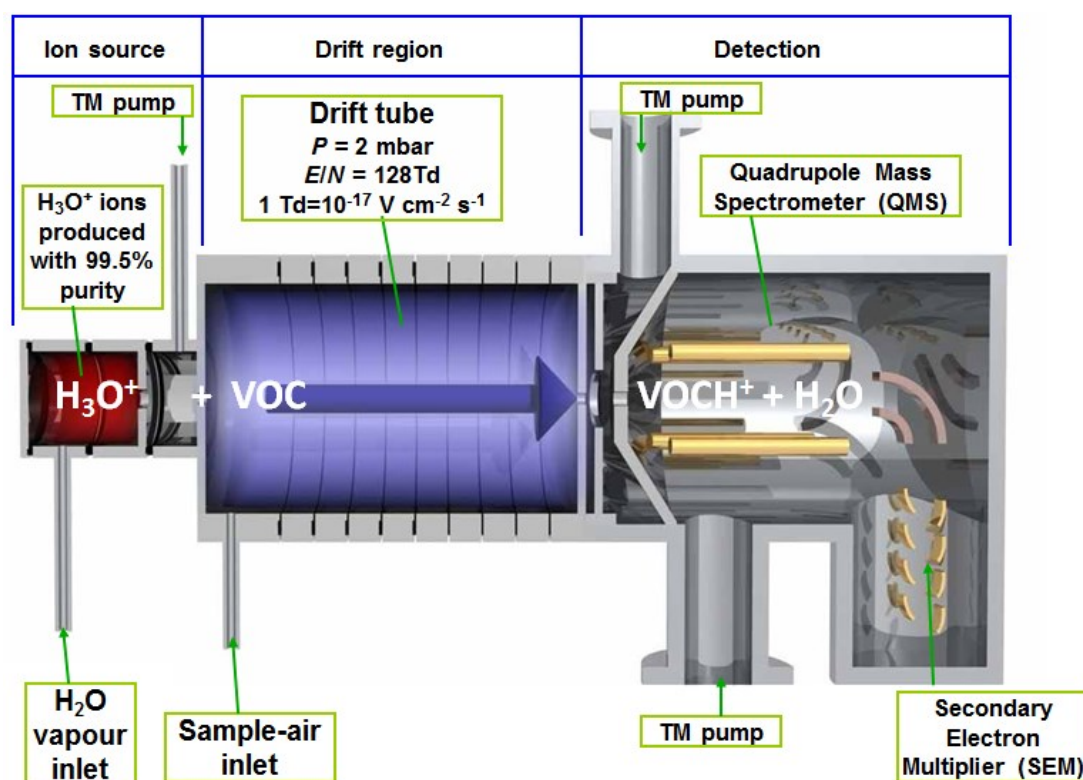
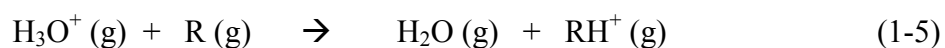


Figure 1-4 Schematic diagram of a PTR-MS (Misztal, 2010). The instrument is comprised of 3 main sections: the ion source ( $\text{H}_3\text{O}^+$  ions are formed); the drift region ( $\text{H}_3\text{O}^+$  ions undergo proton-transfer reactions with trace components of air); and the detection region (protonated analyte molecules are detected by a secondary electron multiplier (SEM)). TM refers to turbo molecular pumps used to sustain a constant pressure of  $\sim 2 \text{ mbar}$  in the drift tube and  $\sim 1 \times 10^{-5} \text{ mbar}$  in the quadrupole mass analyser. Sample air inlet flow rate is also used to maintain drift tube pressure.

$\text{H}_3\text{O}^+$  primary ions are formed in a hollow cathode ion source on the order of  $1 \times 10^6$  ions per second under normal operating conditions. Reagent ions pass into the drift tube, which is under the influence of an electric field ( $E$ ) with a typical value of  $\sim 60 \text{ V cm}^{-1}$  and is held at a pressure in the region of 2 mbar, by introducing ambient air at a flow rate of  $\sim 100 \text{ mL min}^{-1}$ . Analyte molecules react with  $\text{H}_3\text{O}^+$  ions to form protonated molecules as shown in Equation 1-5:



where R is some trace component of air. As Equation 1-5 requires R to have a proton affinity greater than that of water ( $691 \text{ kJ mol}^{-1}$  (Blake et al., 2009)) in order to be irreversible, bulk components of air such as  $\text{O}_2$ ,  $\text{N}_2$  and  $\text{CO}_2$  do not react due to their low proton affinities. On the other hand, many VOCs have a proton affinity high enough to undergo proton-transfer reactions on every collision. Table 1-2 lists the proton affinities of the main components of air as well as some common VOCs.

**Table 1-2 List of proton affinities for common components of air and example VOCs. Data obtained from [www.ionicon.com](http://www.ionicon.com) and Blake et al. (2009).**

Molecule	Proton affinity / $\text{kJ mol}^{-1}$
Oxygen	421
Nitrogen	494
Carbon dioxide	541
Ozone	626
Methane	544
<b>Water</b>	<b>691</b>
Formaldehyde	715
Methanol	753
Acetaldehyde	769
Acetone	812
MACR	812
Isoprene	832
MVK	837

Protonated molecules then pass through a quadrupole mass analyser where molecules are separated by their mass to charge ratio ( $m/z$ ), and a signal is detected through collision with a secondary electron multiplier (SEM). The use of a soft method of

ionisation means that complex fragmentation patterns are avoided. This is highly advantageous when dealing with ambient air containing an extensive range of trace components, as the most abundant ion detected is normally the protonated molecular ion ( $\text{RH}^+$ ). The electric field, temperature and pressure of the drift tube need to be optimised so that the  $E/N$  ratio (where  $N$  is the number density of buffer gas molecules, i.e., air) is in the normal operating range of 120 – 130 Td (1 Townsend =  $10^{-17} \text{ cm}^2 \text{ V molecule}^{-1}$ ). This range gives a good compromise between molecular ion fragmentation and reagent ion clustering. Increasing the  $E/N$  ratio (by increasing  $E$  or decreasing drift tube pressure) would prevent reagent ion hydration ('water clustering':  $\text{H}_3\text{O}^+\text{H}_2\text{O}$ ) but would increase the degree of fragmentation of molecular ions. On the other hand, decreasing the  $E/N$  ratio would prevent molecular ion fragmentation, but increase reagent ion clustering.

One of the main challenges in measuring VOC fluxes using PTR-MS is the determination of compound lag time. This is defined as the time offset between a series of vertical wind speed data and a series of VOC mixing ratio<sup>1</sup> measured by a PTR-MS due to the delay caused by transit time through the sampling line (Taipale et al., 2010) in addition to instrument response time and collection of the disjunct sample series. A lag time must therefore be determined and applied to data series for accurate calculation of flux values.

The lag time can be determined using one of several methods which have been reviewed in detail elsewhere (Miształ, 2010; Taipale et al., 2010). The most prevalent approach involves calculating the covariance as a function of lag time within a reasonable time window based on the dimensions of the sampling line. The lag time is then taken as that which results in maximum covariance. Although popular amongst the PTR-MS community, this method can lead to overestimation of fluxes. This approach was applied for measurements detailed in Chapter 2.

---

<sup>1</sup> the abundance of one component relative to that of all other components, on a molar basis.

A newly developed approach (Misztal, 2010) involves subdividing the flux averaging period. Lag times are calculated separately for each sub-period and the median lag time is applied for the entire averaging period. This has proved to be a suitable alternative (Taipale et al., 2010) and was used in Chapter 3 of this work.

### 1.5.3.2 Recent developments of PTR-MS

In addition to PTR-MS, an instrument incorporating a time of flight (TOF) analyser has also been developed, giving greater mass resolution, and allowing the simultaneous acquisition of all  $m/z$  channels, eliminating the need for disjunct sampling (Jordan et al., 2009b). The PTR-TOF-MS remains much more expensive than PTR-MS however.

It has recently been demonstrated that a standard PTR-MS can be used to resolve isobaric compounds such as monoterpenes (Misztal et al., 2012). This was achieved by using an alternating rather than constant drift voltage and examining fragmentation patterns, which differed between monoterpenes.

Until recently, the PTR-MS has been used as a gas-phase analytical instrument; however some recent studies have modified the traditional, commercial instrument to be suitable for online analysis of secondary organic aerosols (Hellén et al., 2008). A more recent example involves the addition of a thermal desorption (TD) unit at the front-end to enable the PTR-MS to be capable of directly sampling gas-phase and aerosol-phase organic components (Holzinger et al., 2010b) which has since been applied in field campaigns (Holzinger et al., 2010a). The assembly is capable of making measurements of aerosol chemical composition every 15 minutes. It also has the advantage of being capable of automatically switching between aerosol and gas-phase measurements through the use of valves.

Another development has seen the capability of switching to alternative reagent ions (Jordan et al., 2009a). The commercially available instrument is capable of switching between  $\text{H}_3\text{O}^+$ ,  $\text{NO}^+$  and  $\text{O}_2^+$  reagent ions in less than 10 s. This combines the sensitivity of PTR-MS with the capability of being able also to detect compounds

with a proton affinity lower than water and the ability to distinguish between isobaric compounds (Jordan et al., 2009a).

## 1.6 Research aims

The primary aim of this work was to quantify fluxes of VOCs from a variety of plant canopies. Further to this, the use of PTR-MS allowed identification of fluxes of a wider variety of VOCs than isoprene and monoterpenes, which had been the main focus of VOC studies prior to appropriate instrumental developments.

A temperate, coniferous forest was chosen as a study site due to no previous canopy-scale measurements being carried out on the species Douglas fir (*Pseudotsuga menziesii*). A review of literature also showed a lack of data for non-terpenoid emissions.

Field measurements of canopy-scale fluxes and mixing ratios were also recorded for two crops, elephant grass (*Miscanthus x giganteus*) and willow (*Salix spp.*). These crops were studied due to their increasing use as bioenergy feedstocks as a way of addressing climate change and uncertainty in energy security. Associated impacts on VOC emission, and therefore on air quality, as a result of land use change had not previously been investigated.

Field measurements of isoprene and monoterpene fluxes from a temperate peat bog were collected. Previous measurements from this ecosystem have only been reported for sub-Arctic and boreal sites. Additionally, field manipulation studies were carried out to investigate the effect of wet nitrogen deposition on fluxes, simulating future increased atmospheric nitrogen concentrations.

To enhance understanding of transitions of VOCs from gas to aerosol phase, chamber experiments were carried out to probe atmospheric reactions of monoterpenes.

## 1.7 Thesis structure

The subsequent chapters of this thesis detail all experimental work. A more thorough review of relevant literature for each particular chapter is given in their respective

introductions. Specific technical details of the methods used are also given in each chapter.

Chapter 2 presents results of above- and in-canopy mixing ratios and fluxes from a Douglas fir forest in The Netherlands.

Fluxes and mixing ratios above two different bioenergy crops (*Miscanthus* and willow) from a field campaign in Lincolnshire, UK are compared in Chapter 3. This chapter is based on an article now published (Copeland et al., 2012).

A third dataset of field measurements is presented in Chapter 4, detailing flux measurements from a temperate peat bog (Whim Moss, UK). Effects of field manipulation studies are also discussed.

The final dataset in Chapter 5 reports laboratory experiments using a reaction chamber to investigate the atmospheric reactions of monoterpenes in the presence of isoprene.

The main conclusions are summarised and compared in Chapter 6.

## Chapter 2: VOC mixing ratios and fluxes above a Douglas fir forest

In this chapter, results from an intensive field campaign are presented. Mixing ratios and fluxes of VOCs were measured within and above a Douglas fir forest in Speulderbos, Netherlands. It was observed that emissions of monoterpenes were comparable to previous studies of *Pseudotsuga menziesii*, with the standard emission factor for the first and second halves of the campaign measured to be 1.15 and 0.82  $\mu\text{g g}_{\text{dw}}^{-1} \text{h}^{-1}$ , with temperature coefficients of 0.266 and 0.063  $^{\circ}\text{C}^{-1}$ , respectively. Isoprene standard emission factors for the two halves of the campaign were determined to be 0.10 and 0.18  $\mu\text{g g}_{\text{dw}}^{-1} \text{h}^{-1}$ , respectively. The first study of canopy-scale, non-terpenoid emissions was also undertaken and fluxes of oxygenated VOCs were also significant. This highlights the importance of quantifying a wider variety of VOCs from biogenic sources, other than isoprene and monoterpenes.

### 2.1 Introduction

Biogenic VOC emissions from vegetation (Steiner and Goldstein, 2007) are estimated as about 10 times greater globally than VOC emissions from anthropogenic sources (Guenther et al., 1995). The dominant BVOC is isoprene (Guenther et al., 2006), estimated to contribute 44% of global VOC flux, with monoterpenes contributing 11%, and other reactive VOCs and other VOCs contributing 22.5% apiece. Coniferous forests are normally associated with monoterpene emissions and low (or zero) isoprene emissions (Geron et al., 2000; Karl et al., 2009). A study in the USA reported Douglas fir to be within the top 10 monoterpene-emitting tree species regionally and nationally (Geron et al., 2000).

Several studies have investigated emissions of monoterpenes from Douglas fir on the leaf and branch scale. A study of bigcone Douglas fir (*Pseudotsuga macrocarpa*) measured a total standard monoterpene emission rate (at 30  $^{\circ}\text{C}$ ) of 1.1  $\mu\text{g g}_{\text{dw}}^{-1} \text{h}^{-1}$  (Arey et al., 1995), with  $\alpha$ -pinene and limonene as major components and  $\beta$ -pinene and 3-carene also detected. Another study reported a standardised value of 0.44  $\mu\text{g g}_{\text{dw}}^{-1} \text{h}^{-1}$  for coastal Douglas fir (*Pseudotsuga menziesii*) (Pressley et al., 2004). The highest reported standardised flux was 2.60  $\mu\text{g g}_{\text{dw}}^{-1} \text{h}^{-1}$  monoterpenes (standardised

to 30 °C) in addition to  $1.72 \mu\text{g g}_{\text{dw}}^{-1} \text{h}^{-1}$  isoprene (at 30 °C and  $1000 \mu\text{mol m}^{-2} \text{s}^{-1}$ ) from *P. menziesii* (Drewitt et al., 1998). It has also been shown that needle monoterpene concentration can be used to predict emission rate at constant temperature due to the linear relationship between the two parameters (Lerdau et al., 1995).

Several studies have investigated the impact of varying environmental stressors on synthesis and emission of monoterpenes from Douglas fir. One study showed that increased CO<sub>2</sub> mixing ratio increased the photosynthetic rate in mature needles but did not affect needle monoterpene concentration or emission rate. It was predicted that elevated CO<sub>2</sub> in addition to a 4 °C rise in growth temperature would result in a 50% increase in monoterpene emission due to increases in biomass and leaf area index (LAI) but, experimentally, needle monoterpene concentrations were unaffected (Constable et al., 1999).

In contrast, another study observed that elevated CO<sub>2</sub> exposure or temperature resulted in decreased needle monoterpene concentrations. The additive effect of increases in both factors resulted in a 64% reduction in concentration (Snow et al., 2003). Although monoterpene emission rates were not measured, the theory that needle concentrations can be used as a proxy (Lerdau et al., 1995) would imply an expected decrease under elevated temperature and/or CO<sub>2</sub> mixing ratio scenarios. This is contrary to other observations that needle concentrations are unaffected by CO<sub>2</sub> mixing ratio and temperature (Constable et al., 1999).

Additionally, it has been reported that high soil nitrogen levels will stimulate shoot growth and therefore decrease carbon available for secondary pathways, such as monoterpene emissions (Lerdau et al., 1995). These results could not account for the observations by Snow et al. (2003) which were N-limited, yet showed a decreased monoterpene pool and no shoot growth. There was however evidence of increased root carbon flux which would compete with monoterpene production pathways. The contrasting results of Constable et al. (1999) also observed no correlation between N availability and needle monoterpene concentrations. It was suggested that the discrepancy in results between the two studies was due to a limited concentration

range of samples and low sampling frequency in the Constable study (Constable et al., 1999; Snow et al., 2003).

Most studies of Douglas fir to date have focused solely on isoprene and monoterpenes. One study which investigated a wider range of VOCs emitted from saplings detected monoterpenes, sesquiterpenes, their oxygenated products (including 2-methyl-3-buten-2-ol (MBO)), methyl salicylate and a homoterpene ( $C_{11}H_{18}$ ) (Joó et al., 2011). Changing emission patterns under heat and biotic stress were also investigated.

One previous study at the Speuld site (Figure 2-1) measured forest floor and above-canopy mixing ratios of  $\alpha$ -pinene,  $\beta$ -pinene, 3-carene and limonene (Dorsey et al., 2004). Total monoterpene mixing ratios were highest at night, peaking at  $\sim 0.5$  ppbv between 20:00 and 03:00. It was also observed that forest floor mixing ratios were greater than those measured above-canopy, attributed to large amounts of surface leaf litter. These results corroborate a separate study (Peters et al., 1994) which also found peak concentrations within the same time window – a result of limited atmospheric mixing at night – and observed that concentrations at 21 m above ground were two times those at 36 m. Measurements of other VOCs were not made in either study.

Because of predicted global environmental change and ambiguity in resultant effects on monoterpene emissions, the lack of data for non-terpenoid emissions, and variation in measured standard emission factors, quantification of VOC emissions from Douglas fir warrants further research. The aim of this study was to quantify fluxes and mixing ratios of BVOCs above and within a Douglas fir canopy. The measurements were in addition to a wider study into particles and inorganic reactive gases as part of the EU NitroEurope research programme ([www.nitroeuropa.eu](http://www.nitroeuropa.eu)).

## 2.2 Methods

### 2.2.1 Sampling site

The field measurements were carried out from 15 June to 10 July 2009 at an established measurement site in Speulderbos forest near Garderen, Netherlands ( $52^{\circ} 15' \text{ N}$ ,  $5^{\circ} 41' \text{ E}$ , 50 m amsl, Figure 2-1) which was operated by RIVM (National Institute of Public Health and Environmental Protection). The forest comprised a dense, homogeneous monoculture of mature Douglas fir (*Pseudotsuga menziesii*, ~2.3 ha, Figure 2-2), planted in 1960, within a larger forested area (50 km<sup>2</sup>). The maximum canopy height was around 32 m. There was almost no tree foliage below 8 m with very little light penetrating to the forest floor due to the typical stem separation being only a few metres. The soil was characterised as orthic podzol/holtpodzol with loamy sand texture.

The nearest settlements to the site were Garderen (2.5 km SE, population ~2,000), Putten (5.7 km WNW, population ~23,000) and Ermelo (6.6 km NW, population ~26,000), while the nearest major city was Apeldoorn (19 km ESE, population ~156,000). There was very little traffic on surrounding roads.



**Figure 2-1 Location of the Speulderbos measurement site in The Netherlands.**



**Figure 2-2** Aerial view of the Speuld measurement site. Grey lines show footpaths through the forest. The location of the sampling tower is indicated by the white marker. (Map attributable to ©2012 Aerodata International Surveys, Geoeye (Imagery) and ©2012 Google (map data)).

Flux footprints for the sampling site were predicted using a simple parameterisation model (Kljun et al., 2004) using minimum, maximum and mean friction velocity values. Model results are shown in Figure 2-3. The largest distance for 80% flux contribution over the range of friction velocities encountered (660 m) was within a uniform area of the forest for all wind directions (Figure 2-4).

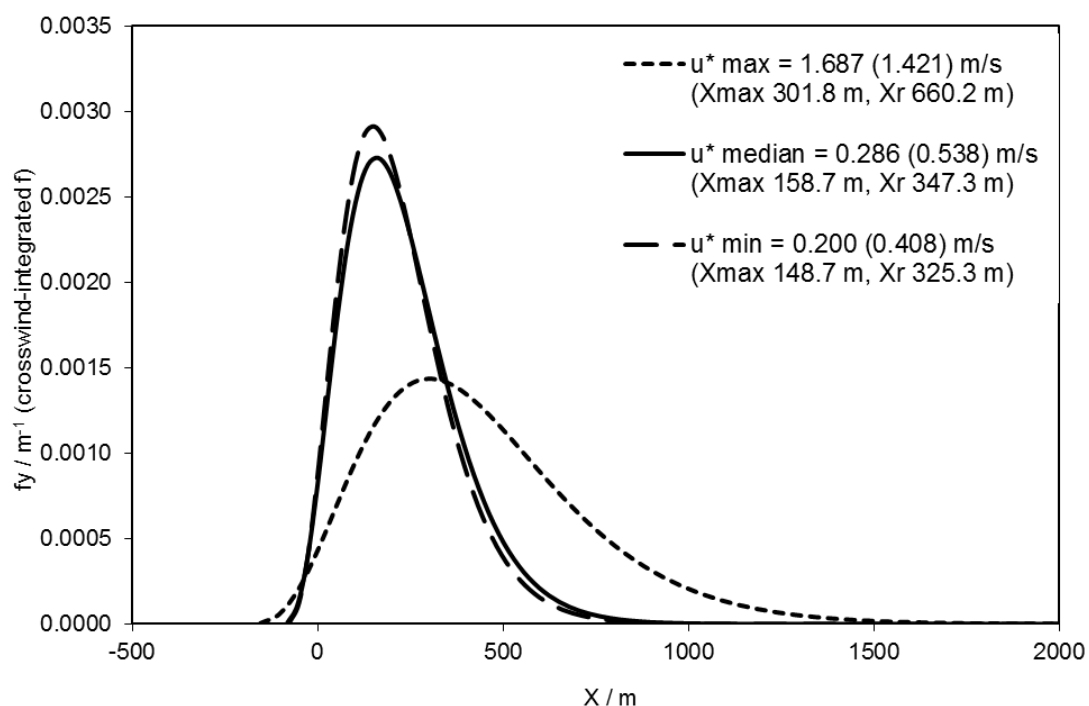


Figure 2-3 Modelled flux footprints for Speuld measurements. The following parameters were used: measurement height  $z_m$  45 m; roughness length  $z_0$  3.2 m (estimated as 1/10th of the canopy height, 32 m); boundary layer height  $h$  1000 m. Crosswind integrated footprint functions ( $f_y$ ) were calculated for minimum, median and maximum values of  $u^*$  (1 sd of the vertical wind speed,  $\sigma_w$ , shown in brackets) as indicated on the graph. The distance at which maximum contribution can be expected, and at which 80% of the flux is contained, are given as  $X_{max}$  and  $X_r$ , respectively.



Figure 2-4 Map showing the predicted radius of the maximum 80% flux footprint using a simple parameterisation model (Kljun et al., 2004). The blue marker indicates the location of the sampling tower within Speuld forest. (Map data ©2012 Google Imagery ©2012 TerraMetrics. Radius plotted using [www.freemaptools.com](http://www.freemaptools.com)).

### 2.2.2 PTR-MS set-up

BVOC mixing ratios and fluxes above the forest canopy were measured using proton transfer reaction mass spectrometry (PTR-MS) (Blake et al., 2009) coupled with virtual disjunct eddy covariance (vDEC) (Karl et al., 2002; Rinne et al., 2001).

The PTR-MS used in this study (Ionicon Analytik, Innsbruck, Austria) was fitted with an extra turbopump connected to the detection chamber, and Teflon instead of Viton rings in the drift tube (Davison et al., 2009; Misztal et al., 2010). Pfeiffer turbopumps replaced the Varian equivalents. The drift tube conditions were held constant throughout (pressure 1.7 mbar, temperature 45 °C, voltage 478 V) to maintain an  $E/N$  ratio of  $\sim 130$  Td ( $1 \text{ Td} = 10^{-17} \text{ V cm}^2$ ).

A scaffolding tower approximately 45 m high with platforms at 2 m height intervals had previously been installed at the site and was used for the campaign. The PTR-MS sampling inlet and 20 Hz sonic anemometer (WindmasterPro, Gill Instruments) were positioned above the canopy at the top of the tower. Air was sampled at  $23.5 \text{ L min}^{-1}$  through a 50 m PTFE inlet line (1/4" OD, 3/16" ID) with a T-piece for sub-sampling into the PTR-MS inlet at a rate of  $250 \text{ mL min}^{-1}$ . Condensation of water vapour in the inlet line was prevented by wrapping with self-regulating heating tape (Omega, UK type SRF3-2C). Data were logged using a program written in LabVIEW<sup>2</sup> (Version 8.5, National Instruments).

### 2.2.3 Determination of VOC mixing ratios and fluxes

The PTR-MS signal was calibrated explicitly for several VOCs using a mixed gas calibration cylinder (Apel-Riemer Environmental Inc., USA) containing 1 ppmv each of formaldehyde, methanol, acetonitrile, acetone, acetaldehyde, isoprene and 0.18 ppmv (R)-(+)-limonene. The calibration gas was diluted with VOC-scrubbed air to produce 6 samples with concentrations of 0.5, 1.0, 10, 20, 30 and 50% of the pure calibration gas standard. A relative transmission curve was then constructed to determine empirical calibration coefficients for other VOCs under study not present

---

<sup>2</sup> Acknowledgements to Pawel Misztal.

in the standard (Taipale et al., 2008). Calibrations were carried out in the lab before commencement of the field campaign, and on 8 July during the campaign, to determine sensitivity as a function of  $m/z$ , normalised to  $1 \times 10^6$  primary ion counts (normalised counts per second, ncps ppbv<sup>-1</sup>). Limits of detection were calculated as the ratio of twice the standard deviation of the background ion counts ( $\sigma_{background}$ ) for a particular  $m/z$  divided by the sensitivity,  $S$  (ncps ppbv<sup>-1</sup>) (Karl et al., 2003):

$$LOD = \frac{2 \sigma_{background}}{S} \quad (2-1)$$

For the first 10 days of measurements (18-28 June) the PTR-MS was run in multiple ion detection (MID) mode for two 25 min sampling periods per hour. During these periods only the targeted VOC ions listed in Table 2-1 were measured, with dwell times of 0.5 s, in addition to the primary ion H<sub>3</sub>O<sup>+</sup>, and water cluster (H<sub>2</sub>O)H<sub>3</sub>O<sup>+</sup>, which had dwell times of 0.2 s. The sensitivities and limits of detection for the target ions are also included in Table 2-1.

The remaining 10 min per hour were used for full mass scans in the range 21 – 206 amu at a dwell time of 1 s per amu. For one 5 min period, ambient air was scanned to allow information about the full VOC composition to be acquired. For a further 5 min per hour, ‘zero air’ was scanned to determine the instrument background. Zero air was achieved by sampling ambient air through a custom-made zero-air generator comprising a glass tube packed with platinum wool and a 50:50 mixture of platinum mesh and activated charcoal heated to 200 °C. The background spectrum was subtracted in subsequent processing of data.

**Table 2-1 Compounds measured during the Speuld field campaign including dwell times, sensitivities and limits of detection during the first (up to 20:00 on 29<sup>th</sup> June) and second (from 20:00 on 29<sup>th</sup> June) halves of the campaign.**

<i>m/z</i> [amu]	Contributing compound(s)	Formula	Dwell time [s]	Sensitivity [ncps ppbv <sup>-1</sup> ]	Limit of detection [ppbv]	
					First half	Second half
21	water isotope	H <sub>2</sub> <sup>18</sup> O	0.2	-	-	-
33	methanol	CH <sub>4</sub> O	0.5	9.53	0.58	0.95
37	water cluster	(H <sub>2</sub> O) <sub>2</sub>	0.2	-	-	-
45	acetaldehyde	C <sub>2</sub> H <sub>4</sub> O	0.5	11.1	0.21	0.27
59	acetone	C <sub>3</sub> H <sub>6</sub> O	0.5	10.1	0.10	0.11
	propanal					
60	trimethylamine (TMA)	N(CH <sub>3</sub> ) <sub>3</sub>	0.5	8.25	0.09	0.13
69	isoprene	C <sub>5</sub> H <sub>8</sub>	0.5	2.42	0.24	0.26
	furan					
	methyl butenol fragment					
71	methyl vinyl ketone (MVK)	C <sub>4</sub> H <sub>6</sub> O	0.5	4.84	0.13	0.14
	methacrolein (MACR)					
81	monoterpene fragment (MT81)		0.5	1.9	0.36	0.28
83	(Z)-3-hexenol fragment		0.5	1.1	0.69	0.60
	(E)-3-hexenol fragment					
	(E)-2-hexenol fragment					
	hexanal fragment					
	(E,Z)-2-hexenyl acetate fragment					
87	2-methyl-3-buten-2-ol (MBO)	C <sub>5</sub> H <sub>10</sub> O	0.5	1	0.65	0.71
93	<i>p</i> -cymene fragment	C <sub>7</sub> H <sub>8</sub>	0.5	0.9	1.08	0.69
	toluene					
137	monoterpene (MT137)	C <sub>10</sub> H <sub>16</sub>	0.5	0.235	3.03	2.44
149	estragole	C <sub>10</sub> H <sub>12</sub> O	0.5	0.2	3.77	5.55

As the PTR-MS was run in MID mode, fewer data points were generated than required for direct eddy covariance due to the non-continuous manner in which the quadrupole mass analyser measures each  $m/z$ . The set-up resulted in 30,000 wind speed measurements and up to 203 VOC measurements in each 25 min sampling period. The lag time between PTR-MS and wind speed data due to the residence time in the sampling inlet line and the disjunction between sonic and PTR-MS data was determined by finding the maximum in cross-correlation between vertical wind speed and VOC mixing ratio as a function of lag time (with 15 s window). An analysis program written in LabVIEW<sup>3</sup> was used to determine lag times separately for each compound within each 25 min flux sampling period. Mean lag times throughout the campaign were in the range 6.5 to 7.1 s. This includes an estimated transition time of 2.3 s between the sampling point and analyser input; the remainder mostly resulted from delays in the data-handling software.

Quality control criteria were applied to filter data for periods of low friction velocity ( $u^* < 0.15 \text{ m s}^{-1}$ ), non-stationarity, large spikes in vertical wind speed or VOC concentration, and where  $< 10,000$  data points (5.5 % of all data) were acquired in a 25 min sampling period. Most discarded data occurred during night when turbulence was low (48.3% of all data points). High frequency flux losses due to the relatively slow disjunct VOC sampling frequency (2 Hz, compared to 20 Hz sonic data capture) were estimated using empirical ogive analysis (Ammann et al., 2006) for each 25 min period and flux values were corrected accordingly. Standard rotations of the coordinate frame were applied to correct for sonic anemometer tilt for each 25 min period separately.

The main source of error when using the vDEC method is due to counting statistics at small dwell times of the QMS. Appropriately long integration times are therefore used. Calculation of  $\sigma_{background}$  for determination of LOD was therefore derived using an appropriate number of zero air points to match the time length of data points. Each diurnal time point measurement represents 25 min of data, while each zero air

---

<sup>3</sup> Acknowledgments to Pawel Misztal.

point is the mean of 5 min. Therefore, 5 times the number of zero air points as data points are used for calculating  $\sigma_{background}$ . For example, a single diurnal time-step averaged over 10 days (as in the first half of the measurement campaign) will represent:

$$10 \text{ day} \times 25 \text{ min} = 250 \text{ min} \quad (2-2)$$

Since each zero air point is 5 min,

$$\frac{250 \text{ min}}{5 \text{ min}} = 50 \text{ data points} \quad (2-3)$$

50 zero air data points were therefore used in the calculation of LOD for the first half of the campaign. Similarly, the second half of the campaign comprised 9 days, therefore 45 zero air data points were used to calculate  $\sigma_{background}$  and hence LOD for the second half of the campaign.

#### 2.2.4 In-canopy gradient measurements

From 30 June to 7 July in-canopy, in addition to above-canopy, mixing ratios were measured. A winched, pulley system allowed continuous movement of the PTR-MS inlet between heights of 4 and 32 m. During this period, above-canopy measurements were taken during the first half of every hour (hh:05 to hh:30) and in-canopy measurements were taken in the latter half of every hour (hh:35 to hh:00). Full mass scans of ambient air and zero air were taken for 5 min intervals at hh:00 and hh:30 respectively. PAR and temperature were also measured from the gradient system.

#### 2.2.5 Chromatographic analysis of ambient air samples

Ambient air samples were collected for subsequent GC-MS analysis to supplement PTR-MS data. Samples were collected from above the canopy (~40 m) approximately hourly from 08:10 to 20:08 on 6 July 2009. Samples were also taken at heights of 32, 18 and 4 m above ground level at 3 points throughout the day (~09:30, 13:30 and 17:30) on 1 and 6 July 2009. A mass-flow controlled Pocket Pump (210-1000 Series, SKC Inc.) was used to pump air at  $150 \text{ mL min}^{-1}$  for 15 min through stainless steel tubes (6 mm O.D.) packed with 200 mg Tenax TA and 100

mg CarboTrap adsorbents (Markes International Ltd., UK). Prior to sampling, packed tubes had been conditioned at 300 °C for 15 min with a flow of helium.

Analyses were carried out using a Hewlett-Packard 5890/5970 GC-MS with an automated thermal desorption unit (ATD 400, Perkin Elmer) connected via a 200 °C heated transfer line. Transfer of samples from the adsorbent tubes was performed in two steps: heat to 280 °C for 5 min at 25 mL min<sup>-1</sup> to desorb samples onto a Tenax-TA cold trap at -30 °C, followed by transfer to the GC column at 300 °C for 6 min. Chromatographic separation utilised an Ultra-2 column (Agilent Technologies, 50 m × 0.2 mm ID × 0.11 µm film, 5% phenylmethyl silica) and a temperature program of 35 °C for 2 min, heat at 5 °C min<sup>-1</sup> to 160 °C, heat at 10 °C min<sup>-1</sup> to 280 °C, and hold for 5 min.

Calibration was carried out using a mixed monoterpene in methanol standard (10 ng µL<sup>-1</sup> α-pinene, β-pinene, α-phellandrene, 3-carene and limonene (Sigma Aldrich, UK)). Aliquots of the monoterpene standard (0, 1, 3 and 5 µL) were injected onto 4 adsorbent tubes with helium carrier gas. Tubes continued to be purged with helium for 2 min after the standard injection to ensure complete adsorption. The limits of detection for α-pinene and limonene were 0.23 and 0.30 ng on column, corresponding to mixing ratios of 18 and 24 pptv, respectively, for a 2.25 L sample.

## 2.3 Results

### 2.3.1 Above canopy fluxes

As described in Section 2.2.3, above-canopy fluxes were measured throughout the campaign. The full time series of all VOC fluxes above Douglas fir along with  $u^*$  and sensible heat flux are shown in Figure 2-5.

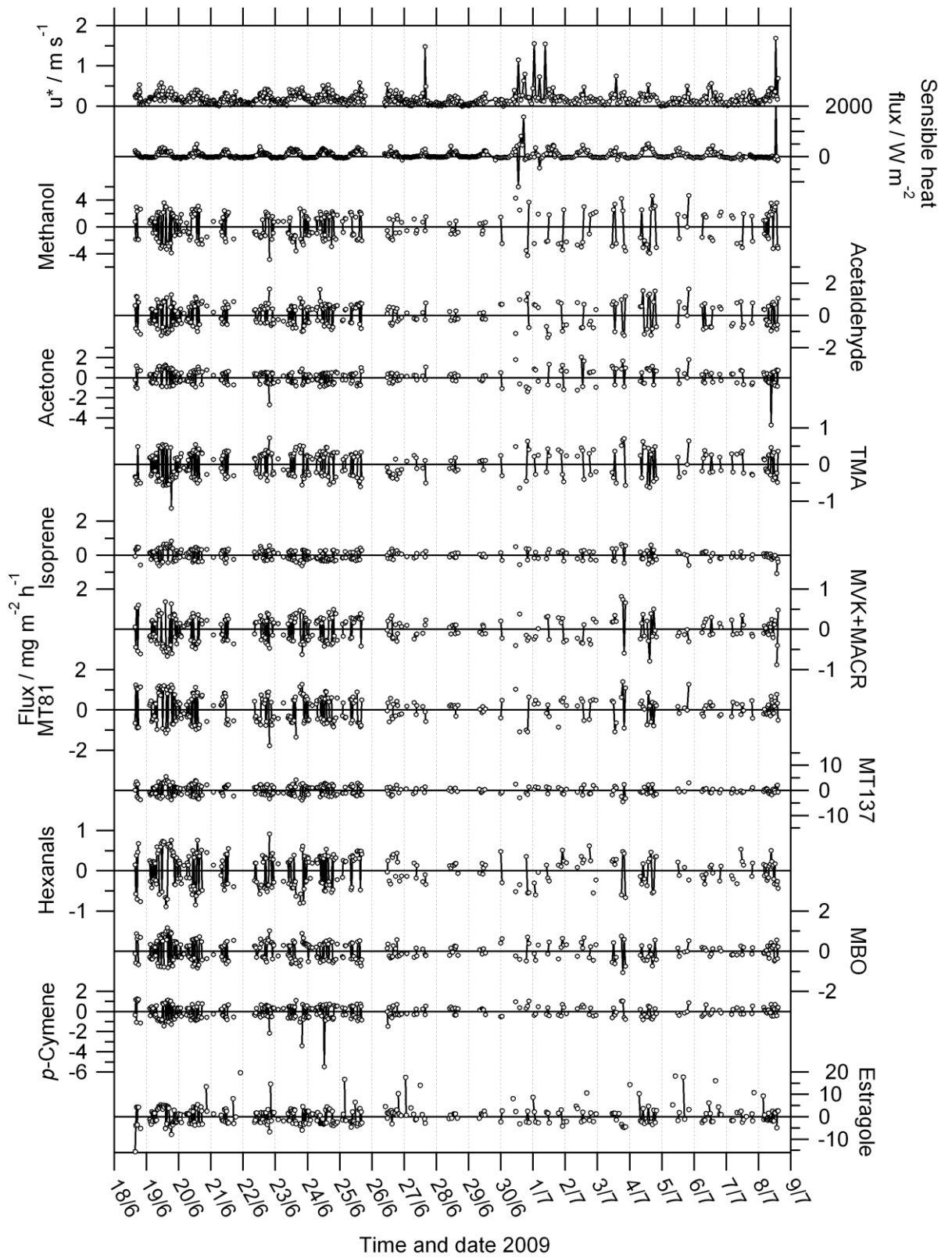
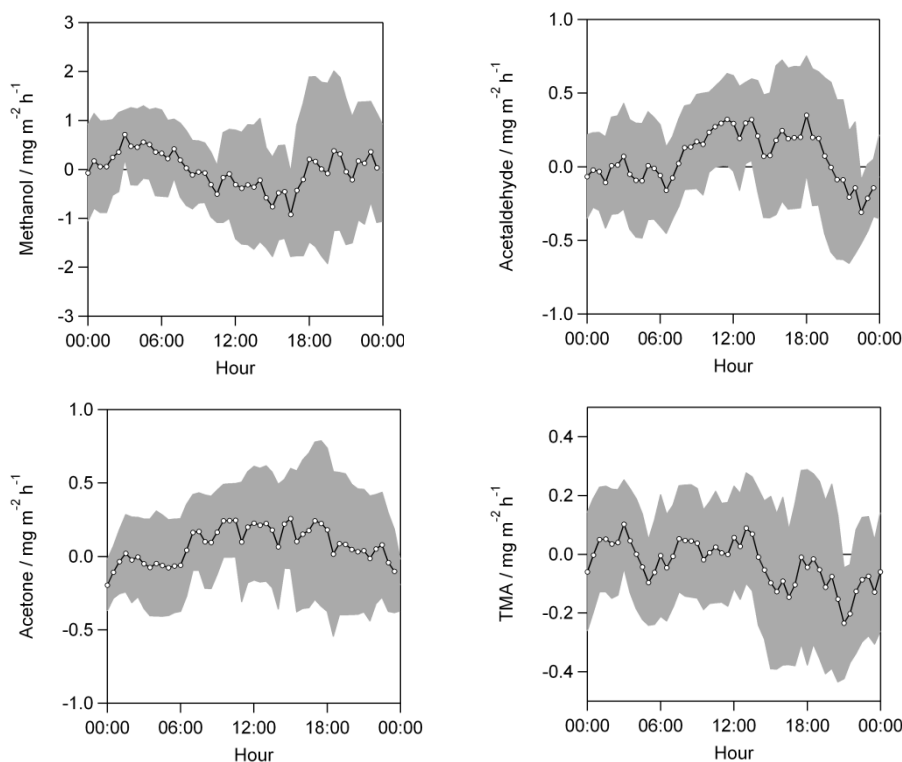
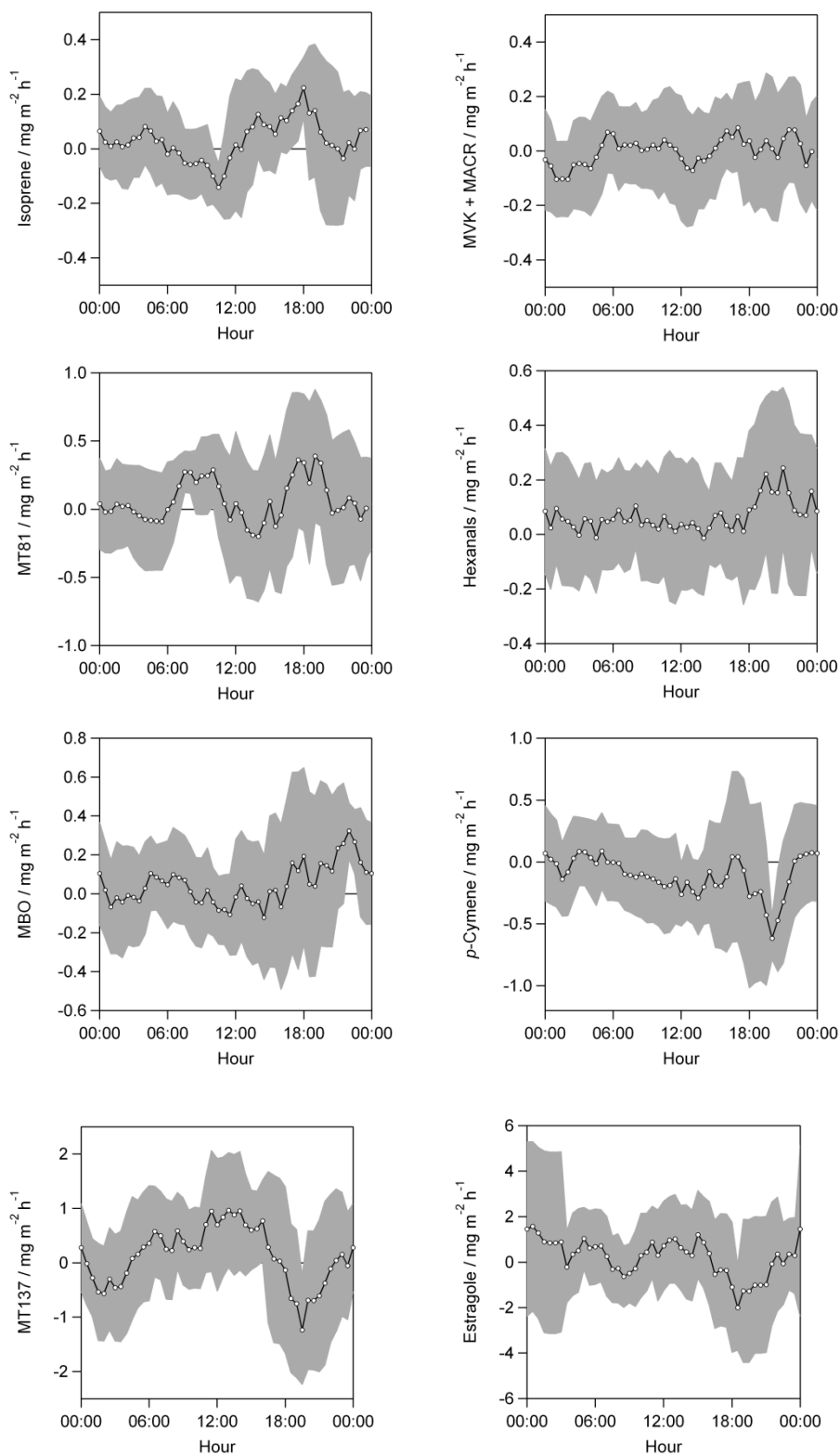


Figure 2-5 Time series of VOC fluxes measured above Douglas fir. Dashed gridlines denote midnight. Note the variable flux scales.

Two periods of missing data 25-26 June and 3 July were due to problems with a data communication cable and failure of the sampling pump, respectively. Most missing data at night time was due to filtering of low  $u^*$  values. The winch set up commenced 29 June at 20:00. From then on, above canopy data are hourly rather than every half hour. Because of this difference in frequency of data points between the first and second half of the campaign, the data were treated as two separate sets for diurnal averaging.

Diurnal profiles of VOC fluxes for the first half of the campaign (prior to the winch set-up) are shown in Figure 2-6. Median values were first calculated for each half-hourly time step and used to plot a 3-hourly running mean e.g. the data point plotted for 12:00 is the mean of median values from 10:30 to 13:30 i.e. 7 time steps. This was done to make diurnal trends clearer, which were not obvious using diurnal means for each time step due to raw data being relatively noisy. Errors due to day-to-day variability are denoted by grey error bands and represent  $\pm 1$  standard deviation based on 10 days of data.





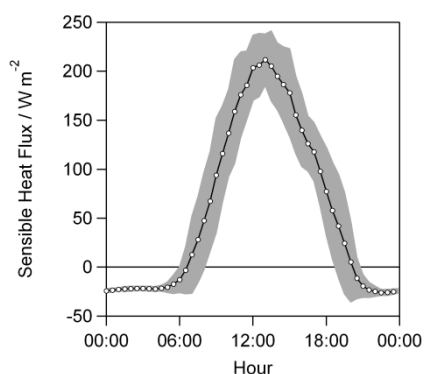


**Figure 2-6 Average diurnal profiles of VOC fluxes above Douglas fir and of sensible heat flux, prior to 20:00 on 29th June 2009. Data points are the mean of median values for a  $\pm 1.5$  hour time window. Note the variable scales. Grey areas show variability calculated as  $\pm 1$  sd.**

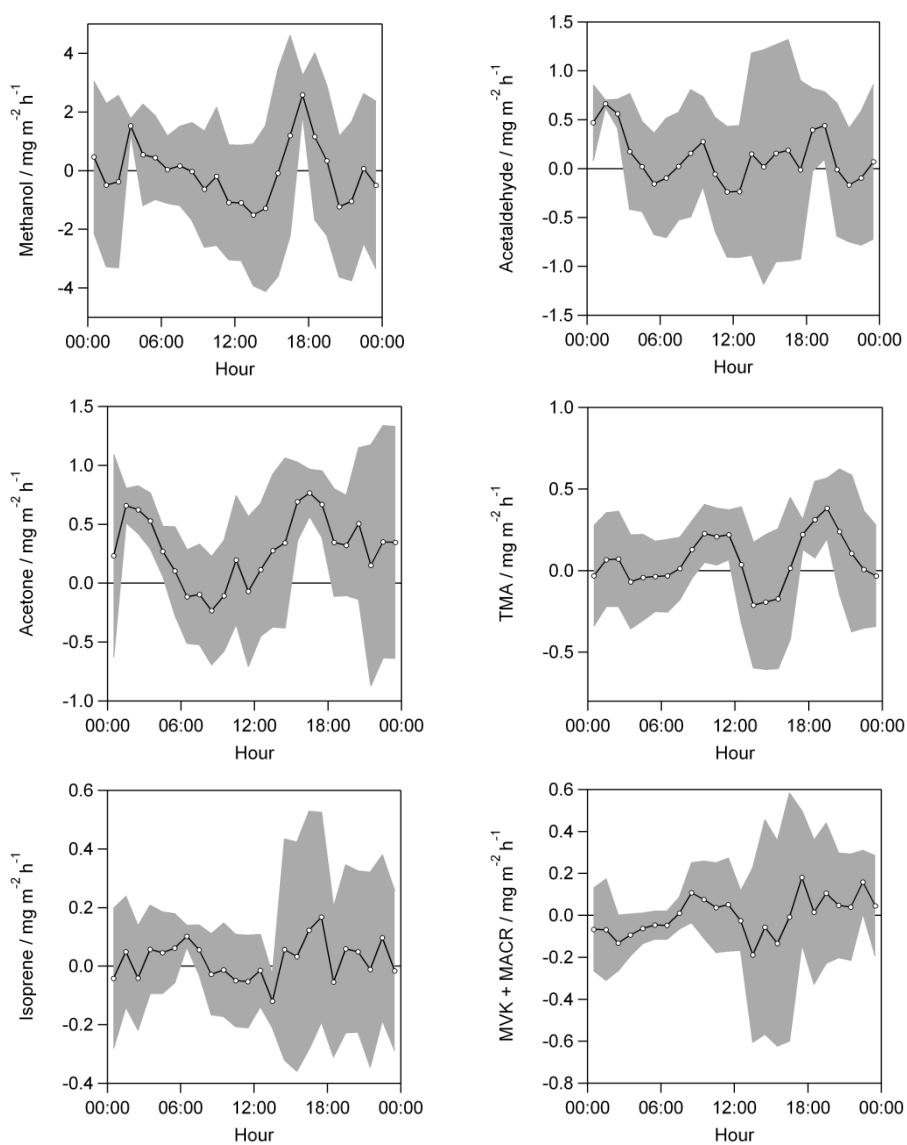
Flux data were somewhat noisy for all VOCs measured. Positive daytime fluxes were discernible for acetaldehyde, acetone and monoterpenes which showed emission during daylight hours and near-zero or depositional fluxes at night following the sharp decrease in sensible heat flux. Methanol and isoprene behaved similarly, all with minima during the day and maxima in the evening or at night. This was particularly pronounced for isoprene, which had a sharp increase in flux between 12:00 and 18:00 – coinciding with maximum in-canopy PAR – before decreasing rapidly to zero towards sunset. The diurnal pattern of the isoprene oxidation products MVK + MACR fluctuated throughout the day with positive fluxes in the morning and early evening – when isoprene emissions declined but photochemistry would have still enabled formation of the products through isoprene oxidation.

Fluxes of hexanals and MBO were around zero except for some positive fluxes between 18:00 and 00:00. Conversely, TMA, *p*-cymene and estragole were deposited in the evening, with TMA and *p*-cymene fluxes around zero for the remainder of the day, while estragole had positive fluxes overnight.

There was a discrepancy in monoterpene fluxes determined from  $m/z$  81 and  $m/z$  137 ions with the latter giving higher flux values. This difference may be due to differences in fragmentation patterns between monoterpenes, as has been observed in other studies (Rinne et al., 2007). Measurements for MT137 were also below LOD –

as they were for hexanals, MBO, *p*-cymene and estragole – therefore measurement at MT81 was likely to be more reliable.

Diurnal profiles of VOC fluxes for the second half of the campaign (during which set-up) are shown in Figure 2-7.



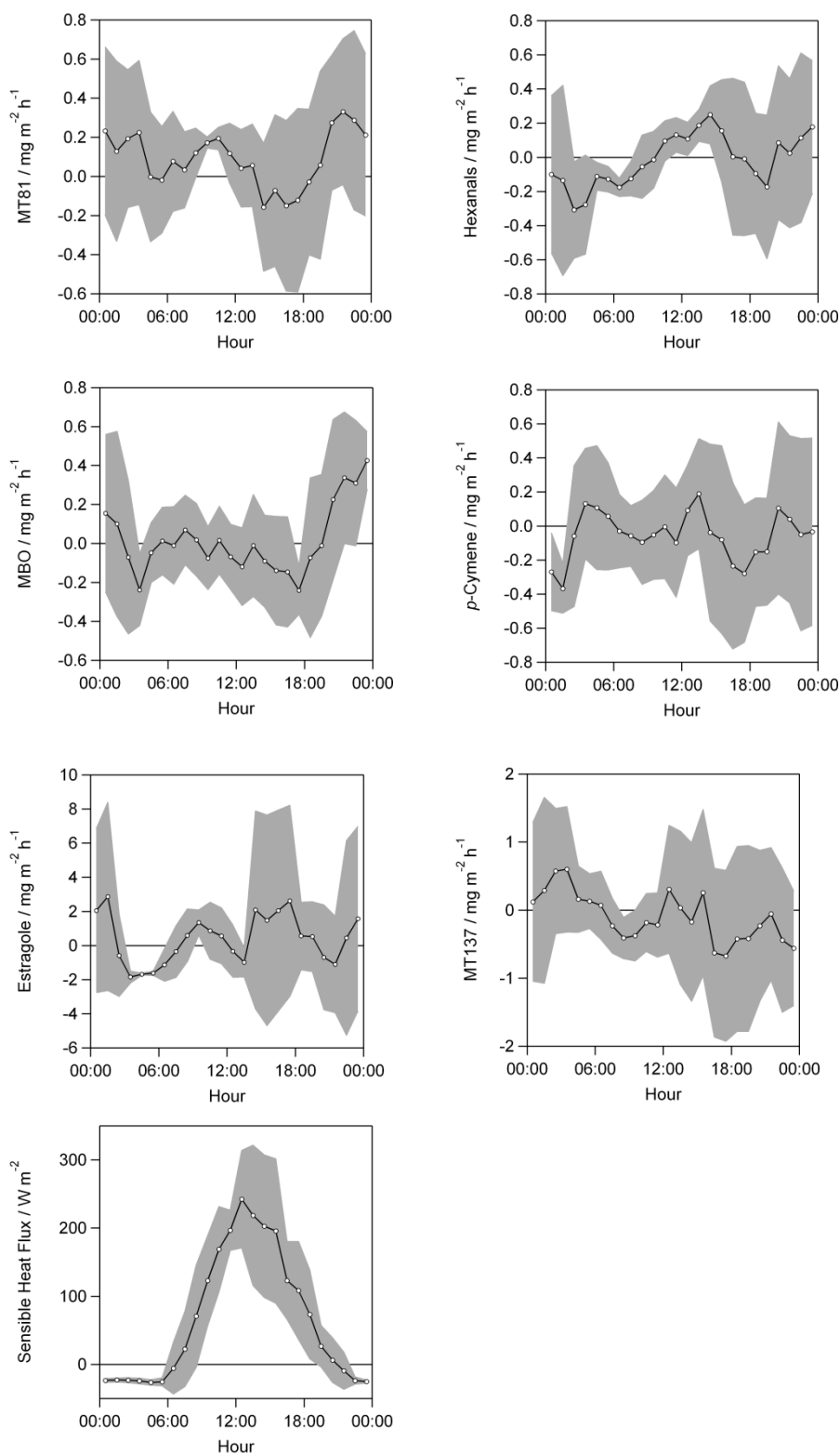


**Figure 2-7** Average diurnal profiles of VOC fluxes above Douglas fir and of sensible heat flux, after 20:00 on 29 June 2009. Data points are the mean of median values for a  $\pm 1.5$  hour time window. Note the variable scales. Grey areas show variability calculated as  $\pm 1$  sd.

Diurnal profiles from the second half were noisier for the second half of the campaign due to less frequent sampling. Absolute flux values tended to be greater during the second half data, as were temperatures. Diurnal patterns showed some similarities to those observed in the first half of the campaign but were much less distinct.

### **2.3.2 Above-canopy mixing ratios**

As described in Section 2.2, above-canopy mixing ratios were measured throughout the campaign. The full time series of all measured species, along with temperature are shown in Figure 2-8.

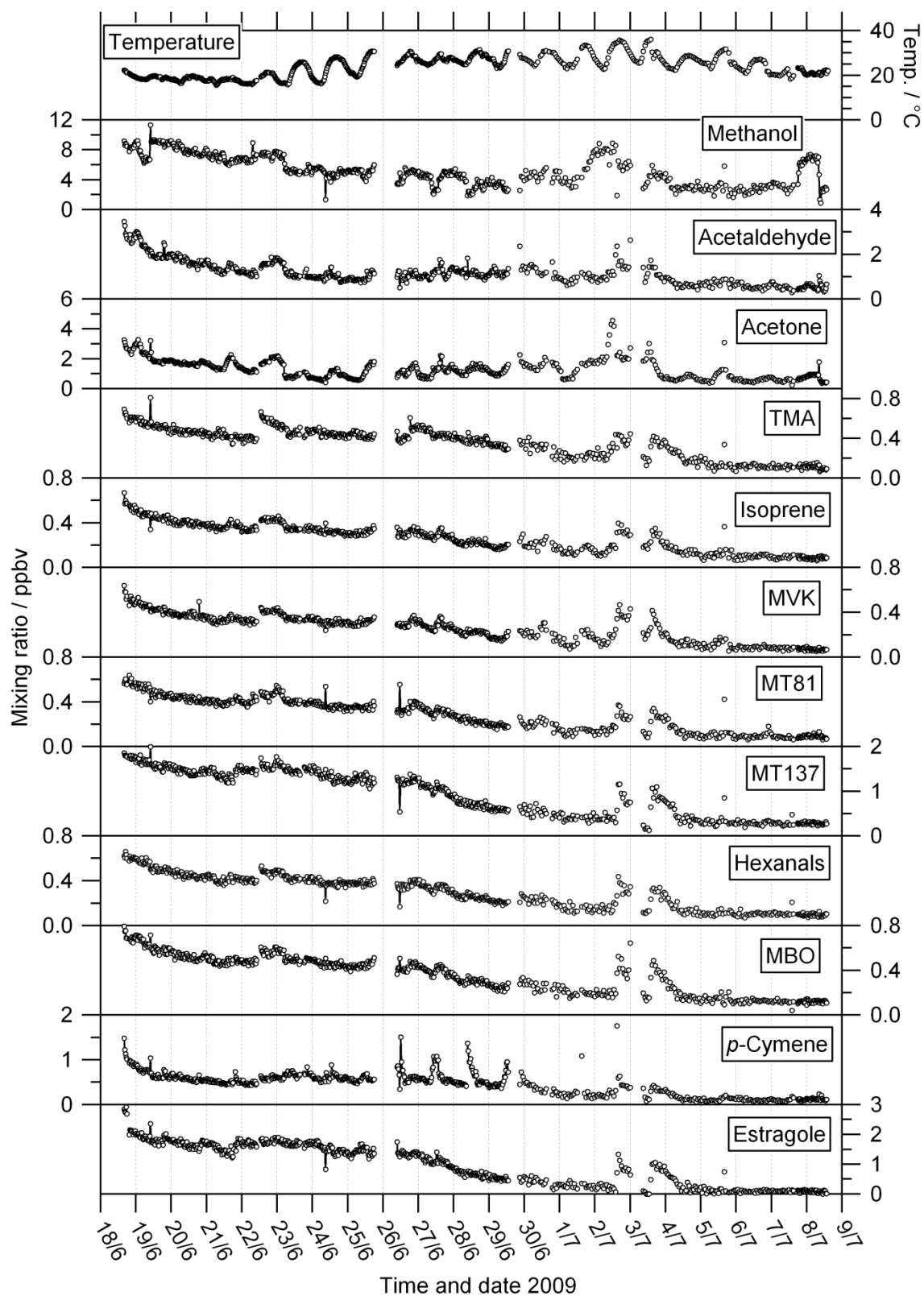
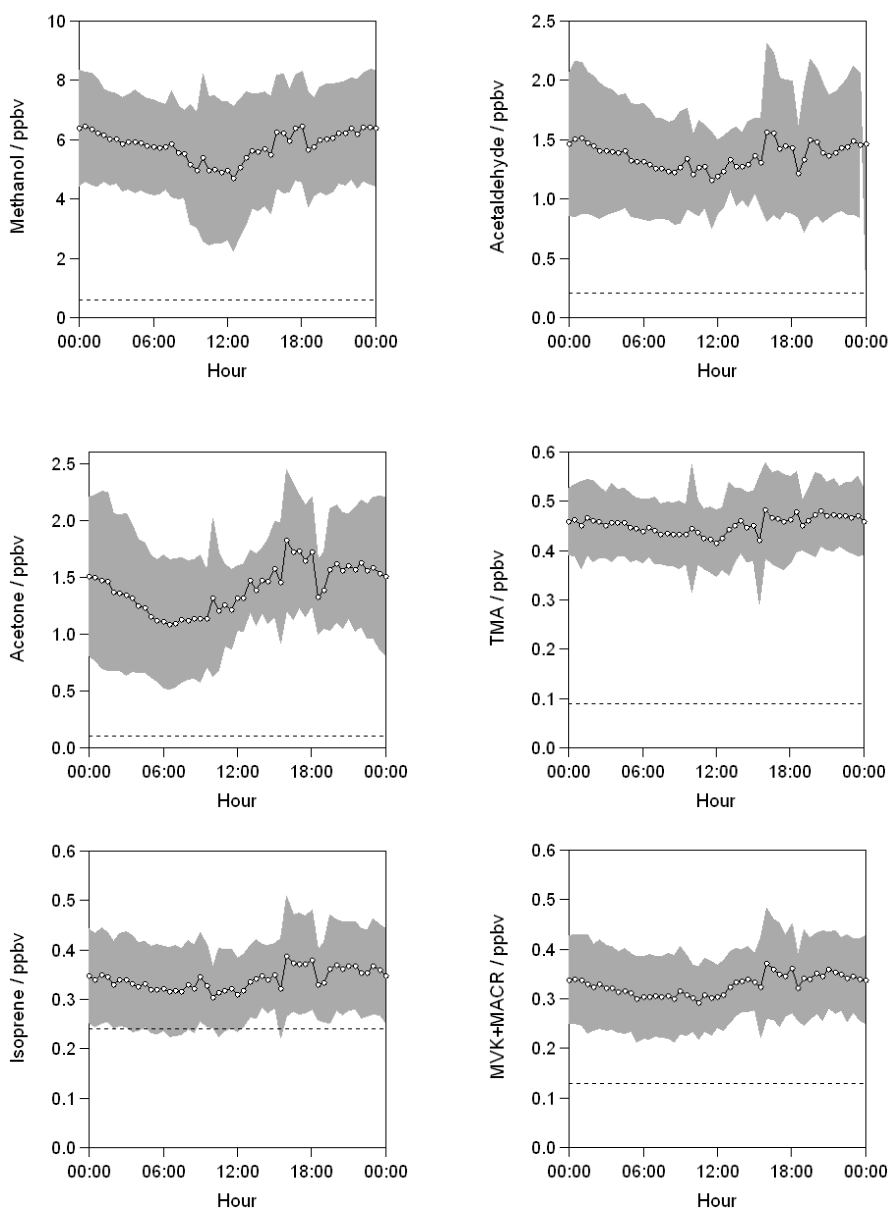
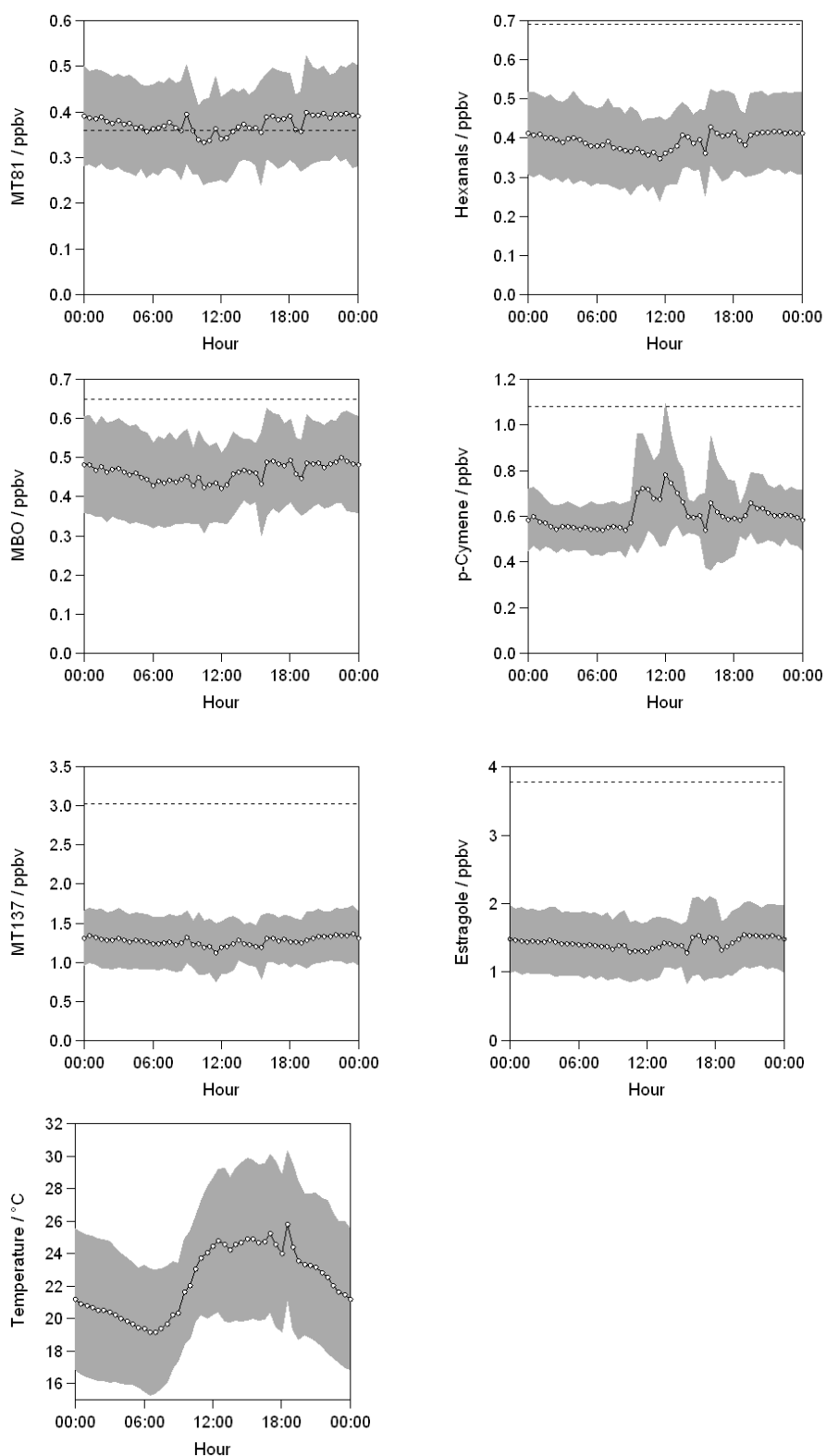


Figure 2-8 Time series of VOC mixing ratios, and of temperature, measured above Douglas fir. Dashed gridlines denote midnight. Note the variable mixing ratio scales.

As with the flux data, two periods of missing data 25-26 June and 3 July were due to problems with a data communication cable and failure of the sampling pump, respectively. The break in data on 29 June was due to setting up the winch system.

Mixing ratio data were treated as two separate sets for diurnal averaging. Diurnal profiles of VOC mixing ratios for the first half of the campaign (prior to the winch set-up) are shown in Figure 2-9.

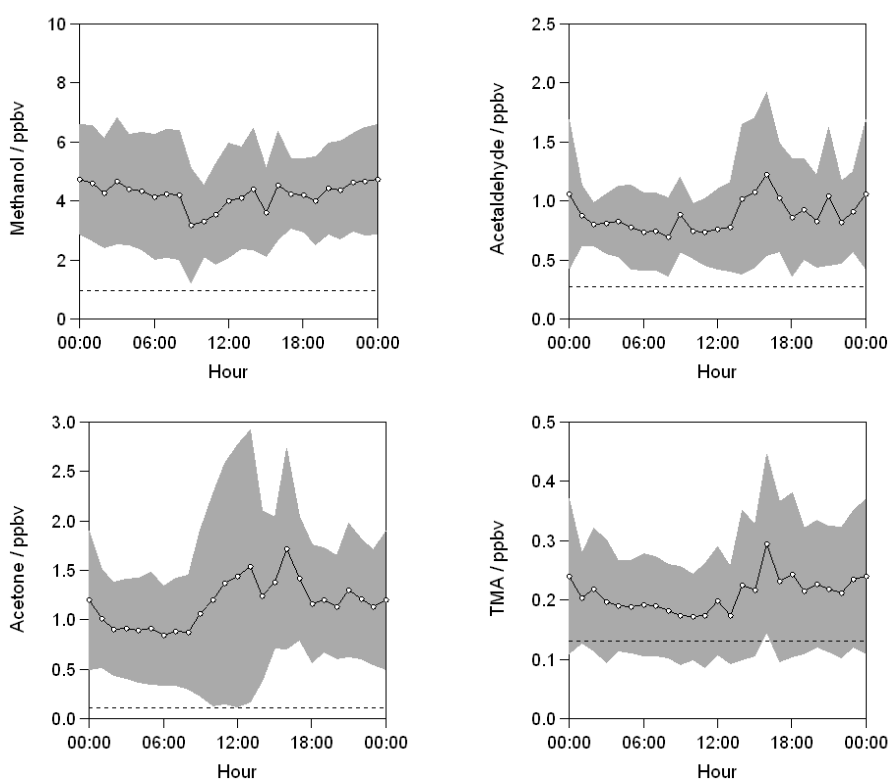


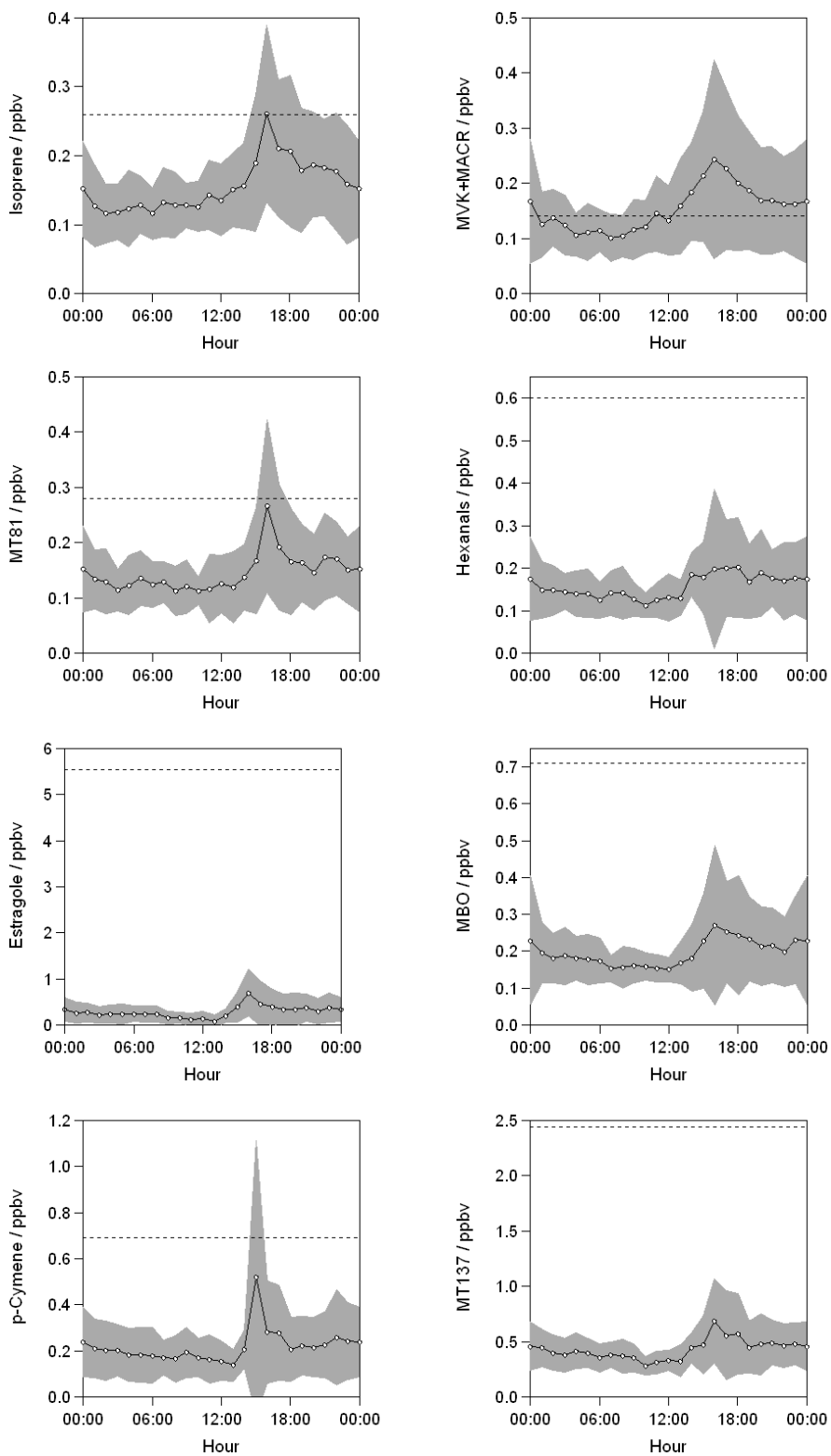


**Figure 2-9 Average diurnal profiles of VOC mixing ratios above Douglas fir, and of temperature, before 20:00 on 29 June 2009. Note the variable scales. Dashed lines denote LOD. Grey areas show variability calculated as  $\pm 1$  sd of the averaged half-hourly values of all measurements.**

All compounds – except *p*-cymene – had a similar diurnal pattern of minima around midday and maxima at night. The amplitude of diurnal cycle was small for most compounds, with methanol, acetaldehyde and acetone showing the most pronounced variation. *p*-Cymene had a relatively constant mixing ratio for most of the day with elevated mixing ratio from mid-morning to mid-afternoon. Hexanals, MBO, *p*-cymene, MT137 and estragole mixing ratios were below the calculated LOD therefore results are not reliable. However, all show a discernible diurnal pattern within a narrow uncertainty band, and have therefore been presented. It may have been that the zero-air generator was inefficient at removing these higher mass compounds, resulting in higher background counts, or that the reliability of removal of the compounds was not consistent, resulting in a high LOD.

Diurnal profiles of VOC mixing ratios for the second half of the campaign (during the winch set-up) are shown in Figure 2-10.





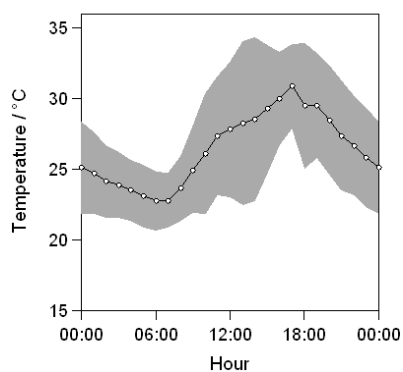


**Figure 2-10 Average diurnal profiles of VOC mixing ratios above Douglas fir, and of temperature, after 20:00 on 29th June 2009. Note the variable scales. Dashed lines denote LOD. Grey areas show variability calculated as  $\pm 1$  sd of the averaged half-hourly values of all measurements.**

Mixing ratios were lower for the second half of the campaign for all VOCs, although temperatures were higher. All diurnal profiles showed similar trends to those observed during the first half of the campaign, with minima around midday. However, greater distinctions in maxima were observed in the evening before mixing ratios reduced slightly at night. They remained constant until reducing towards midday. There was a correspondingly distinct maximum in temperature and lower variability in temperature throughout the day compared to the first half of the campaign (as shown in Figure 2-9). Only methanol, acetaldehyde, acetone and TMA had mixing ratios above calculated LODs, however all VOCs showed a discernible diurnal pattern within a narrow error band, and have therefore been presented.

The identity of monoterpenes present was verified using adsorption tube sampling and GC-MS analysis (Section 2.2.5). The diurnal variation in above-canopy monoterpene mixing ratios by these measurements is shown in Figure 2-11.

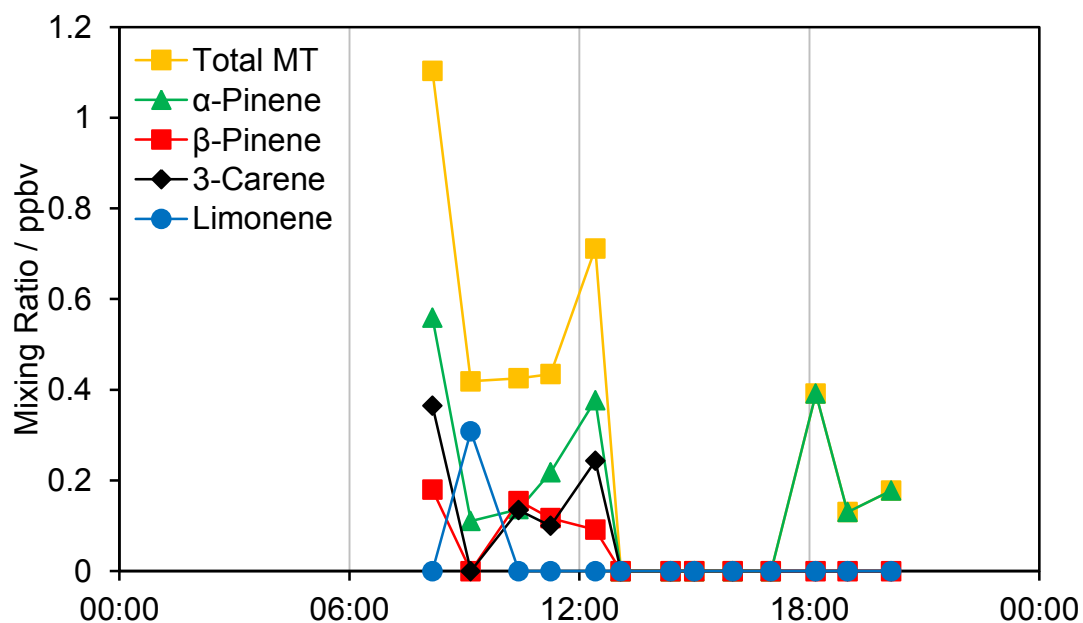
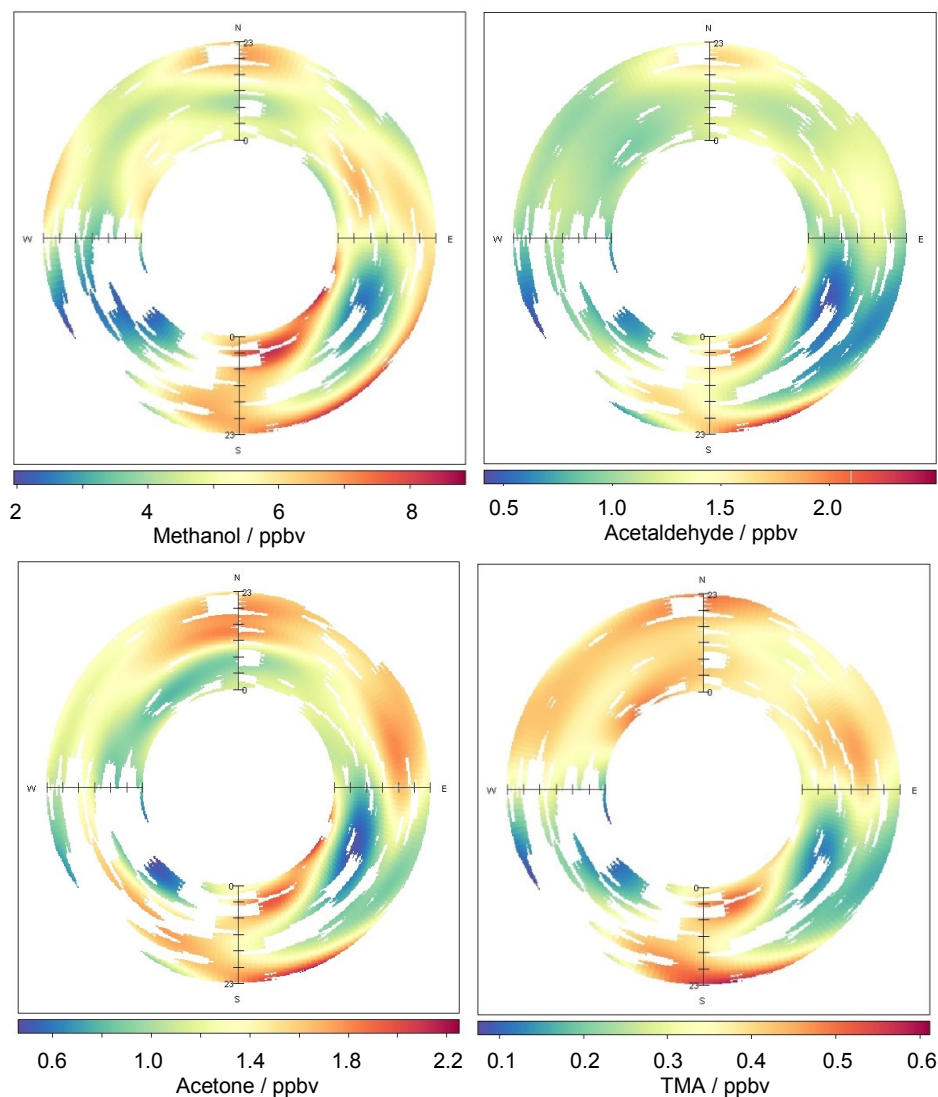


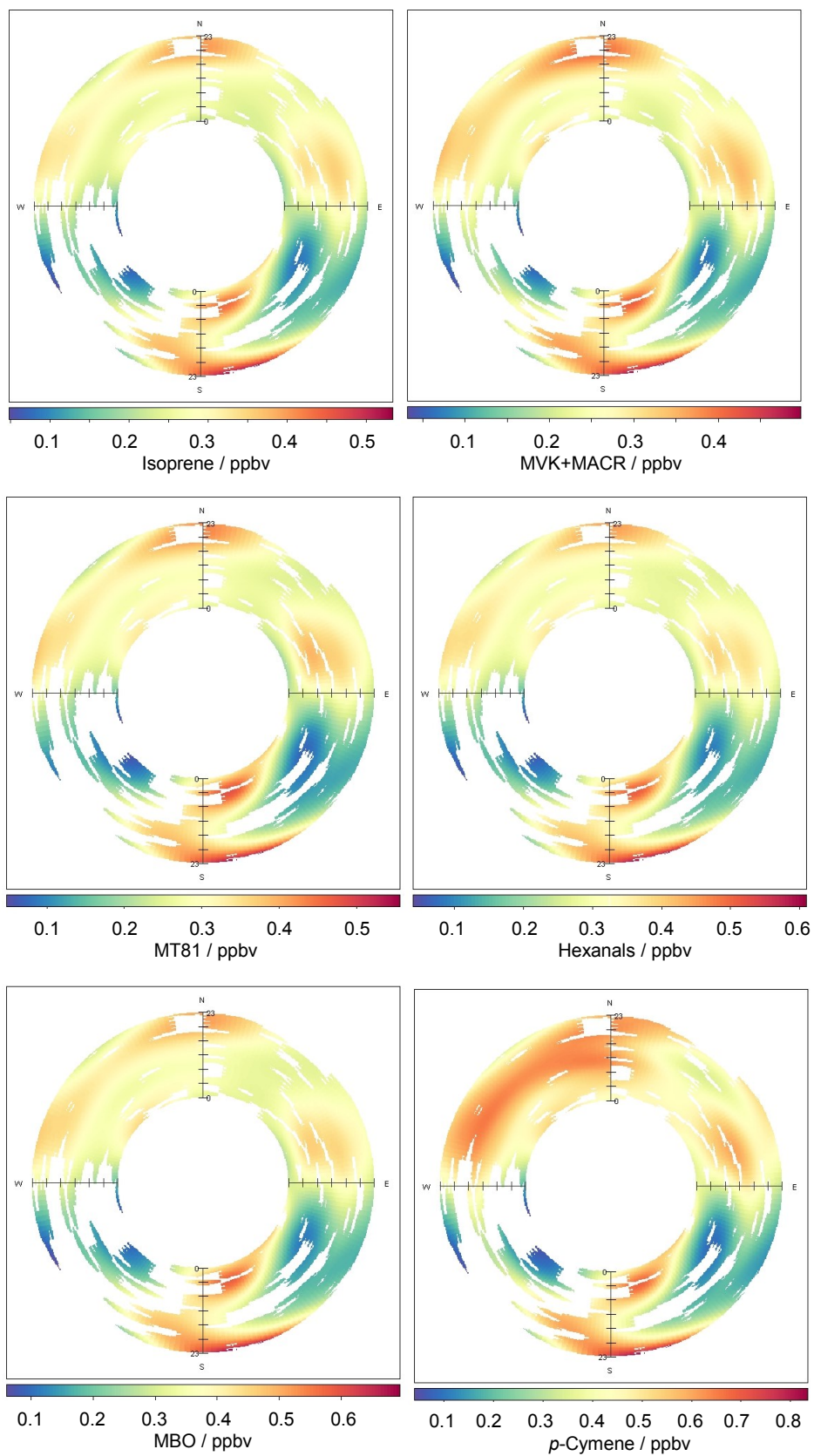
Figure 2-11 Diurnal variation in monoterpene mixing ratios above the Douglas fir canopy (40m). Samples were collected using adsorption tubes on 6 July 2009.

Figure 2-11 shows that GC-MS samples captured the diurnal variation in monoterpenes. Mixing ratios for all monoterpenes decreased during the morning and were not detected between 13:00 and 18:00. Mixing ratios then rose again in the early evening.  $\alpha$ -Pinene had the highest mixing ratio throughout the day, followed by 3-carene and  $\beta$ -pinene. Only a small quantity of limonene was detectable at 09:00. There was good agreement with results from PTR-MS measurements for diurnal pattern and magnitude of mixing ratios (Figure 2-9 and Figure 2-10).

### 2.3.2.1 Directional diurnal variation

To ascertain the location of potential sources of VOCs, annuli were plotted to show the diurnal variation in mixing ratio as a function of wind direction for all campaign data, shown in Figure 2-12. Time of day is represented through the increasing radius of the annulus (0 to 23 hours), direction the wind is coming from by degrees (0 to 359°, E = 90°) and colour denotes mixing ratio according to the scale for each individual VOC.





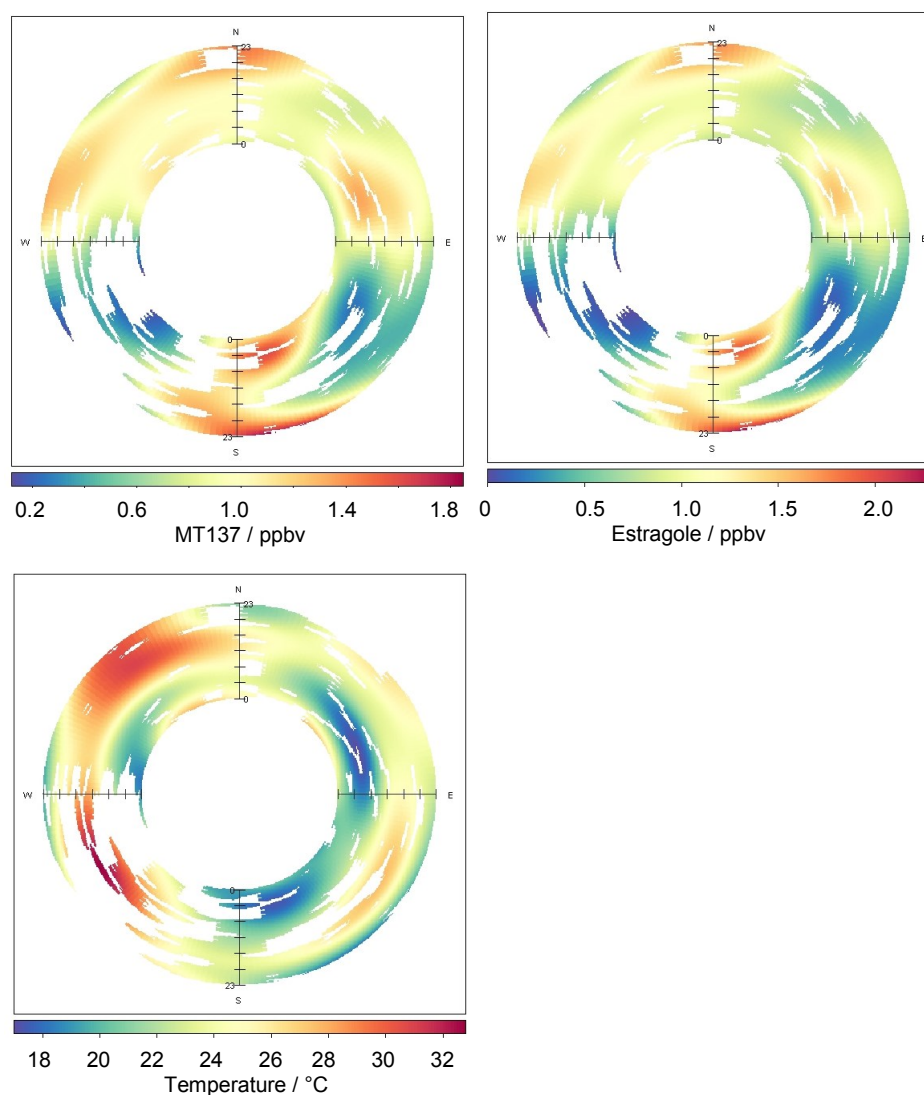


**Figure 2-12 Annuli of diurnal variation in VOC mixing ratio as a function of wind direction for all campaign data. Colour corresponds to mixing ratio according to the scale for each individual plot. Temperature (°C) is shown for comparison. (White space indicates insufficient data.)**

Figure 2-12 shows that all compounds analysed have a similar directional pattern. Mixing ratios were, in general, higher when the wind direction was from 270 to 90° or directly south. Increased mixing ratios were observed at night time and in the evening when the wind was from a SSW and N direction, respectively. Mixing ratios were lower when the wind was from SW and SE directions, but there were also fewer data points from those directions. All compounds followed this diurnal trend although the amplitude of diurnal variation differed. In addition, *p*-cymene and TMA also had high mixing ratios in the evening from the NW sector.

The temperature annulus shows that temperatures increased during the second half of the day, and were particularly elevated during westerly wind directions. The directional dependence of mixing ratios did not however mirror the directional variation in temperature. As the atmospheric lifetimes of the compounds measured were, in some instances, of the order of days, it is likely that sources from outside the forest were also measured. Atmospheric lifetimes of all measured compounds are shown in Table 2-2.

**Table 2-2 Typical atmospheric lifetimes of compounds investigated for the Speuld campaign.**

Compound(s)	Atmospheric lifetimes			
	OH	O <sub>3</sub>	NO <sub>3</sub>	
Methanol <sup>a</sup>	15 d		>220 d	
Acetaldehyde <sup>a</sup>	11 h	>4.5 y	17 d	
Acetone <sup>a</sup>	61 d	>4.5 y	>8 y	
Trimethylamine (TMA) <sup>b</sup>	4.6 - 7 h	5.9 d	<53 d	
Isoprene <sup>a</sup>	2 h	1.3 d	50 min	
Methyl vinyl ketone (MVK) <sup>a</sup>	9 h	3.6 d		
Methacrolein (MACR) <sup>a</sup>	5 h	15 d	10 d	
Monoterpenes	$\alpha$ -pinene <sup>c</sup>	3 h	5 h	5 min
	$\beta$ -pinene <sup>c</sup>	1.8 h	1.1 d	27 min
	3-carene <sup>c</sup>	1.6 h	11 h	7 min
	limonene <sup>c</sup>	49 min	2 h	5 min
Hexanals <sup>d</sup>	7 h			
2-methyl-3-buten-2-ol (MBO) <sup>e</sup>	2.1 h			
<i>p</i> -Cymene <sup>f</sup>	1 d	>330 d	1.3 y	
Estragole <sup>g</sup>	55 min	18 h		

References:

<sup>a</sup> (Harrison and Hester, 1995), [OH]  $1.6 \times 10^6 \text{ cm}^{-1}$ , [O<sub>3</sub>]  $7 \times 10^{11} \text{ cm}^{-1}$ , [NO<sub>3</sub>]  $5 \times 10^8 \text{ cm}^{-1}$

<sup>b</sup> (Lee and Wexler, 2013), [OH]  $1 \times 10^6 \text{ cm}^{-1}$ , [O<sub>3</sub>]  $2.5 \times 10^{11} \text{ cm}^{-1}$ , [NO<sub>3</sub>]  $5 \times 10^8 \text{ cm}^{-1}$

<sup>c</sup> (Atkinson and Arey, 2003), [OH]  $2 \times 10^6 \text{ cm}^{-1}$ , [O<sub>3</sub>]  $7 \times 10^{11} \text{ cm}^{-1}$ , [NO<sub>3</sub>]  $2.5 \times 10^8 \text{ cm}^{-1}$

<sup>d</sup> (Jiménez et al., 2007), [OH]  $1 \times 10^6 \text{ cm}^{-1}$

<sup>e</sup> (Schade and Goldstein, 2001), [OH]  $2 \times 10^6 \text{ cm}^{-1}$

<sup>f</sup> (Corchnoy and Atkinson, 1990), [OH]  $1.5 \times 10^6 \text{ cm}^{-1}$ , [O<sub>3</sub>]  $7 \times 10^{11} \text{ cm}^{-1}$ , [NO<sub>3</sub>]  $2.4 \times 10^8 \text{ cm}^{-1}$

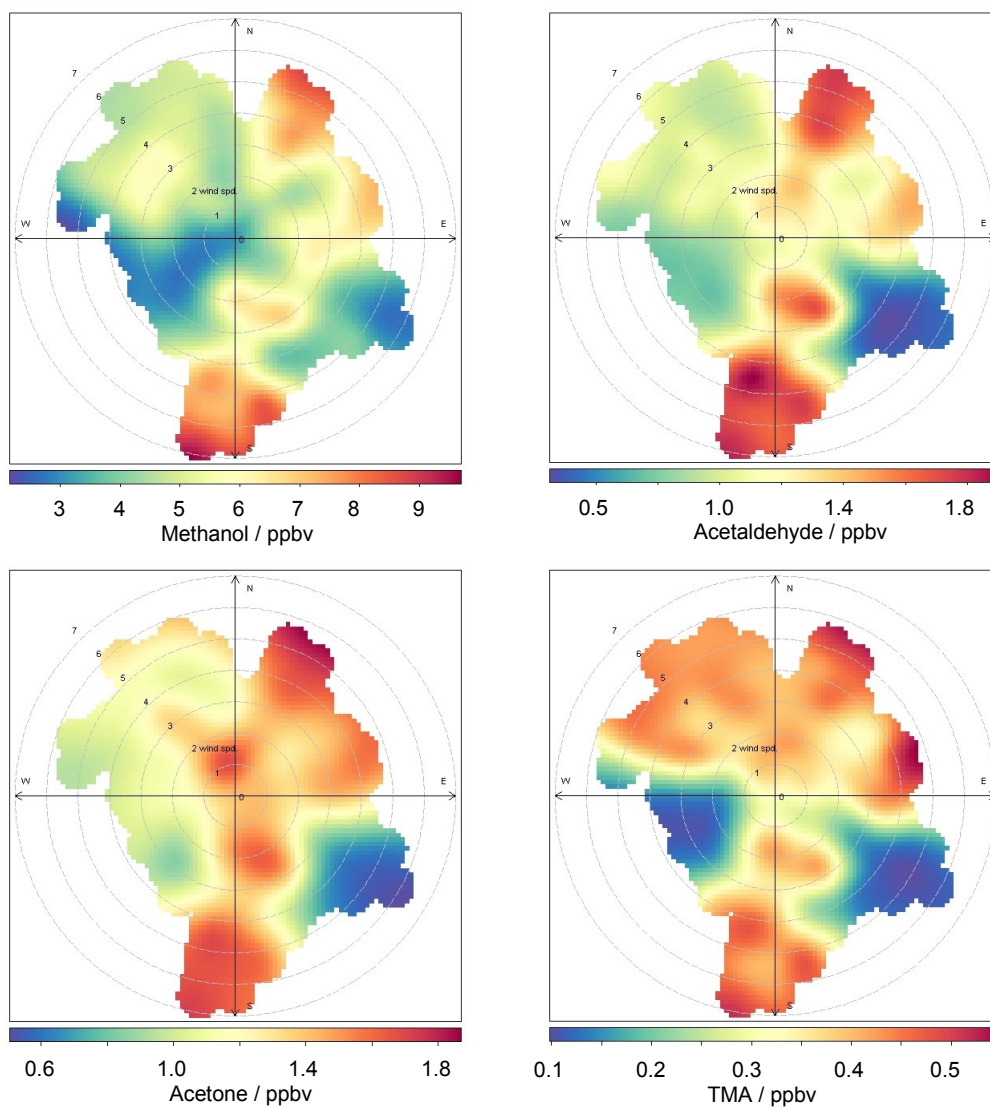
<sup>g</sup> (Bouvier-Brown et al., 2009), [OH]  $5.4 \times 10^6 \text{ cm}^{-1}$ , [O<sub>3</sub>]  $1.18 \times 10^{12} \text{ cm}^{-1}$

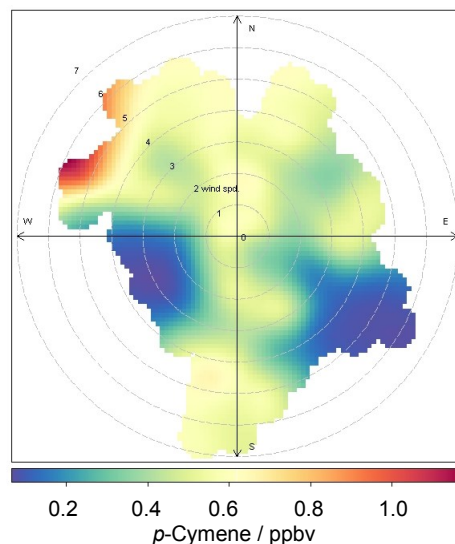
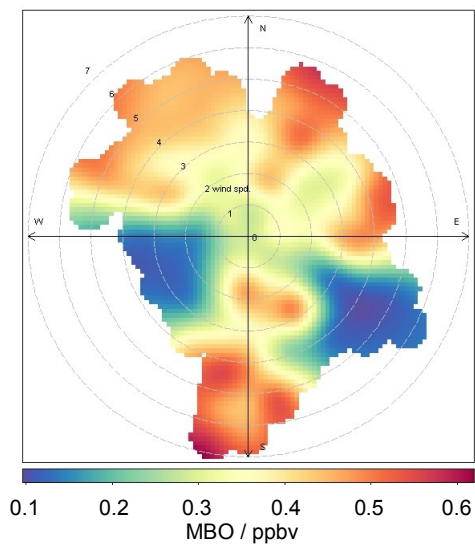
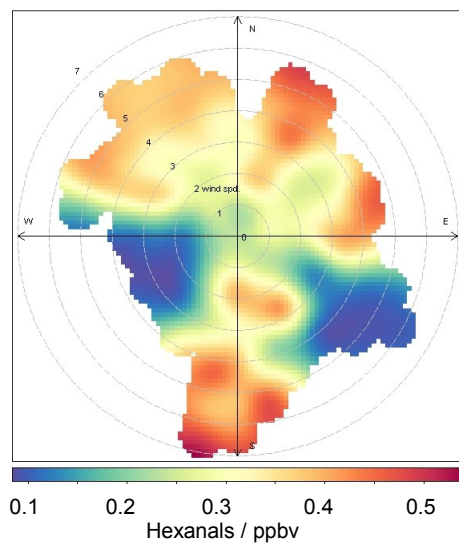
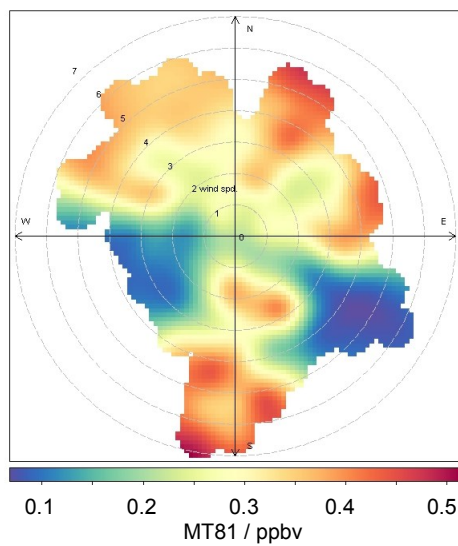
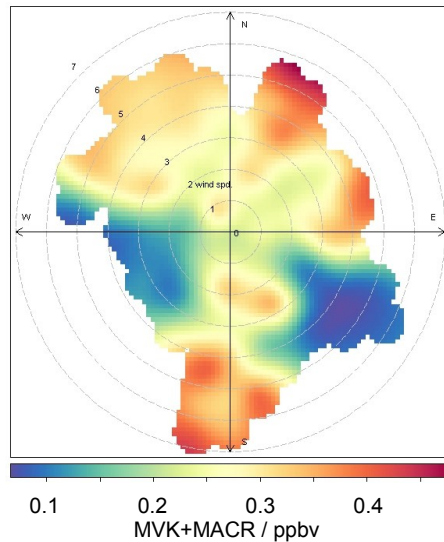
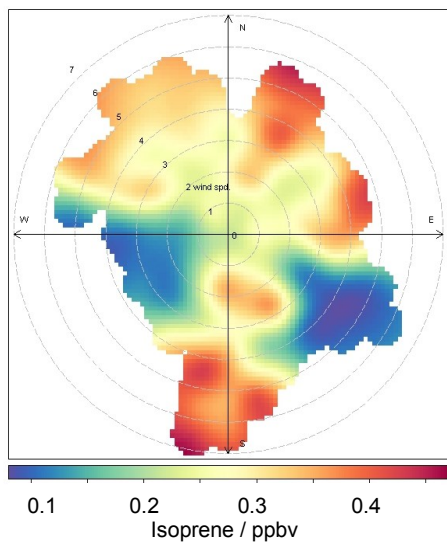
Table 2-2 shows that many of the compounds measured have lifetimes sufficiently long enough to be transported to the site from long range sources. The use of wind

speed data can help attribute how far sources may be from the sampling site, as shown in Section 2.3.2.2.

### 2.3.2.2 Wind direction/speed trends

To aid the identification of the locality of potential VOC sources, bivariate polar plots were prepared to show how mixing ratios vary by wind direction and wind speed (Figure 2-13), combining data from both halves of the field campaign.





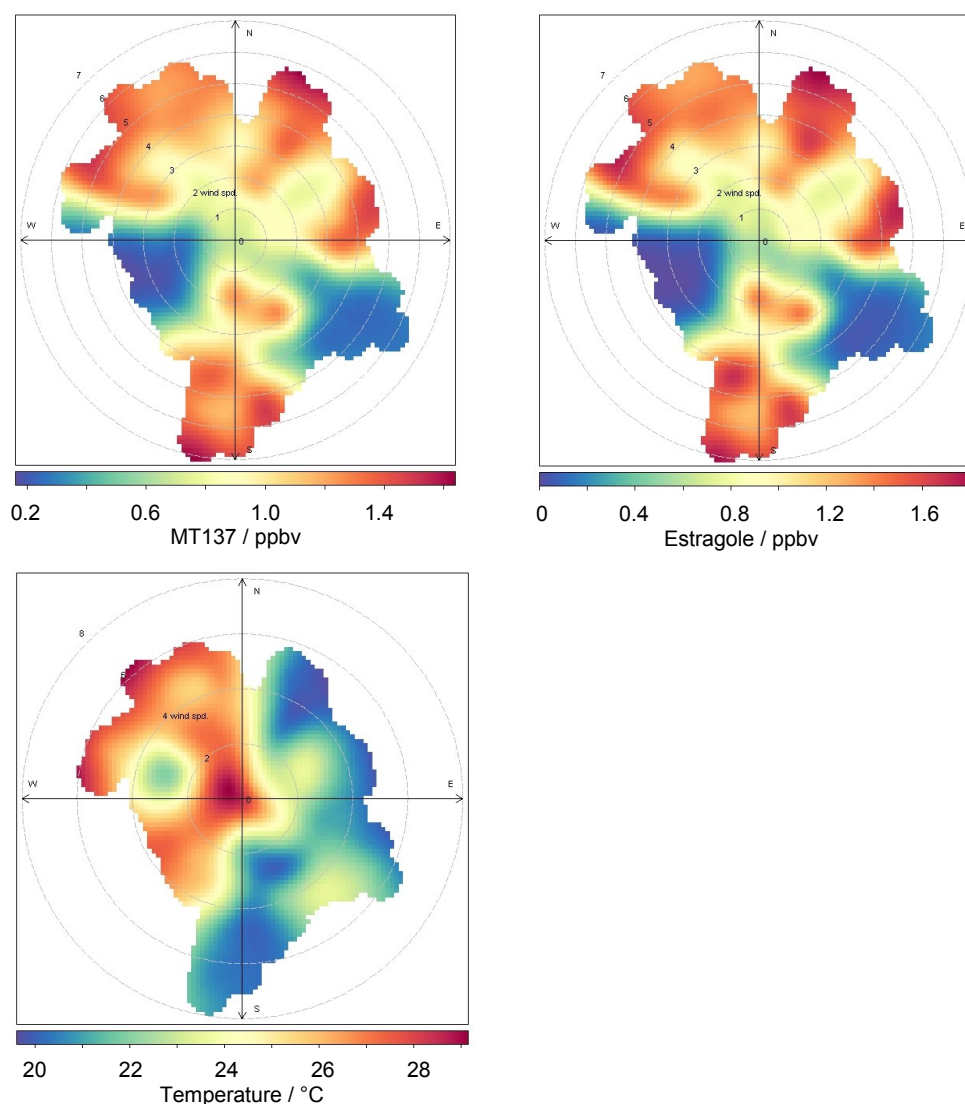


**Figure 2-13 Bivariate plots showing how VOC mixing ratio varies by wind speed and wind direction. Polar coordinates correspond to wind direction, radial distance indicates wind speed ( $\text{m s}^{-1}$ ) and colour denotes VOC mixing ratio according to the key for each individual plot. Temperature ( $^{\circ}\text{C}$ ) is shown for comparison.**

Figure 2-13 shows that most compounds behaved similarly showing enhanced mixing ratios when the wind was from S or NE directions, particularly for high wind speeds (suggesting contributions from distant sources). Additionally, more localised sources – when wind speeds were lower – were particularly evident for acetone and for all other compounds when wind direction was from S. With the exception of acetaldehyde, acetone and methanol, mixing ratios were also elevated when wind was from the NW sector, coinciding with higher temperatures. In fact, highest

mixing ratios of *p*-cymene were observed in this sector, which was the only compound with a spatial pattern notably different to all others.

With regards to the wider area, the forest is bordered by a large heather area 1.5 km to the east. Forest surrounds the site for at least several kilometres in all other directions. The nearest sizable urban area lies 6 km to the northwest of the site at the towns of Ermelo and Putten (combined populations ~50,000). On a wider scale (Figure 2-14), the Speuld site lies within a larger area of land mostly covered by deciduous forest and natural vegetation extending 50 km in a north-south direction and covering an area of ~870 km<sup>2</sup> (Clevers et al., 2007). Outside the wider forested area, a large area of arable land making up most of the Flevopolder region 970 km<sup>2</sup> lies 15 km NW. Amsterdam is ~55 km WNW. At a horizontal wind speed of 2 m s<sup>-1</sup>, it would take less than 8 h to travel this distance; much shorter than some of the atmospheric lifetimes of measured compounds (Table 2-2).

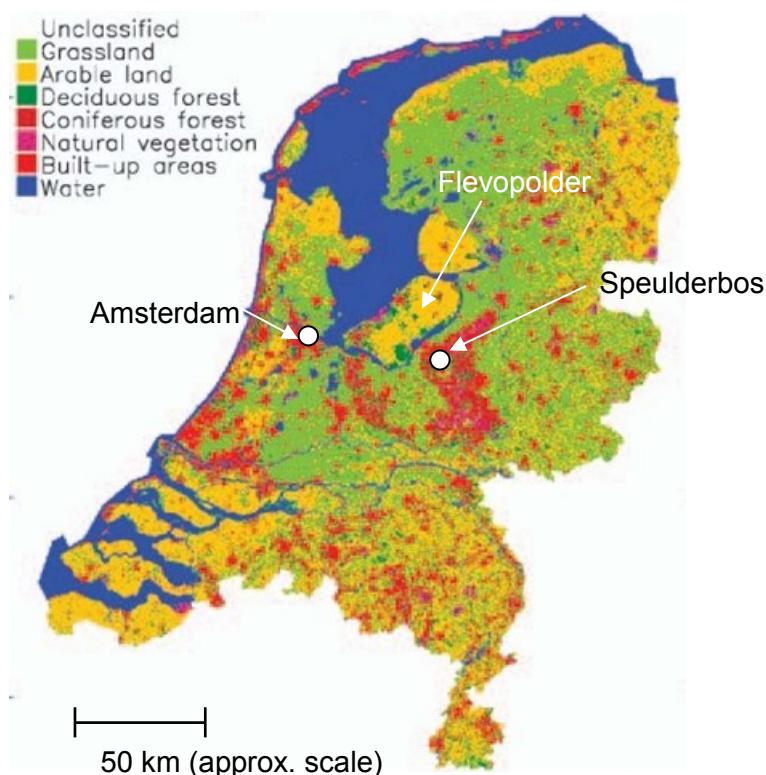


Figure 2-14 Land use map of The Netherlands. Adapted from Figure 7 in Clevers et al. (2007).

It is likely that the tendency for high mixing ratios in N and S directions is due to the wider forested area, as this is the most dominant land use in these directions. Of all compounds also showing high mixing ratios in the NW sector, TMA and hexanals have lifetimes of the order of several hours, therefore the arable region to NW may be a source of these compounds. Indeed, animal husbandry is cited as the main source of atmospheric TMA (Ge et al., 2011) with slurry application a minor contributor (Kuhn et al., 2011), and hexanals are known to be emitted during grass cutting (Davison et al., 2008; Karl et al., 2005b).

High *p*-cymene mixing ratios in NW may also be due to these sources, although *p*-cymene emission is more commonly associated with deciduous broadleaf forests (Geron et al., 2000). Alternatively, as *p*-cymene is detected at the same mass as toluene (normally from anthropogenic sources), it may be possible that it is the latter which was detected. Possible sources could have been in the vicinity of urban centres such as Putten/Ermelo or further afield towards Amsterdam, as the relatively long lifetime (2.4 day, OH) would make longer range transport feasible.

### **2.3.3 In-canopy mixing ratios**

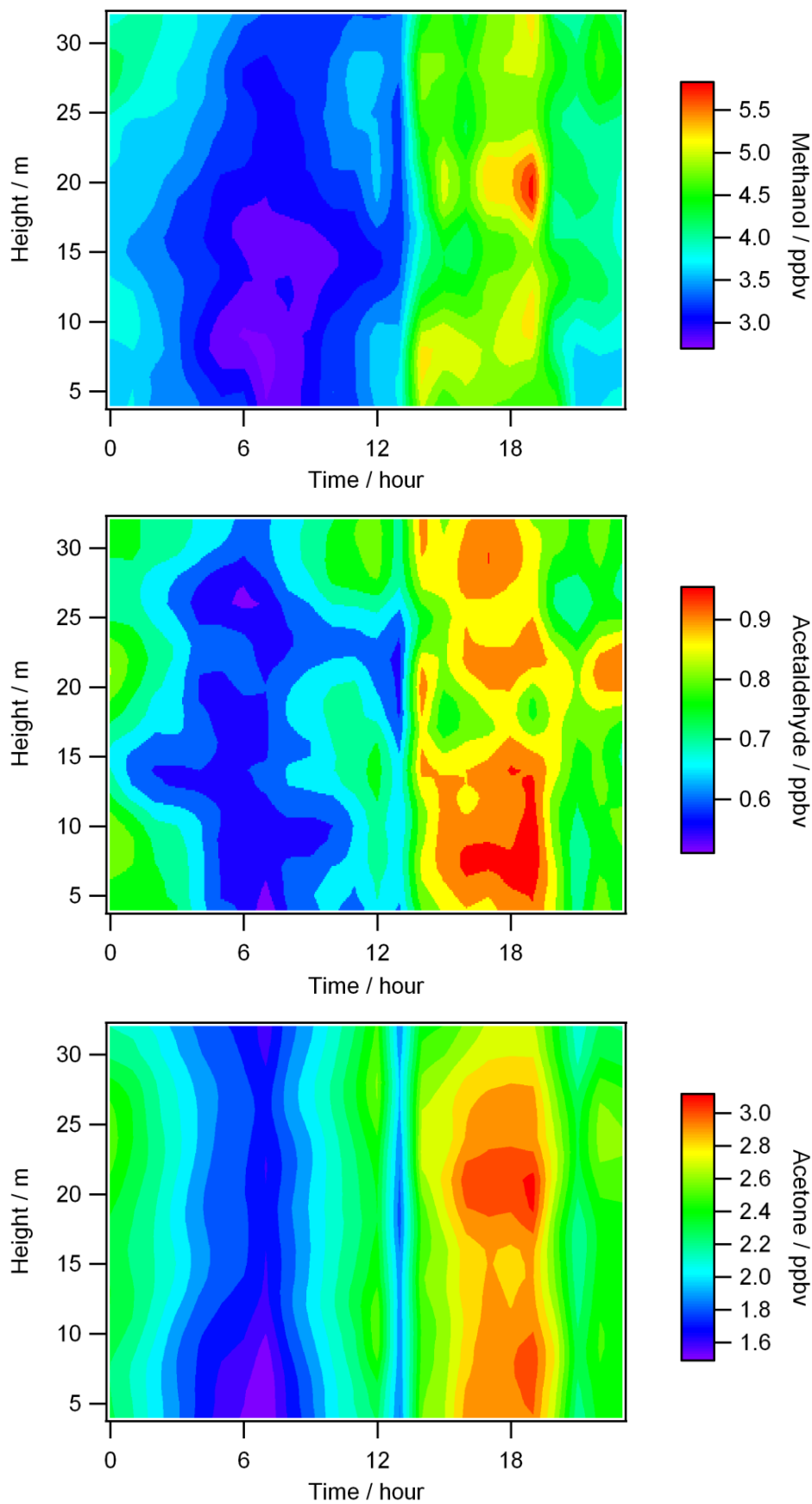
As described in Section 2.2.4, in-canopy mixing ratios were measured during the second half of the campaign from 30 June to 7 July.

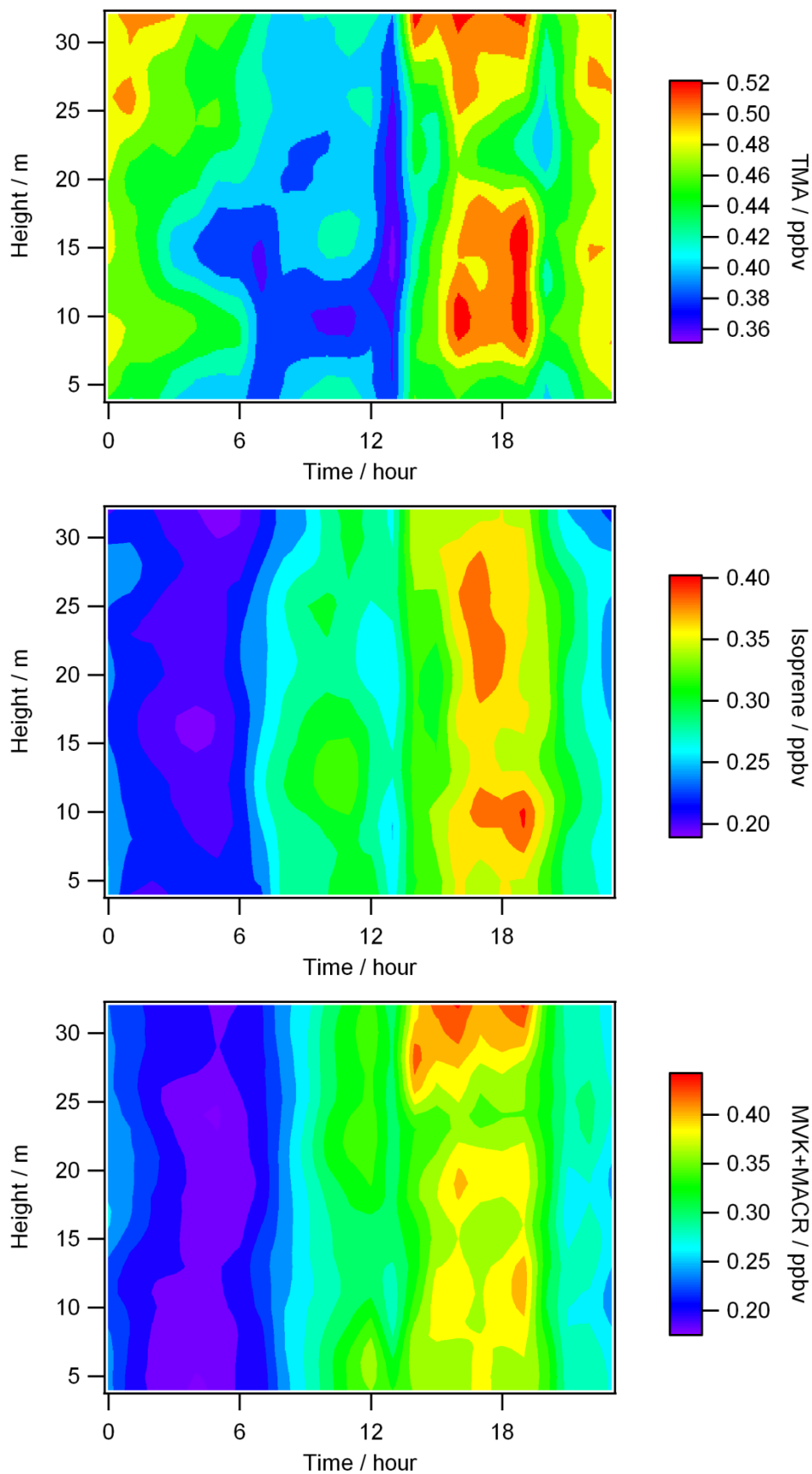
#### **2.3.3.1 Winch sampling**

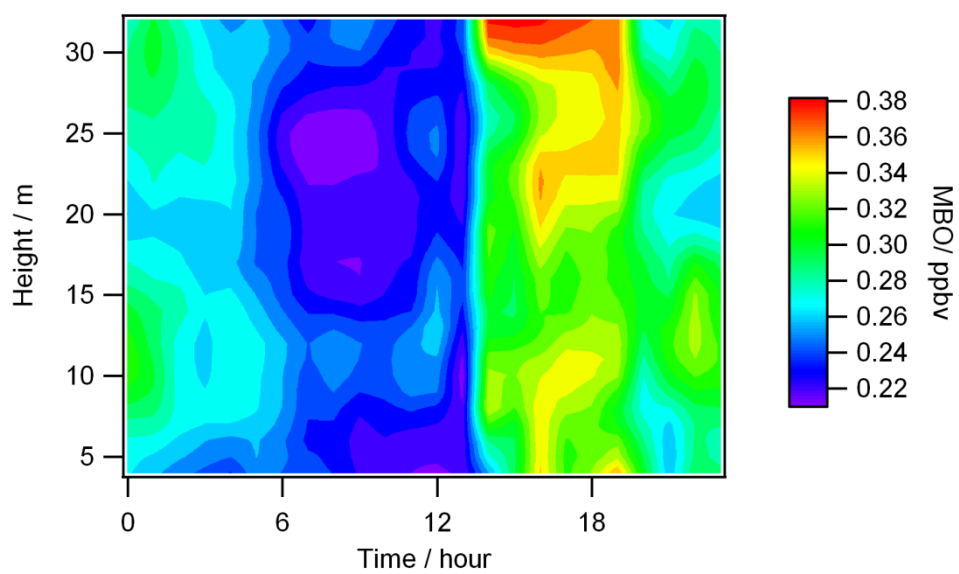
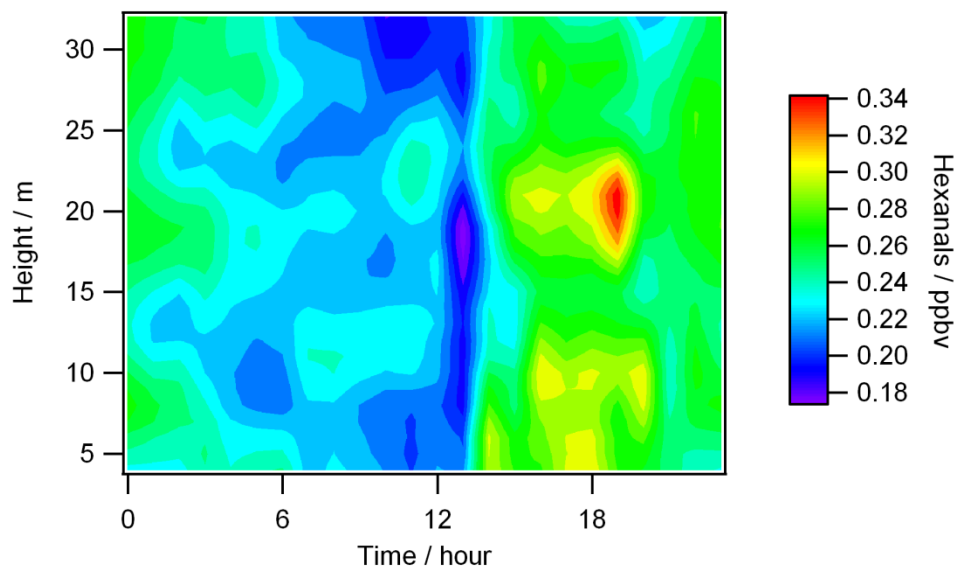
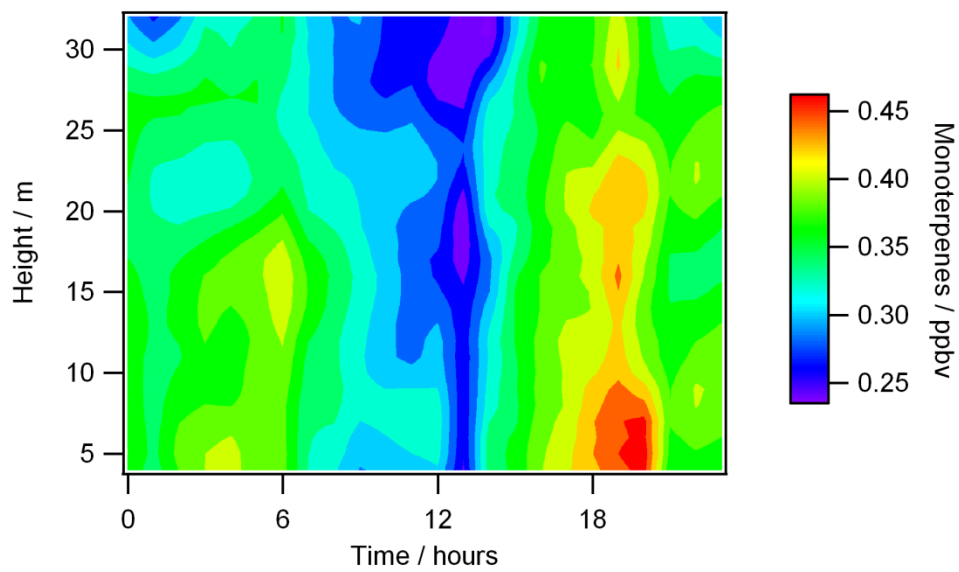
Plots visualising the variation in mixing ratio as a function of time and height for all measured compounds are shown in Figure 2-15<sup>4</sup>.

---

<sup>4</sup> Acknowledgments to Amy Tavendale for producing these plots.







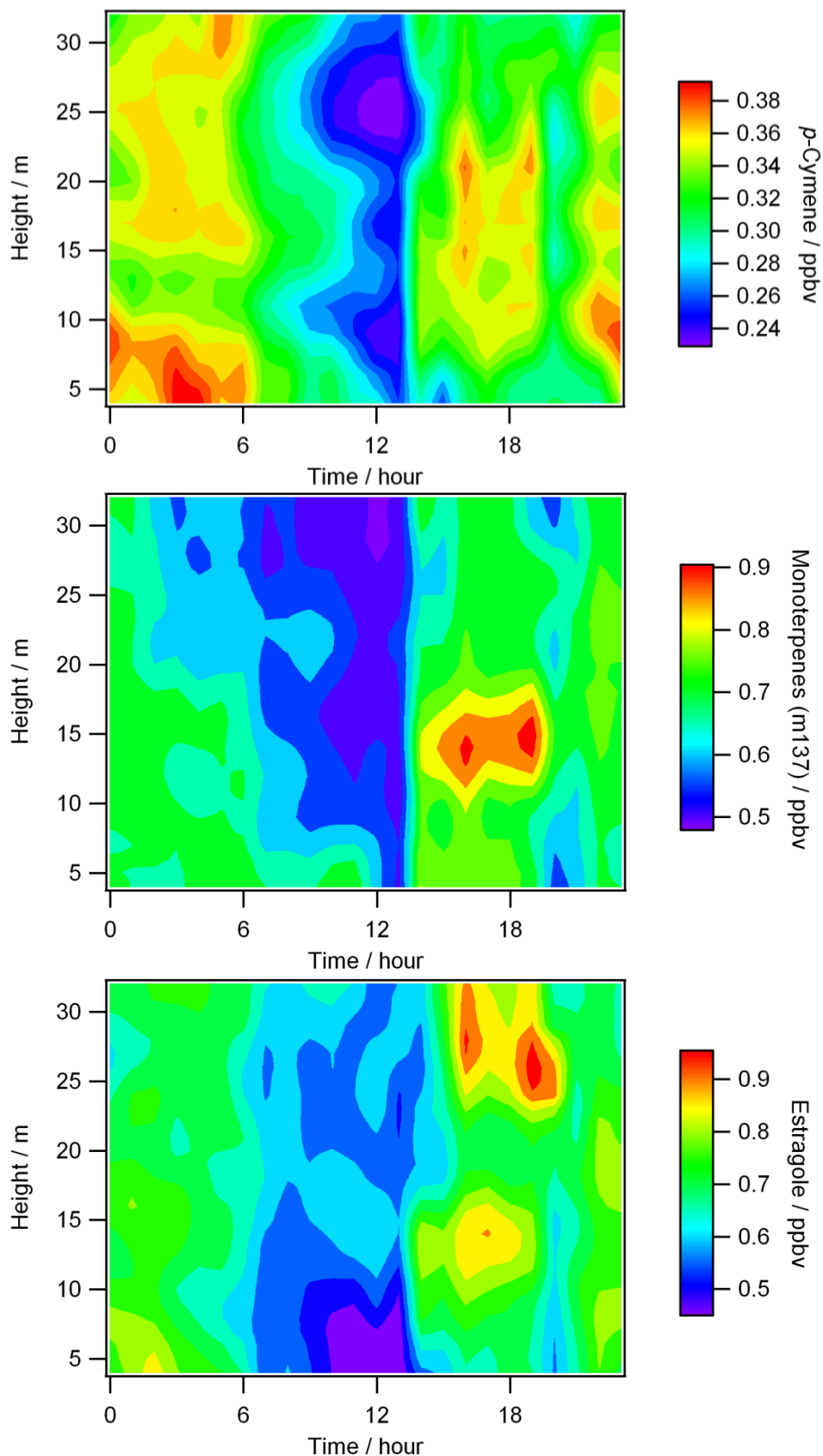


**Figure 2-15** In-canopy mixing ratios (ppbv, denoted by colour) as a function of time of day (hour, x-axis) and canopy height above ground (m, y-axis). Note the variable mixing ratio scales.

Mixing ratios were generally higher than those measured above the canopy (Figure 2-9 and Figure 2-10). All compounds show a similar diurnal pattern to those observed for above-canopy measurements, with mixing ratios increasing throughout the second half of the day. Maxima were at ~18:00, corresponding to reduced vertical mixing and continued temperature-dependant emissions.

Methanol, acetaldehyde, acetone, isoprene, monoterpenes and hexanals had peak mixing ratios within the canopy at ~18:00, with distinct minima around 06:00 for all except monoterpenes (minimum ~13:00). Isoprene mixing ratios decreased more rapidly than other compounds, reaching the minimum by midnight. Acetaldehyde, acetone and monoterpenes had particularly elevated mixing ratios toward the bottom of the canopy (5-10 m), as had been observed for monoterpenes during previous work (Dorsey et al., 2004). This could be explained by the large amount of leaf litter on the forest floor acting as a source.

MVK + MACR, MBO and estragole had peak mixing ratios at the top of the canopy. For MVK + MACR, this can be explained by formation in-canopy through photo-oxidation of isoprene, rather than from primary emission, therefore peak mixing ratio coincides with predicted highest PAR at the top of the canopy. Pine species are known to be a source of MBO (Harley et al., 1998) with emission dependant on both light and temperature (Holzinger et al., 2005). Estragole emission is from both storage pools – similar to monoterpenes – and directly after synthesis in a light and temperature driven mechanism – similar to MBO (Bouvier-Brown et al., 2009). Increased PAR higher in the canopy may therefore explain the mixing ratio profile of both of these compounds, while storage pool emissions of estragole result in a slower decline in mixing ratios overnight.

TMA and *p*-cymene profiles differed from all others and were less structured. TMA mixing ratios were, in general greater towards the top of the canopy, except for ~18:00 when mixing ratios were elevated at all heights. Mixing ratios also remained high overnight. Peak *p*-cymene mixing ratios were between 22:00 and 06:00 low in the canopy (5-10 m).

### 2.3.3.2 GC-MS samples

In-canopy samples for GC-MS analysis were also taken at three different heights (4, 18 and 32 m) and at three time steps throughout the day (morning, afternoon, evening). This was repeated on two days (1 and 6 July 2009) and the average total monoterpene mixing ratios in the canopy are presented in Figure 2-16.

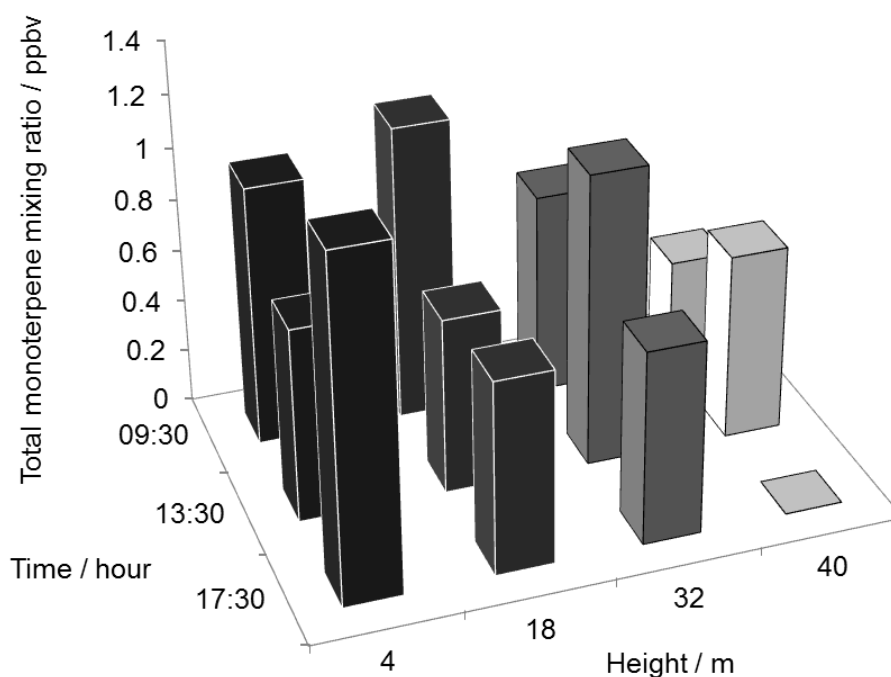


**Figure 2-16** Average total monoterpene mixing ratios within the Douglas fir canopy. Samples were taken at three heights (4, 18 and 32 m) and at three times during the day (morning, afternoon, evening). Results shown are the averages of two sampling days (1 and 6 July) except for 40 m samples which were only taken on 6 July 2009.

Figure 2-16 compares fairly well with in-canopy PTR-MS measurements (Figure 2-15). Within the canopy (4 and 18 m) mixing ratios are highest in the morning and evening, and lowest in the afternoon as was measured by PTR-MS. Conversely, peak mixing ratios measured in the afternoon were greater at the top of the canopy (32 m) and above (40 m). In general mixing ratios were larger at lower heights, again consistent with PTR-MS results. The composition of total monoterpenes as a function of height is illustrated in Figure 2-17.

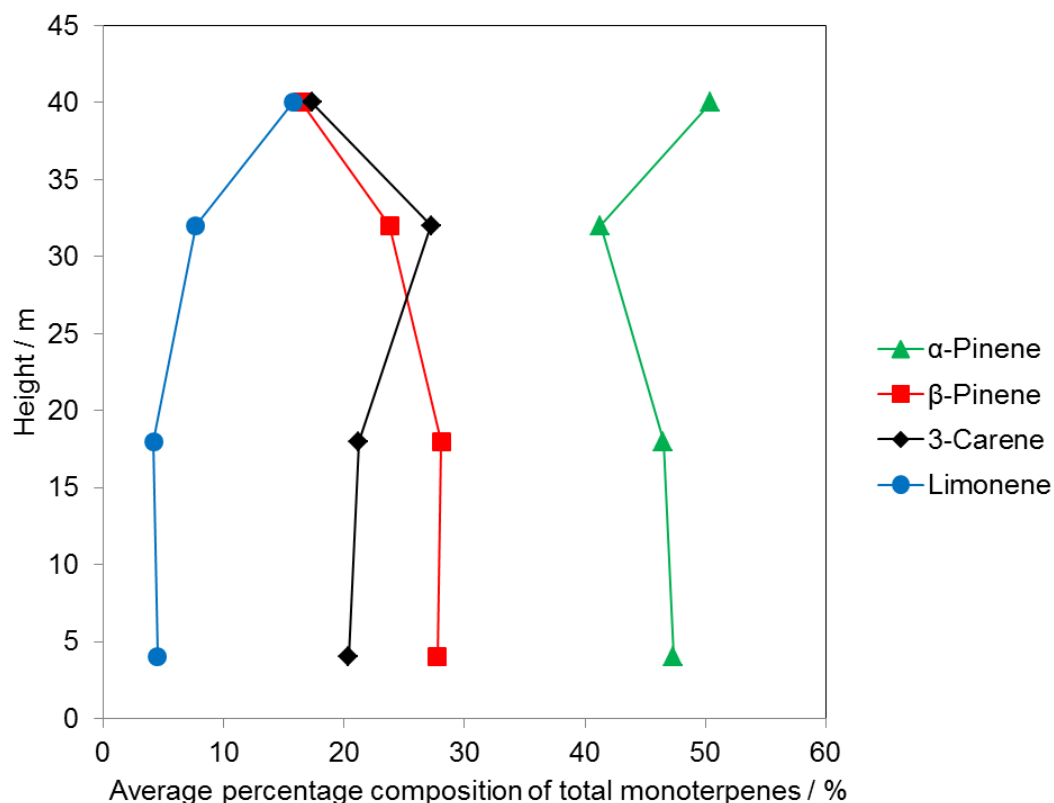


**Figure 2-17 Monoterpene composition as a function of height above ground within the Douglas fir canopy. Each data point is a mean of 6 repeat measurements. Canopy top is at 32 m.**

Figure 2-17 shows that  $\alpha$ -pinene is the dominant monoterpene at all heights. Its percentage contribution towards total monoterpenes decreases with height to a minimum at the canopy top (32 m), before increasing again above the canopy. The exact opposite was observed for 3-carene, which increased in percentage up to 32 m before decreasing above the canopy. Limonene contributes least although the percentage increases with canopy height. The profile of  $\beta$ -pinene is the opposite to that of limonene, showing a steady decrease with height until the percentage contribution is the same as for limonene at a height of 40 m. These results are consistent with a previous study at the Speuld site (Peters et al., 1994), and another study which suggested that  $\alpha$ -pinene,  $\beta$ -pinene and 3-carene account for 95 % monoterpene emissions from Douglas fir (Lerdau et al., 1995). This is reflected in Figure 2-17, except for measurements above the canopy (40 m) which may have been influenced by sources from the wider area.

## 2.4 Discussion

### 2.4.1 Terpenoids

Monoterpene mixing ratios measured in this study are in agreement with previous studies at the site. Total monoterpene mixing ratios were generally higher at night, peaking at 23:30 (1.76 ppbv) and 16:00 (0.95 ppbv) during the first and second halves of the campaign, respectively. They were also greater towards the forest floor suggesting a source low in the canopy, which may be explained by the large amounts of leaf litter and fallen branches, as has been suggested previously (Dorsey et al., 2004; Peters et al., 1994).

A disparity between monoterpene fragment mixing ratios measured at  $m/z$  81 and 137 was observed. The relationship between quantification at the two different ions is shown in Figure 2-18.

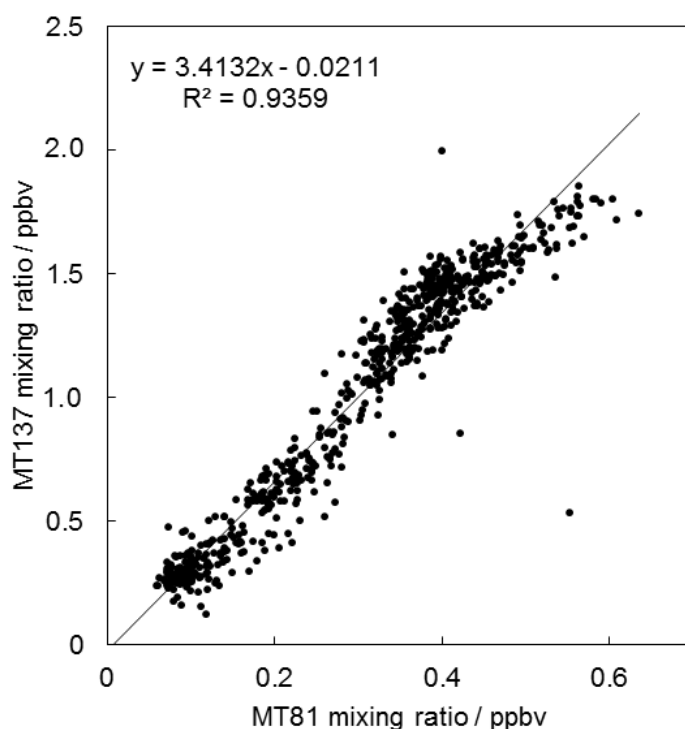


**Figure 2-18 Relationship between the half-hour averaged mixing ratios of  $m/z$  137 against those of  $m/z$  81. The black line shows the linear regression (equation shown inset).**

Figure 2-18 shows that the relationship between the two masses is linear, as has been observed elsewhere (Rinne et al., 2005), with a MT137 to MT81 ratio of around 3.4.

The origin of this observed difference is due to differing fragmentation patterns of varying monoterpenes in the PTR-MS, which have been shown to depend on drift tube  $E/N$  ratio (Misztal et al., 2012; Tani et al., 2003).

Monoterpene fluxes from plant sources have been shown to increase exponentially with temperature (Guenther et al., 1993; Pressley et al., 2004), according to the G93 algorithm,

$$E_{meas} = E_s e^{\beta(T - T_s)} \quad (2-4)$$

where  $E_{meas}$  is the measured emission rate at leaf temperature  $T$  ( $^{\circ}\text{C}$ ),  $E_s$  is the standard (basal) emission rate at  $30^{\circ}\text{C}$  ( $T_s$ ) and  $\beta$  is an empirical temperature coefficient, normally between  $0.06$  and  $0.14^{\circ}\text{C}^{-1}$ . Only weak relationships were observed for diurnal flux data from the first and second halves of the campaign ( $R^2 = 0.177$  and  $0.074$  respectively). The low correlations of  $E_{meas}$  with  $T$  are likely due to noisy flux data and being close to the instrument LOD. Nonetheless, the standard monoterpene emission rates for the first and second halves of the campaign were calculated to be  $1.15$  and  $0.82 \mu\text{g g}_{\text{dw}}^{-1} \text{h}^{-1}$ , with temperature coefficient of  $0.266$  and  $0.063^{\circ}\text{C}^{-1}$ , respectively. These values are compared with other studies of Douglas fir in Table 2-3. Foliar density  $D$  was estimated at  $600 \text{ g}_{\text{dw}} \text{ m}^{-2}$  (Guenther et al., 1994).

It can be seen from Table 2-3 that the standard monoterpene emission factors from this study were within the range of previously derived values for *Pseudotsuga menziesii*. All other studies used branch enclosure methods (see Section 1.5.1). Despite the PTR-MS method giving canopy-averaged results, this does not result in a bias towards lower emission factors as may be expected for isoprene emission factors; monoterpene emissions are only temperature dependent, and not proportional to PAR, so although parts of the canopy would have been shaded, this should not have affected monoterpene emissions. Only temperature differences within the canopy would have resulted in deviations from comparable studies. The temperature coefficient measured in the second half of the study was in agreement with the generally accepted value for most plants (Guenther et al., 1993) while for the first half of the campaign it was closer to that of stressed trees (Joó et al., 2011).

Although Douglas fir trees – and coniferous species in general – are thought to be non-emitters of isoprene, fluxes were discernible, as they were for the isoprene oxidation products MVK and MACR. Their above-canopy mixing ratios showed a diurnal pattern throughout the campaign also. Figure 2-15 shows that peak isoprene mixing ratios occur throughout the canopy, whilst the MVK and MACR mixing ratio peaks at the top of the canopy, ~32 m. This supports the hypothesis that the forest canopy is a source of isoprene, which is oxidised to form MVK and MACR, peaking at the top of the canopy where PAR is greatest. As isoprene emission from plants is strongly influenced by light and leaf temperature, the canopy-level emission,  $F$ , was recalculated as a standard emission factor ( $\varepsilon$ ) normalised to a standard leaf temperature of 303 K and PAR flux of  $1000 \mu\text{mol m}^{-2} \text{s}^{-1}$ , as described by the G95 algorithm (Guenther et al., 1995),

$$\varepsilon = \frac{F}{D \gamma} \quad (2-5)$$

where  $D$  is foliar density ( $\text{g dry weight m}^{-2}$ ) and  $\gamma$  is a non-dimensional activity adjustment factor to account for the effect of light and temperature:

$$\gamma = C_L C_T \quad (2-6)$$

The light dependence,  $C_L$ , is defined by

$$C_L = \frac{\alpha c_L Q}{\sqrt{1 + \alpha^2 Q^2}} \quad (2-7)$$

where  $\alpha$  (0.0027) and  $c_L$  (1.066) are empirical coefficients and  $Q$  is PAR flux ( $\mu\text{mol m}^{-2} \text{s}^{-1}$ ). The temperature dependence  $C_T$ , is defined by

$$C_T = \frac{\exp\left(\frac{c_{T1}(T - T_s)}{RT_s T}\right)}{1 + \exp\left(\frac{c_{T2}(T - T_M)}{RT_s T}\right)} \quad (2-8)$$

where  $T$  is leaf temperature (K),  $T_s$  is leaf temperature at standard conditions (303 K),  $R$  is the universal gas constant ( $8.314 \text{ J K}^{-1} \text{ mol}^{-1}$ ), and  $c_{T1}$  ( $95000 \text{ J mol}^{-1}$ ),  $c_{T2}$  ( $230000 \text{ J mol}^{-1}$ ) and  $T_M$  (314 K) are empirical coefficients.

Values of above-canopy PAR and temperature, and of isoprene flux (from Figure 2-6 and Figure 2-7), at hourly intervals during the campaign were used for the calculation of  $\gamma$  and  $F$  respectively. Foliar density  $D$  was estimated at  $600 \text{ g}_{\text{dw}} \text{ m}^{-2}$  for *Pseudotsuga spp.* (Guenther et al., 1994) Hourly emission factors  $\varepsilon$  were then determined for isoprene for the first and second halves of the campaign, and were calculated to have peak values of  $0.77$  and  $0.75 \text{ } \mu\text{g g}_{\text{dw}}^{-1} \text{ h}^{-1}$ , respectively. Mean daytime values of  $0.10$  and  $0.18 \text{ } \mu\text{g g}_{\text{dw}}^{-1} \text{ h}^{-1}$  were calculated to allow comparison, in Table 2-3, with mean values from other studies. Standard isoprene emission factors from this study were within the range of previously derived values for *Pseudotsuga spp.* (Table 2-3).

**Table 2-3 Comparison of standardised emission rates of monoterpenes and isoprene from Douglas fir.**

Species	Monoterpenes / $\mu\text{g g}_{\text{dw}}^{-1} \text{h}^{-1}$	Temperature coefficient / $^{\circ}\text{C}^{-1}$	Isoprene / $\mu\text{g g}_{\text{dw}}^{-1} \text{h}^{-1}$	Measurement type	Reference
<i>Pseudotsuga menziesii</i>	1.15 (first half) 0.82 (second half)	0.266 (first half) 0.063 (second half)	0.10 (first half) 0.18 (second half)	Canopy-scale, PTR-MS	This study
"	$0.44 \pm 0.16$	$0.14 \pm 0.05$		Dynamic branch enclosure, mature forest	(Pressley et al., 2004)
"	$0.8 \pm 0.2$ (healthy) $6.8$ (stressed)	$0.133 \pm 0.013$ (healthy) $0.316$ (stressed)		Dynamic branch enclosure, saplings	(Joó et al., 2011)
"	1.81		<0.11	-	(Guenther et al., 1994)
"	2.0		1.0	-	(Karl et al., 2009)
"	$2.3 \pm 1.4$		$1.5 \pm 1.6$	-	(Kesselmeier and Staudt, 1999)
"	$2.60 \pm 1.63$	assumed to be $0.09 \pm 0.025$	$1.72 \pm 1.85$	Dynamic branch enclosure, mature trees	(Drewitt et al., 1998)
<i>Pseudotsuga macrocarpa</i>	$1.1 \pm 0.3$		0.0	Dynamic branch enclosure, immature tree (greenhouse)	(Arey et al., 1995)

### 2.4.2 Non-terpenoids

This study investigated non-terpenoids at the Speuld site for the first time. Only one previous study could be found which qualitatively measured other VOCs from Douglas fir saplings (Joó et al., 2011). Positive fluxes were observed for all compounds except TMA and *p*-cymene/toluene which were deposited. Peak daily median fluxes of some oxygenated compounds were higher than in other studies of coniferous forests. Methanol and acetaldehyde fluxes (2.6 and 0.7 mg m<sup>-2</sup> h<sup>-1</sup>, respectively, from Figure 2-7) were higher than those measured in a subalpine, coniferous forest in the USA where fluxes peaked at 1 and 0.4 mg m<sup>-2</sup> h<sup>-1</sup>, respectively (Karl et al., 2002). Acetone fluxes were the same at both sites (0.8 mg m<sup>-2</sup> h<sup>-1</sup>). Results at Speuld were also higher than those measured in a Scots pine canopy (Hyytiälä, Finland) for methanol, acetaldehyde and acetone (0.4, 0.15 and 0.3 mg m<sup>-2</sup> h<sup>-1</sup>, respectively (Rinne et al., 2007)). In both studies, measurements were carried out during summer (June and July, respectively). Daily temperatures at the subalpine site in USA peaked at ~17 °C. In contrast, peak temperatures at the Finnish site were only slightly cooler (~25 °C) than in the results presented here, however, night-time minimum temperatures were much cooler (~14 °C). Cooler temperatures may therefore account for lower measured fluxes at other sites compared to this study.

In-canopy mixing ratio measurements further support Douglas fir as a source of methanol, acetaldehyde, acetone, hexanals, MBO and estragole. It has been shown in several studies that decaying plant material is a source of oxygenated VOCs, such as for ponderosa pine (Schade and Goldstein, 2001), loblolly pine (Karl et al., 2005a) and decaying spruce needles (Warneke et al., 1999). As there was a thick layer of leaf litter on the forest floor, it is feasible that this could have been a source of oxygenated VOCs, particularly acetaldehyde and acetone which had highest mixing ratios near the forest floor.

Above-canopy mixing ratios of all VOCs were observed to follow a similar diurnal trend of maxima in the evening or at night, with methanol, acetaldehyde, acetone, TMA, isoprene and MVK + MACR all being above the LOD. This can be explained

by reduced radical sink chemistry at night, coupled with reduced vertical mixing, resulting in accumulation within a shallower boundary layer.

Above canopy mixing ratios of all compounds appeared to be predominantly influenced by the wider forested area, with more distant sources also identified, particularly for TMA and *p*-cymene. Arable land NW of the site was thought to be the source of elevated TMA mixing ratios, which would also explain the depositional flux profile. Elevated mixing ratios at *m/z* 93 were potentially attributable to anthropogenic toluene, since Figure 2-13 shows elevated mixing ratios associated with urban areas in WNW direction. PTR-MS measurements are unable to distinguish between different compounds of the same mass however, therefore it is not possible to say conclusively the species detected or source.

Due to the difference in frequency of data points between the first half of the campaign (above-canopy only) and the second half (in-canopy and above-canopy measurements), diurnal variation plots were presented as two separate data sets. It was observed that temperatures were higher during the second half of the campaign. As would be expected for VOCs of biogenic origin, this would explain the greater fluxes measured. On the other hand, mixing ratios were generally lower during the second half of the field campaign. This could be explained by enhanced radical sink chemistry or by greater dilution. Figure 2-19 shows the time series of wind speed throughout the campaign.

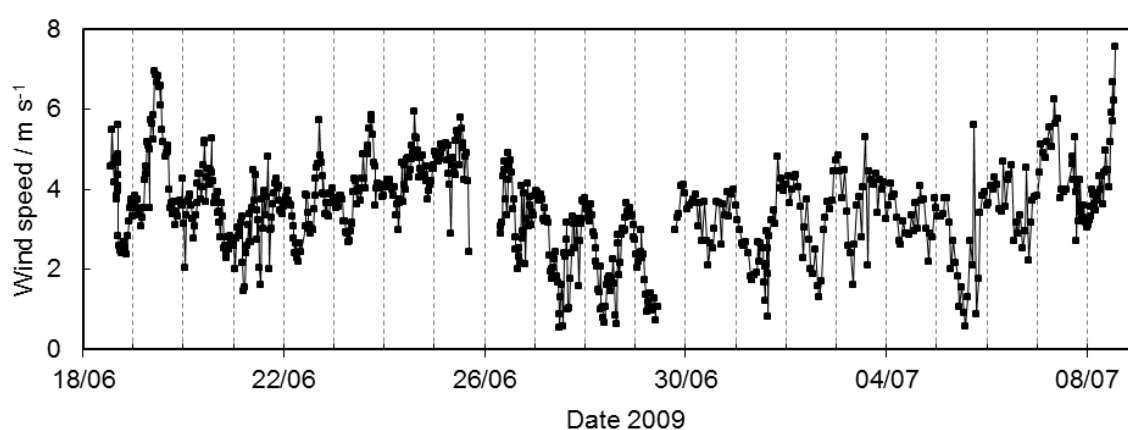


**Figure 2-19** Time series of wind speed measured above the Douglas fir canopy. Grey gridlines denote midnight.

It can be seen from Figure 2-19 that the diurnal pattern of wind speed changes throughout the campaign. Until 26 June there are distinct maxima in wind speeds around midday. From 27 June onwards, maxima occur around midnight. This is most pronounced on 2 and 3 July. This may explain the reduced mixing ratios during the second half of the campaign; although reduced radical sink chemistry caused mixing ratios to increase at night, the increases were not as pronounced as during the first half of the campaign because of increased mixing.

## 2.5 Conclusions

Using PTR-MS with the disjunct eddy correlation method, emissions of VOCs from a Douglas fir forest in Speuld, The Netherlands were quantified. Monoterpene results were comparable to other studies of Douglas fir, with the standard emission factor of 1.15 and 0.82  $\mu\text{g g}_{\text{dw}}^{-1} \text{h}^{-1}$ , and temperature coefficients of 0.266 and 0.063  $^{\circ}\text{C}^{-1}$  for the first and second halves of the campaign, respectively. The mean standard emission factors for isoprene were calculated as 0.1 and 0.18  $\mu\text{g g}_{\text{dw}}^{-1} \text{h}^{-1}$ , respectively. Fluxes of non-terpenoid VOCs were also significant, and had peak fluxes greater than has been measured for other coniferous species. This is the first study of non-terpenoid, canopy-scale emissions from a Douglas fir canopy and highlights the importance of quantifying a wider variety of VOCs from biogenic sources, other than isoprene and monoterpenes. Further work could include isolation of sources within the forest, as there was evidence that leaf litter could be an important source of VOCs in addition to the tree canopy.

## Chapter 3: VOC emissions from *Miscanthus* and short rotation coppice willow bioenergy crops

This chapter is based on a published article included in Appendix I.

*Miscanthus x giganteus* and short rotation coppice (SRC) willow (*Salix spp.*) are increasingly important bioenergy crops. Above-canopy fluxes and mixing ratios of volatile organic compounds (VOCs) were measured in summer for the two crops at a site near Lincoln, UK, by proton transfer reaction mass spectrometry (PTR-MS) and virtual disjunct eddy covariance. The isoprene emission rate above willow peaked around midday at  $\sim 1 \text{ mg m}^{-2} \text{ h}^{-1}$ , equivalent to  $20 \text{ } \mu\text{g g}_{\text{dw}}^{-1} \text{ h}^{-1}$  normalised to  $30^\circ\text{C}$  and  $1000 \text{ } \mu\text{mol m}^{-2} \text{ s}^{-1}$  PAR, much greater than for conventional arable crops. Average midday peak isoprene mixing ratio was  $\sim 1.4$  ppbv. Acetone and acetic acid also showed small positive daytime fluxes. No measurable fluxes of VOCs were detected above the *Miscanthus* canopy. Differing isoprene emission rates between different bioenergy crops, and the crops or vegetation cover they may replace, means the impact on regional air quality should be taken into consideration in bioenergy crop selection.

### 3.1 Introduction

Bioenergy crops are those grown specifically for energy production rather than food, as a means of mitigating two problems associated with the use of traditional fossil fuels: anthropogenic climate forcing and energy security (McKay, 2006). Such crops contribute to carbon neutrality since  $\text{CO}_2$  produced during the combustion of the crop is offset by the  $\text{CO}_2$  sequestered during growth. There is also potential for long-term storage of carbon via uptake by soil through plant roots (Grogan and Matthews, 2002). Consequently, cultivation of bioenergy crops is increasing rapidly. For example, power generators in the UK are required to increase to 15.4% by 2015/16 the energy derived from renewable sources (DTI, 2005), with biomass being acknowledged as a key resource in achieving this target.

Although bioenergy crops are perceived to be carbon neutral, full life-cycle analysis needs also to take account of changes in emissions of other potent greenhouse gases such as CH<sub>4</sub> or N<sub>2</sub>O. Also, few studies have investigated volatile organic compound (VOC) emissions from bioenergy crops. Biogenic VOC emissions from vegetation (Steiner and Goldstein, 2007) are estimated as about 10 times greater globally than VOC emissions from anthropogenic sources (Guenther et al., 1995). The dominant BVOC is isoprene (Guenther et al., 2006), but other important compounds include oxygenated VOCs and terpenoids.

Emissions of VOCs are important for several reasons. Their rapid oxidation chemistry, particularly in the presence of NO<sub>x</sub>, affects the oxidative capacity of the atmosphere, the generation of tropospheric ozone (Atkinson, 2000), of concern for human and plant health (Ashmore, 2005) and as a radiative forcing gas, and on formation of secondary organic particles, which likewise affect human health (Dockery et al., 1993) and radiative forcing (Kulmala et al., 2004).

The potential for BVOC emissions from crops to have a significant impact on atmospheric composition has been demonstrated in the tropics (Hewitt et al., 2009). The aim of this study was to determine fluxes of BVOCs for two bioenergy crops grown in the UK and elsewhere: short rotation coppice (SRC) willow (*Salix spp.*), a woody crop grown in dense plantations of multi-stemmed plants and harvested every 3 years; and *Miscanthus x giganteus*, a perennial grass native to Asia, of the same taxonomic group as sugarcane, sorghum and maize (Naidu et al., 2003) but more resilient to lower temperature whilst maintaining high CO<sub>2</sub> assimilation and biomass conversion efficiency. The crop grows up to 3.5 m per year (Rowe et al., 2009), and is harvested annually between January and March. The chipped and dried biomass of both crops is used to fuel biomass burners or to co-fire existing coal-fired power stations.

Fluxes from this work are compared with those for conventional UK arable crops to assess the potential impact of this land-use change on atmospheric chemistry.

## 3.2 Methods

### 3.2.1 Sampling site

The field measurements were carried out from mid-July to mid-August 2010 near Lincoln, UK (53° 19' N, 0° 35' W). Figure 3-1 shows the layout of the site, which consisted of several fields of *Miscanthus*, willow and wheat, located within an area of predominantly flat arable fields separated by hedgerows and isolated areas of mixed deciduous woodland. Mean annual rainfall at the site was 600 mm and the soil was a fine loam, overlying Charnmouth mudstone. The nearest settlement (population: 113), which had a relatively busy through-road, was ~0.7 km to the southeast. A minor road running east-west was situated 0.3 km to the south.

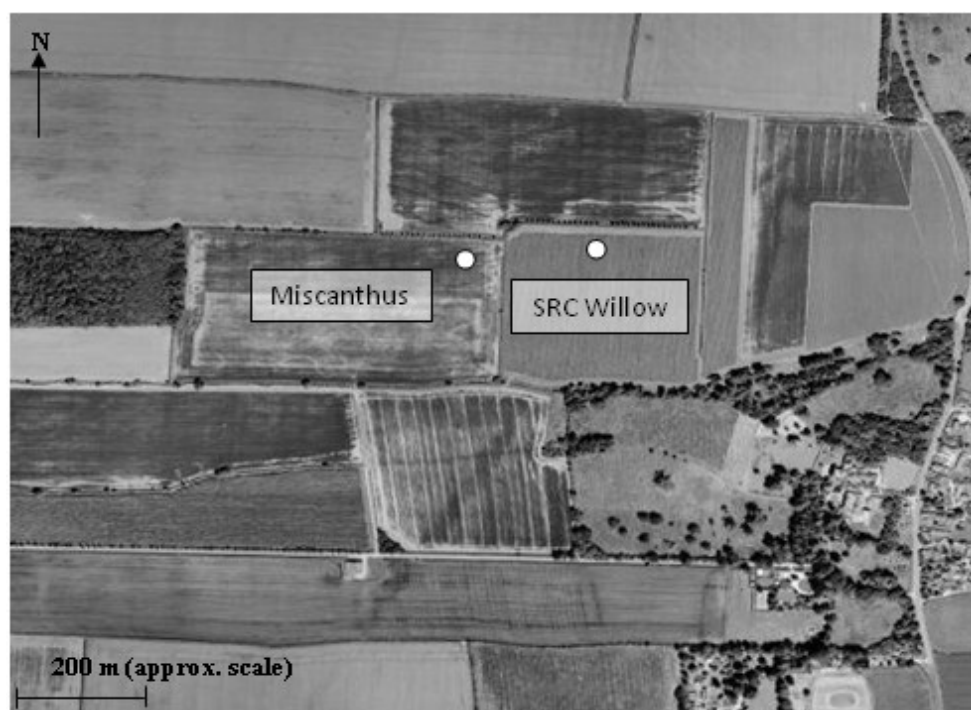


Figure 3-1 Aerial view of the *Miscanthus* and willow plantations. The white dots denote the measurement locations at the NE corner of the *Miscanthus* field and the N edge of the SRC willow field. (Map attributable to: ©2001 DigitalGlobe, GeoEye, Getmapping plc, Infoterra Ltd & Bluesky, TerraMetrics. Map data ©2011 Google).

The *Miscanthus* plot (~11 ha, planted in spring 2006) was surrounded by the following vegetation types: hedgerow and wheat to the north; willow to the east; deciduous trees to the west; willow and wheat to the south. Crop height was typically

2.5 m. Sampling was carried out from 16<sup>th</sup> July to 2<sup>nd</sup> August 2010, near the NE corner of the plot, downwind of the prevailing wind direction, at an inlet height of approximately 4 m.

The willow plot (~6.5 ha, planted in 2001 with five different genotypes) was bounded as follows: a row of deciduous trees and a ploughed field to the north; *Miscanthus* to the west; mixed deciduous woodland to the south; wheat to the east. Typical canopy height was 4 m. Sampling was carried out from 5<sup>th</sup> to 13<sup>th</sup> August 2010 at an inlet height of 6.7 m on the north edge of the field. Trees were planted in pairs of rows 1.3 m apart, with 0.6 m spacing within each pair.

Flux footprints for both sampling sites were predicted using a simple parameterisation model (Kljun et al., 2004). Model results are shown in Figure 3-2. For the *Miscanthus* measurements, the largest distance for 80% flux contribution over the range of friction velocities encountered (122 m) was within the area of the *Miscanthus* field throughout the south-westerly sector (180 – 270°). For the willow measurements, the largest distance for 80% flux contribution (185 m) meant there may have been some small flux contributions from outside the willow field when wind was from the west. Flux contribution was otherwise within the willow field for the whole southerly wind sector (90 – 270°). These sectors were used for directional filtering of data prior to deriving diurnal averages. Directionally-filtered data comprised 23% and 71% of all data for *Miscanthus* and willow, respectively.

Harvesting activities in surrounding farms during this study may have affected results, particularly during *Miscanthus* measurements, and are discussed later.

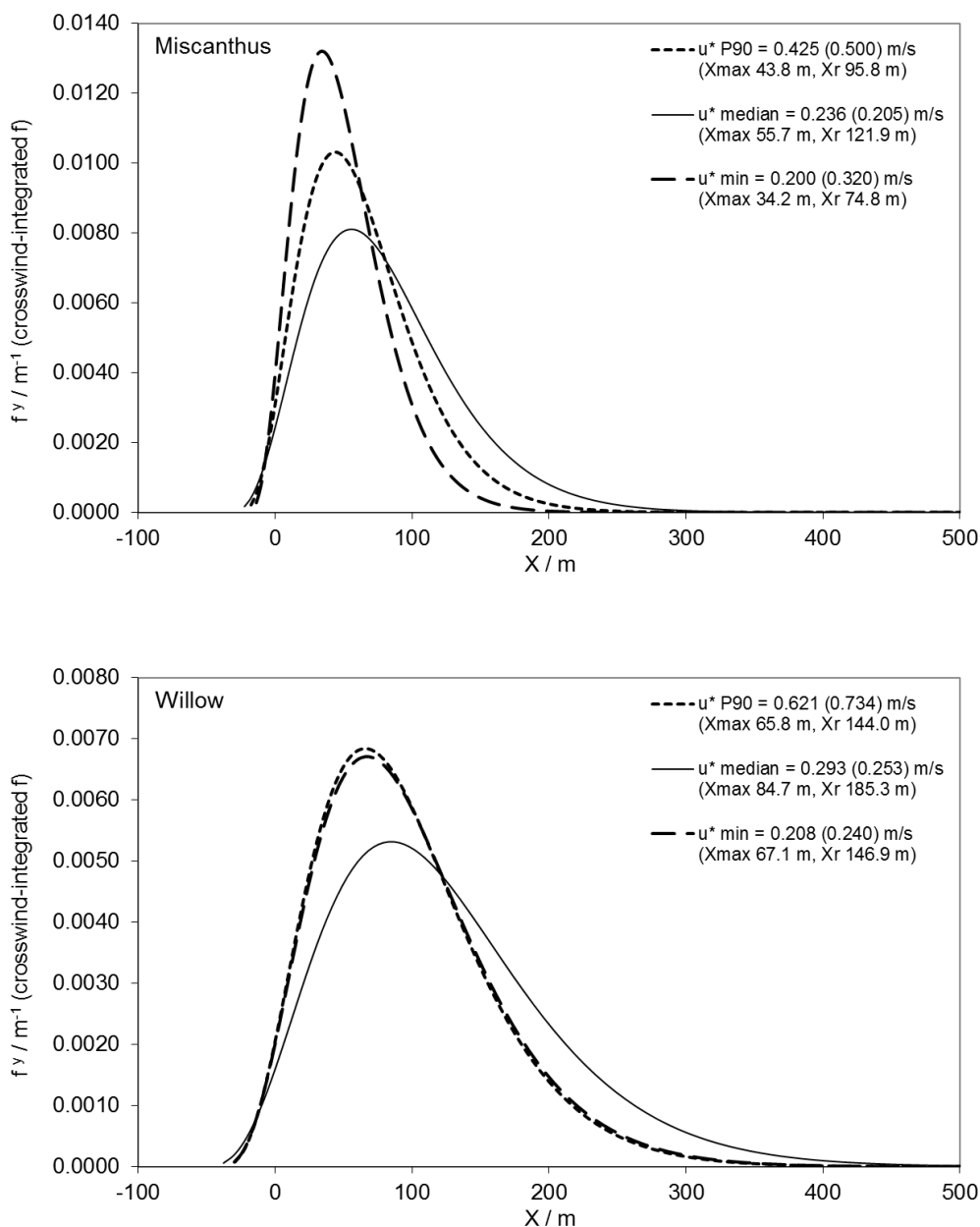


Figure 3-2 Modelled flux footprints for *Miscanthus* and SRC willow measurements. The following parameters were used. *Miscanthus*: measurement height  $z_m$  4 m; roughness length  $z_0$  0.25 m (estimated as 1/10th of the canopy height, 2.5 m); boundary layer height  $h$  1000 m. SRC willow:  $z_m$  6.7 m;  $z_0$  0.4m;  $h$  1000 m. Footprints were calculated for 90th percentile (P90), median and minimum values of  $u^*$  (1 sd of the vertical wind speed,  $\sigma_w$ , shown in brackets) as indicated on the graphs. The distance at which maximum contribution can be expected, and at which 80% of the flux is contained, are given as  $X_{max}$  and  $X_r$ , respectively.

### 3.2.2 PTR-MS set-up

BVOC mixing ratios and fluxes above both crop canopies were measured using PTR-MS (Blake et al., 2009) coupled with virtual disjunct eddy covariance (vDEC) (Karl et al., 2002; Rinne et al., 2001). PTR-MS is a ‘soft’ chemical ionisation method in which hydronium ions ( $\text{H}_3\text{O}^+$ ) formed in a hollow cathode ion source pass into a drift tube subject to an electric field ( $E$ ) into which the ambient air is also introduced. As most VOC molecules have a proton affinity greater than water, they react with  $\text{H}_3\text{O}^+$  ions to form protonated products, predominantly the protonated molecular ion, but also fragments or clusters. The extent of fragmentation/clustering can be controlled by tuning the  $E/N$  ratio ( $N$  is the  $\text{H}_3\text{O}^+$  ion density).

The PTR-MS used in this study (Ionicon Analytik, Innsbruck, Austria) was fitted with an extra turbopump connected to the detection chamber, and Teflon instead of Viton rings in the drift tube (Davison et al., 2009; Misztal et al., 2010). Pfeiffer turbopumps replaced the Varian equivalents. The drift tube conditions were held constant throughout (pressure 2 mbar, temperature 40 °C, voltage 572 V) to maintain an  $E/N$  ratio of  $\sim 130$  Td ( $1 \text{ Td} = 10^{-17} \text{ V cm}^2$ ).

The sampling inlet and 20 Hz sonic anemometer (WindmasterPro, Gill Instruments) were positioned above the canopy using a telescopic mast. Air was sampled at  $30 \text{ L min}^{-1}$  through a 20 m PTFE inlet line (1/4" OD, 3/16" ID) with a T-piece for sub-sampling into the PTR-MS inlet at a rate of  $100 \text{ mL min}^{-1}$ . Condensation of water vapour in the inlet line was prevented by wrapping with self-regulating heating tape (Omega, UK type SRF3-2C). Data were logged using a program written in LabVIEW (Version 8.5, National Instruments).

### 3.2.3 Determination of VOC mixing ratios and fluxes

The PTR-MS signal was calibrated explicitly for several VOCs using a mixed gas calibration cylinder (Apel-Riemer Environmental Inc., USA) containing 1 ppmv each of formaldehyde, methanol, acetonitrile, acetone, acetaldehyde, isoprene and 0.18 ppmv d-limonene. The calibration gas was diluted with VOC-scrubbed air to produce 6 samples with concentrations of 0.5, 1.0, 10, 20, 30 and 50% of the pure calibration gas standard. A relative transmission curve was then constructed to determine

empirical calibration coefficients for other VOCs under study not present in the standard (Taipale et al., 2008). Calibrations were carried out in the lab before commencement of the field campaign, and on 22<sup>nd</sup> July during the campaign. Concentrations of gases in the calibration cylinder were verified using GC-MS calibrated with its own independent standards (details given in Section 3.2.4).

The PTR-MS was run in multiple ion detection (MID) mode for two 25 min sampling periods per hour. During these periods only the targeted VOC ions listed in Table 3-1 were measured, with dwell times of 0.5 s, in addition to the primary ion  $\text{H}_3\text{O}^+$ , and water cluster  $(\text{H}_2\text{O})\text{H}_3\text{O}^+$ , which had dwell times of 0.2 s. The sensitivities (ncps ppbv<sup>-1</sup>) and limits of detection (ppbv) for the target ions for the *Miscanthus* and willow campaigns are also included in Table 3-1. LODs were calculated as the ratio of twice the standard deviation of the background ion counts for a particular  $m/z$  throughout the campaign divided by the sensitivity (Karl et al., 2003).

The remaining 10 min per hour were used for full mass scans in the range 21 – 206 amu at a dwell time of 1 s per amu. For one 5 min period, ambient air was scanned to allow information about the full VOC composition to be acquired. For a further 5 min per hour, ‘zero air’ was scanned to determine the instrument background. Zero air was achieved by sampling ambient air through a custom-made zero-air generator comprising a glass tube packed with platinum wool and a 50:50 mixture of platinum mesh and activated charcoal heated to 200°C. The background spectrum was subtracted in subsequent processing of data.

As the PTR-MS was run in MID mode, fewer data points were generated than required for direct eddy covariance due to the non-continuous manner in which the quadrupole mass analyser measures each  $m/z$ . The set-up resulted in 30,000 wind speed measurements and up to 441 VOC measurements in each 25 min sampling period (depending on how many VOCs were being measured). The total lag time between PTR-MS and wind speed data was determined by examining the cross-correlation between vertical wind speed and VOC mixing ratio as a function of lag time (with 15 s window). Total lag includes residence time in the sampling inlet line but also lag associated with collection and data writing of a full cycle of analysis by

disjunct sampling and the response of the PTR-MS. The median of the lag times for each 5 min sub-period was used to calculate the flux in that 25 min period (Misztal, 2010). For example, the average lag-time for isoprene above the willow was 9.58 s, with a standard deviation between 25 min periods of 1.41 s. This method produced less variable lag times than those derived using the prevalent MAX method in cross-correlation function (~72% lower sd), and has been shown to be a practical alternative (Taipale et al., 2010).

Quality controls were used to filter data for periods of low friction velocity ( $u^* < 0.15 \text{ m s}^{-1}$ ), non-stationarity, large spikes in vertical wind speed or VOC concentration, and where <20000 data points were acquired in a 25 min sampling period. Most discarded data occurred during night when turbulence was low. High frequency flux losses due to the relatively slow disjunct VOC sampling frequency (0.25 Hz, compared to 20 Hz sonic data capture) were estimated using empirical ogive analysis (Ammann et al., 2006) for each 25 min period. At least 78% of flux was captured for all individual 25 min data periods, and values were corrected accordingly. Standard rotations of the coordinate frame were applied to correct for sonic anemometer tilt for each 25 min period separately.

**Table 3-1 Compounds measured during the field campaign including dwell times, sensitivities and limits of detection.**

<i>m/z</i> [amu]	Contributing compound(s)	Formula	Dwell time [s]	Sensitivity [ncps ppbv <sup>-1</sup> ]	Limit of detection [ppbv]	
					<i>Miscanthus</i>	Willow
21	water isotope	H <sub>2</sub> <sup>18</sup> O	0.2	-	-	-
33	methanol	CH <sub>4</sub> O	0.5	4.1	1.41	2.03
37	water cluster	(H <sub>2</sub> O) <sub>2</sub>	0.2	-	-	-
45	acetaldehyde	C <sub>2</sub> H <sub>4</sub> O	0.5	12	0.44	0.21
59	acetone propanal	C <sub>3</sub> H <sub>6</sub> O	0.5	11	0.41	0.06
61	acetic acid	C <sub>2</sub> H <sub>4</sub> O <sub>2</sub>	0.5	10	0.08	0.06
69	isoprene furan methyl butenol fragment	C <sub>5</sub> H <sub>8</sub>	0.5	3.5	0.13	0.12
71	methyl vinyl ketone (MVK) methacrolein (MACR)	C <sub>4</sub> H <sub>6</sub> O	0.5	6.2	0.06	0.07
73	methyl ethyl ketone (MEK)	C <sub>4</sub> H <sub>8</sub> O	0.5	6.0	0.11	0.08

### 3.2.4 Chromatographic analysis of ambient air samples

Ambient air samples were collected for chromatographic analysis, to confirm the identity of the VOC components measured by the PTR-MS, approximately hourly from 06:53 to 16:20 on 23 September 2010 above *Miscanthus* and from 06:32 to 17:30 on 11 August 2010 above willow (at ~1 m above the canopies). Sampling above *Miscanthus* was carried out at a later date because initial samples taken during the intensive campaign were lost due to GC-MS instrument failure. A mass-flow controlled Pocket Pump (210-1000 Series, SKC Inc.) was used to pump air at 100 mL min<sup>-1</sup> for 15 min through stainless steel adsorbent tubes (6 mm OD) packed with 200 mg Tenax TA and 100 mg CarboTrap (Markes International Ltd., UK). Prior to sampling, packed tubes were conditioned at 300 °C for 15 min with a flow of helium.

Analyses were carried out using a Hewlett-Packard 5890/5970 GC-MS with an automated thermal desorption unit (ATD 400, Perkin Elmer) connected via a 200 °C heated transfer line. Transfer of samples from the adsorbent tubes was performed in two steps: heat to 280 °C for 5 min at 25 mL min<sup>-1</sup> to desorb samples onto a Tenax-TA cold trap at -30 °C, followed by transfer to the GC column at 300 °C for 6 min. Chromatographic separation utilised an Ultra-2 column (Agilent Technologies, 50 m × 0.2 mm ID × 0.11 µm film, 5% phenylmethyl silica) and a temperature program of 35 °C for 2 min, heat at 5 °C min<sup>-1</sup> to 160 °C, heat at 10 °C min<sup>-1</sup> to 280 °C, and hold for 5 min.

Calibration was carried out using a mixed monoterpene in methanol standard (10 ng µL<sup>-1</sup> α-pinene, β-pinene, α-phellandrene, 3-carene and limonene (Sigma Aldrich, UK)) and an isoprene in nitrogen gas standard (700 ppbv, BOC Gases, UK). Aliquots of the monoterpene standard (0, 1, 3 and 5 µL) were injected onto 4 adsorbent tubes with helium carrier gas. Tubes continued to be purged with helium for 2 min after the standard injection. Isoprene calibration tubes were prepared by slowly (over a period of about 2 min) injecting 0, 10, 30 and 50 mL of the gas standard onto 4 adsorbent tubes, while purging with helium. The limits of detection for isoprene, α-pinene and limonene were 0.16, 0.23 and 0.30 ng on column, corresponding to mixing ratios of 38, 27 and 35 pptv, respectively, for a 1.5 L sample.

### 3.2.5 Meteorological measurements

Photosynthetically active radiation (PAR), rainfall, temperature and relative humidity were available as part of long-term measurements at the site, carried out by CEH.

## 3.3 Results

### 3.3.1 *Miscanthus*

The time series of VOC fluxes above *Miscanthus* are shown in Figure 3-3 along with  $u^*$  and sensible heat flux. Two periods of missing data 21<sup>st</sup> – 22<sup>nd</sup> and 25<sup>th</sup> – 27<sup>th</sup> July were due to failure of the sampling pump. Data in the first few days were relatively noisy, showing no particular diurnal trend up to 20<sup>th</sup> July. This was likely due to elevated  $O_2^+$  impurities during transport of the instrument, due to air in the water vapour inlet system, resulting in less reliable primary ion counts or higher LOD. Additionally, episodes of rainfall on 17<sup>th</sup>, 18<sup>th</sup>, 20<sup>th</sup> and 22<sup>nd</sup> July may have resulted in a reduction in mixing ratio of VOCs where emission is proportional to PAR.

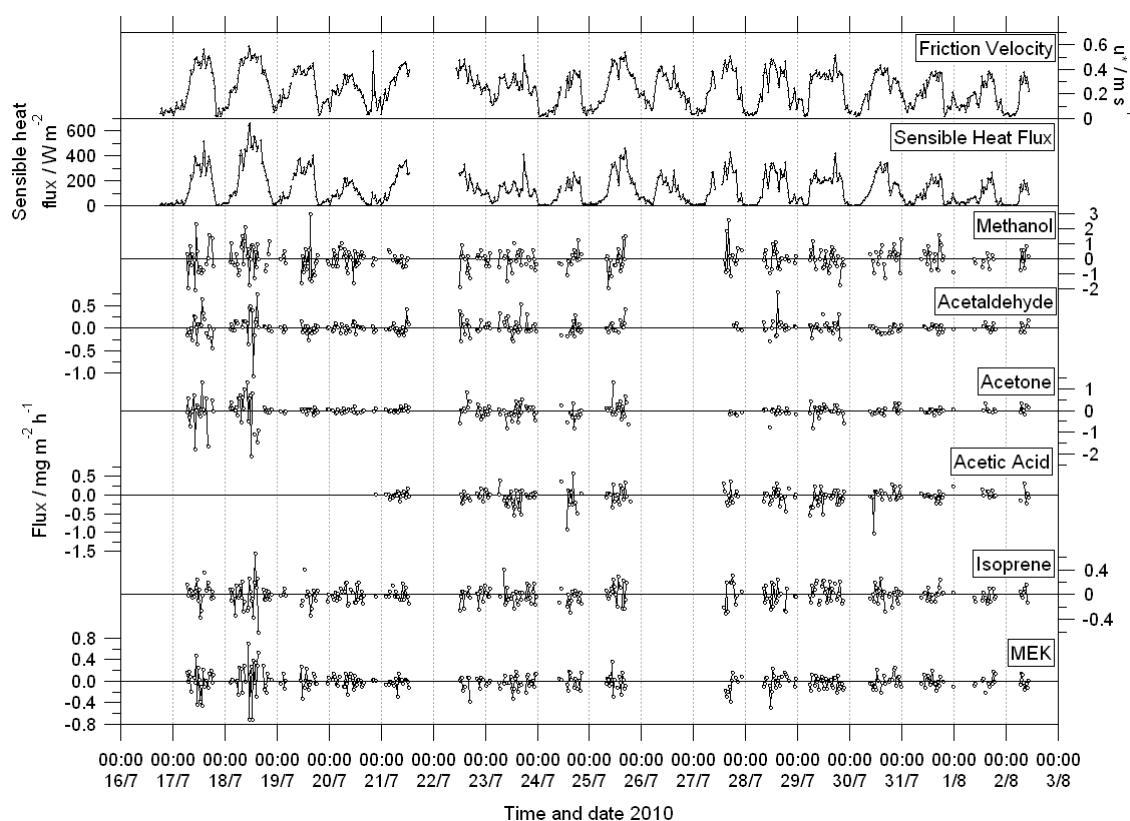


**Figure 3-3** Time series of VOC fluxes measured above *Miscanthus*. Dashed gridlines denote midnight. Note the variable flux scales. Note, spikes in data have been removed to allow day-to-day variation in fluxes to be seen more clearly. Data removed from this figure were still included in diurnal averaging (Figure 3-4).

Small net emissions of isoprene and MEK from *Miscanthus* during daytime were just discernible, most noticeable on 18<sup>th</sup> July when sensible heat flux was also at its maximum. However, in general, flux data were somewhat noisy for all VOCs measured, and mostly not significantly different from zero. The directionally-filtered diurnal averages of VOC fluxes are shown in Figure 3-4. As described earlier, the relevant sector for the *Miscanthus* measurements was south-west (180 – 270°). The mixing ratios of MVK+MACR (the first-generation oxidation products of isoprene) showed no diurnal pattern and were below LOD, so no data for these species are shown.

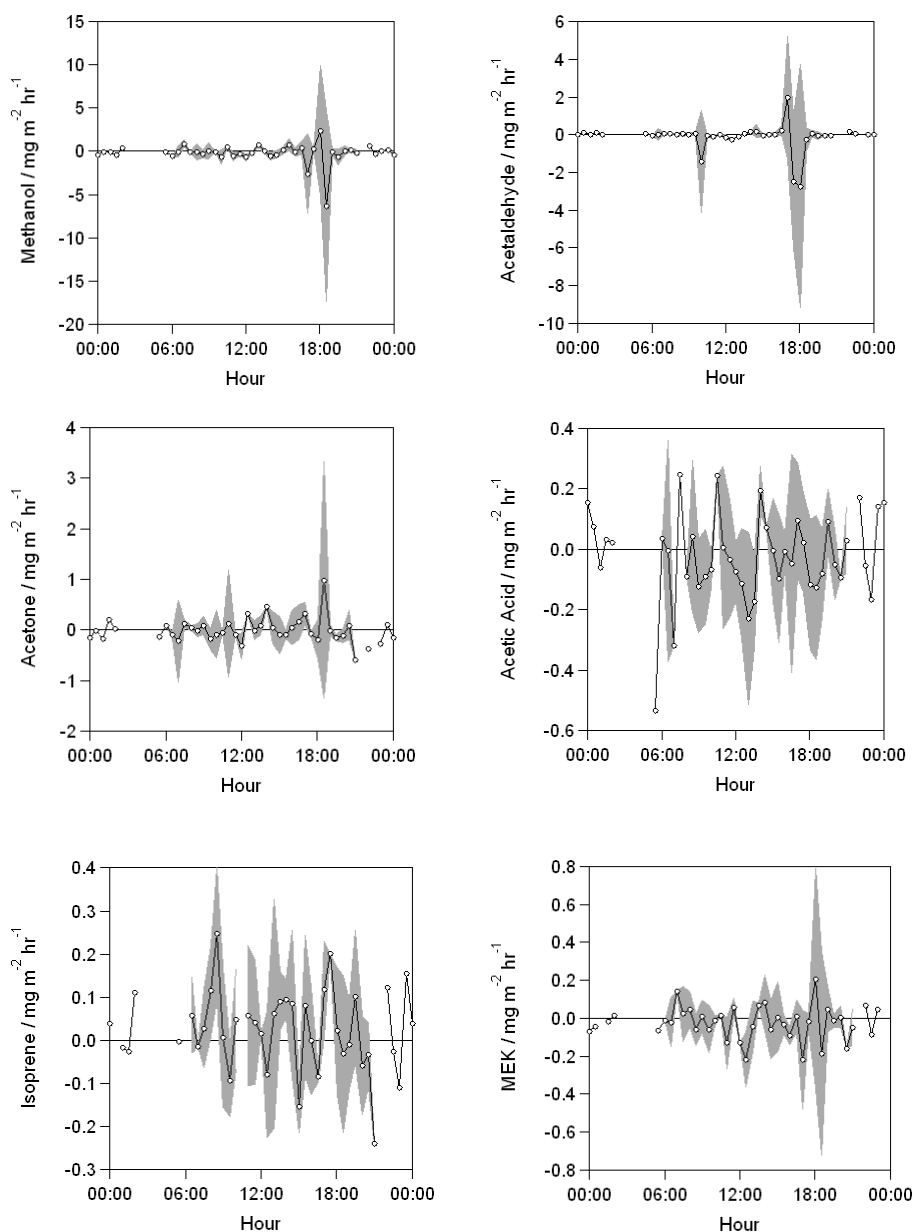


**Figure 3-4** Average diurnal profiles of VOC fluxes above *Miscanthus* when wind direction was between 180 and 270° (i.e. from over the *Miscanthus* field). Note the variable scales. Grey areas represent variability calculated as  $\pm 1$  sd of the averaged half-hourly values of all measurements. A profile for MVK+MACR is not included due to insufficient data.

The time series of VOC mixing ratios above *Miscanthus* are shown in Figure 3-5. For the period 27<sup>th</sup> July to 2<sup>nd</sup> August, mixing ratios of all measured VOCs had maxima at night except for isoprene whose mixing ratios were elevated in late afternoon.

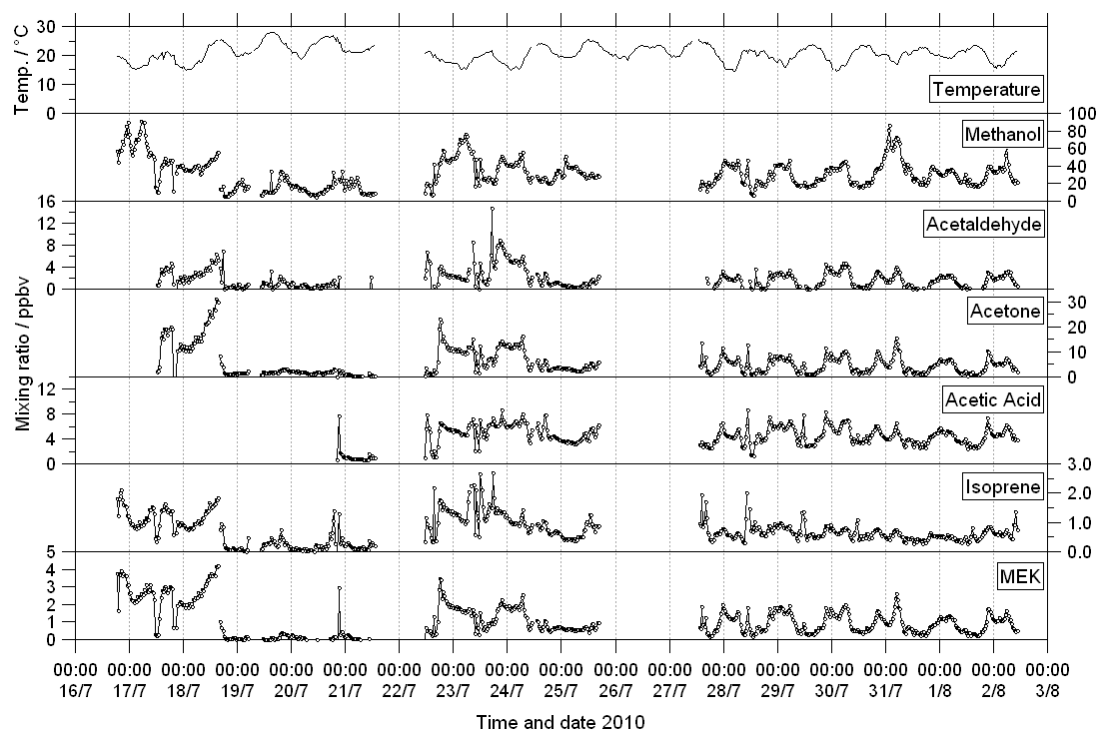


**Figure 3-5** Time series of VOC mixing ratios, and of temperature, measured above *Miscanthus*. Dashed gridlines denote midnight. Note the variable mixing ratio scales.

The average diurnal VOC mixing ratios above *Miscanthus* are shown in Figure 3-6. Methanol, acetaldehyde, acetone, acetic acid and MEK had similar diurnal profiles in mixing ratio. All showed a minimum mixing ratio around midday. The isoprene mixing ratio peaked around midday consistent with observation of a possible small isoprene flux above *Miscanthus* (Figure 3-4). No isoprene or monoterpenes were detected in the GC-MS analysis of adsorption tube sampling above the *Miscanthus* canopy.

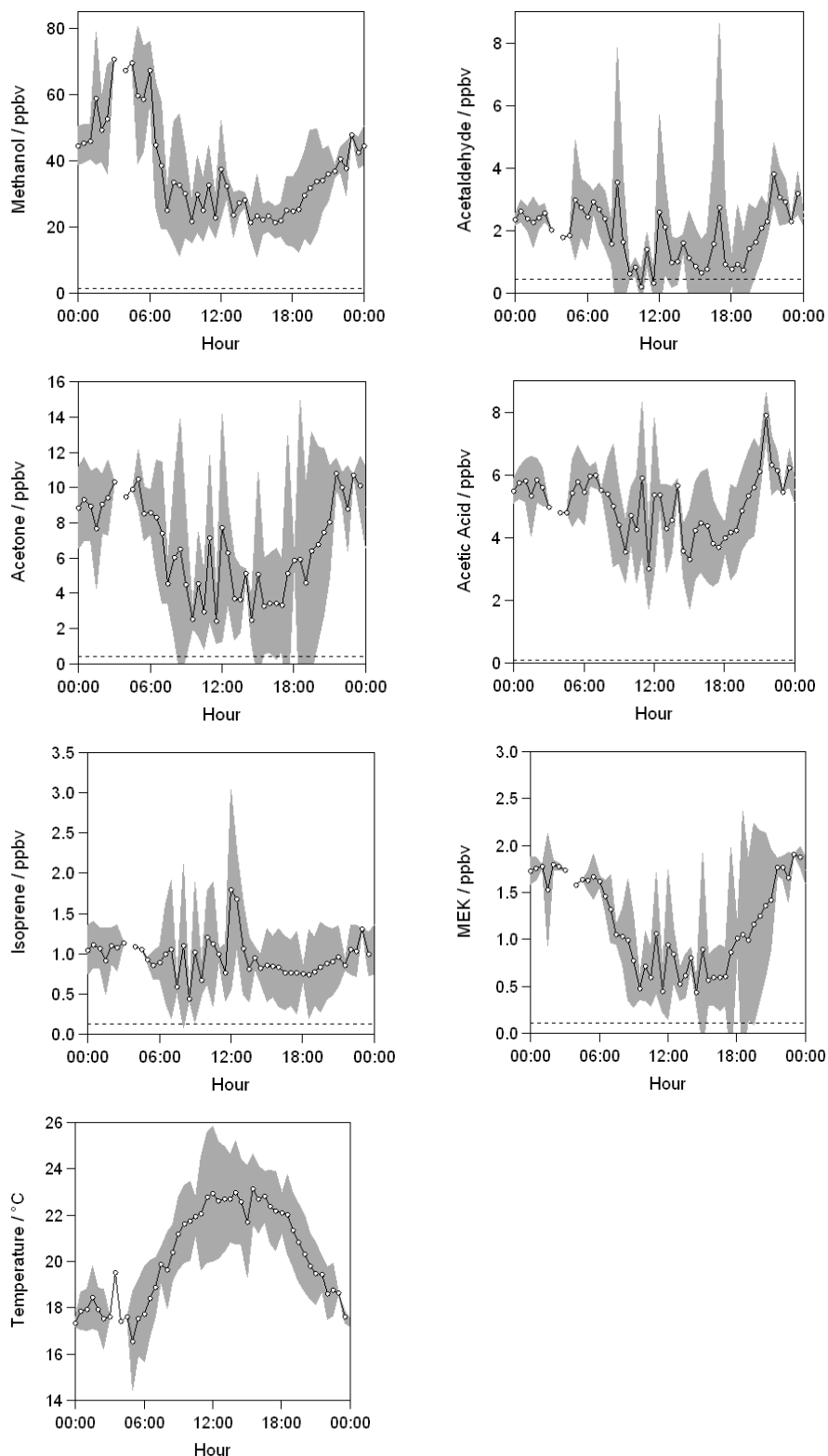


**Figure 3-6** Average diurnal profiles of VOC mixing ratios above *Miscanthus*, and of temperature, when wind direction was between 180 and 270° (i.e. from over the *Miscanthus* field). Note the variable scales. Dashed lines denote LOD. Grey areas represent variability calculated as  $\pm 1$  sd of the averaged half-hourly values of all measurements.

### 3.3.2 Short rotation coppice willow

The time series of VOC fluxes, and  $u^*$  and sensible heat, measured above willow are shown in Figure 3-7. Missing data on 10<sup>th</sup> and 12-13<sup>th</sup> August were due to failure of the mobile power supply.

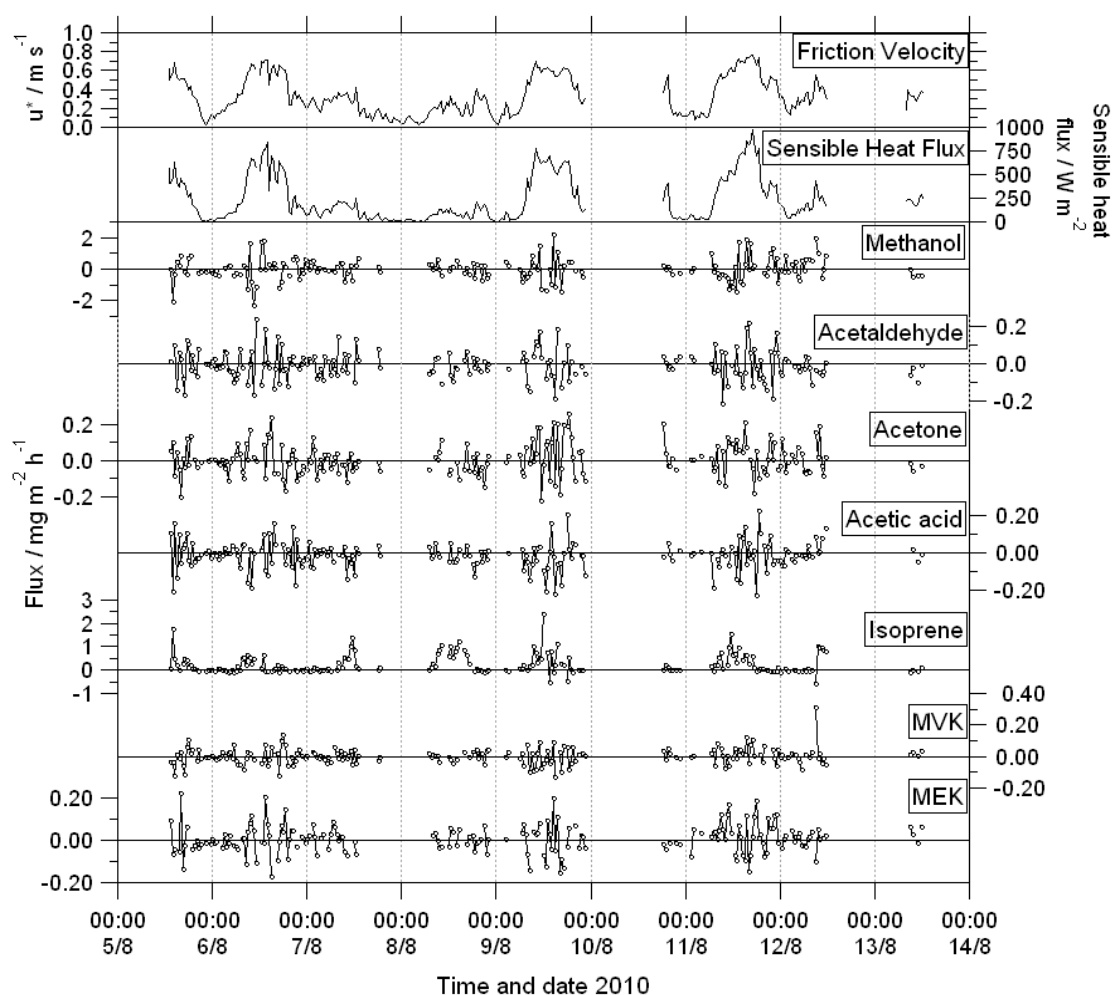


**Figure 3-7** Time series of VOC fluxes measured above willow canopy. Dashed gridlines denote midnight. Note the variable scales.

Data were directionally filtered to include only those from over the willow field (90 – 270°) before diurnally averaging (Figure 3-8). Willow showed a distinct diurnal pattern of isoprene flux, peaking at  $\sim 1 \text{ mg m}^{-2} \text{ h}^{-1}$  around midday and decreasing to zero overnight, driven by the strong dependence of isoprene emissions on temperature and PAR. All other VOC measured showed positive and negative fluxes throughout the day, with no significant net positive or negative daily flux overall.

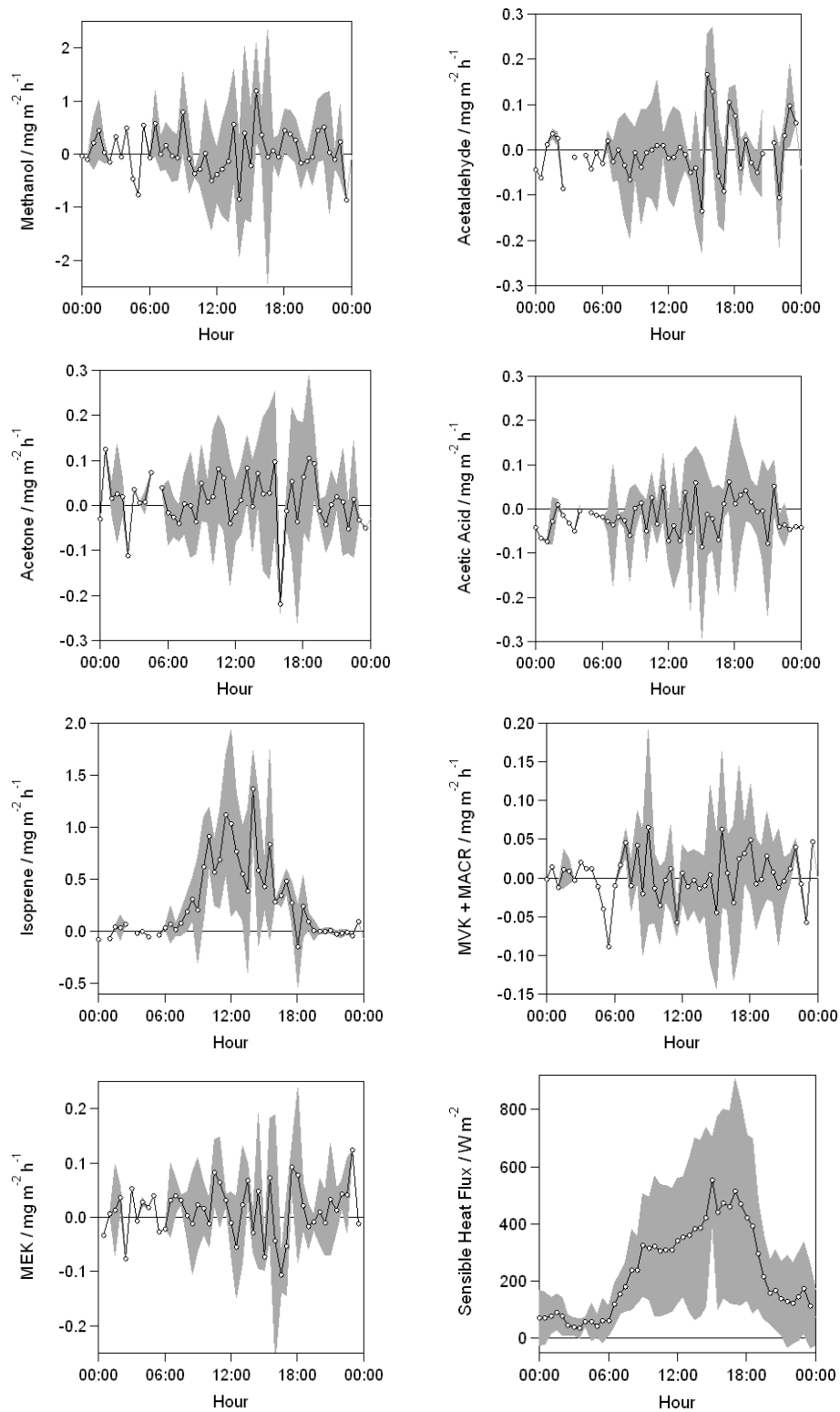


**Figure 3-8** Average diurnal profiles of VOC fluxes above willow, and of sensible heat flux, when wind direction was between  $90$  and  $270^\circ$  (i.e. from over the willow field). Note the variable scales. Grey areas show variability calculated as  $\pm 1$  sd of the averaged half-hourly values of all measurements.

Figure 3-9 shows the time series of VOC mixing ratios and temperature above SRC willow. The time series showed clear diurnality in mixing ratios of all VOCs measured, except for methanol.

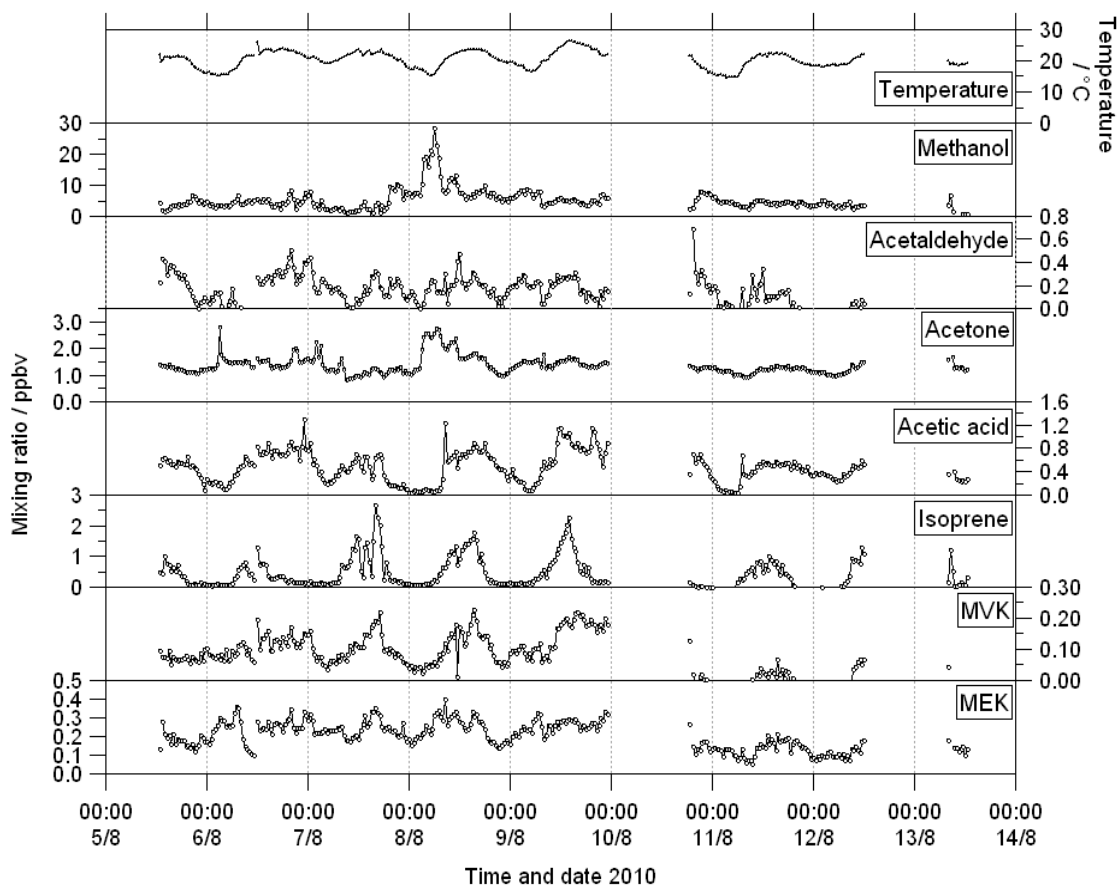


**Figure 3-9** Time series of VOC mixing ratios, and of temperature, measured above willow. Dashed gridlines denote midnight. Note the variable mixing ratio scales.

The directionally-filtered diurnal averages of mixing ratio over the willow are shown in Figure 3-10.

Isoprene had a dominant maximum mixing ratio in early afternoon ( $\sim 1$  ppbv), temporally coincident with the temperature profile, and low mixing ratios at night. Figure 3-10 also plots the isoprene mixing ratios determined by adsorption tube sampling and GC-MS analysis. There was good agreement. Small quantities of the monoterpenes  $\alpha$ -pinene and limonene were also detected by GC-MS, but no diurnal patterns were discernible in these data.

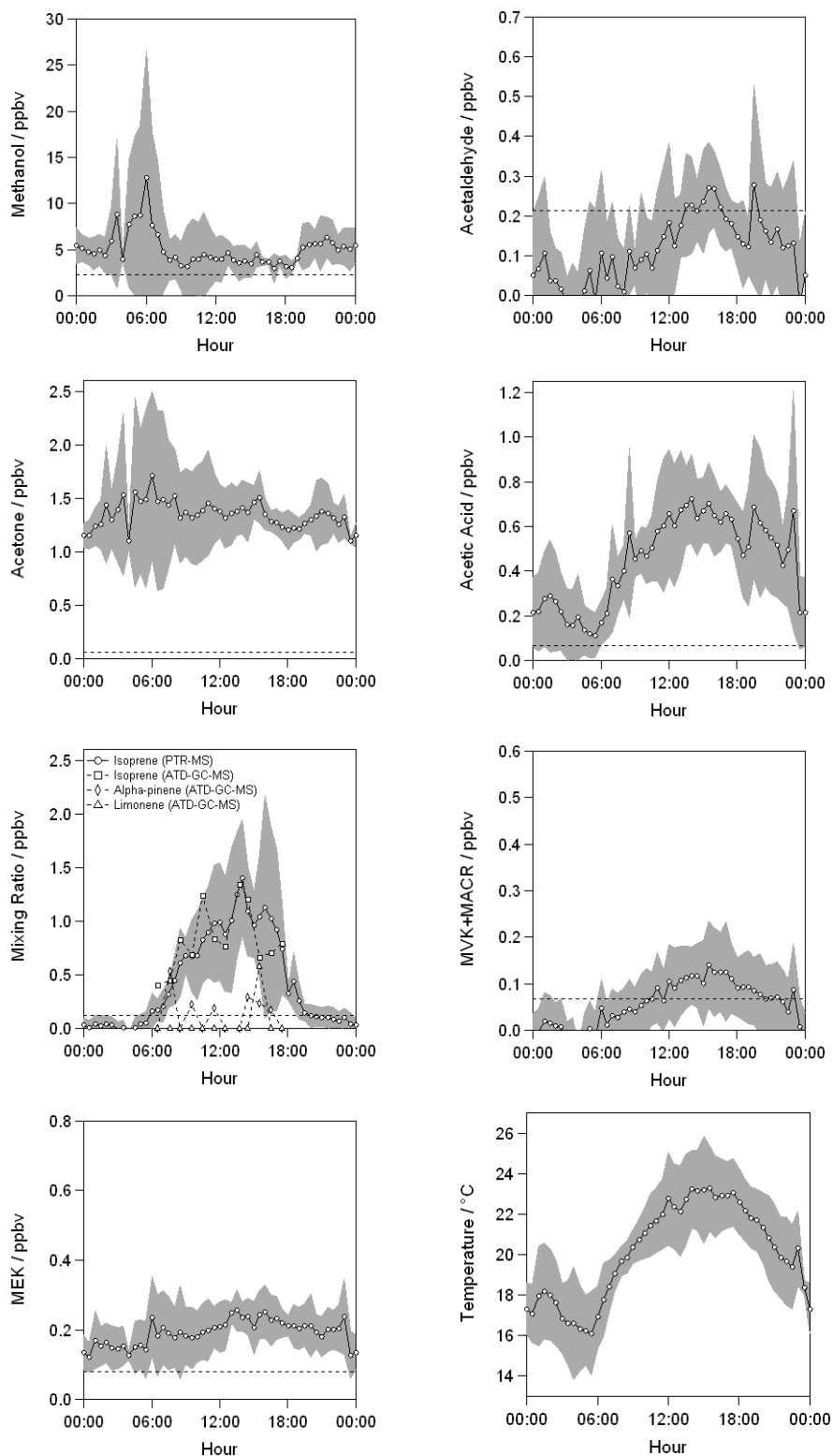


**Figure 3-10** Average diurnal profiles of VOC mixing ratios above willow, and of temperature, when wind direction was between 90 and 270° (i.e. from over the willow field). Note the variable scales. Dashed lines denote LOD. Grey areas represent variability calculated as  $\pm 1$  sd of the averaged half-hourly values of all measurements.

Acetic acid, acetaldehyde and MVK+MACR also showed diurnal profiles with maxima in the afternoon and minima around 6 am, closely mirroring daily temperature variation. The amplitude of the daytime maximum of MEK mixing ratio was considerably less. Acetone exhibited low diurnal variability but with the small maximum in early morning similar to the observation of *Miscanthus*.

As isoprene oxidation is the only known source of MVK and MACR, the ratio of MVK+MACR to isoprene mixing ratios can be used to examine the degree of isoprene oxidation (Figure 3-11).

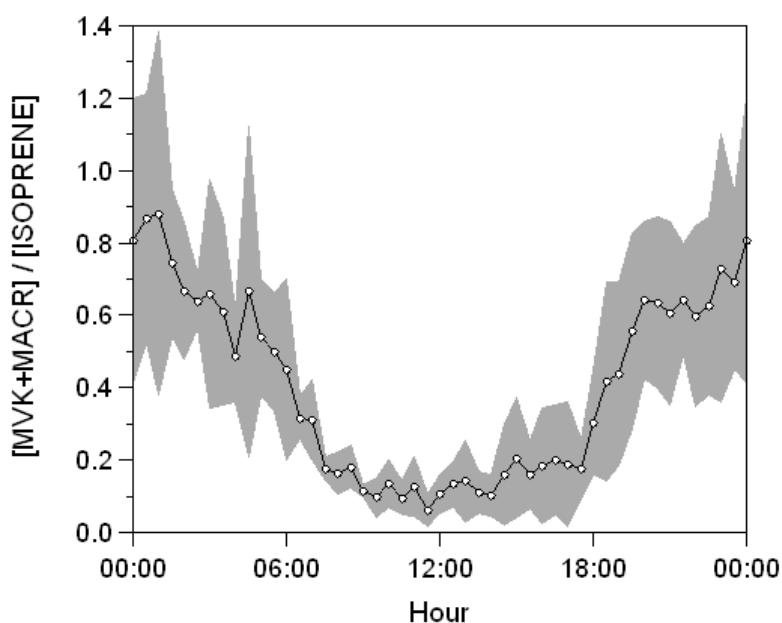


**Figure 3-11 Average diurnal profile of [MVK+MACR]:[isoprene] ratio above the willow canopy. Grey areas represent variability calculated as  $\pm 1$  sd of the averaged half-hourly values of all measurements.**

The [MVK+MACR]:[isoprene] ratio peaked around midnight with an average value of about 0.8 when isoprene was not being emitted and MVK+MACR were not undergoing photochemical loss or dispersion. At dawn there was a rapid decline in the ratio as the canopy responded to increasing PAR and temperature hence isoprene emissions increased, and the boundary layer depth also increased. The minimum ratio of  $\sim 0.1$  occurred for several hours around midday. The ratio rose in late afternoon as isoprene emissions declined but isoprene oxidation continued.

The average measured daytime [MVK+MACR]:[isoprene] ratio of 0.24 is comparable with those from other northern latitude studies. A daytime ratio of 0.23 was measured in a rural Canadian forest clearing (Biesenthal et al., 1998), 0.12 was reported for a mixed forest in Michigan, USA (Apel et al., 2002) and 0.4 – 0.8 in a deciduous forest in Pennsylvania, USA (Martin et al., 1991).

### 3.3.3 Standardised isoprene emission

As isoprene emission from plants is strongly influenced by light and leaf temperature, the canopy-level emission,  $F$ , was recalculated as a standard emission factor ( $\varepsilon$ ) normalised to a standard leaf temperature of 303 K and PAR flux of 1000  $\mu\text{mol m}^{-2} \text{s}^{-1}$ , as described by the G95 algorithm (Guenther et al., 1995),

$$\varepsilon = \frac{F}{D\gamma} \quad (3-1)$$

where  $D$  is foliar density ( $\text{g dry weight m}^{-2}$ ) and  $\gamma$  is a non-dimensional activity adjustment factor to account for the effect of light and temperature:

$$\gamma = C_L C_T \quad (3-2)$$

The light dependence,  $C_L$ , is defined by

$$C_L = \frac{\alpha c_L Q}{\sqrt{1 + \alpha^2 Q^2}} \quad (3-3)$$

where  $\alpha$  (0.0027) and  $c_{LI}$  (1.066) are empirical coefficients and  $Q$  is PAR flux ( $\mu\text{mol m}^{-2} \text{s}^{-1}$ ). The temperature dependence  $C_T$ , is defined by

$$C_T = \frac{\exp\left(\frac{c_{T1}(T - T_s)}{RT_s T}\right)}{1 + \exp\left(\frac{c_{T2}(T - T_M)}{RT_s T}\right)} \quad (3-4)$$

where  $T$  is leaf temperature (K),  $T_s$  is leaf temperature at standard conditions (303 K),  $R$  is the universal gas constant ( $8.314 \text{ J K}^{-1} \text{ mol}^{-1}$ ), and  $c_{T1}$  ( $95000 \text{ J mol}^{-1}$ ),  $c_{T2}$  ( $230000 \text{ J mol}^{-1}$ ) and  $T_M$  (314 K) are empirical coefficients.

Values of above-canopy PAR and temperature, and of isoprene flux (from Figure 3-8), at hourly intervals during the willow campaign were used for the calculation of  $\gamma$  and  $F$  respectively. Foliar density  $D$  was estimated at  $150 \text{ g}_{\text{dw}} \text{ m}^{-2}$  for *Salix spp.* (Karl et al., 2009). Hourly emission factors  $\varepsilon$  were then determined for isoprene from willow, and were found to have a peak value of  $25 \text{ } \mu\text{g g}_{\text{dw}}^{-1} \text{ h}^{-1}$  at 10:00. A mean midday value of  $20 \text{ } \mu\text{g g}_{\text{dw}}^{-1} \text{ h}^{-1}$  for  $12:00 \pm 2 \text{ h}$  was determined to allow comparison, in Table 3-2, with mean values from other studies.

Table 3-2 shows that the emission factor from this study was within the range of values derived previously for *Salix spp.* The slightly lower measurements derived in this work and in the other above-canopy study (Olofsson et al., 2005) were canopy-averaged emissions factors which included leaves which were in shade as well as those in direct sunlight. It was therefore expected that these measurements would result in lower standard emission factors than from individual branch or leaf-level experiments.

**Table 3-2 Comparison of standardised emission rates of isoprene from willow. REA = relaxed eddy accumulation.**

Species	Standard emission rate / $\mu\text{g g}_{\text{dw}}^{-1} \text{h}^{-1}$	Measurement type	Reference
<i>Salix</i> spp.	20	Canopy-scale, PTR-MS	This study
<i>Salix</i> spp.	28	Branch enclosure	(Owen and Hewitt, 2000)
<i>Salix alba</i>	18	Branch enclosure, lab conditions	(Pio et al., 1993)
<i>Salix alba</i>	37.2	-	(Karl et al., 2009)
<i>Salix babylonica</i>	115	-	(Winer et al., 1983)
<i>Salix caprea</i>	18.9	Branch enclosure	(Karl et al., 2009)
<i>Salix caroliniana</i>	12.5	Air-exchange branch enclosure	(Zimmerman, 1979)
<i>Salix nigra</i>	25.2	Whole plant, air-exchange chamber	(Evans et al., 1982)
<i>Salix phylicifolia</i>	32	Branch enclosure	(Hakola et al., 1998)
<i>Salix viminalis</i>	12	Canopy-scale, REA	(Olofsson et al., 2005)

### 3.4 Discussion

In the context of SRC willow as a bioenergy crop, the significant isoprene emission factor could potentially impact local and regional air quality by affecting tropospheric ozone production and SOA formation. Conventional agricultural crops are regarded as being low emitting species. For example, wheat and oats are estimated as having isoprene emission factors in the range 0 - 0.5  $\mu\text{g g}_{\text{dw}}^{-1} \text{h}^{-1}$  (Karl et al., 2009; König et al., 1995), while those for rapeseed, rye and barley are zero (Karl et al., 2009; Kesselmeier and Staudt, 1999). Replacement of conventional crops with SRC willow would therefore result in increased isoprene emission. A recent study examined the impact of SRC crop cultivation in Europe (Ashworth et al., 2012). It was concluded that monthly mean increases in ozone and BSOA (+1% and +5% respectively) from low level planting scenarios were significant enough to affect regional air quality and therefore warrant consideration in short term local impact assessments, as well as life cycle analysis of bioenergy crops.

At the end of 2009, total UK plantings of *Miscanthus* and SRC willow were 12,700 and 6,400 ha respectively (DEFRA, 2009). A government report stated that there is potential in the UK to increase bioenergy crop cultivation substantially by a further 350,000 ha by 2020, accounting for ~6% of total UK arable land (DEFRA, 2007), with the assumption that 70% would be *Miscanthus* and SRC willow (Rowe et al., 2009). In the case of 70% being converted solely to SRC willow, then a UK-wide increase of up to 7.35 tonne  $\text{h}^{-1}$  in emissions of isoprene would result (assuming zero isoprene emissions from the land prior to conversion to willow, 150  $\text{g}_{\text{dw}} \text{m}^{-2}$  willow, and an isoprene standard emission rate of 20  $\mu\text{g g}_{\text{dw}}^{-1} \text{h}^{-1}$  determined here). This UK-wide increase can be treated as a maximum hourly increase in isoprene emission, since the standardised emission factor assumes a temperature of 30 °C, much higher than UK annual mean of 8.6 °C (1971 – 2000 average<sup>5</sup>). An improved and more realistic scale-up model could be done by obtaining real temperature and PAR data for regions of the UK where bioenergy crops are likely to be planted. Emission rate

---

<sup>5</sup> [www.metoffice.gov.uk](http://www.metoffice.gov.uk)

will also vary throughout the year according to stage in the plant life cycle in addition to monthly variation in temperature and PAR.

Total VOC emissions in the UK are estimated at 751,000 tonnes annually (DEFRA, 2013). Solvents are the main emission source, accounting for 46 %, with fossil fuel extraction, industrial processes and road transport combined contributing 39 %. Biogenic emission sources of VOCs in the UK are not reported therefore can be regarded as negligible in comparison to anthropogenic sources. The importance of any predicted increase of isoprene due to increased bioenergy crop planting is therefore likely to be of low significance. In the extreme scenario described above, a UK-wide increase of 7.35 tonne h<sup>-1</sup> would account for a maximum of 8.6 % of current annual UK VOC estimates. Clearly, the contribution will be much lower than this if real temperature and PAR data, and the limited growing season of the crop are considered.

The standard emission factor for isoprene from SRC willow measured in this study was 26.5 g C ha<sup>-1</sup> h<sup>-1</sup>. This is an order of magnitude higher than was determined for total emission of VOCs from the biofuel crop switchgrass (Eller et al., 2011), where emissions were dominated by oxygenated VOCs and isoprene contributed less than 8%. Low VOC fluxes from *Miscanthus* were also reported in a recent study (Crespo et al., 2012), with modest emissions of methanol, acetaldehyde and acetone in the same order of magnitude as for switchgrass (Eller et al., 2011).

For *Miscanthus*, the near-zero values of flux at night were in contrast to the increase in mixing ratios of oxygenated VOCs (Figure 3-5 and Figure 3-6). Since reliability of the eddy covariance technique depends on friction velocity, the greater boundary layer stability at night (hence low friction velocity) resulted in unreliable night time flux measurements. It may therefore be possible that night time fluxes were non-zero. A more likely scenario is that increasing VOC mixing ratios at night were affected by sources in the wider area. Towards the start of the measurement period, several of the surrounding fields were subject to harvesting and subsequent ploughing activities, which are known to be a source of oxygenated VOCs (Karl et al., 2001). Mixing ratios of methanol, acetaldehyde and acetone were comparable to

those measured in previous field experiments of crop cutting (Warneke et al., 2002). The enhanced mixing ratios towards dusk, and at night can be explained by reduced radical sink chemistry, together with accumulation within a shallower nocturnal boundary layer from reduced vertical transport and mixing, as demonstrated by the lower wind speed and  $u^*$  at night (Figure 3-3). During willow measurements, atypical increases in mixing ratios of methanol, acetone and acetic acid on 8<sup>th</sup> August may also have been caused by further harvesting activity in the wider area.

### 3.5 Conclusions

Measurements of above-canopy fluxes and mixing ratios of VOCs revealed significant emissions of isoprene from short rotation coppice willow, with a standard emission factor of  $20 \mu\text{g g}_{\text{dw}}^{-1} \text{h}^{-1}$ . No significant emissions were measured from *Miscanthus*. This is the first field study of bioenergy crops in the UK and shows that a change in land use from conventional to bioenergy crops could result in increased isoprene emissions. Bioenergy crop species choice should therefore include consideration of their impact on regional air quality. Further work could include measurement of VOC emissions from *Miscanthus* and SRC willow during senescence and harvesting.

## Chapter 4: VOC emissions from a temperate peat bog

In this chapter, results from a field experiment are presented. Static enclosure measurement using adsorbent tubes and GC-MS analysis were used to determine fluxes of isoprene and monoterpenes from an ombrotrophic bog at Whim Moss, ~30 km south of Edinburgh, UK. Standardised (30 °C and 1000  $\mu\text{mol m}^{-2} \text{s}^{-1}$ ) emission factors were 590 and 1.5  $\mu\text{g m}^{-2} \text{h}^{-1}$  for isoprene and monoterpenes, respectively. The effects of wet  $\text{NO}_3^-$  or  $\text{NH}_4^+$  treatment (equivalent to 64 kg N  $\text{ha}^{-1} \text{y}^{-1}$ ) on VOC emissions was also investigated and it was found that both nitrate and ammonium treatment reduced isoprene emissions, while nitrate treatment increased  $\beta$ -pinene emission compared to control plots experiencing only background deposition of N (measured to be 8 kg N  $\text{ha}^{-1} \text{y}^{-1}$ ). Increasing atmospheric nitrogen concentrations are therefore predicted to have an impact on VOC emission.

### 4.1 Introduction

Boreal and subarctic peatlands are estimated to be a significant carbon store covering an estimated 350 million hectares globally (Gorham, 1991) and storing 270 to 370 Pg C (Turunen et al., 2002). Their high carbon storage ability, even in waterlogged conditions, has led to methane and carbon dioxide fluxes from peatlands to be well studied. Despite their extensive coverage and known carbon store, however, very little work has focused on investigating the potential for peatlands to emit non-methane VOCs.

Some Finnish studies have investigated BVOC emissions from peatlands and the impact of changing environmental factors on these emissions. A microcosm experiment (Tiiva et al., 2007b) investigated the effect of elevated ozone exposure on isoprene emissions, for mixed *Sphagnum papillosum* and *Eriophorum vaginatum*. It was found that, although increased ozone exposure did not significantly affect isoprene emissions over two consecutive growing seasons, there was some evidence that when also coupled with warmer weather conditions, isoprene emissions were larger and more variable.

To determine possible effects due to the depletion in stratospheric ozone – particularly at high latitudes – the same group also found that under enhanced UV-B exposure, isoprene emissions increased from peatland dominated by *Warnstorfia exunnulata*, *Eriophorum russeolum* and *Carex limosa* (Tiiva et al., 2007a). Again, the effect was particularly pronounced in conjunction with warm weather. The same species were also found to be a source of 16 different VOCs (Faubert et al., 2010a), though emissions were modest in comparison to isoprene. It was also determined that enhanced UV-B had no overall effect on BVOC emissions (excluding isoprene), although variable water-table depths were found to influence emissions (Faubert et al., 2010a; Faubert et al., 2010b).

Nitrogen emissions have increased rapidly since the 19<sup>th</sup> century due to agriculture and fossil fuel combustion (Fowler et al., 2004), with these anthropogenic sources now exceeding natural sources globally by nearly a factor of two (Galloway, 1998). Increased atmospheric N can enter ecosystems as either wet (via precipitation) or dry (as a gas or aerosol) deposition and can be in the reduced ( $\text{NH}_x$ : e.g.  $\text{NH}_3$  or  $\text{NH}_4^+$ ) or oxidised ( $\text{NO}_y$ : e.g.  $\text{NO}$ ,  $\text{NO}_2$ ,  $\text{HNO}_3$ ) form (Stevens et al., 2011). Due to increased food demand, the increase in terrestrial deposition of both reduced and oxidised N is predicted to continue by up to 133% and 70% of 1990s level by 2050, respectively (Galloway et al., 2004; Stevens et al., 2011).

Increased N deposition has been shown in many studies to have an impact on plants (Leith et al., 2001; Leith et al., 1999; Stevens et al., 2011; Van Den Berg et al., 2005). However, no studies of the effect of enhanced N deposition on VOC emissions could be found for peatland vegetation, although there have been studies on the effect of N *availability* on VOC emissions for other vegetation types. For example, Lerdau et al. (1995) investigated the effect of nitrogen availability on Douglas fir in a greenhouse study. It was reported that higher nitrogen treatment resulted in higher leaf monoterpene concentrations, and greater resultant fluxes. Nitrogen treatments were supplied by addition of fertiliser solution through the soil.

Although no studies report the effect of nitrogen deposition on VOC emissions, previous studies have shown that N deposition onto upland species resulted in

increased above-ground biomass for some plant species (as dry  $\text{NH}_3$  and wet  $\text{NH}_4\text{Cl}$  (Leith et al., 2001), and wet  $\text{NH}_4\text{NO}_3$  (Leith et al., 1999)). It is reasonable to hypothesise therefore that there may be some resultant effect on VOC emissions.

The aim of this work was to measure isoprene and monoterpene fluxes from a Scottish peatland. An established field experiment was deemed to be suitable for also investigating the impact of separate enhanced  $\text{NO}_3^-$  and  $\text{NH}_4^+$  deposition on VOC emissions from peatland vegetation (Sheppard et al., 2004).

## 4.2 Methods

### 4.2.1 Site location and description

The field site was Whim Moss (Figure 4-1), located ~30 km south of Edinburgh ( $3^\circ 16' \text{W}$  and  $55^\circ 46' \text{N}$ ), 280 m amsl, with average annual rainfall of 900 mm. The ombrotrophic bog is described as being transitional between lowland raised and blanket bog.

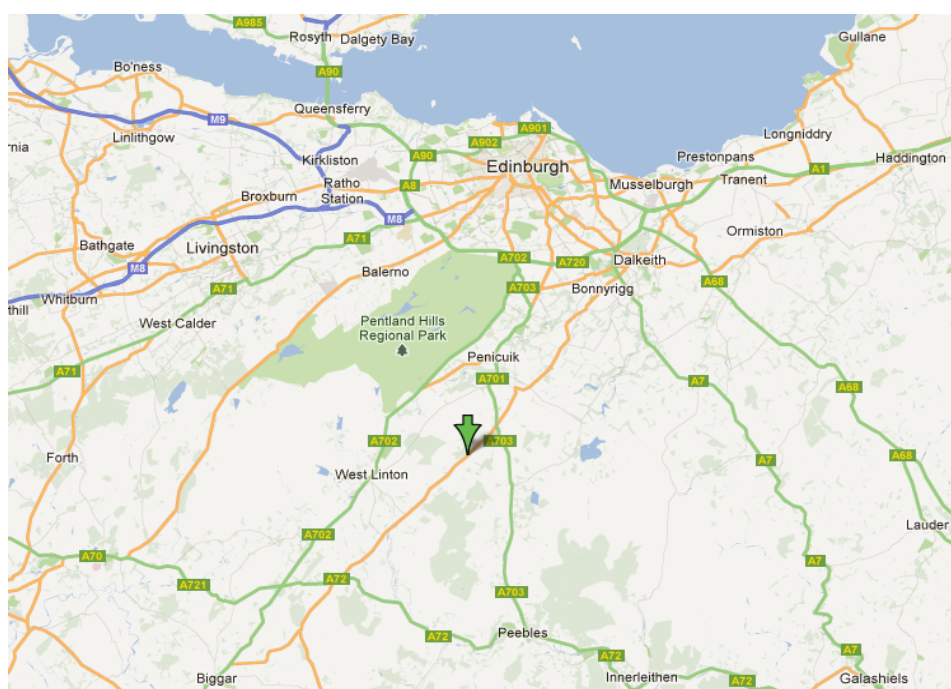


Figure 4-1 Location of Whim Moss experimental field site in relation to Edinburgh. (Attributable to ©2012 Google).

Experimental plots cover a total area of ~0.5 ha and are accessed using a 1 km network of boardwalks to avoid damage to vegetation and hydrology (Figure 4-2). The site was set up as a research facility in 2002 and experimental N treatments are on-going (Sheppard et al., 2004). The following meteorological parameters are continuously recorded: rainfall, wind speed and direction, air and soil temperature, and solar and net radiation.



**Figure 4-2** Aerial view of Whim Moss field site, showing the boardwalk layout, within which 44 sampling plots are arranged. (Map attributable to ©2013 DigitalGlobe, Getmapping plc. Map data ©2013 Google).

### 4.2.2 N-treatment plots

A schematic diagram of the plot layout is shown in Figure 4-3. The field site uses automated sprinklers to supply dilute solutions containing  $\text{NH}_4^+$  or  $\text{NO}_3^-$  – coinciding with rain events – to a series of 44 plots (4 replicate blocks of 11 treatments; see Figure 4-3). Plots are treated with 8, 24, or 56  $\text{kg N ha}^{-1} \text{y}^{-1}$  (in addition to the ambient background deposition of 8  $\text{kg N ha}^{-1} \text{y}^{-1}$ ) as either reduced ( $\text{NH}_4\text{Cl}$ ) or oxidised ( $\text{NaNO}_3$ ) nitrogen. In addition, 8 and 56  $\text{kg N ha}^{-1} \text{y}^{-1}$  plots are treated with P and K as  $\text{K}_2\text{HPO}_4$ . Circular plot areas ( $12.5 \text{ m}^2$ ) are placed 3 m apart, and assigned

as adjacent pairs of oxidised and reduced N treatments. Plots are otherwise randomly assigned within each replicate block.

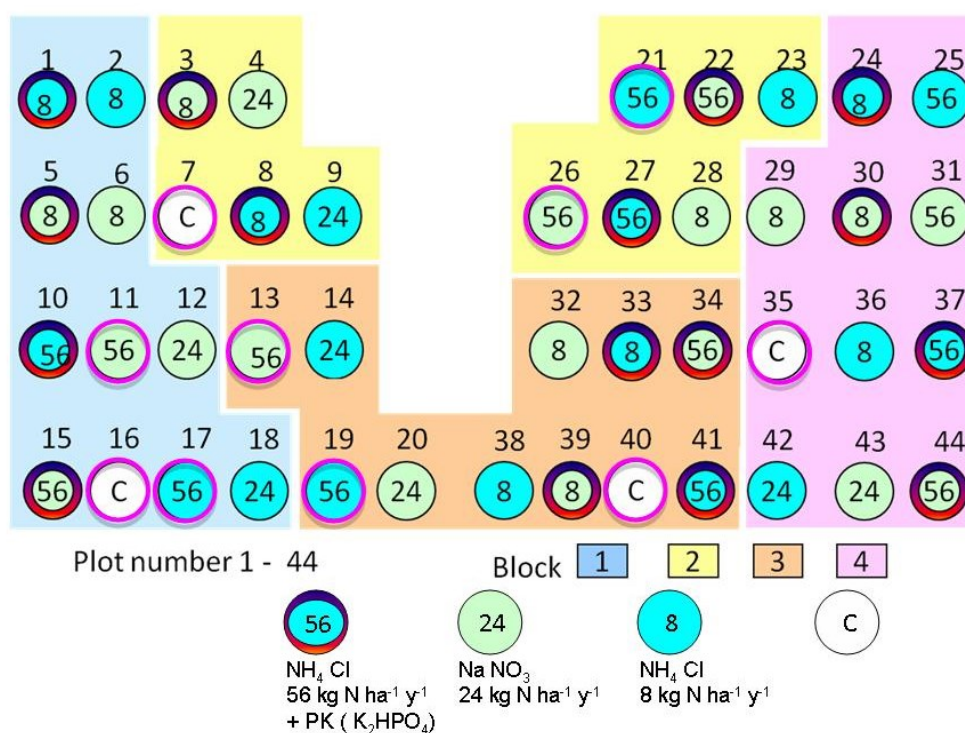


Figure 4-3<sup>6</sup> Schematic diagram showing treatment plots at Whim Moss. Plots are numbered 1 to 44, and are arranged in 4 replicate blocks. Numbers inside the circles indicate the deposition treatment received (kg N ha<sup>-1</sup> y<sup>-1</sup>) in addition to the 8 kg N ha<sup>-1</sup> y<sup>-1</sup> background deposition. The colour of the circle indicates whether N was in reduced NH<sub>4</sub>Cl (turquoise) or oxidised NaNO<sub>3</sub> (pale green) form, or were control plots (C) receiving no additional treatment other than background N (8 kg N ha<sup>-1</sup> y<sup>-1</sup>). A purple/red outer circle shows plots which also received P and K. Plots circled pink indicate the plots used in this study.

A more detailed description of the treatment system is available elsewhere (Sheppard et al., 2004). Only control plots 7, 16, 35, 40, reduced NH<sub>4</sub><sup>+</sup> plots 17, 19, 21 and NO<sub>3</sub><sup>-</sup> plots 11, 13 and 26 were used during this study (as indicated by pink outer circles in Figure 4-3).

<sup>6</sup> Acknowledgements to Lucy Sheppard, CEH Edinburgh.

### 4.2.3 Plot sampling

Sampling visits to the site were carried out on 24 October (13:20 to 14:56) and 14 November 2011 (10:29 to 11:45), when only control plots were sampled (plots 7, 16, 35, and plots 7, 16, 35 and 40, on the two visits, respectively).

A comparative study to investigate diurnality of fluxes from different sample treatment plots was carried out on 22 July 2011. Samples were simultaneously taken from control, and  $\text{NH}_4^+$  and  $\text{NO}_3^-$  treated plots at 3 points throughout the day, according to the sampling plan shown in Table 4-1.

**Table 4-1 Sampling plan of  $\text{NO}_3^-$ ,  $\text{NH}_4^+$  and control plot comparison study carried out at Whim Moss on 22 July 2011. Plots with  $56 \text{ kg N ha}^{-1} \text{ y}^{-1}$  ammonium or nitrate treatment were investigated. Three replicates of each treatment type were used, and plots of the same treatment type were sampled simultaneously at the start (T1) and end (T2) of the enclosure time (mins from start of experiment).**

	Plot Number								
	Block 1			Block 2			Block 3		
	11 ( $\text{NO}_3^-$ )	16 (C)	17 ( $\text{NH}_4^+$ )	26 ( $\text{NO}_3^-$ )	7 (C)	21 ( $\text{NH}_4^+$ )	13 ( $\text{NO}_3^-$ )	40 (C)	19 ( $\text{NH}_4^+$ )
T1	0	15	30	0	15	30	0	15	30
T2	60	75	90	60	75	90	60	75	90

T1 and T2 denote the times in minutes from the start of the experiment at which sampling commenced. Three replicates of each treatment type were taken (blocks 1, 2 and 3) with three people starting a sampling sequence simultaneously (one person per block). All four blocks could not be sampled due to limits on the number of people and equipment available to take simultaneous samples. Sampling time was 10 min, therefore sequential sampling of nitrate, control and ammonium plots were synchronized at 15 minute intervals, as were the 10 min T2 sampling points after the enclosure time. This allowed 10 min for sampling and 5 min set-up time between each sample plot. The entire sampling sequence of 9 plots, shown in Table 4-1, was carried out at start points of 09:00, 12:00 and 15:00 to examine diurnality. Enclosure of plots and sampling was therefore carried out 09:00 to 10:40, 12:00 to 13:40 and

15:00 to 16:40. This allowed for chamber lids to be removed from the sampling collars for 1 h 20 min between each time step.

Further comparative samples were collected on 1 and 6 February 2012, when two duplicates of  $\text{NH}_4^+$  (plots 11 and 26),  $\text{NO}_3^-$  (plots 17 and 21) and control (plots 7 and 16) samples were taken between 10:00 and 11:40.

Temperature and PAR data were available for all sampling days from ongoing long-term measurements at the site, and represent ambient rather than in-chamber conditions.

## **4.2.4 Chamber sampling**

### **4.2.4.1 Field measurements**

The set-up used during chamber sampling is illustrated in Figure 4-4. Soil sampling collars (diameter 39.5 cm) remained inserted into the peat permanently and were randomly positioned within each of the measurement plots. At the time of flux measurement, a transparent, polystyrene chamber (33 L) was placed on a soil collar. Commercially available, bell-shaped, gardening cloches were modified for use as static chambers. Sampling valves from Tedlar™ sampling bags were affixed to the top of the sampling chambers. Foam adhesive sealant was placed around the base of the chambers to provide a more effective seal between the chambers and soil collars.

With the chamber sampling valve open, an adsorbent sample tube (6 mm OD) packed with 200 mg Tenax TA and 100 mg CarboTrap (Markes International Ltd., UK) was connected inline and a 2 L sample of air was pre-concentrated onto the tube using a mass-flow controlled Pocket Pump (210-1000 Series SKC Inc., USA) by sampling at  $200 \text{ mL min}^{-1}$  for 10 min. The valve was then closed before removing the sample tube. The chamber remained in place for 1 h before collecting another sample, resulting in a total enclosure time of 1 h 10 min. All packed tubes had been conditioned at  $300 \text{ }^\circ\text{C}$  for 15 min with a flow of helium prior to use for sampling.



**Figure 4-4** Experimental set-up used during sampling of a chamber enclosure. A transparent, polystyrene chamber (33 L) was positioned onto a soil collar (which remains in the soil permanently). A mass-flow controlled pump was used to draw a 2 L air sample through an adsorbent tube, connected in-line to the sampling valve at the top of the chamber.

#### **4.2.4.2 Effect of chamber on radiative transmission**

Because VOC emissions are dependent on PAR and temperature, chambers used for static enclosure sampling ideally need to be transparent to PAR. The optical transmission of the polystyrene material from which the chambers were made was investigated by analyzing a small piece of chamber material in a bench-top UV-visible spectrophotometer in the range 200 – 900 nm to encompass the PAR region (400 – 700 nm). Figure 4-5 shows that mean absorbance in the PAR region is 0.14, indicating that ~72 % PAR is transmitted through the chamber material.

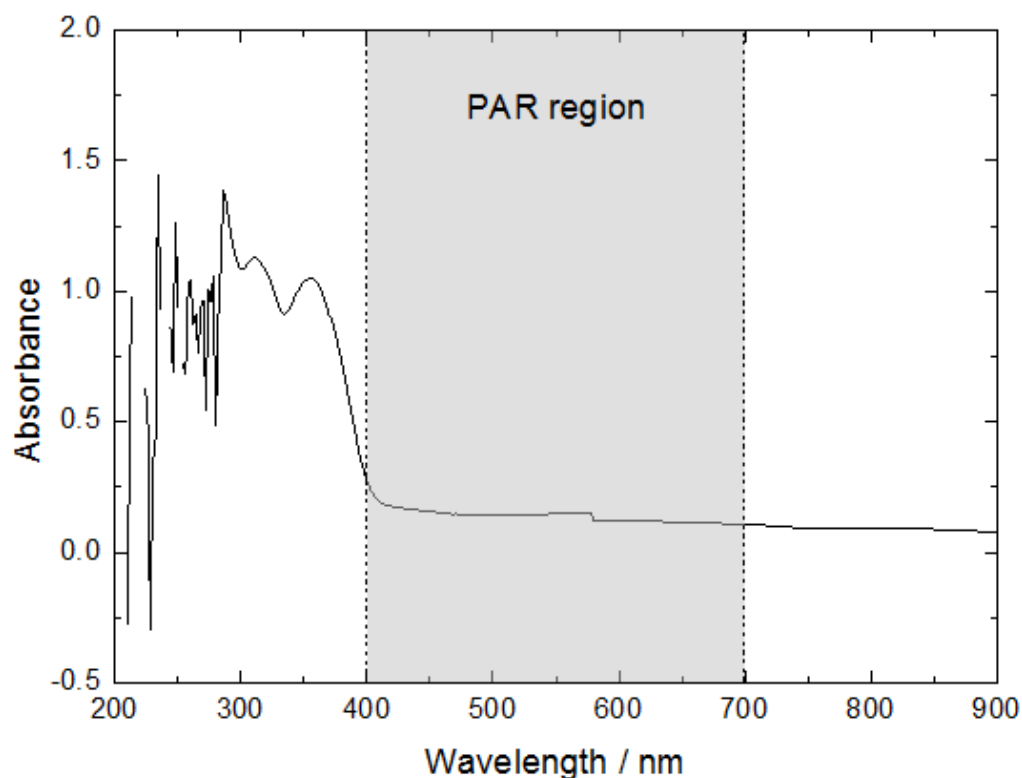


Figure 4-5 Absorption of radiation in the UV-visible range by the polystyrene chamber material. The grey region (400 - 700 nm) indicates the wavelengths of photosynthetically active radiation (PAR).

#### 4.2.4.3 Effect of chamber on VOC adsorption

The chamber material was also assessed for VOC adsorption. Ideally, equipment used for VOC sampling should be inert to the analyte, so that loss of sample to surfaces is avoided and also to ensure there is no carry-over, where VOCs may stick to a surface during sampling, then desorb during subsequent sampling at another sample site.

The chambers were tested for VOC adsorption in the laboratory by placing two chambers onto an inert Teflon surface, before pre-concentrating a 2 L sample of air from each onto adsorbent tubes (as described in Section 4.2.4.1). Isoprene (500 mL) was then added to one of the chambers and ambient air (500 mL) to the other. Another 2 L sample was then taken from each chamber after around 1 min. Both chambers were then inverted to allow flushing in ambient air for 3 min before placing them back on the Teflon surface to take a final 2 L sample.

Both chambers had approximately the same concentration of isoprene at the start ( $2.28 \pm 0.08$  ppbv). The concentration in the chamber to which isoprene had been added increased to 6.00 ppbv (the concentration in the control chamber was 2.67 ppbv) and after flushing, the concentration was 0.66 ppbv (1.04 ppbv in the control chamber).

As the chamber which had been injected with isoprene did not have an elevated mixing ratio after flushing, it can be assumed that there was no substantial carry over effect due to adsorption of isoprene on the chamber surface. The chamber mixing ratio did not however increase as much as expected. Given the known quantity of isoprene added and the volume of the chamber, an increase to  $\sim 12.5$  ppbv would have been expected yet the mixing ratio only increased to around half that. This could be explained by inadequate mixing of the isoprene in the chamber after injection, or from a poor seal between the chamber and the Teflon surface, resulting in some sample leakage.

#### **4.2.4.4 Sampling enclosure time**

Chamber enclosure time needed to be long enough to allow concentrations of VOCs to be high enough to be analytically detectable but not be too long to interfere significantly with plant biology. For example, enclosing for too long may have resulted in an increased temperature or humidity, thus altering the natural VOC flux.

Due to their higher atmospheric concentrations, sampling for atmospheric gases such as  $\text{CO}_2$  or  $\text{CH}_4$  requires only a small volume, so several samples can be collected throughout the enclosure period to give a more accurate representation of how flux varies with time. However, because a relatively large sample volume is needed to pre-concentrate VOCs, sampling multiple time points throughout an enclosure period would result in a significant dilution effect due to the removal of a large proportion of the chamber headspace. This could have a feedback effect on flux of VOCs from the vegetation under study.

The trade-off between accurately time-resolved fluxes versus sample dilution effects was investigated. 2 L samples were collected at time = 0 and 135 min from

enclosures at 3 different plots. On the same 3 plots (on a different day with similar weather conditions) the enclosure period was again kept constant, but 2 L samples were collected at time = 0, 45, 90 and 135 min.

It was observed that flux initially increased with increasing enclosure time before falling slightly by 135 min. However, due to sampling logistics and for practical reasons it was decided that collecting multiple time-point samples was not feasible. Therefore samples at time = 0 and 60 min were taken throughout this study.

#### **4.2.5 Sample analysis and flux calculations**

Analyses of sampling tubes were carried out using a Hewlett-Packard 5890/5970 GC-MS with an automated thermal desorption unit (ATD 400, Perkin Elmer) connected via a 200 °C heated transfer line. Transfer of samples from the adsorbent tubes was performed in two steps: heat to 280 °C for 5 min at 25 mL min<sup>-1</sup> to desorb samples onto a Tenax-TA cold trap at -30 °C, followed by transfer to the GC column by heating the trap at 300 °C for 6 min. Chromatographic separation utilised an Ultra-2 column (Agilent Technologies, 50 m × 0.2 mm ID × 0.11 µm film, 5% phenylmethyl silica) and a temperature program of 35 °C for 2 min, heat at 5 °C min<sup>-1</sup> to 160 °C, heat at 10 °C min<sup>-1</sup> to 280 °C, and hold for 5 min.

Calibration was carried out using a mixed monoterpene in methanol standard (10 ng µL<sup>-1</sup> α-pinene, β-pinene, α-phellandrene, 3-carene and limonene (Sigma Aldrich, UK)) and an isoprene in nitrogen gas standard (700 ppbv, BOC Gases, UK). Aliquots of the monoterpene standard (0, 1, 3 and 5 µL) were injected onto 4 adsorbent tubes with helium carrier gas. Tubes continued to be purged with helium for 2 min after the standard injection. Isoprene calibration tubes were prepared by slowly (over a period of about 2 min) injecting 0, 10, 30 and 50 mL of the gas standard onto 4 adsorbent tubes, while purging with helium. The limits of detection for isoprene, α-pinene, β-pinene, 3-carene and limonene were 2.0, 2.0, 0.12, 1.1 and 2.4 ng on column, corresponding to mixing ratios of 360, 174, 11, 93 and 208 pptv, respectively, for a 2 L sample.

The raw data gave the on-tube mass of VOC at the start and end of enclosure time. To calculate flux over the enclosure time, total chamber mass of VOC for the start and end samples had to be determined first, as shown in Equation 4-1.

$$\text{Total chamber mass} = \frac{\text{Sample mass from tube (ng)}}{\text{Sample volume (m}^3\text{)}} \times \text{Chamber volume (m}^3\text{)} \quad (4-1)$$

*Chamber volume* includes the volume within the chamber (33 L) as well as the soil collar, which varied for each plot due to differences in vegetation volume. The collar volume had been previously determined for each collar as part of on-going measurements at the site<sup>7</sup>. *Sample volume* in all cases was 2 L. Fluxes were then calculated using Equation 4-2.

$$\text{Flux} = \frac{\text{Difference in mass (ng)}}{\text{Surface area (m}^2\text{)} \times \text{Enclosure time (h)}} \quad (4-2)$$

*Difference in mass* refers to the difference in total chamber VOC mass between samples taken before and after the enclosure time as calculated from Equation 4-1. *Surface area* for the soil collars was 0.12254 m<sup>2</sup> in all cases.

#### 4.2.5.1 Error calculations

Error sources in flux measurements include uncertainties in both the sampling and analytical procedures. Assumed sources of error were:

- The mass difference,  $\Delta m$ , as described in Equation 4-2, which is discussed in more detail below.
- The chamber volume,  $V$ , assumed to be  $\pm 0.05$  L ( $5 \times 10^{-5}$  m<sup>3</sup>)
- The surface area,  $A$ , within the sampling collar, estimated to be  $3.1 \times 10^{-4}$  m<sup>2</sup>
- The enclosure time,  $t$ , which was estimated to be  $\pm 0.5$  min ( $8.33 \times 10^{-3}$  h)

---

<sup>7</sup> Sarah Leeson, CEH Edinburgh, 6 Feb 2012.

The most significant source of error was  $\Delta m$ , denoting the uncertainty in the VOC mass difference between T2 and T1 samples, i.e., before and after enclosure. Mass values were calculated by GC measurement and derived by interpolation from a calibration curve, as described in Section 4.2.5; therefore the linear regression was used as an estimate of all random uncertainties associated with the analytical process. The standard deviation in  $y$  values ( $s_{y/x}$ ) is expressed as:

$$s_{y/x} = \sqrt{\frac{\sum(y_i - \hat{y}_i)^2}{n - 2}} \quad (4-3)$$

where  $y_i$  are measured  $y$ -values,  $\hat{y}_i$  are  $y$ -values calculated using the calibration curve, and  $n$  is the number of standards used to construct the calibration curve.

For a given signal  $y_o$  the mass  $x_o$  can be determined from the calibration curve and will have an associated uncertainty,  $s_{x_o}$  calculated as:

$$s_{x_o} = \frac{s_{y/x}}{b} \sqrt{1 + \frac{1}{n} + \frac{(y_o - \bar{y})^2}{b^2 \sum(x_i - \bar{x})^2}} \quad (4-4)$$

where  $b$  is the slope, and  $\bar{x}$  and  $\bar{y}$  are the mean standard mass and detector response respectively.  $s_{x_o}$  was determined for both T1 and T2 samples (corresponding to before and after enclosure respectively) and the combined overall uncertainty associated with the mass difference,  $\Delta m$ , was calculated as:

$$s_{\Delta m} = \sqrt{s_{T1}^2 + s_{T2}^2} \quad (4-5)$$

Finally, overall uncertainty in flux values was calculated as:

$$s_F = F \times \sqrt{\left(\frac{s_{\Delta m}}{\Delta m}\right)^2 + \left(\frac{s_V}{V}\right)^2 + \left(\frac{s_t}{t}\right)^2 + \left(\frac{s_A}{A}\right)^2} \quad (4-6)$$

## 4.3 Results

### 4.3.1 VOC fluxes from control plots

By examining only samples from control plots, the effects of vegetation cover, temperature and PAR on VOC fluxes was first investigated.

#### 4.3.1.1 Vegetation cover effects

Visits to Whim Moss on 24 October and 14 November 2011 were used to sample only from control plots. The aim of these sampling visits was to determine how vegetation type may affect VOC emissions. Weather conditions on these two days were similar, allowing fluxes to be compared over both days while minimizing any effect of varying temperature or PAR. Additionally, weather conditions were comparable on 1 and 6 February therefore control plot samples from these dates have also been included for comparison. Figure 4-6 to Figure 4-10 show VOC emissions as a function of vegetation cover for all vegetation types present in chamber plots 7, 16, 35 and 40.

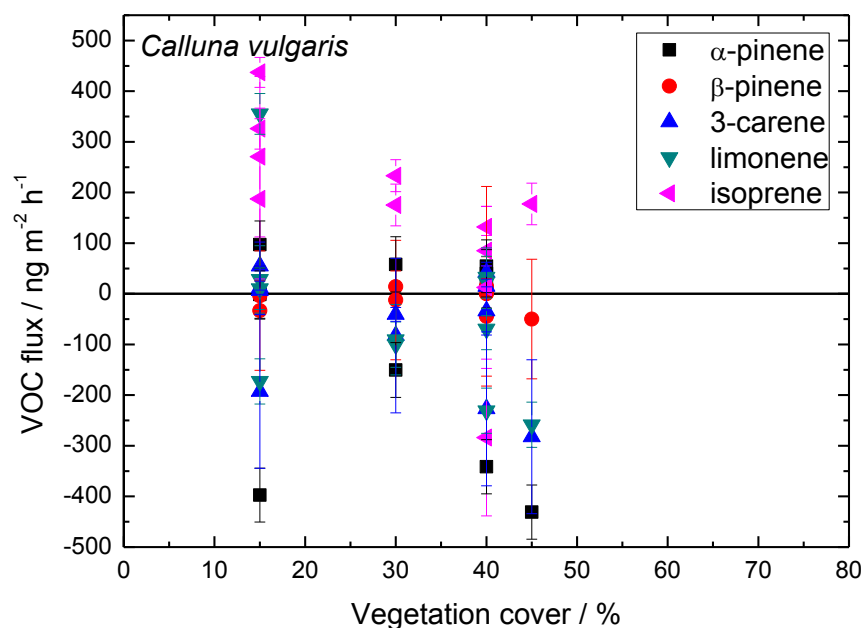


Figure 4-6 VOC flux (from control plots 7, 16, 35 and 40) as a function of percentage vegetation cover for *Calluna vulgaris*. Error bars incorporate analytical and sampling uncertainties.

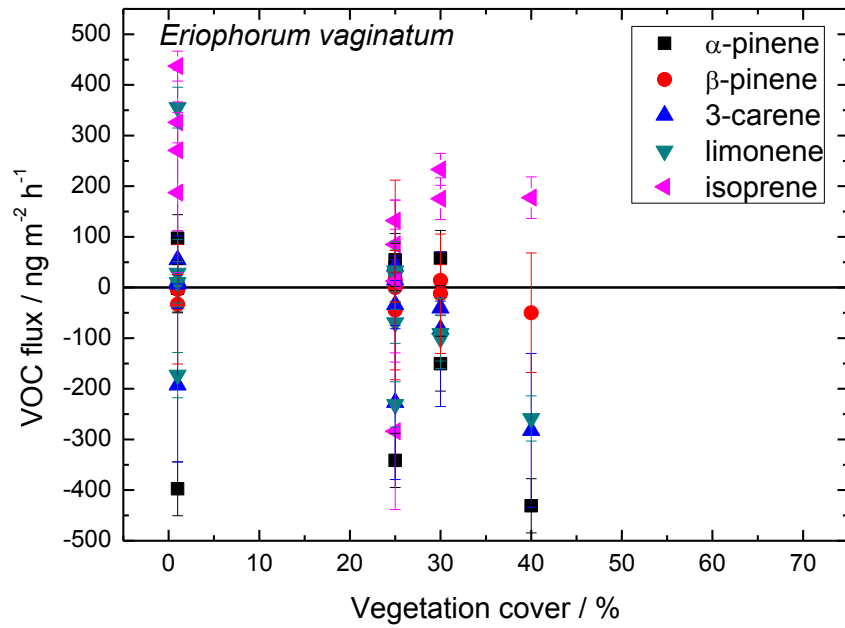


Figure 4-7 VOC flux (from control plots 7, 16, 35 and 40) as a function of percentage vegetation cover for *Eriophorum vaginatum*. Error bars incorporate analytical and sampling uncertainties.

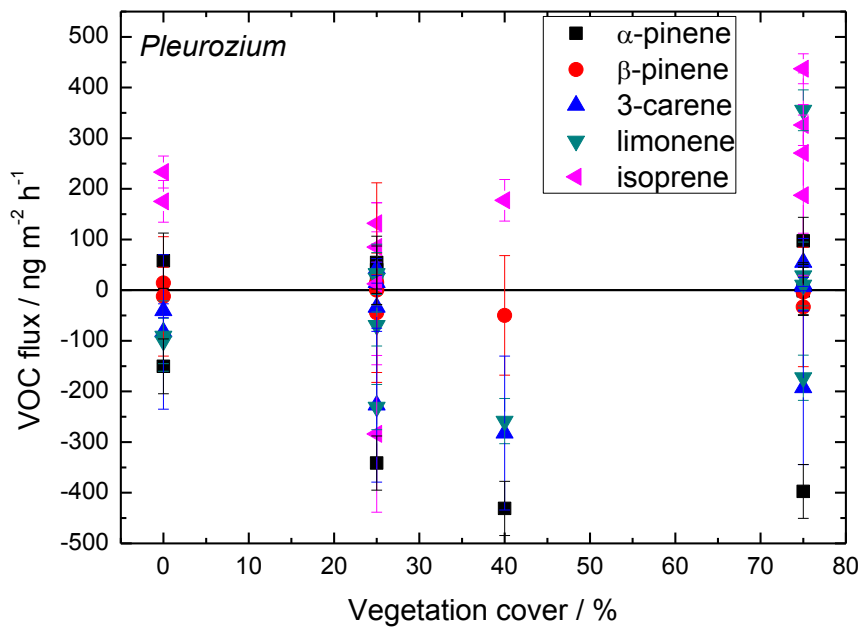


Figure 4-8 VOC flux (from control plots 7, 16, 35 and 40) as a function of percentage vegetation cover for *Pleurozium*. Error bars incorporate analytical and sampling uncertainties.

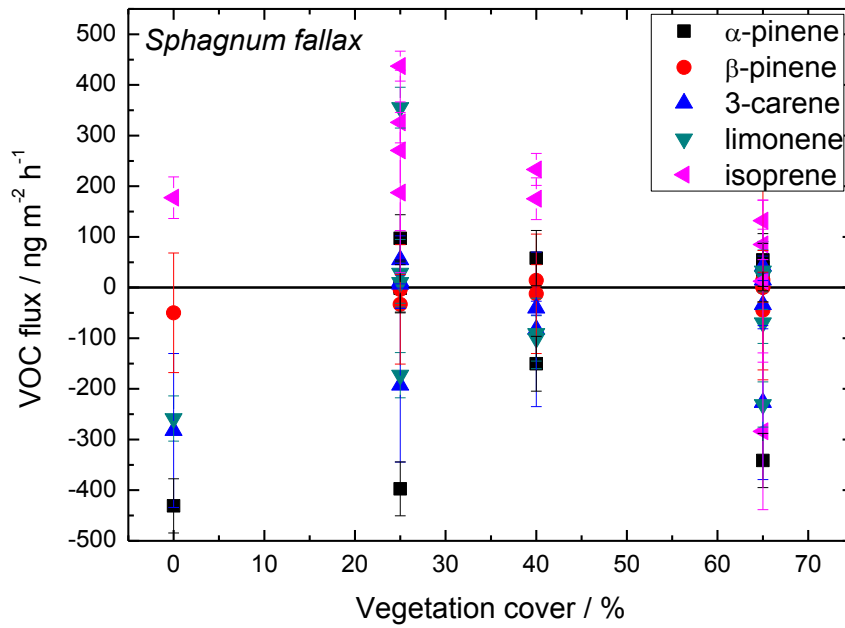


Figure 4-9 VOC flux (from control plots 7, 16, 35 and 40) as a function of percentage vegetation cover for *Sphagnum fallax*. Error bars incorporate analytical and sampling uncertainties.

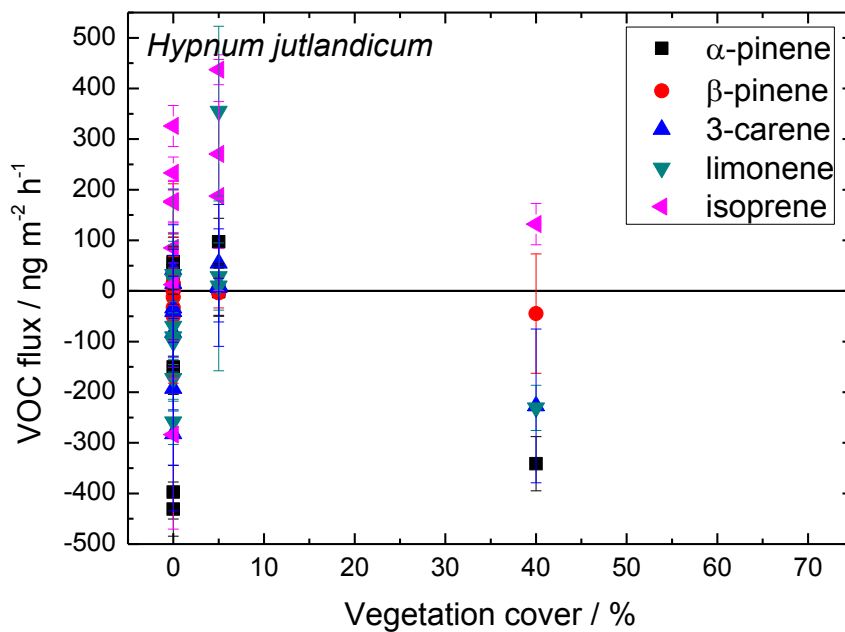


Figure 4-10 VOC flux (from control plots 7, 16, 35 and 40) as a function of percentage vegetation cover for *Hypnum jutlandicum*. Error bars incorporate analytical and sampling uncertainties.

Figure 4-8 shows that isoprene flux increased with % area *Pleurozium* cover ( $y = 3.024x + 38.4$ ,  $R^2: 0.15$ ). This supports previous studies which found *Pleurozium* to be a moderate isoprene emitter (Hanson et al., 1999). On the other hand, isoprene flux decreased as cover of all other species increased.  $\beta$ -pinene fluxes were near zero for all plant species and therefore show no correlation to vegetation cover. Fluxes of  $\alpha$ -pinene, 3-carene and limonene were mostly depositional and showed no correlations to vegetation cover.

Other vegetation species were present in smaller quantities or in fewer sample plots than the species presented, so it is not possible to quantify the relationship between their cover and VOC fluxes. As samples were collected in winter, it is likely that temperatures were too low for a true representation of emission potential from each of the species to be established.

#### **4.3.1.2 Temperature effects**

Control plot samples from 22 July, 24 October and 14 November 2011, and 1 and 6 February 2012 were used to investigate the relationship between temperature and emission. Plots of VOC flux as a function of air temperature are shown in Figure 4-11 to Figure 4-15. Since in-chamber temperatures were not recorded, the mean ambient air temperature during the sample enclosure times was used. An exponential fit was applied for data for all compounds. Grey data points denoting four negative flux values on plots for  $\alpha$ -pinene and 3-carene (Figure 4-11 and Figure 4-13, respectively) appeared to be outliers and were not included in the data fitting. Uncertainties were also much larger for these data points, particularly for 3-carene. These data correspond to samples taken on 14 November 2011, but there were no known sampling issues which may have led to greater uncertainties in this sample set. It is possible that these negative data represent a fixed depositional flux to vegetation surfaces.

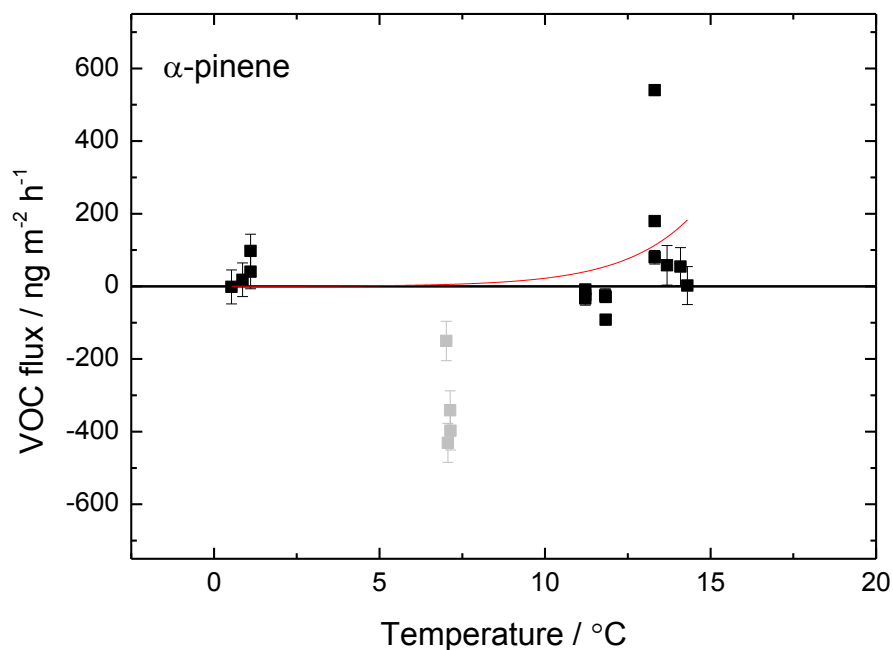


Figure 4-11  $\alpha$ -pinene flux (from control plots 7, 16, 35 and 40) as a function of ambient air temperature. The red line shows an exponential fit,  $Flux = 0.170 e^{0.488 T}$ .

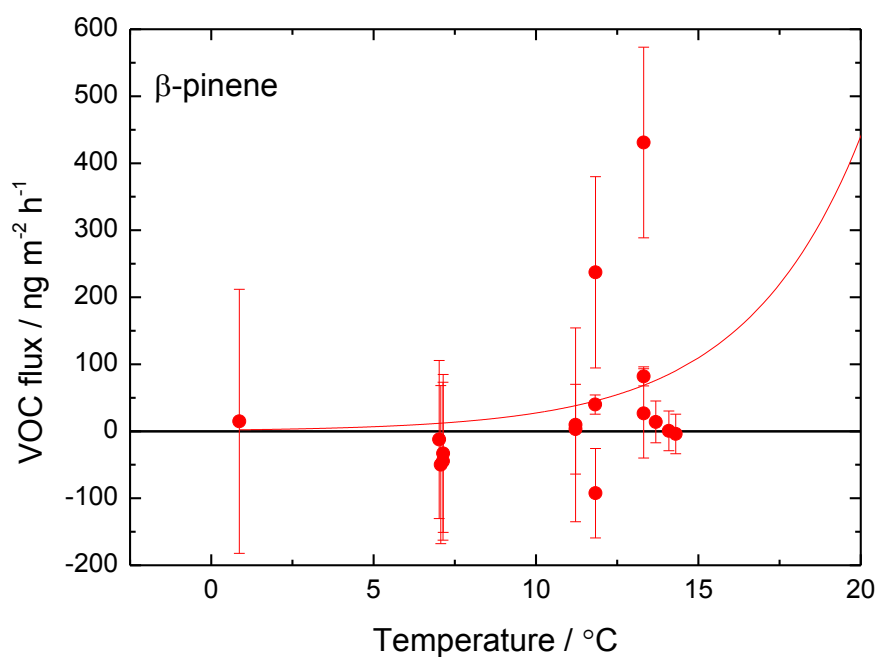


Figure 4-12  $\beta$ -pinene flux (from control plots 7, 16, 35 and 40) as a function of ambient air temperature. The red line shows an exponential fit,  $Flux = 1.69 e^{0.278 T}$ .

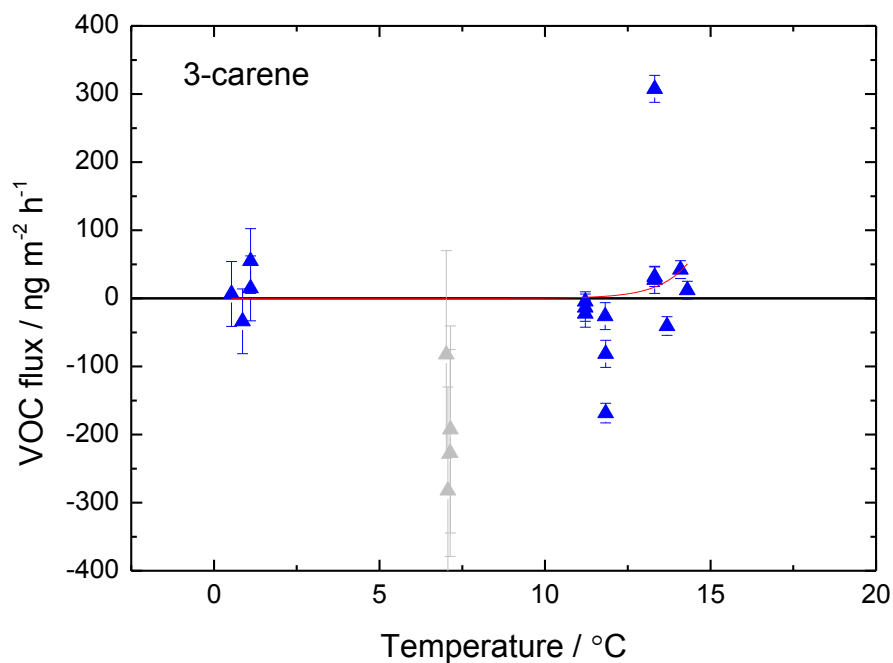


Figure 4-13 3-carene flux (from control plots 7, 16, 35 and 40) as a function of ambient air temperature. The red line shows an exponential fit,  $Flux = 4.51 \times 10^{-6} e^{1.14 T}$ .

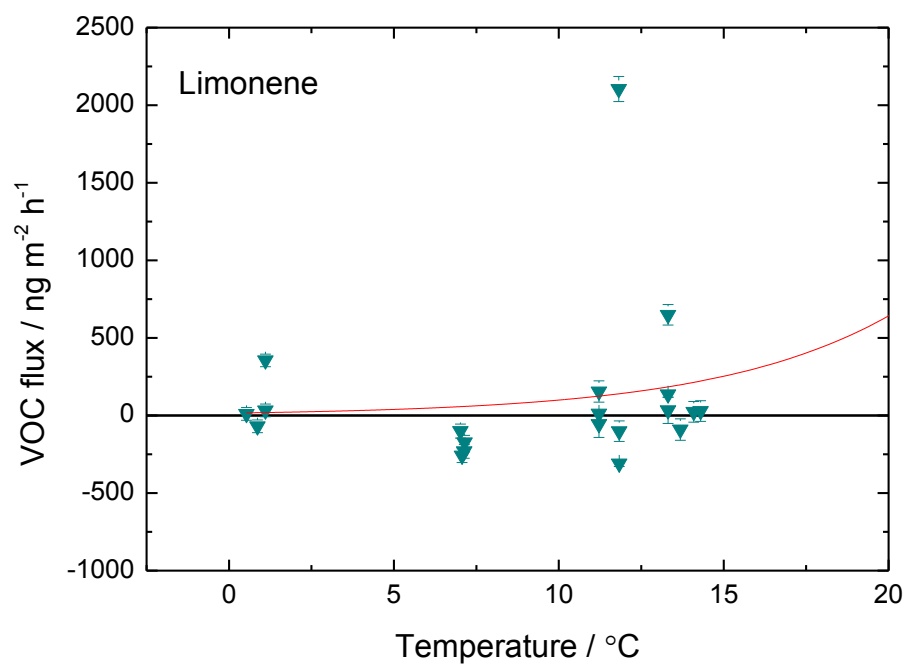
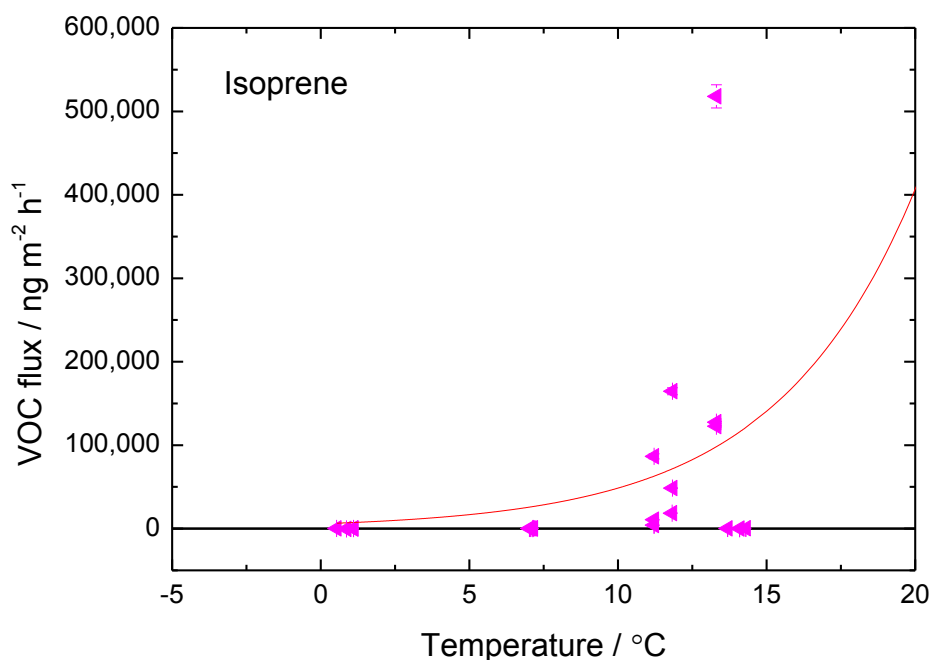


Figure 4-14 Limonene flux (from control plots 7, 16, 35 and 40) as a function of ambient air temperature. The red line shows an exponential fit,  $Flux = 15.4 e^{0.186 T}$ .



**Figure 4-15** Isoprene flux (from control plots 7, 16, 35 and 40) as a function of ambient air temperature. The red line shows an exponential fit,  $Flux = 5802 e^{0.213 T}$ .

The ecosystem showed the empirical expected exponential increase in fluxes with increasing temperature (Guenther et al., 1993). For all VOCs, fluxes were near-zero or negative for all temperatures below 10 °C. Above this threshold, fluxes increased steeply with temperature. This compares well to other studies which found a steep response above 15 °C (Holst et al., 2010).

An exponential relationship of the form  $Flux = a e^{(b T)}$  comparable to the G93 algorithm was evident above a threshold temperature, where  $Flux$  is expressed as  $ng\ m^{-2}\ h^{-1}$  and  $T$  is air temperature in °C. Fitting parameters  $a$  and  $b$ , and their associated uncertainties are summarised in Table 4-2.

**Table 4-2 Fitting parameters for the relationship between VOC flux  $F$  ( $\text{ng m}^{-2} \text{h}^{-1}$ ), and temperature  $T$  ( $^{\circ}\text{C}$ ), where  $F = a e^{(bT)}$ . Standard errors are shown in parentheses.**

VOC	$a$	$b$	$R^2$
$\alpha$ -pinene	0.170 (1.42)	0.488 (0.619)	0.0408
$\beta$ -pinene	1.69 (11.2)	0.278 (0.501)	0.0204
3-carene	$4.51 \times 10^{-6}$ ( $2.22 \times 10^{-4}$ )	1.13547 (3.52)	-0.0460
limonene	15.4 (102)	0.186 (0.513)	-0.0293
isoprene	5802 (18046)	0.213 (0.239)	0.0886

Uncertainties associated with fitting parameters are greater than the actual values of  $a$  and  $b$  for all terpenes. This shows that there is poor correlation between the measured data and the Guenther et al. (1993) model. Low  $R^2$  parameters also confirm poor fit to the model. This is likely due to limited data points, particularly at higher temperatures above the threshold value. Measurements over a greater temperature range would need to be obtained to determine whether vegetation at Whim follows the model described by Guenther et al. (1993).

#### 4.3.1.3 PAR effects

Control plot samples from 22, July, 24 October, 14 November 2011, and 1 and 6 February 2012 were used to investigate any relationship between PAR and VOC fluxes. Plots of VOC flux as a function of PAR are shown in Figure 4-16 to Figure 4-20. Since in-chamber PAR values were not recorded, the mean ambient PAR throughout sample enclosure times was used. As was the case for the temperature plots, 4 outlying data points were excluded from exponential fits of  $\alpha$ -pinene and 3-carene data (Figure 4-16 and Figure 4-18, respectively).

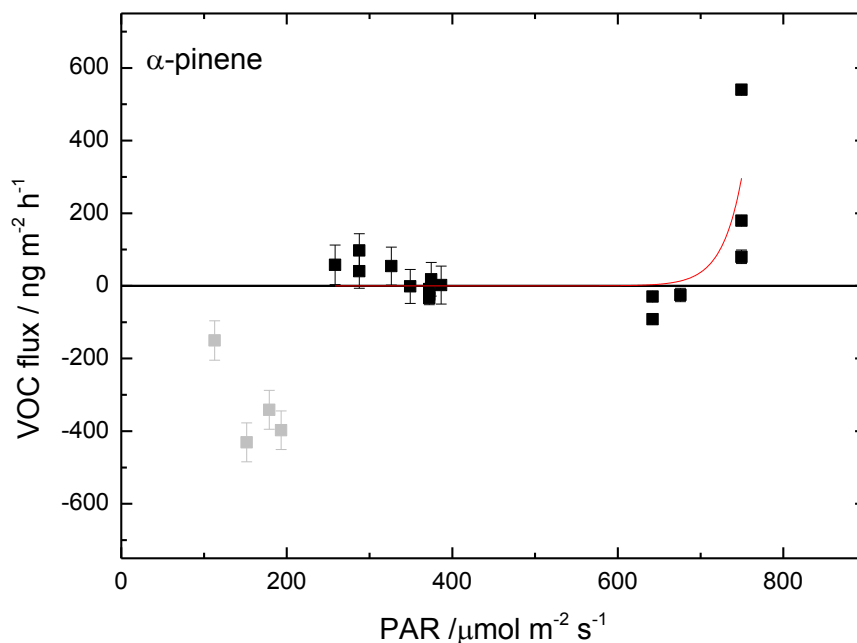


Figure 4-16  $\alpha$ -pinene flux (from control plots 7, 16, 35 and 40) as a function of PAR. The red line shows an exponential fit,  $Flux = 6.83 \times 10^{-12} e^{0.0419 PAR}$ .

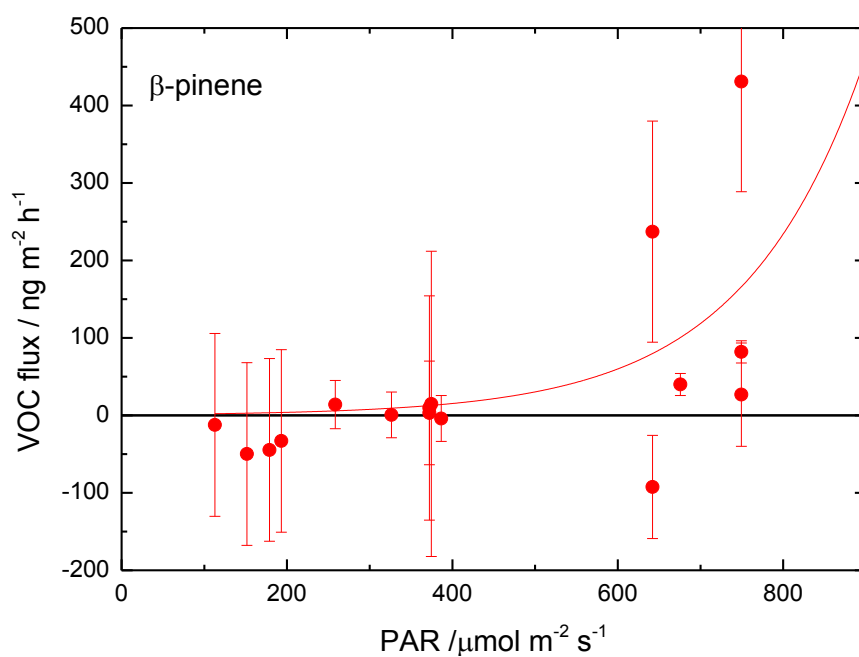


Figure 4-17  $\beta$ -pinene flux (from control plots 7, 16, 35 and 40) as a function of PAR. The red line shows an exponential fit,  $Flux = e^{0.00682 PAR}$ .

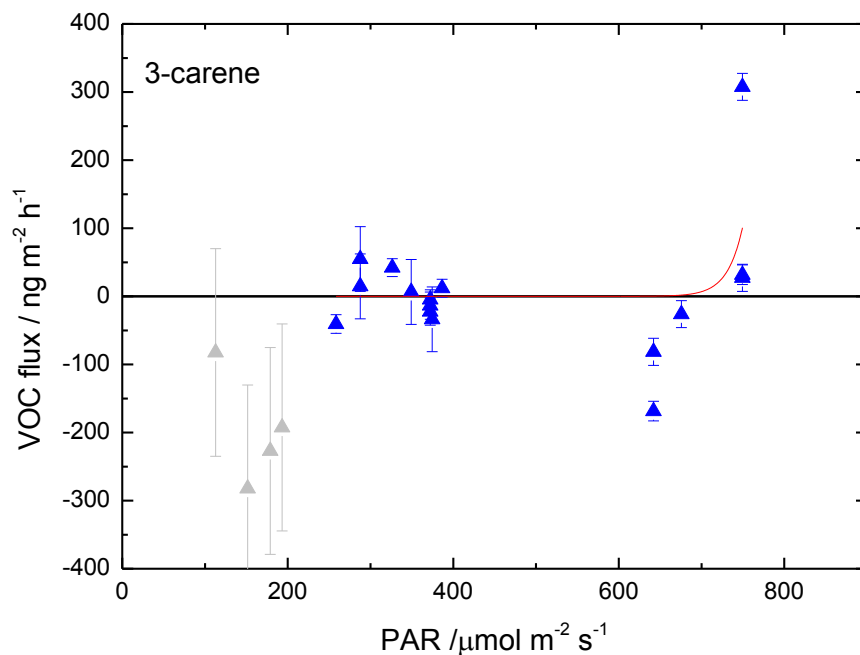


Figure 4-18 3-carene flux (from control plots 7, 16, 35 and 40) as a function of PAR. The red line shows an exponential fit,  $Flux = 2.02 \times 10^{-16} e^{0.0544 PAR}$ .

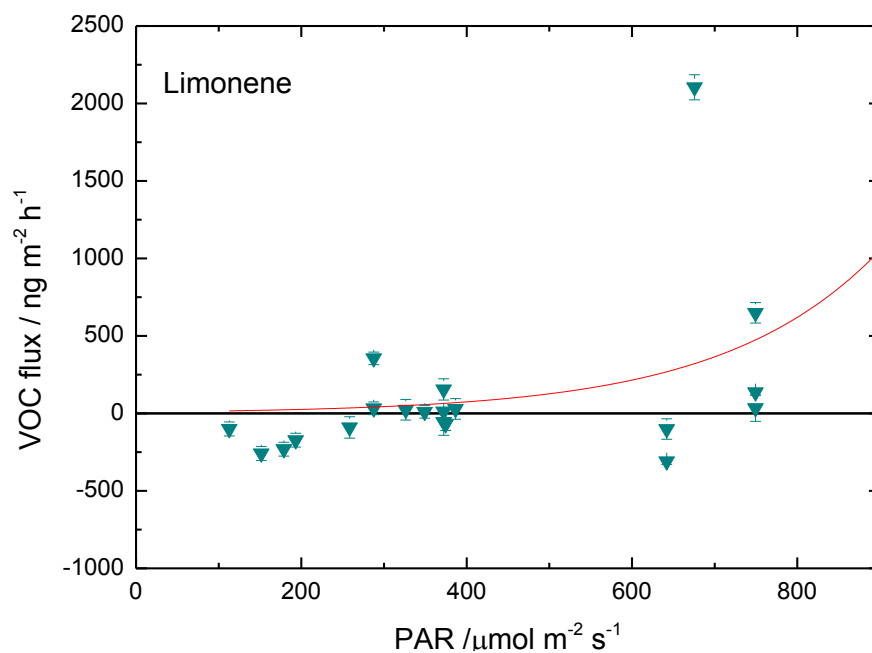
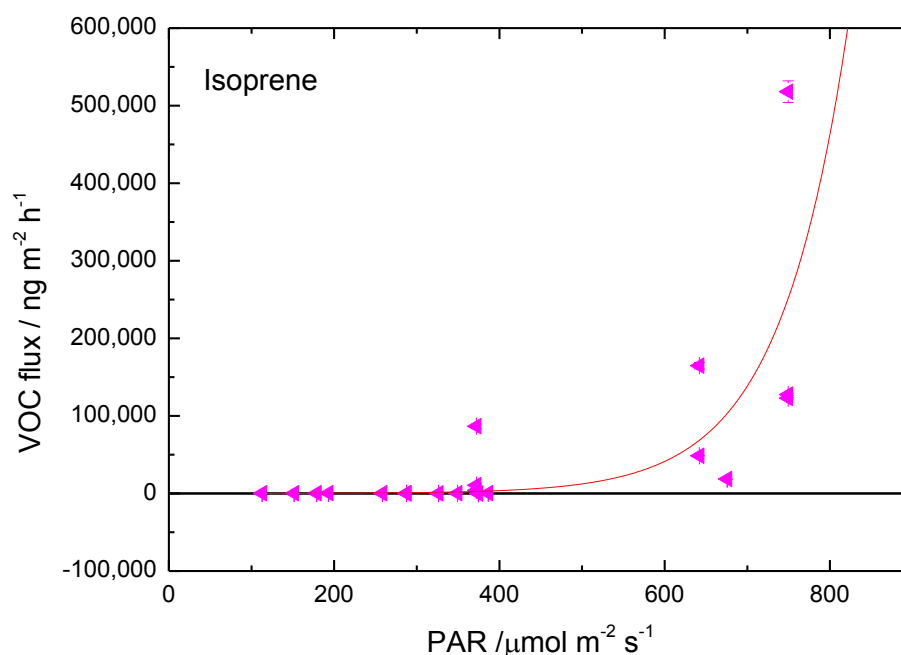


Figure 4-19 Limonene flux (from control plots 7, 16, 35 and 40) as a function of PAR. The red line shows an exponential fit,  $Flux = 8.93 e^{0.0053 PAR}$ .



**Figure 4-20** Isoprene flux (from control plots 7, 16, 35 and 40) as a function of PAR. The red line shows an exponential fit,  $Flux = 29.2 e^{0.0121 PAR}$ .

Similar to the trends observed for temperature, all fluxes were near-zero or negative for PAR values below around  $400 \mu\text{mol m}^{-2} \text{s}^{-1}$ . Above this value, fluxes increased with PAR. Again, an exponential relationship of the form  $Flux = a e^{(b PAR)}$  was evident for  $\beta$ -pinene, limonene and isoprene above a threshold PAR value, where  $Flux$  is expressed as  $\text{ng m}^{-2} \text{h}^{-1}$  and  $PAR$  is air temperature in  $\mu\text{mol m}^{-2} \text{s}^{-1}$ . Fitting parameters  $a$  and  $b$ , and their associated uncertainties are summarised in Table 4-3.

**Table 4-3** Fitting parameters for the relationship between VOC flux,  $F$  ( $\text{ng m}^{-2} \text{h}^{-1}$ ), and  $PAR$  ( $\mu\text{mol m}^{-2} \text{s}^{-1}$ ), where  $F = a e^{(b PAR)}$ . Standard errors are shown in parentheses.

VOC	$a$	$b$	$R^2$
$\alpha$ -pinene	$6.83 \times 10^{-12}$ ( $5.10 \times 10^{-10}$ )	0.0419 (0.0996)	0.594
$\beta$ -pinene	-	0.00682 ( $3.89 \times 10^{-4}$ )	0.330
3-carene	$2.02 \times 10^{-16}$ ( $1.00 \times 10^{-13}$ )	0.0544 (0.661)	0.182
limonene	8.93 (39.3)	0.00530 (0.00614)	0.0952
isoprene	29.2 (145)	0.0121 (0.00668)	0.515

Uncertainties associated with fitting parameters are high, particularly for  $a$ . As for the fittings of flux to temperature described in Section 4.3.1.2, this is likely due to limited data points, particularly at higher PAR values above the threshold. Relationships between PAR and fluxes of  $\beta$ -pinene, limonene and isoprene were stronger than those observed for temperature.

#### 4.3.1.4 Standardised isoprene and monoterpene emissions

As isoprene emission from plants is influenced by light and temperature, measured emissions,  $F$ , were recalculated as a standard emission factor ( $\varepsilon$ ) normalised to a standard leaf temperature of 303 K and PAR flux of  $1000 \mu\text{mol m}^{-2} \text{s}^{-1}$ , as described by the G95 algorithm (Guenther et al., 1995),

$$\varepsilon = \frac{F}{\gamma} \quad (4-7)$$

where  $\gamma$  is a non-dimensional activity adjustment factor to account for the effect of light and temperature:

$$\gamma = C_L C_T \quad (4-8)$$

The light dependence,  $C_L$ , is defined by

$$C_L = \frac{\alpha c_L Q}{\sqrt{1 + \alpha^2 Q^2}} \quad (4-9)$$

where  $\alpha$  (0.0027) and  $c_{LI}$  (1.066) are empirical coefficients and  $Q$  is PAR flux ( $\mu\text{mol m}^{-2} \text{s}^{-1}$ ). The temperature dependence  $C_T$ , is defined by

$$C_T = \frac{\exp\left(\frac{c_{T1}(T - T_s)}{RT_s T}\right)}{1 + \exp\left(\frac{c_{T2}(T - T_M)}{RT_s T}\right)} \quad (4-10)$$

where  $T$  is leaf temperature (K),  $T_s$  is leaf temperature at standard conditions (303 K),  $R$  is the universal gas constant ( $8.314 \text{ J K}^{-1} \text{ mol}^{-1}$ ), and  $c_{T1}$  ( $95000 \text{ J mol}^{-1}$ ),  $c_{T2}$  ( $230000 \text{ J mol}^{-1}$ ) and  $T_M$  (314 K) are empirical coefficients.

The mean estimate obtained for isoprene emissions was  $586 \pm 262 \mu\text{g m}^{-2}$  (ground area)  $\text{h}^{-1}$  standardised to  $30 \text{ }^\circ\text{C}$  and  $1000 \mu\text{mol m}^{-2} \text{ s}^{-1}$  PAR.

Similarly, standardised monoterpene emissions can be expressed using a temperature dependent algorithm (Guenther et al., 1993)

$$E_{meas} = E_s e^{[\beta(T - T_s)]} \quad (4-11)$$

where  $E_{meas}$  is the measured emission rate at leaf temperature  $T$  (K),  $E_s$  is the standard (basal) emission rate at  $303 \text{ K}$  ( $T_s$ ) and  $\beta$  is an empirical temperature coefficient, normally between  $0.06$  and  $0.14 \text{ K}^{-1}$ , but best estimated as  $0.09 \text{ K}^{-1}$  for all plants and monoterpenes (Guenther et al., 1993). Total monoterpene fluxes (taken as the sum of  $\alpha$ -pinene,  $\beta$ -pinene, 3-carene and limonene) and ambient temperatures were used to determine a standard emission factor and temperature coefficient by plotting  $\ln(E_{meas})$  against  $T - T_s$ , giving a straight line with gradient  $\beta$  and intercept  $\ln(E_s)$ . In order to obtain values of  $\ln(E_{meas})$ , only data points with a positive total monoterpene flux could be used. As such, only 10 out of a total of 20 samples could be used. The plot is shown in Figure 4-21.

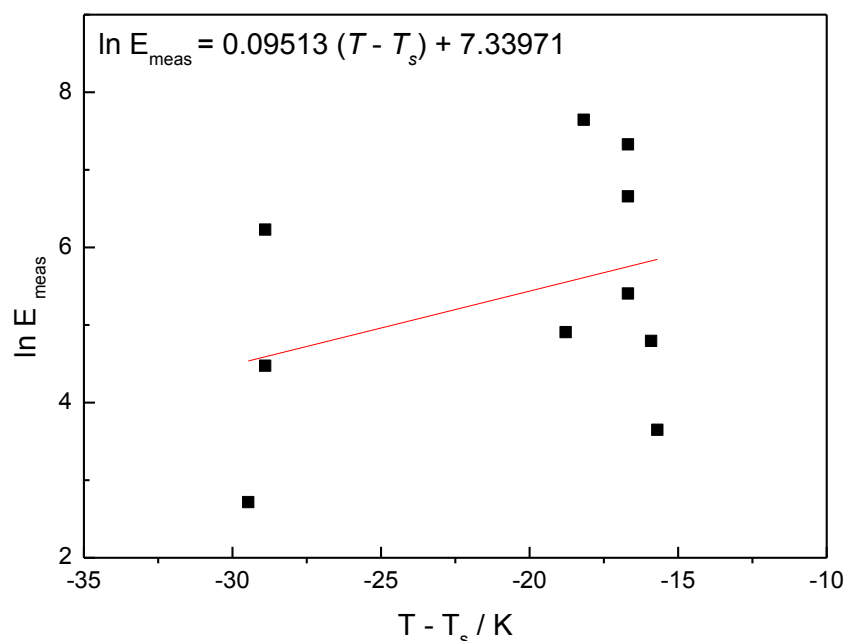


**Figure 4-21** Graph of  $\ln E_{meas}$  against  $T - T_s$  (K). The red line shows a linear regression of the form  $\ln E_{meas} = \beta (T - T_s) + \ln E_s$ , where  $E_{meas}$  is the total monoterpene emission (in  $\text{ng m}^{-2} \text{h}^{-1}$ ) at temperature,  $T$ .  $E_s$  is the basal emission rate at standard temperature  $T_s$  (303 K). The temperature coefficient  $\beta$ , was found to be  $0.0951 (\pm 0.0088) \text{ K}^{-1}$  and  $E_s$  was  $1.54 (\pm 1.89) \mu\text{g m}^{-2} \text{h}^{-1}$ .

The temperature coefficient was found to be  $0.095 (\pm 0.009) \text{ K}^{-1}$  and standard emission rate was  $1.54 (\pm 1.89) \mu\text{g m}^{-2} \text{h}^{-1}$ . A comparison of these values (along with standard isoprene emission rate) against similar boreal wetland studies is shown in Table 4-4.

Table 4-4 shows that the standardized isoprene emission rate derived in this study falls within the range of values from previous studies in other wetland sites. In contrast, the standardized monoterpene emission flux determined here was lower. However, only one other study reported monoterpene emissions on an area basis (Janson et al., 1999). Previous studies of individual plant species have, however, shown peatland species to be low emitters of monoterpenes, for example: *Calluna vulgaris*, *Eriophorum vaginatum*, *Eriophorum angustifolium* and *Erica tetralix* are reported to have standardized emission rates of 2.42, 0.1, 0.1 and  $0.14 \mu\text{g g}_{\text{dw}}^{-1} \text{h}^{-1}$ , respectively. Other vegetation types present in sampling plots at Whim have been reported to be non-emitters of monoterpenes (Stewart et al., 2003).

**Table 4-4 Comparison of standardised monoterpene and isoprene emission rates for boreal wetland studies.**

Species or site	Monoterpenes / $\mu\text{gC m}^{-2} \text{h}^{-1}$	Isoprene / $\mu\text{g m}^{-2} \text{h}^{-1}$	Measurement type	Reference
Whim, Scotland	1.54	586	Static chamber	This study
Boreal <i>Sphagnum</i> peatland, central Finland		1015	Static chambers on open-field microcosms	(Tiiva et al., 2007b)
<i>Sphagnum</i> fen, southern Finland		680	REA	(Haapanala et al., 2006)
<i>Sphagnum</i> fen, southern Sweden	102	462	Grab samples (Tenax tubes)	(Janson et al., 1999)
Sub-arctic wetland, northern Sweden		373 (standardised to 20 °C)	PTR-MS	(Holst et al., 2010)
Moss and sedge dominated fen, SW Finland		224	Static chamber	(Hellén et al., 2006)

### 4.3.2 Effects of N-treatment on VOC emissions

Experiments were carried out to assess the relationship between N-treatment and VOC emissions. Additionally, samples collected on 22 July 2011 were used to examine the diurnal variation in VOC fluxes. Triplicate samples were collected for each treatment type at three time-steps throughout the day as described in Section 4.2.3. Results are presented in Figure 4-22 to Figure 4-26.

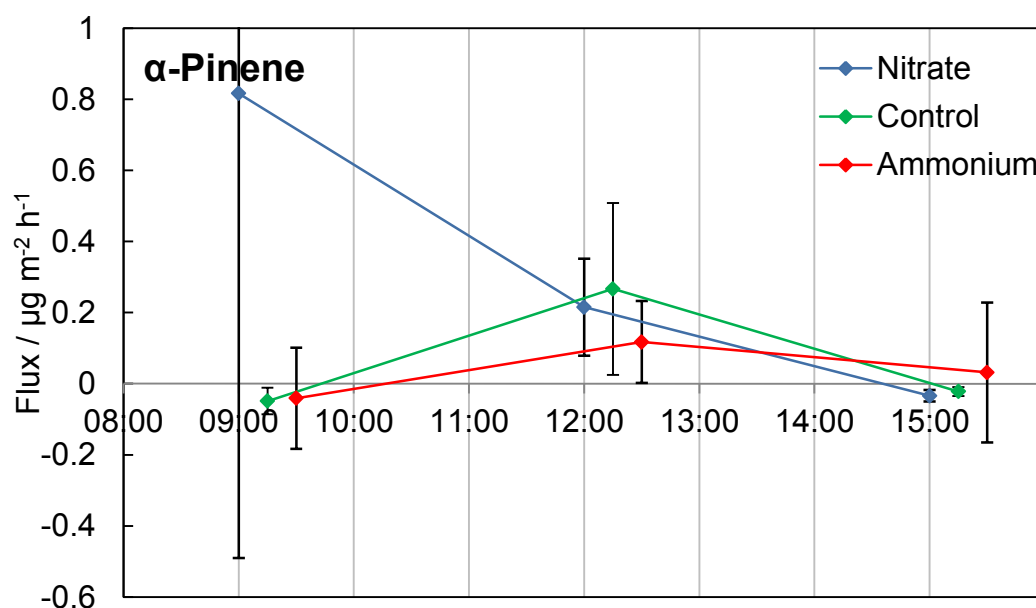


Figure 4-22 Diurnal variation of  $\alpha$ -pinene flux for control, nitrate and ammonium-treated plots. Each data point is the mean measurement from three replicate sample plots. Error bars denote 1 sd.

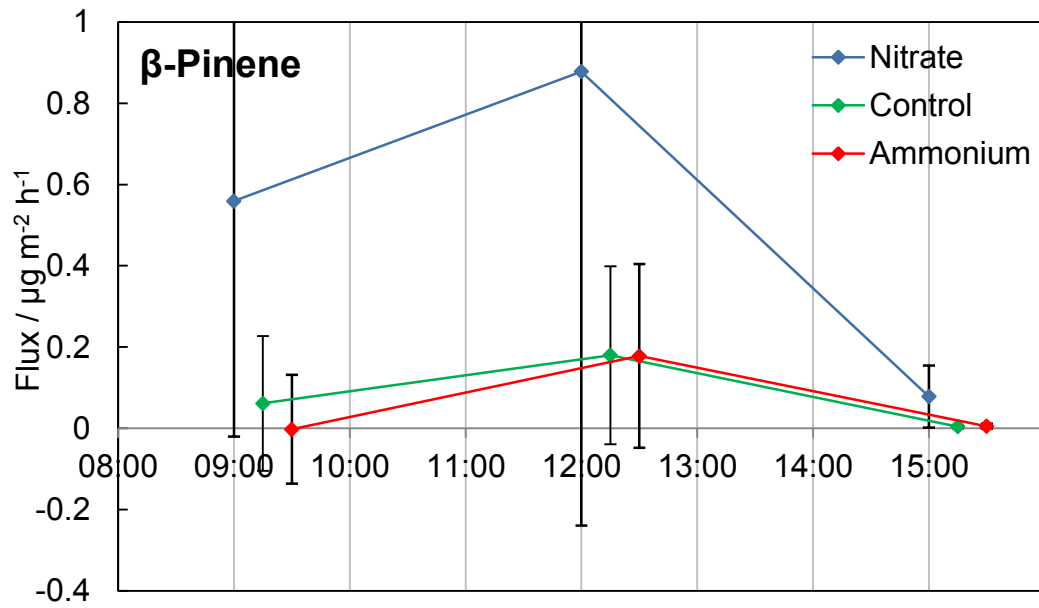


Figure 4-23 Diurnal variation of  $\beta$ -pinene flux for control, nitrate and ammonium-treated plots. Each data point is the mean measurement from three replicate sample plots. Error bars denote 1 sd.

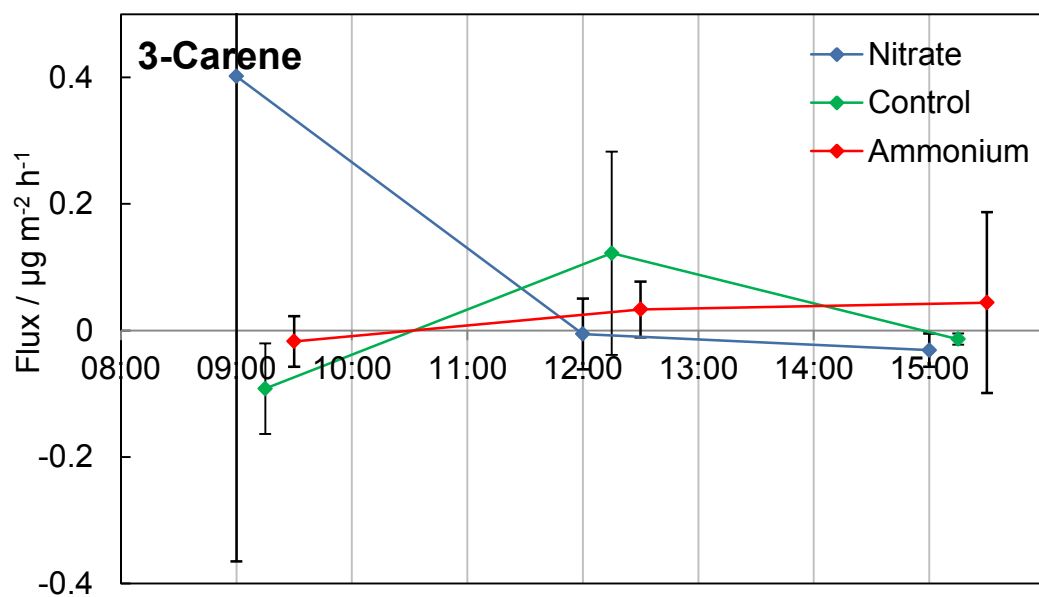


Figure 4-24 Diurnal variation of 3-carene flux for control, nitrate and ammonium-treated plots. Each data point is the mean measurement from three replicate sample plots. Error bars denote 1 sd.

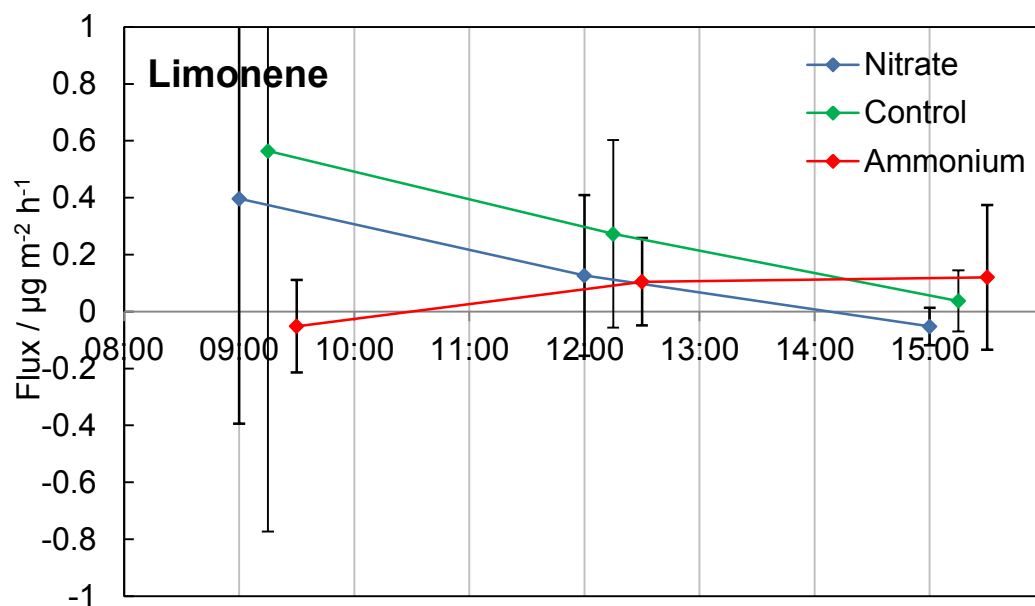


Figure 4-25 Diurnal variation of limonene flux for control, nitrate and ammonium-treated plots. Each data point is the mean measurement from three replicate sample plots. Error bars denote 1 sd.

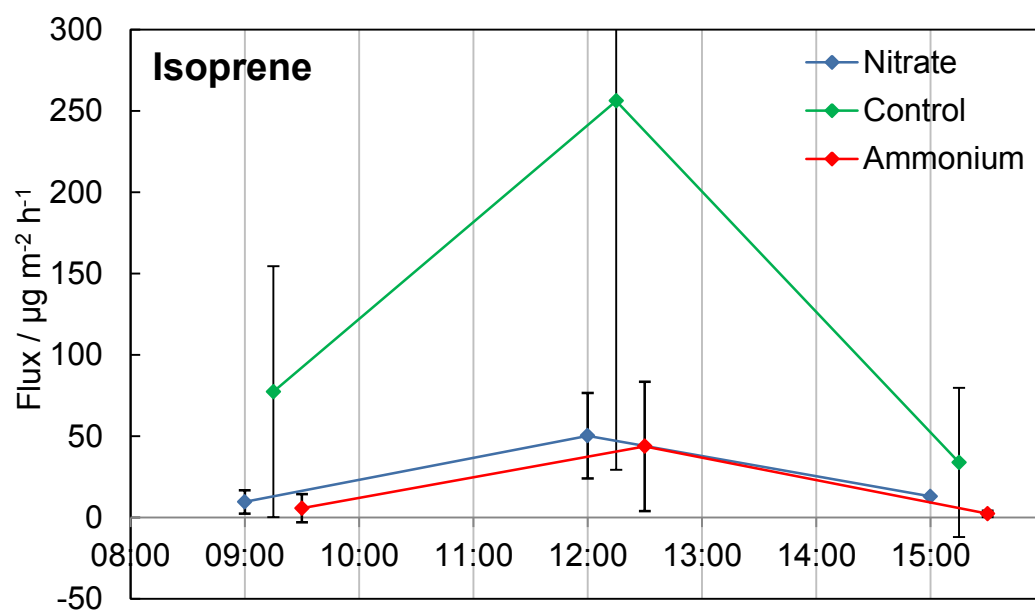


Figure 4-26 Diurnal variation of isoprene flux for control, nitrate and ammonium-treated plots. Each data point is the mean measurement from three replicate sample plots. Error bars denote 1 sd.

Most diurnal patterns were typical for biogenic VOCs, with smaller fluxes in the morning and afternoon. Largest fluxes were generally measured around noon for all VOCs and treatment types with the exception of  $\alpha$ -pinene, 3-carene and limonene

from nitrate-treated plots, and limonene from the control plots. Variability in these instances was large and in all cases was due to one outlying data point of the three replicates, corresponding to plots 13 and 40 for nitrate and control means, respectively.

Figure 4-26 shows that isoprene fluxes followed the expected diurnal pattern for all three treatment types. Fluxes were positive and peaked around noon coinciding with peak temperature and PAR. Fluxes from plots treated with nitrate and ammonium were similar in magnitude and both were substantially lower than from control plots. An independent, 1-tailed t-test comparing all 9 data points taken throughout the day for a particular treatment type against the control samples, showed that both nitrate and ammonium reduced isoprene flux with  $P < 0.05$  significance ( $t(16) = 1.83$ ,  $P = 0.043$ , and  $t(16) = 1.95$ ,  $P = 0.034$ , respectively).

Vegetation cover was examined to establish whether the difference in fluxes may be attributable to differences in vegetation cover. All three control plots contained *Pleurozium* (mean cover 33 %), while there was none in any of the N-treated plots. It was shown for control plots (Figure 4-8) that isoprene emission was positively correlated to *Pleurozium* cover. This could therefore explain the observed difference of fluxes from N-treated plots. Additionally, *S. fallax* cover was higher in control plots (30 % mean) than in nitrate or ammonium-treated plots (12 and 1 %, respectively). Although no positive correlation with isoprene flux was observed from control plots in this study (Figure 4-9), *Sphagnum* species are described in previous literature as high isoprene emitters (Haapanala et al., 2006; Janson and De Serves, 1998).

Another major difference in vegetation cover between control and treated plots was leaf litter cover, which was not present in control plots but averaged 37 % and 42 % respectively for nitrate and ammonium-treated plots. It may be possible that VOCs emitted from live vegetation are deposited onto leaf litter, thus reducing the measured flux. Reduced isoprene emissions from N-treated plots may be explained entirely by vegetation effects. However, it is not clear – and beyond the scope of this

study – whether the differences in isoprene fluxes are a secondary effect due to changes in vegetation cover induced by N-treatment.

$\beta$ -Pinene fluxes also appeared to be affected by N-treatment (Figure 4-23). Fluxes from control and ammonium-treated plots were similar, while nitrate-treated plots had larger fluxes in the morning and at noon. An independent, 1-tailed t-test for all 9 data points taken throughout the day for each treatment showed that fluxes from ammonium-treated plots were not significantly different from control plots ( $t(16) = 0.29$ ,  $P = 0.388$ ). Fluxes from nitrate-treated plots were higher than the control samples, and on the significance threshold ( $t(16) = 1.72$ ,  $P = 0.052$ ).

Nitrate-treated plots had higher *C. vulgaris* cover (40 %) than either control or ammonium-treated plots (33 and 2 %, respectively). Additionally, *H. jutlandicum* cover was greater (32, 15 and 12 % for nitrate, control and ammonium plots, respectively). *S. capillifolium* and *Vaccinium oxycoccus* (cranberry) were also present in the nitrate-treated plot with the highest  $\beta$ -pinene fluxes (plot 11) but absent from all other plots. *C. vulgaris* has been shown in other studies to be a monoterpene emitter with emission potential of  $2.42 \mu\text{g g}_{\text{dw}}^{-1} \text{h}^{-1}$  (Stewart et al., 2003), but information about speciation of monoterpene fluxes could not be found. Only isoprene emission data is available for *V. oxycoccus* (Drewitt et al., 1998) and *Sphagnum* species (Ekberg et al., 2011; Hanson et al., 1999) with no data reported for monoterpene fluxes.

Again, it is not possible to ascertain whether the difference in  $\beta$ -pinene fluxes between treatment types is a secondary result of altered vegetation due to N-treatment. Previous studies at Whim and laboratory studies concluded that wet ammonium treatment increased *Calluna* but reduced *Sphagnum* cover (Sheppard et al., 2011; Van Den Berg et al., 2005); therefore N-treatment would certainly be expected to have an effect on VOC emissions, whether through change in biomass cover or as a direct impact of N availability.

Duplicate samples of control, ammonium and nitrate treated plots were also taken on 1 and 6 February 2012 to determine the effect of treatment type on VOC emissions. The results are shown in Figure 4-27 and Figure 4-28, respectively.

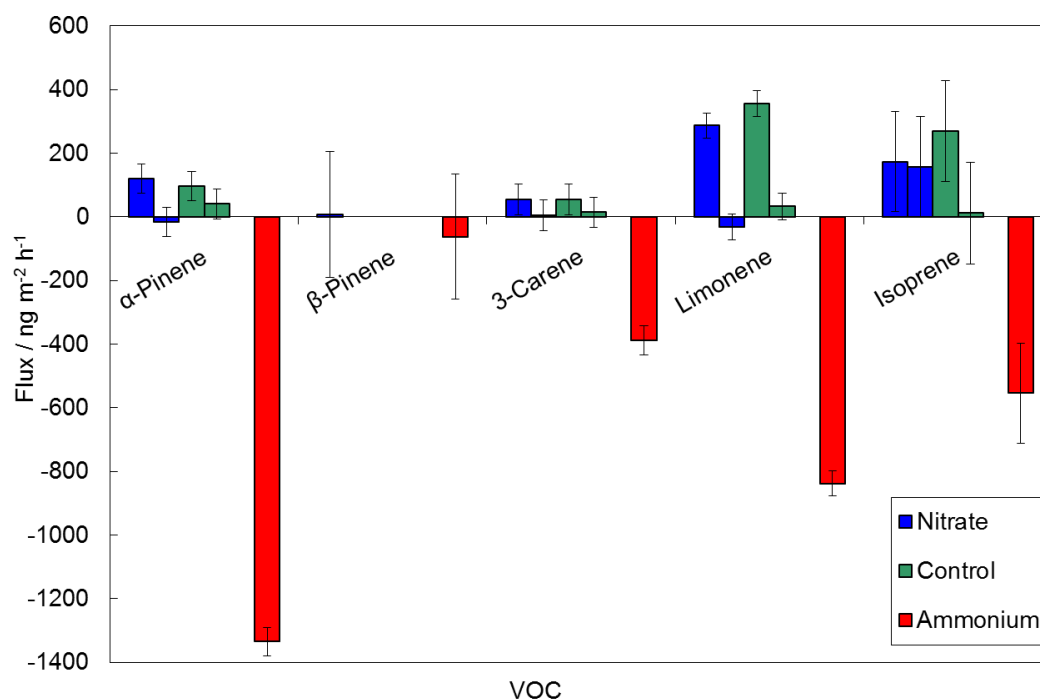


**Figure 4-27 VOC fluxes of 4 monoterpenes and isoprene from duplicates of nitrate-treated (plots 11 and 26), control (16 and 7) and ammonium-treated (17 and 21) sample plots on 1 February 2012. Error bars incorporate analytical and sampling uncertainties.**

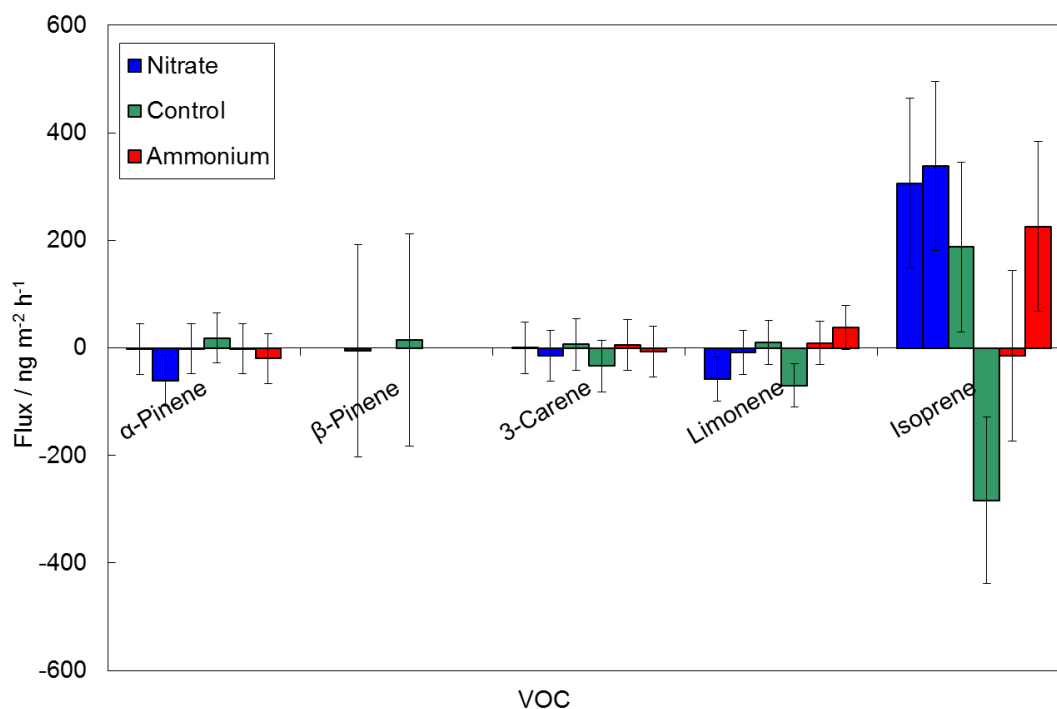


**Figure 4-28 VOC fluxes of 4 monoterpenes and isoprene from duplicates of nitrate-treated (plots 11 and 26), control (16 and 7) and ammonium-treated (17 and 21) sample plots on 6 February 2012. Error bars incorporate analytical and sampling uncertainties.**

Fluxes were around an order of magnitude lower than samples collected in summer (Figure 4-22 to Figure 4-26). One of the samples taken from an ammonium treated plot on 1 February failed, so only one sample was available for this date (Figure 4-27). It can be seen from Figure 4-27 that VOC fluxes from the sampled ammonium plot showed deposition for all VOCs, and were substantially different from fluxes for all other sampled plots. Figure 4-29 shows the vegetation cover of each of the samples plots.

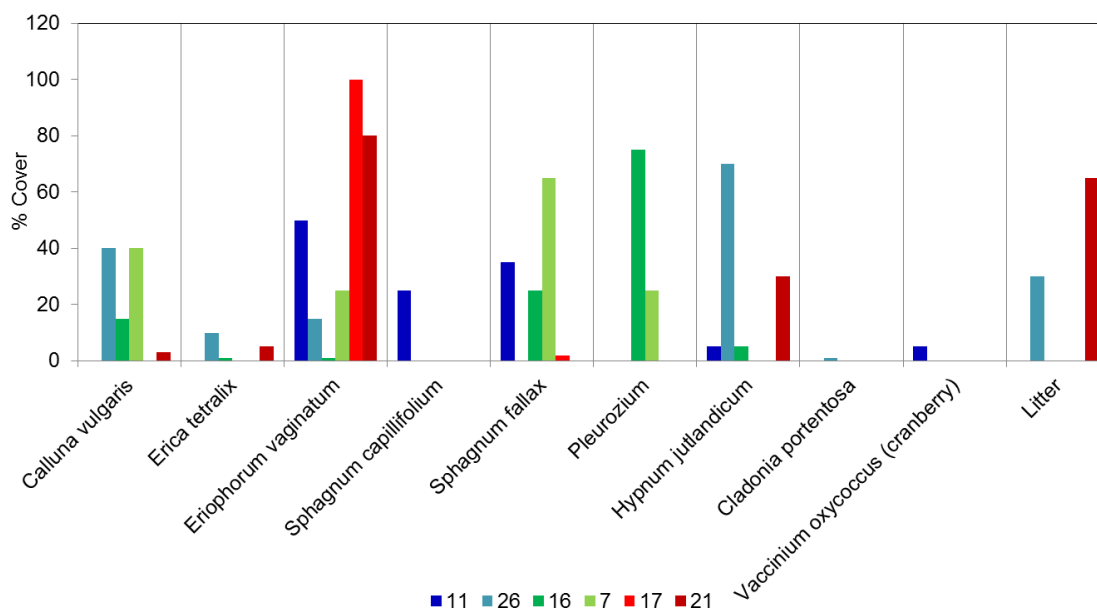


**Figure 4-29** Percentage vegetation cover of the six plots sampled on 1 and 6 February 2012 and 22 July 2011. Blue bars denote those treated with nitrate, green denote control plots and red denote those treated with ammonium.

Figure 4-29 shows that the dominant species in plot 21 is *E. vaginatum*, with smaller areas of *H. jutlandicum*, *E. tetralix* and *C. vulgaris*. It was shown in Figure 4-7 that for control plots, as cover of *E. vaginatum* increased, flux decreased. This may in part explain the observed deposition in Figure 4-27. Additionally, a large area of leaf litter was recorded in plot 21 which may account for the large depositional fluxes. The only other plot to have leaf litter cover was plot 26, which also showed deposition for all VOCs, except isoprene, on both sampling days.

Other than the noticeable difference for plot 21 on 1 February, fluxes were relatively low compared to other sampling days due to low temperatures. As a result, differences in fluxes due to varying N-treatments were difficult to discern for these sampling days, and statistical tests showed no significant difference in fluxes between treatments.

## 4.4 Discussion

The work here presents the first study of emissions of VOCs from a temperate peatbog at Whim Moss, Scotland. To our knowledge, it is also the first study to assess the relationship between N-treatment and VOC fluxes.

Most reported studies of VOC emissions from wetlands have been carried out in Scandinavia with no reported studies in the UK or at other lower latitude sites. Temperature and PAR has been shown in all studies to affect emissions. However, even in studies which had lower mean temperature and PAR conditions, isoprene emissions were still significant. Further investigation into the potential of wetlands as a source of VOCs in more temperate regions is therefore justified.

As well as differences in meteorological conditions, variation in VOC fluxes between – and even within – this study and other sites (Table 4-4) can be accounted for by differences in vegetation cover. Studies of individual plants have been conducted for some of the more dominant species; however further work could focus on extending knowledge of emission potentials to other species. Additionally, plant developmental stage will affect VOC emissions and was not investigated here.

Limitations with the method used in this study may have affected the accuracy of measured fluxes. The use of a static chamber is not ideal, due to the potential for impact on plant emissions as a result of altering temperature and humidity, as well as the local ambient concentration of the VOCs being measured. Tests on the chamber suggested that measurements may underestimate the true value, either due to inadequate mixing within the chamber, or leaks due to a poor seal with the soil collar. There is therefore potential for improvement in the enclosure design.

Improvements to the sampling method could include the use of a fan within chambers to ensure that air is well-mixed. This may also help alleviate condensation of water on the inside of the chamber surface. Also, temperature and PAR measurements within the chambers would give more a more accurate indication of plant conditions rather than using ambient measurements.

Despite the method limitations, this work nonetheless provides a valuable, comparative study to investigate the effects of N-treatment on VOC emissions. There was evidence that isoprene and  $\beta$ -pinene fluxes were affected by nitrate treatment in both cases, and also ammonium in the case of isoprene. What was not clear was whether the variations in VOC emissions were as a direct result of N-treatment, or whether they were a secondary effect of change in vegetation cover due to N-treatment. There is evidence for the latter from previous research carried out at Whim (Sheppard et al., 2011). In either case, further understanding of the associated changes to VOC emissions is important, given the predicted rise in atmospheric N concentrations and sensitivity of peatland ecosystems to atmospheric composition and deposition.

## 4.5 Conclusions

Static enclosure measurements of VOC fluxes revealed a temperate peatland to be a source of isoprene and monoterpenes, with standardised (30 °C and 1000  $\mu\text{mol m}^{-2} \text{s}^{-1}$ ) emission factors of 590 and 1.5  $\mu\text{g m}^{-2} \text{h}^{-1}$ , respectively. The effects of wet  $\text{NO}_3^-$  or  $\text{NH}_4^+$  treatment (equivalent to 64 kg N  $\text{ha}^{-1} \text{y}^{-1}$ ) on VOC emissions was also investigated and it was found that both nitrate and ammonium treatment reduced isoprene emissions, while nitrate treatment increased  $\beta$ -pinene emission compared to control plots experiencing only background deposition of N (8 kg N  $\text{ha}^{-1} \text{y}^{-1}$ ). Further work could include experiments to confirm the impact of N-treatment on VOC emissions from individual species, either under field or laboratory conditions. This would allow impacts on VOC emissions to be assessed as a result of vegetation cover change due to increased atmospheric nitrogen concentrations.

## Chapter 5: Effect of isoprene on the gas-phase oxidation of monoterpenes

In this chapter, results from laboratory experiments are presented. A reaction chamber was used to investigate the gas-phase loss of a monoterpene in the presence of isoprene, under three different concentration scenarios. Limonene and  $\alpha$ -pinene were investigated separately under varying isoprene mixing ratio. PTR-MS was used to measure the rate of decrease of monoterpene, which, for  $\alpha$ -pinene, was found to be slowest when isoprene mixing ratio was greater. The opposite result was observed for limonene. The observed trends were explained by differences in the atmospheric lifetimes of  $\alpha$ -pinene or limonene in comparison to that of isoprene.

### 5.1 Introduction

As an extension to previous chapters, not only is it important to quantify VOC emissions from the biosphere to the atmosphere, it is also important to understand the chemistry of emitted species. As described in Chapter 1, VOCs undergo oxidation reactions in the atmosphere to form secondary organic aerosol (SOA) in gas-to-particle processes, and have long been recognised as a source of particle formation in the atmosphere (Went, 1960). Large uncertainties still exist however in the processes and quantities involved in the formation of SOA.

Current estimates of the contribution of biogenic sources to global SOA production are variable. A global modelling study predicted that biogenic sources contribute 2.5 – 44 Tg  $y^{-1}$  SOA (Tsigaridis and Kanakidou, 2003), while bottom-up approaches based on aerosol yields for individual compounds resulted in estimates of 12 – 70 Tg  $y^{-1}$  (Kanakidou et al., 2005). A top-down approach on the other hand resulted in estimates as high as 510 – 910 Tg  $y^{-1}$  (Goldstein and Galbally, 2007).

In addition to uncertainties in gas-to-aerosol processes, unknowns still exist in how SOA may impact on climate. Some studies have suggested negative feedback effects between increasing temperature, VOC emissions and SOA production (Goldstein et al., 2009; Kulmala et al., 2004; Mentel et al., 2013). It is suggested that increased global temperatures will increase VOC emissions, and thus increase atmospheric

SOA formation. The SOA particles will then attenuate global warming due to their cooling effect by scattering of solar radiation.

Additionally, there are currently uncertainties about the potential for synergistic effects of multiple VOC emissions on secondary pollutants. This is important for future predictions of atmospheric composition, as land use changes or climate change may result not only in changes of VOC species emitted, but also their relative ratios.

It has been hypothesised that, although isoprene is itself not considered a major contributor to SOA (Kanakidou et al., 2005) – accounting for around 2 Tg y<sup>-1</sup> SOA (Claeys et al., 2004) – it may inhibit nucleation of aerosol particles from monoterpenes by acting as a sink of OH radicals due to its high reactivity (Kiendler-Scharr et al., 2009). The study by Kiendler-Scharr et al. (2009) was carried out using chamber experiments on unseeded air, therefore is not necessarily representative of real atmospheric conditions, where pre-existing aerosol particles provide a surface for VOC oxidation products to partition onto (Hamilton et al., 2011).

The results suggest that if relative emissions of isoprene increase due to increasing global temperatures or land use change, SOA formation from monoterpenes could be reduced. This would therefore reduce the negative radiative forcing effects of aerosol particles, thus potentially amplifying global warming.

Controlled chamber experiments were conducted to investigate loss of gas phase compounds. The aim of the chamber experiments was to investigate the effect of varying isoprene concentration in a single monoterpene system, to identify whether isoprene concentration has an effect on the rate of loss of monoterpene. The monoterpenes selected were limonene and  $\alpha$ -pinene to allow differing reactivity of monoterpene to be investigated. The work presented here was part of a larger study including aerosol measurements which will be reported elsewhere.

## 5.2 Methods

Experiments were carried out to investigate the behaviour of gas-phase species during the formation of aerosol particles. Various measurements were taken of both gas- and aerosol-phase, however only PTR-MS data is presented here.

The aerosol chamber used is based within the Centre for Atmospheric Science at University of Manchester. It consists of an 18 m<sup>3</sup> (3 m (H) x 3 m (L) x 2 m (W)) Teflon bag mounted onto 3 aluminium frames. One fixed frame surrounds the centre of the chamber. The other 2 surround the top and bottom vertices of the chamber and can be moved in the vertical direction to allow the bag to be expanded or collapsed during filling/flushing. The bag and frame are contained within an outer housing. One of the walls is fitted with a 6 kW xenon arc lamp and a series of halogen lamps, with the rest of the inner housing being covered with reflective “space blanket” to allow maximum irradiance. The number of lamps used had been carefully selected to replicate the solar spectrum. Air conditioning between the bag and the outer enclosure was used to avoid unwanted heat from the lamps.

Chemical precursors – including organic trace gas species, aerosol seed, oxidant and NO<sub>x</sub> – are all user controlled, as well as environmental factors such as temperature and relative humidity. Figure 5-1 shows a schematic diagram of the components connected to the chamber.

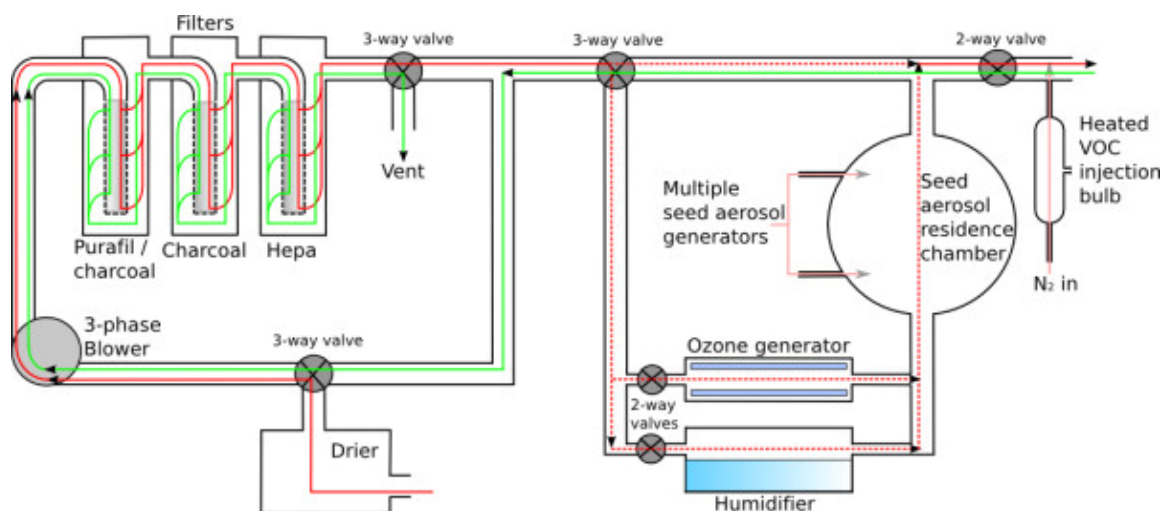


**Figure 5-1<sup>8</sup>** Schematic diagram of the Manchester University aerosol chamber filling system. Green lines show the path taken for air during flushing of the chamber. Red denotes path(s) taken while filling. Note that during filling the air intake always passes over the drier and filters. It may or may not pass through the ozone generator, humidifier or VOC injection bulb, depending on the stage in the fill cycle.

Electro-pneumatic valves are used to control the flow of air during filling/flushing, with the exception of the VOC inlet which is manually controlled by setting a regulator to purge the vessel with nitrogen.

Cleaning of the chamber prior to the commencement of an experiment was achieved firstly by filling the bag with ppm-level ozone in scrubbed lab air overnight. In the morning, this air was flushed from the chamber, and 5 cycles of automatic filling/flushing the bag with scrubbed, dried, rehumidified air ( $3 \text{ m}^3 \text{ min}^{-1}$ ) were carried out.

The final fill cycle was also used to set the temperature and relative humidity conditions required for the experiment ( $26^\circ\text{C}$ , 82%) by diverting air flow through or avoiding the humidifier. Use of 3 filters in series (see Figure 5-1) resulted in  $\text{NO}_x$

<sup>8</sup> Acknowledgments to Rami Alfarra, University of Manchester.

concentrations of < 5 ppbv. Initial ozone concentrations at this stage were typically < 2 ppbv. (NH<sub>4</sub>)<sub>2</sub>SO<sub>4</sub> aerosol seed was introduced by running an aerosol generator for 40 s at 2 bar (2 g L<sup>-1</sup>). The required VOC precursor(s) were added by manually injecting a known volume of sample into a heated injection bulb which was purged with nitrogen into the chamber. The sample volume was calculated based on the required concentration in the chamber, and the approximate volume of the chamber (18 m<sup>3</sup>). Once the fill cycle was complete, air flow was directed to introduce ozone. The ozone generator was switched on for 60 s, and then the air flow passed through for 2 s, achieving a concentration of ~10 ppbv. Experiments were carried out in light. The “lights on” stage signified the start of the experiment, and time = 0.

Several online analytical instruments for analysis of gas- and aerosol-phase species were used to sample from the chamber from before lights on, in addition to the PTR-MS. These are summarised in Table 5-1.

**Table 5-1 Summary of instruments connected to the aerosol chamber with brief descriptions of the parameters measured.**

Instrument	Parameter Measured
Condensation Particle Counter (CPC)	Total aerosol number concentration
Differential Mobility Particle Sizer (DMPS)	Dry and wet particle mobility size up to 0.8µm diameter
Aerosol Mass Spectrometer (AMS)	Chemical composition of aerosol
Hygroscopicity Tandem Differential Mobility Analyser (HTDMA)	Hygroscopic growth factor at 90% RH for several dry sizes
NO <sub>x</sub> Analyser	NO-NO <sub>2</sub> -NO <sub>x</sub> mixing ratio
O <sub>3</sub> Analyser	ozone mixing ratio

A single experiment typically took a full working day, including flush/fill cycles in the morning, in addition to flushing and filling with ppm level ozone in the evening following each experiment, which was left overnight to ensure thorough cleaning of the chamber.

A background scan was measured by filling the chamber with scrubbed lab air as normal but without addition of any precursors. This was done to determine the background quantities of species intrinsic to the chamber and the sampling system of the PTR-MS.

### 5.2.1 PTR-MS set-up and measurements

BVOC mixing ratios were measured using proton transfer reaction mass spectrometry (PTR-MS). The PTR-MS used in this study (Ionicon Analytik, Innsbruck, Austria) was fitted with an extra turbopump connected to the detection chamber, and Teflon instead of Viton rings in the drift tube (Davison et al., 2009; Misztal et al., 2010). Pfeiffer turbopumps replaced the Varian equivalents. The drift tube conditions were held constant throughout (pressure 2.0 mbar, temperature 45 °C, voltage 552 V) to maintain an  $E/N$  ratio of  $\sim 128$  Td ( $1 \text{ Td} = 10^{-17} \text{ V cm}^2$ ).

Air was sampled through a PTFE inlet line into the PTR-MS at a rate of  $\sim 100 \text{ mL min}^{-1}$ . Data were logged using a program written in LabVIEW (Version 8.5, National Instruments).

The PTR-MS signal was calibrated explicitly for several VOCs using a mixed gas calibration cylinder (Apel-Riemer Environmental Inc., USA) containing 1 ppmv each of formaldehyde, methanol, acetonitrile, acetone, acetaldehyde, isoprene and 0.18 ppmv d-limonene. The calibration gas was diluted with VOC-scrubbed air to produce 7 samples with concentrations of 0, 0.5, 1, 10, 20, 30 and 50% of the pure calibration gas standard. A relative transmission curve was then constructed to determine empirical calibration coefficients for other VOCs under study not present in the standard (Taipale et al., 2008). Calibration was carried out on 23 November 2009, with experiments carried out on 18, 19, 20, 24 November and 3 and 4 December 2009.

The PTR-MS was run in multiple ion detection (MID) mode for two 25 min sampling periods per hour. During these periods only the targeted VOC ions listed in Table 5-2 were measured, with dwell times of 2 s, in addition to the primary ion  $\text{H}_3\text{O}^+$ , and water cluster  $(\text{H}_2\text{O})\text{H}_3\text{O}^+$ , which had dwell times of 0.2 s. The sensitivities are also included in Table 5-2.

The remaining 10 min per hour were used for full mass scans in the range 21 – 206 amu at a dwell time of 2 s per amu. Air from within the chamber was scanned to allow information about the full VOC composition to be acquired.

**Table 5-2 Compounds measured during the chamber experiments including dwell times and sensitivities.**

$m/z$ [amu]	Contributing compound(s)	Formula	Dwell time [s]	Sensitivity [ncps ppbv <sup>-1</sup> ]
21	water isotope	$\text{H}_2^{18}\text{O}$	0.2	-
37	water cluster	$(\text{H}_2\text{O})_2$	0.2	-
61	glycolaldehyde	$\text{C}_2\text{H}_4\text{O}$	2	13.6
69	isoprene	$\text{C}_5\text{H}_8$	2	4.09
	furan			
	methyl butenol fragment			
71	methyl vinyl ketone (MVK) methacrolein (MACR)	$\text{C}_4\text{H}_6\text{O}$	2	3.16
73	methylglyoxal	$\text{C}_3\text{H}_4\text{O}_2$	2	2.45
75	hydroxyacetone	$\text{C}_3\text{H}_6\text{O}_2$	2	2.00
81	monoterpene fragment		2	1.58
87	2-methyl-3-buten-2-ol (MBO)	$\text{C}_5\text{H}_{10}\text{O}$	2	1.41
101	isoprene hydroxyhydroperoxide fragment isoprene dihydroxyperoxide fragment		2	1.38
119	isoprene hydroxyhydroperoxide isoprene dihydroxyperoxide	$\text{C}_5\text{H}_{10}\text{O}_3$	2	1
137	monoterpene	$\text{C}_{10}\text{H}_{16}$	2	0.356
139	nopinone/ limona ketone	$\text{C}_9\text{H}_{14}\text{O}$	2	0.356
151	pinonaldehyde/limonaldehyde fragment		2	0.0014
185	pinonic/limononic acid	$\text{C}_{10}\text{H}_{16}\text{O}_3$	2	0.001
187	pinic/limonic acid	$\text{C}_9\text{H}_{14}\text{O}_4$	2	0.001

### 5.2.2 Experiments with a monoterpenes and isoprene

Chamber experiments were carried out using either limonene or  $\alpha$ -pinene. Three experiments were carried out for each monoterpene, using a high, medium or low mixing ratio of isoprene. For the “low” isoprene experiments, no isoprene was added to the chamber, therefore mixing ratios given in Table 5-3 represent background mixing ratio present in the scrubbed air used to fill the chamber (0.50 and 0.25 ppbv for limonene and  $\alpha$ -pinene respectively).

**Table 5-3 Summary of chamber experiments carried out. Mixing ratios at the start of the experiments are shown for VOCs (as measured by the calibrated PTR-MS), oxidant ( $O_3$ ) and  $NO_x$ .**

Monoterpene	[Isoprene] / ppbv	[Monoterpene] / ppbv	[ $O_3$ ] / ppbv	[ $NO_x$ ] / ppbv
Limonene	0.50	15	8.0	3.2
	3.5	11	9.5	2.1
	115	20	11	1.7
$\alpha$ -Pinene	0.25	45	10	2.9
	2.5	43	16	9.0
	43	40	8.5	2.8

### 5.2.3 MCM simulations

Simulations using FACSIMILE4 for Windows (MCPA Software Ltd, UK) were run for comparison with experimental data obtained from limonene and  $\alpha$ -pinene experiments. The chemical mechanistic information was taken from the Master Chemical Mechanism, MCM v3.2 (Jenkin et al., 1997; Saunders et al., 2003), via website: <http://mcm.leeds.ac.uk/MCM>. For limonene experiments, limonene, limonaldehyde, limonic acid, limononic acid, isoprene, MVK and MACR species and their mechanisms were extracted for running simulations in FACSIMILE.  $\alpha$ -pinene, pinonaldehyde, pinic acid, pinonic acid, isoprene, MVK and MACR were extracted for  $\alpha$ -pinene simulations. Light conditions were simulated by constant photolysis rates. Starting concentrations and conditions were set as detailed in Table 5-4. The programs are included in Appendix II.

**Table 5-4 Starting concentrations and conditions for each of the six MCM simulations.**

Experiment	[MT] / ppbv	[Isoprene] / ppbv	[O <sub>3</sub> ] / ppbv	[NO] / ppbv	[NO <sub>2</sub> ] / ppbv	T / K
Limonene	15	0.5	8	2.5	0.7	295.8
	11	3.5	9.5	1.5	0.6	295.2
	20	115	11	1.5	0.2	296.2
$\alpha$ -Pinene	45	0.25	10	2.1	0.8	296.5
	43	2.5	16	8.2	0.8	296.4
	40	43	8.5	2.2	0.6	296.4

Starting parameters were set to match those measured experimentally at the start of chamber experiments.

## 5.3 Results

### 5.3.1 Experimental chamber results

#### 5.3.1.1 $\alpha$ -Pinene results

Raw PTR-MS data from the chamber experiments was rather noisy (included in Appendix III). As such, an exponential fit was applied to the data, which was then offset to start at mixing ratio equal to zero, so that the rate of decrease in  $\alpha$ -pinene could be compared across experiments. Rates of decrease of  $\alpha$ -pinene in the presence of three different concentrations of isoprene are shown in Figure 5-2. Experiments were run for 4 - 5 hours, however only the first hour of data were examined to avoid the possibility of secondary reactions, wall losses and increased SOA causing experimental results to deviate from modeled data.

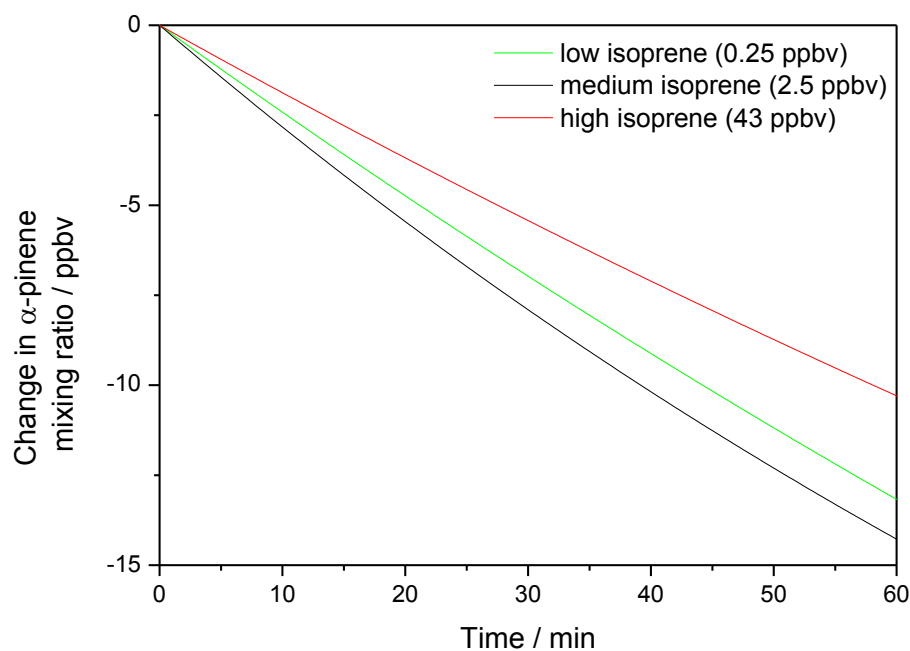


**Figure 5-2 Exponential fits to show rate of decrease of  $\alpha$ -pinene with varying mixing ratios of isoprene. Initial mixing ratios of  $\alpha$ -pinene used were 45, 43 and 40 ppbv for low, medium and high mixing ratios of isoprene respectively.**

Figure 5-2 shows that the highest isoprene mixing ratio (43 ppbv) resulted in the slowest rate of decrease in  $\alpha$ -pinene. Medium and low isoprene mixing ratios (2.5 and 0.25 ppbv respectively) resulted in similar initial rates of loss of  $\alpha$ -pinene, with the mixing ratio starting to plateau for the medium experiment first.

The reaction of a monoterpene with OH radical is a second order reaction with rate equation

$$rate = k [OH][monoterpene] \quad (5-1)$$

where  $k$  is the reaction rate constant. However, because OH is constantly regenerated in the reaction chamber, its concentration can be assumed to be constant and a pseudo-first order rate equation is followed

$$rate = k'[monoterpene] \quad (5-2)$$

where  $k'$  is a pseudo-first order rate constant.

In all  $\alpha$ -pinene experiments, an exponential decrease in mixing ratio was observed according to the pseudo-first order kinetic equation

$$[A]_t = [A]_0 e^{-k't} \quad (5-3)$$

The natural logarithm of measured  $\alpha$ -pinene mixing ratios were therefore plotted against time to determine the pseudo-first order rate constant,  $k'$  for each of the experiments according to the equation

$$\ln[A]_t = \ln[A]_0 - k't \quad (5-4)$$

The linear fits are shown in Figure 5-3.

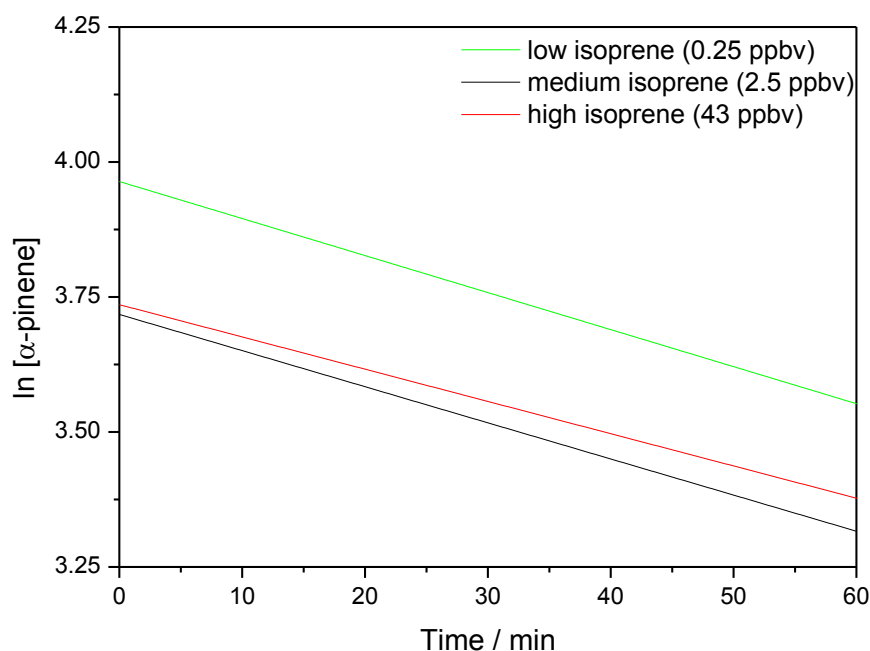


**Figure 5-3** Linear fits of the natural logarithm of  $\alpha$ -pinene mixing ratio against time. Initial mixing ratios of  $\alpha$ -pinene used were 45, 43 and 40 ppbv for low, medium and high mixing ratios of isoprene respectively.

Linear fit equations for  $\alpha$ -pinene experiments are summarised in Table 5-5 along with associated errors (raw data shown in Appendix III).

**Table 5-5 Linear fit parameters for the pseudo-first order decay of  $\alpha$ -pinene, according to the equation  $\ln[A]_t = \ln[A]_0 - k't$ . Numbers in parentheses denote standard errors.**

[isoprene] / ppbv	$\ln[A]_0$	$k' / \text{min}^{-1}$
0.25	3.964 (0.00836)	0.00686 ( $5.30 \times 10^{-5}$ )
2.5	3.718 (0.00834)	0.00669 ( $5.56 \times 10^{-5}$ )
43	3.736 (0.00808)	0.00597 ( $5.83 \times 10^{-5}$ )

The rate of  $\alpha$ -pinene decay was slower at the start of the experiment for low isoprene (Figure III-I). The starting mixing ratio according to the linear logarithm plot (52 ppbv) therefore deviates slightly from the value measured (45 ppbv).

### 5.3.1.2 Limonene results

As with  $\alpha$ -pinene experiments, exponential fits were applied to the data from the three limonene experiments, which were then offset to start at mixing ratio equal to zero, so that the rate of decrease in limonene could be compared across experiments (raw data are included in Appendix III). Rates of decrease of limonene in the presence of three different concentrations of isoprene are shown in Figure 5-4.

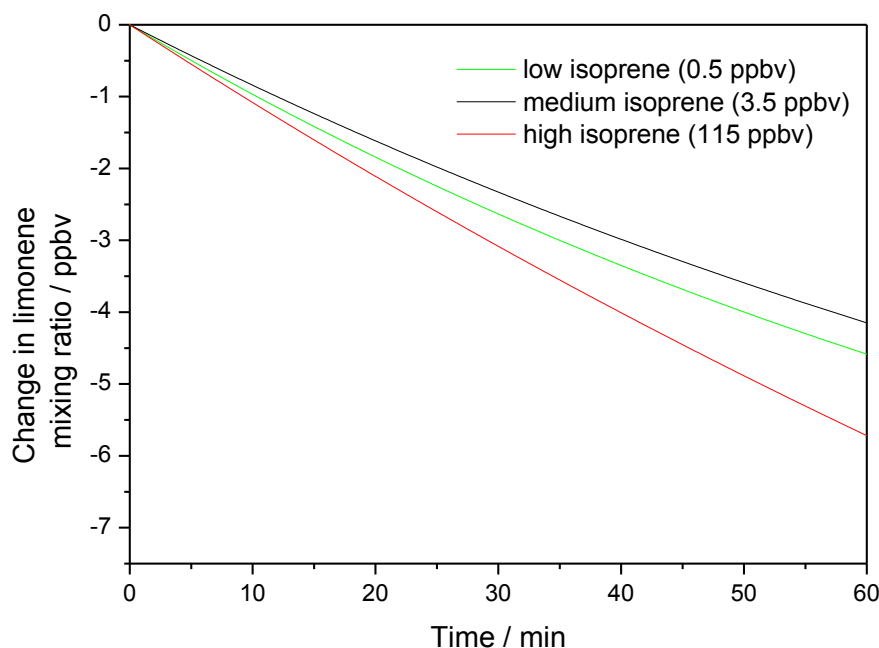


**Figure 5-4** Rate of decrease of limonene with varying mixing ratios of isoprene. Mixing ratios of limonene used were 15, 11 and 20 ppbv for low, medium and high mixing ratios of isoprene respectively.

Figure 5-4 shows that the highest isoprene mixing ratio (115 ppbv) resulted in the fastest rate of decrease in limonene, in contrast to the results from  $\alpha$ -pinene experiments. Similarly to  $\alpha$ -pinene experiments, medium and low isoprene mixing ratios (3.5 and 0.5 ppbv respectively) resulted in similar rates of loss of limonene.

All limonene measurements followed an exponential decrease in mixing ratio according to the pseudo-first order kinetic equation (equation 5-3). The natural logarithm of measured limonene mixing ratios were therefore plotted against time to determine the rate constant,  $k'$  for each of the experiments, and the linear fits are shown in Figure 5-5 (raw data shown in Appendix III).

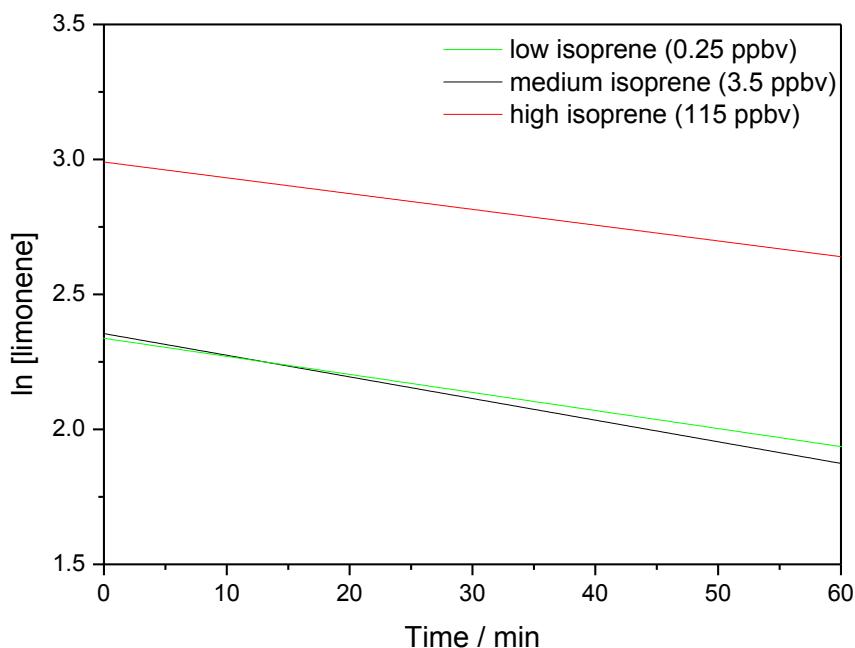


**Figure 5-5** Linear fits of the natural logarithm of limonene mixing ratio against time. Mixing ratios of limonene used were 15, 11 and 20 ppbv for low, medium and high mixing ratios of isoprene respectively.

Linear fit equations for limonene experiments are summarised in Table 5-6 along with associated errors.

**Table 5-6** Linear fit parameters for the pseudo-first order decay of limonene, according to the equation  $\ln[A]_t = \ln[A]_0 - k't$ . Numbers in parentheses denote standard errors.

[isoprene] / ppbv	$\ln[A]_0$	$k' / \text{min}^{-1}$
0.5	2.337 (0.0581)	0.00669 ( $3.87 \times 10^{-4}$ )
3.5	2.355 (0.0273)	0.00802 ( $2.00 \times 10^{-4}$ )
115	2.990 (0.0168)	0.00584 ( $1.65 \times 10^{-4}$ )

## 5.3.2 Simulated MCM results

### 5.3.2.1 $\alpha$ -Pinene MCM simulations

As with experimental results, simulated data were offset to start at mixing ratio equal to zero, so that the rate of decrease in  $\alpha$ -pinene could be compared across experiments. Rates of decrease of  $\alpha$ -pinene in the presence of three different concentrations of isoprene are shown in Figure 5-6.

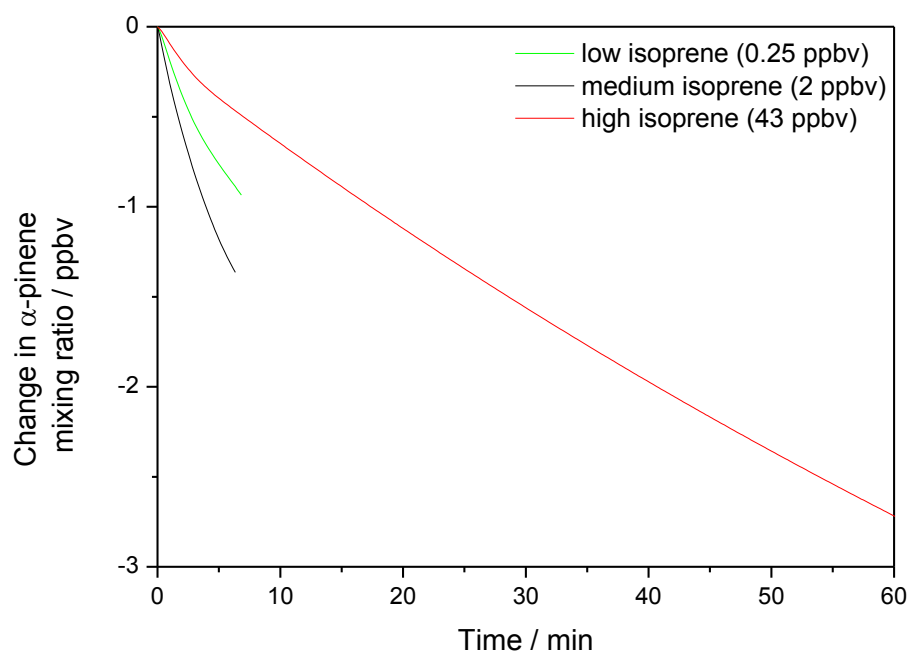


**Figure 5-6** Rate of decrease of  $\alpha$ -pinene with varying mixing ratios of isoprene from MCM simulations. Mixing ratios of  $\alpha$ -pinene used were 45, 43 and 40 ppbv for low, medium and high mixing ratios of isoprene respectively. Note that data output could not be calculated by the model for the full time course for 2 of the runs due to an instability in the model caused by low initial isoprene mixing ratio.

Figure 5-6 shows that the highest isoprene mixing ratio (43 ppbv) resulted in the slowest rate of decrease in  $\alpha$ -pinene. Simulations for low and medium isoprene mixing ratios did not run for the full time series using the conditions set as detailed in Table 5-4 due to an instability caused by depletion of a low initial isoprene mixing ratio. From the available data output, the medium isoprene mixing ratio resulted in the fastest initial rate of  $\alpha$ -pinene decrease.

All  $\alpha$ -pinene decay plots in Figure 5-6 followed an exponential decrease in mixing ratio according to the pseudo-first order kinetic equation (Equation 5-3). The natural logarithm of simulated  $\alpha$ -pinene mixing ratios were therefore plotted against time to determine the rate constant,  $k$  for each of the experiments, shown in Figure 5-7.

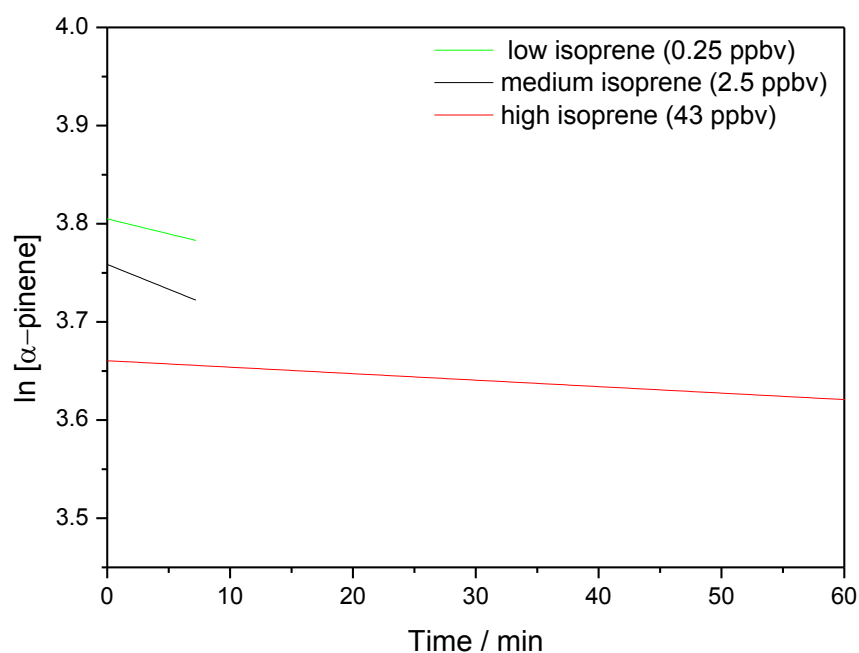


**Figure 5-7** Linear fits of the natural logarithm of  $\alpha$ -pinene mixing ratio against time for MCM simulations. Mixing ratios of  $\alpha$ -pinene used were 45, 43 and 40 ppbv for low, medium and high mixing ratios of isoprene respectively.

Linear fits for Figure 5-7 are summarized in Table 5-7.

**Table 5-7** Linear fit parameters for the pseudo-first order decay of  $\alpha$ -pinene from MCM simulations, according to the equation  $\ln[A]_t = \ln[A]_0 - k't$ . Numbers in parentheses denote standard errors.

[isoprene] / ppbv	$\ln[A]_0$	$k' / \text{min}^{-1}$
0.25	3.805 ( $2.86 \times 10^{-4}$ )	0.00304 ( $7.21 \times 10^{-5}$ )
2.5	3.759 ( $3.89 \times 10^{-4}$ )	0.00504 ( $1.06 \times 10^{-4}$ )
43	3.661 ( $4.77 \times 10^{-4}$ )	$6.601 \times 10^{-4}$ ( $3.06 \times 10^{-6}$ )

### 5.3.2.2 Limonene MCM simulations

Exponential fits were applied to simulated limonene data, which were then offset to start at mixing ratio equal to zero, so that the rate of decrease in limonene could be compared across experiments. Rates of decrease of limonene in the presence of three different concentrations of isoprene are shown in Figure 5-8.

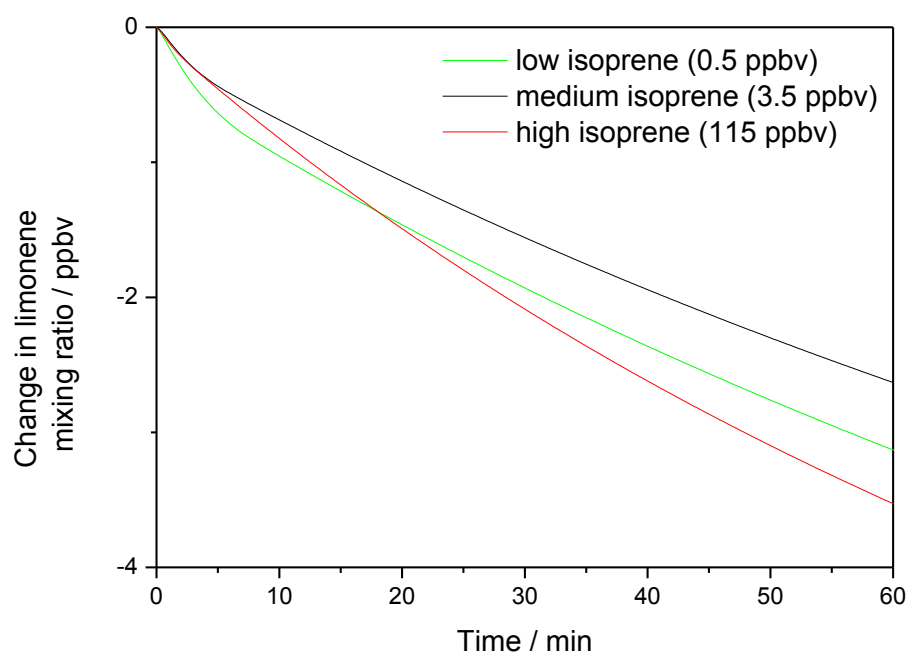


**Figure 5-8** Rate of decrease of limonene with varying mixing ratios of isoprene from MCM simulations. Mixing ratios of limonene used were 15, 11 and 20 ppbv for low, medium and high mixing ratios of isoprene respectively.

It can be seen from Figure 5-8 that the fastest rate of decrease in limonene mixing ratio over 60 min was observed for the highest mixing ratio of isoprene, with the middle isoprene mixing ratio resulting in the slowest rate of decrease in limonene.

All limonene decay plots in Figure 5-8 followed an exponential decrease in mixing ratio according to the pseudo-first order kinetic equation (Equation 5-3). The natural logarithm of simulated limonene mixing ratios were therefore plotted against time to determine the rate constant,  $k'$  for each of the experiments (Figure 5-9), and the linear fits are summarized in Table 5-8.

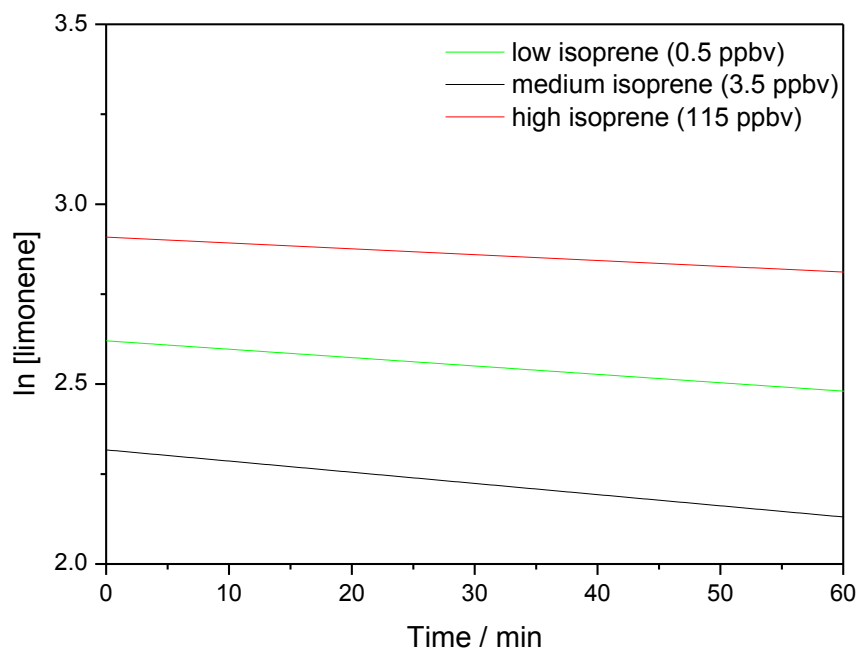


**Figure 5-9** Linear fits of the natural logarithm of limonene mixing ratio against time for MCM simulations. Mixing ratios of limonene used were 15, 11 and 20 ppbv for low, medium and high mixing ratios of isoprene respectively.

**Table 5-8** Linear fit parameters for the pseudo-first order decay of limonene from MCM simulations, according to the equation  $\ln[A]_t = \ln[A]_0 - k't$ . Numbers in parentheses denote standard errors.

[isoprene] / ppbv	$\ln[A]_0$	$k' / \text{min}^{-1}$
0.5	2.620 (0.00121)	0.00233 ( $7.74 \times 10^{-6}$ )
3.5	2.317 (0.00124)	0.00311 ( $7.94 \times 10^{-6}$ )
115	2.908 (0.00149)	0.00162 ( $9.57 \times 10^{-6}$ )

## 5.4 Discussion

Comparison of Figure 5-2 with Figure 5-6, and Figure 5-4 with Figure 5-8, shows that the total decrease in monoterpene mixing ratios was greater for experimentally measured data than for simulated MCM data. This may be explained by losses occurring in the chamber experiments which are not accounted for in the MCM simulations, such as wall losses, dilution effects, or incomplete mixing.

Measured  $k'$  values from the chamber experiments differed from those calculated from MCM simulations. The two sets of  $k'$  values are compared in Figure 5-10 for limonene and  $\alpha$ -pinene.

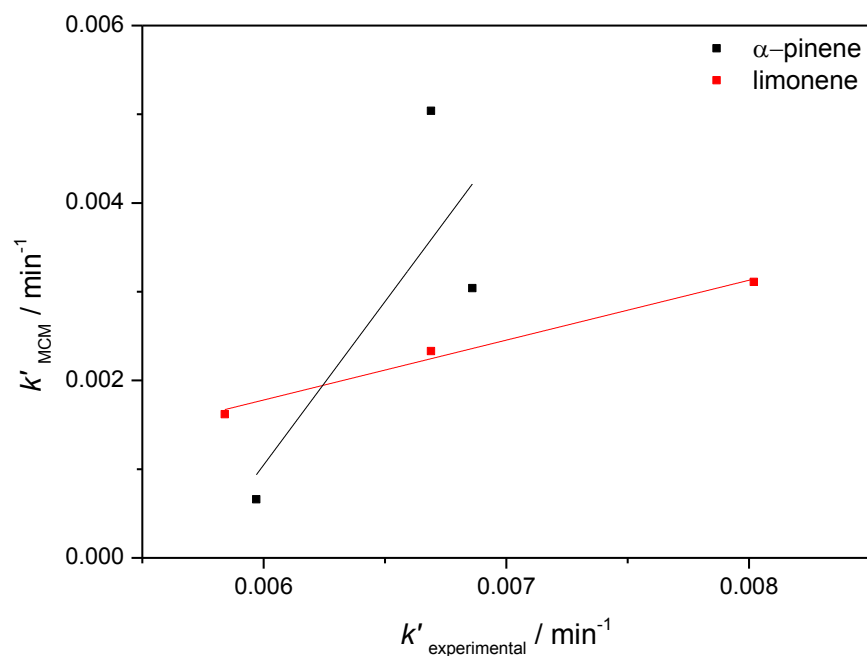


**Figure 5-10 Relationship between  $k'$  values from MCM simulations with those measured from chamber experiments. Linear fit of limonene is  $k'_{\text{MCM}} = 0.675 k'_{\text{experimental}} - 0.0227$  (errors: m 0.0673, c  $4.65 \times 10^{-4}$ ). Linear fit of  $\alpha$ -pinene is  $k'_{\text{MCM}} = 3.68 k'_{\text{experimental}} - 0.0210$  (errors: m 2.82, c 0.0184).**

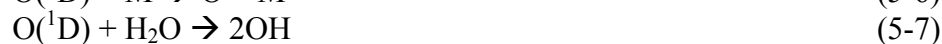
Figure 5-10 shows that for both  $\alpha$ -pinene and limonene, experimental values of  $k'$  showed faster removal rates than those predicted from simple gas-phase reactions only, as simulated in the MCM model. There was a linear relationship between measured and calculated rates however.

Comparison of experimental and simulated results for  $\alpha$ -pinene (Figure 5-2 and Figure 5-6, respectively) shows that there is some agreement in trends. Both showed the slowest rate of decrease in  $\alpha$ -pinene for highest isoprene mixing ratios. This is in agreement with the results of Kiendler-Scharr et al. (2009) who hypothesised that high isoprene suppresses oxidation of monoterpenes.

On the other hand, examination of experimental and simulated results for limonene (Figure 5-4 and Figure 5-8 respectively) reveals results contrary to those for  $\alpha$ -pinene. In both the simulated and experimental data, the highest mixing ratio of isoprene resulted in the fastest rate of decrease in limonene, followed by low then medium isoprene mixing ratios. This is also in contrast to the study by Kiendler-Scharr et al. (2009).

In the study by (Kiendler-Scharr et al., 2009), experimental chamber studies were carried out using VOC emissions from a variety of monoterpene-emitting species (silver birch, beech, Norway spruce and Scots pine) to which varying isoprene quantities had been added. The monoterpene composition was not reported, however all species used in the study except beech are reported to have greater  $\alpha$ -pinene emissions than limonene.  $\alpha$ -Pinene and limonene make up 13.6 and 1.2 % of monoterpene emissions from silver birch (Hakola et al., 1998), 5.7 and 6.3 % from beech (König et al., 1995), 48.1 and 0.9 % from Scots pine (Räisänen et al., 2009), and 49.2 and 6.8 % from Norway spruce (Christensen et al., 2000). Additionally, an MCM simulation was carried out using  $\alpha$ -pinene. It is therefore logical that  $\alpha$ -pinene results from this study should follow those observed by Kiendler-Scharr et al. (2009).

The apparent ability for isoprene to inhibit oxidation of  $\alpha$ -pinene and the contrasting results for limonene can be explained by comparing atmospheric lifetimes (Atkinson and Arey, 2003) of limonene and  $\alpha$ -pinene with isoprene. Assuming  $2.63 \times 10^{11}$  molecules  $\text{cm}^{-3}$  (average 10.5 ppbv ozone used in chamber experiments), the atmospheric lifetime of isoprene with  $\text{O}_3$  is 3.4 days. Those of  $\alpha$ -pinene and limonene are 12.2 h and 5.3 h respectively. Both monoterpenes have lifetimes shorter than that of isoprene, therefore reactions with  $\text{O}_3$  alone cannot explain the differing influence of isoprene on their oxidation rates. As the experiments were carried out under light, hydroxyl radicals will also have been formed in the chamber system according to the reaction scheme:



where Equation 5-5 is initiated by light of wavelengths of 300 – 320 nm. Formation of OH has also been shown to be particularly elevated during ozonolysis experiments where there is high water availability (Tillmann et al., 2010), indicated in this study by high relative humidity.

The lifetime of isoprene for reaction with the OH radical is 1.4 h. That of  $\alpha$ -pinene is 2.6 h, i.e. reaction is slower than that of isoprene hence isoprene is able to scavenge OH and suppress reaction of  $\alpha$ -pinene with OH. Conversely, the atmospheric lifetime of limonene (49 min) is shorter than that of isoprene. Limonene is therefore more able to compete in oxidation reactions than  $\alpha$ -pinene, explaining why higher isoprene mixing ratios did not reduce the rate of limonene oxidation.

To quantify the established link between isoprene mixing ratio and rate of  $\alpha$ -pinene decrease, experimental  $k'$  values are plotted against isoprene mixing ratio in Figure 5-11.

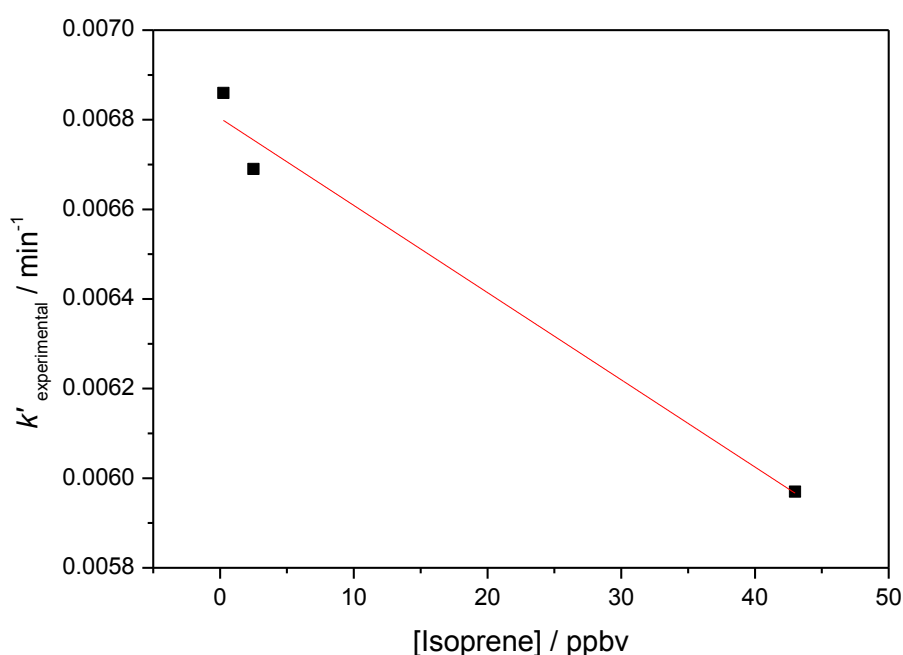


**Figure 5-11 Relationship between experimentally measured  $k'$  value and isoprene mixing ratio. A linear relationship was observed:  $k'_{\text{experimental}} = -1.95 \times 10^{-5} [\text{isoprene}] + 0.00680$  (errors:  $m = 2.63 \times 10^{-6}$ ,  $c = 6.53 \times 10^{-5}$ ,  $R^2 = 0.964$ ).**

Figure 5-11 illustrates that as isoprene mixing ratio was increased, the rate of  $\alpha$ -pinene reaction reduced in a linear relationship. Only three different isoprene mixing ratios were investigated however, and none in the range between 2.5 and 43 ppbv, therefore further experiments could be conducted to verify this relationship.

Results presented here are relevant to areas where there are already primary aerosol sources (e.g. salt spray). Conversion from gas to aerosol phase for isoprene or monoterpene oxidation products will therefore depend on interaction of their oxidation products with the primary aerosol particles (ammonium sulphate in this study). All experiments were conducted on air seeded with ammonium sulphate particles to simulate the majority of environments. This is in contrast to Kiendler-Scharr et al. (2009) who investigated nucleation of SOA from unseeded air, which occurs only in relatively pristine atmospheres.

Further work could focus on running experiments over a greater spread of isoprene mixing ratios, in addition to investigating the effects on other monoterpenes. Other monoterpenes which have OH lifetimes longer than that of isoprene – and would therefore be expected to have their oxidation suppressed – include  $\beta$ -pinene, 2- and 3-carene and camphene, all of which are commonly reported in plant emissions. Examination of the rate of increase of monoterpene oxidation products has not been included here, but could also be examined to corroborate the observed results.

## 5.5 Conclusions

It was found that the rate of  $\alpha$ -pinene oxidation (and hence its loss from the gas-phase) was decreased with increasing isoprene mixing ratio. This was not the case for limonene, which, unlike  $\alpha$ -pinene, has a shorter OH lifetime than isoprene. This has implications for resultant SOA formation which, for  $\alpha$ -pinene (one of the most predominant emitted monoterpenes) may reduce negative feedback of climate warming.

## Chapter 6: Final conclusions

VOC fluxes and mixing ratios were successfully measured at Douglas fir, SRC willow, *Miscanthus* and peatland vegetation sites. Additionally, the effect of isoprene on gas-phase chemistry of monoterpenes was investigated. Implications of all results have been discussed in the individual chapters. Conclusions are summarised here and opportunities for further work discussed.

Results from a Douglas fir forest were successful in corroborating previous VOC measurements of the species, showing emission of monoterpenes. These were the first reported canopy-scale flux measurements for the species, and in addition to terpenoids, oxygenated VOCs were also found emitted from the canopy. The results highlight the importance of quantifying a wider variety of VOCs from biogenic sources. Traditionally, the focus of VOC measurements has been on isoprene and monoterpenes, partly due to lack of appropriate techniques for measuring OVOCs. The usefulness of PTR-MS in simultaneously obtaining data on a range of VOCs at canopy-scale has therefore been demonstrated. There was some evidence from in-canopy measurements that leaf litter could be a source of VOCs in addition to the tree canopy. Further work could therefore focus on verification of these sources by using chamber sampling as outlined in Section 1.5.1 and Chapter 4.

In the experimentally similar study of bioenergy crops, SRC willow was found to be a strong emitter of isoprene. Fluxes were 17 times greater than Douglas fir per unit mass of vegetation. Conversely, the bioenergy crop *Miscanthus* was found to have no detectable fluxes of VOCs. Additionally, comparison with other studies shows that total UK isoprene emissions could be significantly enhanced where SRC willow replaces traditional arable crops such as wheat, barley or oats. The results demonstrate that although bioenergy crops may sequester enough carbon dioxide during growth to offset what is released during combustion, a holistic, full life-cycle approach must be taken when considering their impact on the environment, including exchange of other important trace gases. The effect of land-use change by switching to widespread cultivation of higher VOC emitters has been demonstrated in other studies. As *Miscanthus* can only be grown in warmer temperatures, the impact on air

quality may be a particular issue in regions of the UK where cultivation of SRC willow is agriculturally more viable and therefore more economically favorable. The results presented here only report fluxes during summer for established crops. Work on other crops has shown that leaf wounding can be a strong source of VOCs, particularly OVOCs. Further work should therefore investigate emissions during senescence and harvesting, as well as growth stages of the crop life cycle.

Using the alternative technique of chamber measurements, isoprene and monoterpene fluxes were quantified from a peatland site in Scotland; the first reported measurements from a temperate (rather than sub-arctic or boreal) ecosystem. Despite limitations in the method, it was shown that emissions of terpenoids were comparable to other peatland sites and showed dependence on temperature and light. Due to the varied vegetation cover, results were reported on an area – rather than mass of vegetation – basis. Future work could therefore use enclosures to further probe the VOC emission potential of individual plant species present at the site, under field or laboratory conditions. Additionally, only terpenoids were investigated and so there is scope for inclusion of a wider range of VOCs in future work. Colleagues at CEH are planning further VOC measurements at the site using a relaxed-eddy accumulation (REA) system.

By also sampling from plots which had been exposed to enhanced nitrogen deposition, there was evidence that nitrate and ammonium treatment had varying effects on VOC emissions. While isoprene emissions were reduced by both nitrate and ammonium,  $\beta$ -pinene fluxes were increased by nitrate treatment. This demonstrates the sensitivity of the biosphere to change in atmospheric composition. Since relatively few samples were acquired, further work should aim to provide more data for these investigations. Only sample plots treated with high quantities of nitrogen deposition were investigated. Future work could therefore also be extended to include plots of varying nitrogen deposition to assess the relationship with VOC flux.

Finally, the impact of changing atmospheric composition – in the form of increasing isoprene mixing ratios – on oxidation of monoterpenes was investigated using

chamber experiments. There was evidence to show that the loss of monoterpenes from the gas-phase through oxidation reactions is dependent on isoprene concentration, for monoterpenes with atmospheric lifetime longer than isoprene. This will therefore suppress the potential of monoterpenes to form secondary organic aerosol (SOA) particles due to scavenging of OH radicals by isoprene. The wider implications of this would be that suppressed SOA formation will reduce the negative feedback on climate warming. This study highlights the need for greater understanding of the processes involved in gas-to-aerosol partitioning. It is widely accepted amongst the atmospheric research community that this topic of atmospheric science has one of the lowest levels of scientific understanding. Only  $\alpha$ -pinene and limonene were investigated in this work therefore the process should be verified by examining other monoterpenes. In addition to single monoterpene systems, further work could also include examining mixtures.

A theme throughout this work has been the endeavour to enhance understanding of how VOC emissions may be impacted by environmental change, whether it is in the form of land use, atmospheric composition or climate change. The links between such factors are complex and difficult to disentangle and therefore the understanding of such large scale processes may seem a scientifically daunting task. Nevertheless, the understanding of these global interactions is of fundamental importance for predicting future atmospheric scenarios and the resultant impacts.

## References

Ammann, C., Brunner, A., Spirig, C., Neftel, A., 2006. Technical note: Water vapour concentration and flux measurements with PTR-MS. *Atmospheric Chemistry and Physics* 6, 4643-4651.

Apel, E.C., Riemer, D.D., Hills, A., Baugh, W., Orlando, J., Faloon, I., Tan, D., Brune, W., Lamb, B., Westberg, H., Carroll, M.A., Thornberry, T., Geron, C.D., 2002. Measurement and interpretation of isoprene fluxes and isoprene, methacrolein, and methyl vinyl ketone mixing ratios at the PROPHET site during the 1998 Intensive. *Journal of Geophysical Research: Atmospheres* 107, 4034-4048.

Arey, J., Crowley, D.E., Crowley, M., Resketo, M., Lester, J., 1995. Hydrocarbon emissions from natural vegetation in California's South Coast Air Basin. *Atmospheric Environment* 29, 2977-2988.

Arneth, A., Niinemets, Ü., Pressley, S., Bäck, J., Hari, P., Karl, T., Noe, S., Prentice, I.C., Serça, D., Hickler, T., Wolf, A., Smith, B., 2007. Process-based estimates of terrestrial ecosystem isoprene emissions: incorporating the effects of a direct CO<sub>2</sub>-isoprene interaction. *Atmospheric Chemistry and Physics* 7, 31-53.

Ashmore, M.R., 2005. Assessing the future global impacts of ozone on vegetation. *Plant, Cell and Environment* 28, 949-964.

Ashworth, K., Folberth, G., Hewitt, C.N., Wild, O., 2012. Impacts of near-future cultivation of biofuel feedstocks on atmospheric composition and local air quality. *Atmospheric Chemistry and Physics* 12, 919-939.

Atkinson, R., 2000. Atmospheric chemistry of VOCs and NO<sub>x</sub>. *Atmospheric Environment* 34, 2063-2101.

Atkinson, R., Arey, J., 2003. Gas-phase tropospheric chemistry of biogenic volatile organic compounds: a review. *Atmospheric Environment* 37, S197-S219.

Biesenthal, T.A., Bottenheim, J.W., Shepson, P.B., Li, S.M., Brickell, P.C., 1998. The chemistry of biogenic hydrocarbons at a rural site in eastern Canada. *Journal of Geophysical Research: Atmospheres* 103, 25487-25498.

Blake, R.S., Monks, P.S., Ellis, A.M., 2009. Proton-Transfer Reaction Mass Spectrometry. *Chemical Reviews* 109, 861-896.

Bouvier-Brown, N.C., Goldstein, A.H., Worton, D.R., Matross, D.M., Gilman, J.B., Kuster, W.C., Welsh-Bon, D., Warneke, C., de Gouw, J.A., Cahill, T.M., Holzinger, R., 2009. Methyl chavicol: characterization of its biogenic emission rate, abundance, and oxidation products in the atmosphere. *Atmospheric Chemistry and Physics* 9, 2061-2074.

Christensen, C.S., Hummelshøj, P., Jensen, N.O., Larsen, B., Lohse, C., Pilegaard, K., Skov, H., 2000. Determination of the terpene flux from orange species and Norway spruce by relaxed eddy accumulation. *Atmospheric Environment* 34, 3057-3067.

Claeys, M., Graham, B., Vas, G., Wang, W., Vermeylen, R., Pashynska, V., Cafmeyer, J., Guyon, P., Andreae, M.O., Artaxo, P., Maenhaut, W., 2004. Formation of secondary organic aerosols through photooxidation of isoprene. *Science* 303, 1173-1176.

Clevers, J.G.P.W., Schaepman, M.E., Mùcher, C.A., de Wit, A.J.W., Zurita-Milla, R., Bartholomeus, H.M., 2007. Using MERIS on Envisat for land cover mapping in The Netherlands. *International Journal of Remote Sensing* 28, 637-652.

Constable, J.V.H., Litvak, M.E., Greenberg, J.P., Monson, R.K., 1999. Monoterpene emission from coniferous trees in response to elevated CO<sub>2</sub> concentration and climate warming. *Global Change Biology* 5, 252-267.

Copeland, N., Cape, J.N., Heal, M.R., 2012. Volatile organic compound emissions from *Miscanthus* and short rotation coppice willow bioenergy crops. *Atmospheric Environment* 60, 327-335.

Corchnoy, S.B., Atkinson, R., 1990. Kinetics of the gas-phase reactions of hydroxyl and nitrogen oxide (NO<sub>3</sub>) radicals with 2-carene, 1,8-cineole, *p*-cymene, and terpinolene. *Environmental Science & Technology* 24, 1497-1502.

Crespo, E., Graus, M., Gilman, J.B., Lerner, B.M., Fall, R., Harren, F.J.M., Warneke, C., 2012. Volatile organic compound emissions from elephant grass and bamboo cultivars used as potential bioethanol crop. *Atmospheric Environment* 65, 61-68.

Davison, B., Brunner, A., Ammann, C., Spirig, C., Jocher, M., Neftel, A., 2008. Cut-induced VOC emissions from agricultural grasslands. *Plant Biology* 10, 76-85.

Davison, B., Taipale, R., Langford, B., Misztal, P., Fares, S., Matteucci, G., Loreto, F., Cape, J.N., Rinne, J., Hewitt, C.N., 2009. Concentrations and fluxes of biogenic volatile organic compounds above a Mediterranean macchia ecosystem in western Italy. *Biogeosciences* 6, 1655-1670.

DEFRA, 2007. UK Biomass Strategy. DEFRA.

DEFRA, 2009. Experimental statistics. Non-food crop areas: United Kingdom. DEFRA.

DEFRA, 2013. Emissions of air quality pollutants: 1970 - 2011. DEFRA.

Dockery, D.W., Pope, C.A., Xu, X.P., Spengler, J.D., Ware, J.H., Fay, M.E., Ferris, B.G., Speizer, F.E., 1993. An association between air pollution and mortality in 6 United States cities. *New England Journal of Medicine* 329, 1753-1759.

Dorsey, J.R., Duyzer, J.H., Gallagher, M.W., Coe, H., Pilegaard, K., Weststrate, J.H., Jensen, N.O., Walton, S., 2004. Oxidized nitrogen and ozone interaction with forests. I: Experimental observations and analysis of exchange with Douglas fir. *Quarterly Journal of the Royal Meteorological Society* 130, 1941-1955.

Drewitt, G.B., Curren, K., Steyn, D.G., Gillespie, T.J., Niki, H., 1998. Measurement of biogenic hydrocarbon emissions from vegetation in the Lower Fraser Valley, British Columbia. *Atmospheric Environment* 32, 3457-3466.

DTI, 2005. Implementation guidance for the renewables obligation order 2005. DTI.

Ekberg, A., Arneth, A., Holst, T., 2011. Isoprene emission from Sphagnum species occupying different growth positions above the water table. *Boreal Environment Research* 16, 47-59.

Eller, A.S.D., Sekimoto, K., Gilman, J.B., Kuster, W.C., de Gouw, J.A., Monson, R.K., Graus, M., Crespo, E., Warneke, C., Fall, R., 2011. Volatile organic compound emissions from switchgrass cultivars used as biofuel crops. *Atmospheric Environment* 45, 3333-3337.

Evans, R.C., Tingey, D.T., Gumpertz, M.L., Burns, W.F., 1982. Estimates of isoprene and monoterpene emission rates in plants. *Botanical Gazette* 143, 304-310.

Faubert, P., Tiiva, P., Rinnan, A., Rasanen, J., Holopainen, J.K., Holopainen, T., Kyrö, E., Rinnan, R., 2010a. Non-methane biogenic volatile organic compound emissions from a subarctic peatland under enhanced UV-B radiation. *Ecosystems* 13, 860-873.

Faubert, P., Tiiva, P., Rinnan, A., Raty, S., Holopainen, J.K., Holopainen, T., Rinnan, R., 2010b. Effect of vegetation removal and water table drawdown on the non-methane biogenic volatile organic compound emissions in boreal peatland microcosms. *Atmospheric Environment* 44, 4432-4439.

Finlayson-Pitts, B.J., Pitts Jr, J.N., 2000. Chapter 6 - Rates and mechanisms of gas-phase reactions in irradiated organic – NO<sub>x</sub> – air mixtures, *Chemistry of the Upper and Lower Atmosphere*. Academic Press, San Diego, pp. 179-263.

Fowler, D., O'Donoghue, M., Muller, J.B.A., Smith, R.I., Dragosits, U., Skiba, U., Sutton, M.A., Brimblecombe, P., 2004. A chronology of nitrogen deposition in the UK between 1900 and 2000. *Water, Air, & Soil Pollution: Focus* 4, 9-23.

Galloway, J.N., 1998. The global nitrogen cycle: changes and consequences. *Environmental Pollution* 102, 15-24.

Galloway, J.N., Dentener, F.J., Capone, D.G., Boyer, E.W., Howarth, R.W., Seitzinger, S.P., Asner, G.P., Cleveland, C.C., Green, P.A., Holland, E.A., Karl, D.M., Michaels, A.F., Porter, J.H., Townsend, A.R., Vöosmarty, C.J., 2004. Nitrogen cycles: past, present, and future. *Biogeochemistry* 70, 153-226.

Ge, X., Wexler, A.S., Clegg, S.L., 2011. Atmospheric amines – Part I. A review. *Atmospheric Environment* 45, 524-546.

Geron, C., Rasmussen, R., R. Arnts, R., Guenther, A., 2000. A review and synthesis of monoterpene speciation from forests in the United States. *Atmospheric Environment* 34, 1761-1781.

Goldan, P.D., Kuster, W.C., Fehsenfeld, F.C., Montzka, S.A., 1995. Hydrocarbon measurements in the southeastern United States: The Rural Oxidants in the Southern Environment (ROSE) program 1990. *Journal of Geophysical Research: Atmospheres* 100, 25945-25963.

Goldstein, A.H., Galbally, I.E., 2007. Known and unexplored organic constituents in the Earth's atmosphere. *Environmental Science & Technology* 41, 1514-1521.

Goldstein, A.H., Koven, C.D., Heald, C.L., Fung, I.Y., 2009. Biogenic carbon and anthropogenic pollutants combine to form a cooling haze over the southeastern United States. *Proceedings of the National Academy of Sciences* 106, 8835-8840.

Gorham, E., 1991. Northern peatlands - role in the carbon-cycle and probable responses to climatic warming. *Ecological Applications* 1, 182-195.

Grabmer, W., Graus, M., Lindinger, C., Wisthaler, A., Rappengluck, B., Steinbrecher, R., Hansel, A., 2004. Disjunct eddy covariance measurements of monoterpene fluxes from a Norway spruce forest using PTR-MS. *International Journal of Mass Spectrometry* 239, 111-115.

Grogan, P., Matthews, R., 2002. A modelling analysis of the potential for soil carbon sequestration under short rotation coppice willow bioenergy plantations. *Soil Use and Management* 18, 175-183.

Guenther, A., Hewitt, C.N., Erickson, D., Fall, R., Geron, C., Graedel, T., Harley, P., Klinger, L., Lerdau, M., McKay, W.A., Pierce, T., Scholes, B., Steinbrecher, R., Tallamraju, R., Taylor, J., Zimmerman, P., 1995. A global model of natural volatile organic compound emissions. *Journal of Geophysical Research: Atmospheres* 100, 8873-8892.

Guenther, A., Karl, T., Harley, P., Wiedinmyer, C., Palmer, P.I., Geron, C., 2006. Estimates of global terrestrial isoprene emissions using MEGAN (Model of Emissions of Gases and Aerosols from Nature). *Atmospheric Chemistry and Physics* 6, 3181-3210.

Guenther, A., Zimmerman, P., Klinger, L., Greenberg, J., Ennis, C., Davis, K., Pollock, W., Westberg, H., Allwine, G., Geron, C., 1996. Estimates of regional natural volatile organic compound fluxes from enclosure and ambient measurements. *Journal of Geophysical Research: Atmospheres* 101, 1345-1359.

Guenther, A., Zimmerman, P., Wildermuth, M., 1994. Natural volatile organic compound emission rate estimates for United States woodland landscapes. *Atmospheric Environment* 28, 1197-1210.

Guenther, A.B., Hills, A.J., 1998. Eddy covariance measurement of isoprene fluxes. *Journal of Geophysical Research: Atmospheres* 103, 13145-13152.

Guenther, A.B., Zimmerman, P.R., Harley, P.C., Monson, R.K., Fall, R., 1993. Isoprene and monoterpene emission rate variability: Model evaluations and sensitivity analyses. *Journal of Geophysical Research: Atmospheres* 98, 12609-12617.

Haapanala, S., Rinne, J., Pystynen, K.H., Hellén, H., Hakola, H., Riutta, T., 2006. Measurements of hydrocarbon emissions from a boreal fen using the REA technique. *Biogeosciences* 3, 103-112.

Hakola, H., Rinne, J., Laurila, T., 1998. The hydrocarbon emission rates of tea-leaved willow (*Salix phylicifolia*), silver birch (*Betula pendula*) and European aspen (*Populus tremula*). *Atmospheric Environment* 32, 1825-1833.

Hamilton, J.F., Rami Alfarra, M., Wyche, K.P., Ward, M.W., Lewis, A.C., McFiggans, G.B., Good, N., Monks, P.S., Carr, T., White, I.R., Purvis, R.M., 2011. Investigating the use of secondary organic aerosol as seed particles in simulation chamber experiments. *Atmospheric Chemistry and Physics* 11, 5917-5929.

Hansel, A., Jordan, A., Holzinger, R., Prazeller, P., Vogel, W., Lindinger, W., 1995. Proton transfer reaction mass spectrometry: on-line trace gas analysis at the ppb level. *International Journal of Mass Spectrometry and Ion Processes* 149-150, 609-619.

Hanson, D.T., Swanson, S., Graham, L.E., Sharkey, T.D., 1999. Evolutionary significance of isoprene emission from mosses. *American Journal of Botany* 86, 634-639.

Harley, P., Fridd-Stroud, V., Greenberg, J., Guenther, A., Vasconcellos, P., 1998. Emission of 2-methyl-3-buten-2-ol by pines: A potentially large natural source of reactive carbon to the atmosphere. *Journal of Geophysical Research: Atmospheres* 103, 25479-25486.

Harrison, R.M., Hester, R.E., 1995. *Volatile Organic Compounds in the Atmosphere*. RSC.

Hellén, H., Dommen, J., Metzger, A., Gascho, A., Duplissy, J., Tritscher, T., Prevot, A.S.H., Baltensperger, U., 2008. Using proton transfer reaction mass spectrometry for online analysis of secondary organic aerosols. *Environmental Science & Technology* 42, 7347-7353.

Hellén, H., Hakola, H., Pystynen, K.H., Rinne, J., Haapanala, S., 2006. C<sub>2</sub>-C<sub>10</sub> hydrocarbon emissions from a boreal wetland and forest floor. *Biogeosciences* 3, 167-174.

Hewitt, C.N., Hayward, S., Tani, A., 2003. The application of proton transfer reaction-mass spectrometry (PTR-MS) to the monitoring and analysis of volatile organic compounds in the atmosphere. *Journal of Environmental Monitoring* 5, 1-7.

Hewitt, C.N., MacKenzie, A.R., Di Carlo, P., Di Marco, C.F., Dorsey, J.R., Evans, M., Fowler, D., Gallagher, M.W., Hopkins, J.R., Jones, C.E., Langford, B., Lee, J.D., Lewis, A.C., Lim, S.F., McQuaid, J., Misztal, P., Moller, S.J., Monks, P.S., Nemitz, E., Oram, D.E., Owen, S.M., Phillips, G.J., Pugh, T.A.M., Pyle, J.A., Reeves, C.E., Ryder, J., Siong, J., Skiba, U., Stewart, D.J., 2009. Nitrogen management is essential to prevent tropical oil palm plantations from causing ground-level ozone pollution. *Proceedings of the National Academy of Sciences* 106, 18447-18451.

Holst, T., Arneth, A., Hayward, S., Ekberg, A., Mastepanov, M., Jackowicz-Korczynski, M., Friberg, T., Crill, P.M., Backstrand, K., 2010. BVOC ecosystem flux measurements at a high latitude wetland site. *Atmospheric Chemistry and Physics* 10, 1617-1634.

Holzinger, R., Kasper-Giebl, A., Staudinger, M., Schauer, G., Röckmann, T., 2010a. Analysis of the chemical composition of organic aerosol at the Mt. Sonnblick observatory using a novel high mass resolution thermal-desorption proton-transfer-reaction mass-spectrometer (hr-TD-PTR-MS). *Atmospheric Chemistry and Physics* 10, 10111-10128.

Holzinger, R., Lee, A., Paw, K.T., Goldstein, A.H., 2005. Observations of oxidation products above a forest imply biogenic emissions of very reactive compounds. *Atmospheric Chemistry and Physics* 5, 67-75.

Holzinger, R., Williams, J., Herrmann, F., Lelieveld, J., Donahue, N.M., Röckmann, T., 2010b. Aerosol analysis using a Thermal-Desorption Proton-Transfer-Reaction Mass Spectrometer (TD-PTR-MS): a new approach to study processing of organic aerosols. *Atmospheric Chemistry and Physics* 10, 2257-2267.

Hörtnagl, L., Clement, R., Graus, M., Hammerle, A., Hansel, A., Wohlfahrt, G., 2010. Dealing with disjunct concentration measurements in eddy covariance applications: A comparison of available approaches. *Atmospheric Environment* 44, 2024-2032.

Janson, R., De Serves, C., 1998. Isoprene emissions from boreal wetlands in Scandinavia. *Journal of Geophysical Research: Atmospheres* 103, 25513-25517.

Janson, R., De Serves, C., Romero, R., 1999. Emission of isoprene and carbonyl compounds from a boreal forest and wetland in Sweden. *Agricultural and Forest Meteorology* 98–99, 671-681.

Jenkin, M.E., Saunders, S.M., Pilling, M.J., 1997. The tropospheric degradation of volatile organic compounds: a protocol for mechanism development. *Atmospheric Environment* 31, 81-104.

Jiménez, E., Lanza, B., Martínez, E., Albaladejo, J., 2007. Daytime tropospheric loss of hexanal and trans-2-hexenal: OH kinetics and UV photolysis. *Atmospheric Chemistry and Physics* 7, 1565-1574.

Jóó, É., Dewulf, J., Amelynck, C., Schoon, N., Pokorska, O., Šimpraga, M., Steppe, K., Aubinet, M., Van Langenhove, H., 2011. Constitutive versus heat and biotic stress induced BVOC emissions in *Pseudotsuga menziesii*. *Atmospheric Environment* 45, 3655-3662.

Jordan, A., Haidacher, S., Hanel, G., Hartungen, E., Herbig, J., Märk, L., Schottkowsky, R., Seehauser, H., Sulzer, P., Märk, T.D., 2009a. An online ultra-high sensitivity proton-transfer-reaction mass-spectrometer combined with switchable reagent ion capability (PTR + SRI - MS). *International Journal of Mass Spectrometry* 286, 32-38.

Jordan, A., Haidacher, S., Hanel, G., Hartungen, E., Märk, L., Seehauser, H., Schottkowsky, R., Sulzer, P., Märk, T.D., 2009b. A high resolution and high sensitivity proton-transfer-reaction time-of-flight mass spectrometer (PTR-TOF-MS). *International Journal of Mass Spectrometry* 286, 122-128.

Kanakidou, M., Seinfeld, J.H., Pandis, S.N., Barnes, I., Dentener, F.J., Facchini, M.C., Van Dingenen, R., Ervens, B., Nenes, A., Nielsen, C.J., Swietlicki, E., Putaud, J.P., Balkanski, Y., Fuzzi, S., Horth, J., Moortgat, G.K., Winterhalter, R., Myhre, C.E.L., Tsigaridis, K., Vignati, E., Stephanou, E.G., Wilson, J., 2005. Organic

aerosol and global climate modelling: a review. *Atmospheric Chemistry and Physics* 5, 1053-1123.

Karl, M., Guenther, A., Koble, R., Leip, A., Seufert, G., 2009. A new European plant-specific emission inventory of biogenic volatile organic compounds for use in atmospheric transport models. *Biogeosciences* 6, 1059-1087.

Karl, T., Guenther, A., Jordan, A., Fall, R., Lindinger, W., 2001. Eddy covariance measurement of biogenic oxygenated VOC emissions from hay harvesting. *Atmospheric Environment* 35, 491-495.

Karl, T., Hansel, A., Märk, T., Lindinger, W., Hoffmann, D., 2003. Trace gas monitoring at the Mauna Loa baseline observatory using proton-transfer reaction mass spectrometry. *International Journal of Mass Spectrometry* 223-224, 527-538.

Karl, T., Harley, P., Guenther, A., Rasmussen, R., Baker, B., Jardine, K., Nemitz, E., 2005a. The bi-directional exchange of oxygenated VOCs between a loblolly pine (*Pinus taeda*) plantation and the atmosphere. *Atmospheric Chemistry and Physics* 5, 3015-3031.

Karl, T., Harren, F., Warneke, C., de Gouw, J., Grayless, C., Fall, R., 2005b. Senescing grass crops as regional sources of reactive volatile organic compounds. *Journal of Geophysical Research: Atmospheres* 110, D15302.

Karl, T.G., Spirig, C., Rinne, J., Stroud, C., Prevost, P., Greenberg, J., Fall, R., Guenther, A., 2002. Virtual disjunct eddy covariance measurements of organic compound fluxes from a subalpine forest using proton transfer reaction mass spectrometry. *Atmospheric Chemistry and Physics* 2, 279-291.

Kesselmeier, J., Staudt, M., 1999. Biogenic volatile organic compounds (VOC): An overview on emission, physiology and ecology. *Journal of Atmospheric Chemistry* 33, 23-88.

Kiendler-Scharr, A., Wildt, J., Maso, M.D., Hohaus, T., Kleist, E., Mentel, T.F., Tillmann, R., Uerlings, R., Schurr, U., Wahner, A., 2009. New particle formation in forests inhibited by isoprene emissions. *Nature* 461, 381-384.

Kljun, N., Calanca, P., Rotachhi, M.W., Schmid, H.P., 2004. A simple parameterisation for flux footprint predictions. *Boundary-Layer Meteorology* 112, 503-523.

König, G., Brunda, M., Puxbaum, H., Hewitt, C.N., Duckham, S.C., Rudolph, J., 1995. Relative contribution of oxygenated hydrocarbons to the total biogenic VOC emissions of selected mid-European agricultural and natural plant-species. *Atmospheric Environment* 29, 861-874.

Kuhn, U., Sintermann, J., Spirig, C., Jocher, M., Ammann, C., Neftel, A., 2011. Basic biogenic aerosol precursors: Agricultural source attribution of volatile amines revised. *Geophysical Research Letters* 38, L16811.

Kulmala, M., Suni, T., Lehtinen, K.E.J., Dal Maso, M., Boy, M., Reissell, A., Rannik, U., Aalto, P., Keronen, P., Hakola, H., Back, J.B., Hoffmann, T., Vesala, T., Hari, P., 2004. A new feedback mechanism linking forests, aerosols, and climate. *Atmospheric Chemistry and Physics* 4, 557-562.

Lamb, B., Westberg, H., Allwine, G., Quarles, T., 1985. Biogenic hydrocarbon emissions from deciduous and coniferous trees in the United States. *Journal of Geophysical Research: Atmospheres* 90, 2380-2390.

Langford, B., Davison, B., Nemitz, E., Hewitt, C.N., 2009. Mixing ratios and eddy covariance flux measurements of volatile organic compounds from an urban canopy (Manchester, UK). *Atmospheric Chemistry and Physics* 9, 1971-1987.

Lee, D., Wexler, A.S., 2013. Atmospheric amines – Part III: Photochemistry and toxicity. *Atmospheric Environment* 71, 95-103.

Leith, I., Sheppard, L., Pitcairn, C., Cape, J.N., Hill, P., Kennedy, V., Tang, Y.S., Smith, R., Fowler, D., 2001. Comparison of the effects of wet N deposition ( $\text{NH}_4\text{Cl}$ )

and dry N deposition (NH<sub>3</sub>) on UK moorland species. *Water, Air, & Soil Pollution* 130, 1043-1048.

Leith, I.D., Hicks, W.K., Fowler, D., Woodin, S.J., 1999. Differential responses of UK upland plants to nitrogen deposition. *New Phytologist* 141, 277-289.

Lerdau, M., Matson, P., Fall, R., Monson, R., 1995. Ecological controls over monoterpene emissions from Douglas fir (*Pseudotsuga Menziesii*). *Ecology* 76, 2640-2647.

Lindinger, W., Hansel, A., Jordan, A., 1998. On-line monitoring of volatile organic compounds at pptv levels by means of proton-transfer-reaction mass spectrometry (PTR-MS) medical applications, food control and environmental research. *International Journal of Mass Spectrometry and Ion Processes* 173, 191-241.

Martin, R.S., Westberg, H., Allwine, E., Ashman, L., Farmer, J.C., Lamb, B., 1991. Measurement of isoprene and its atmospheric oxidation products in a central Pennsylvania deciduous forest. *Journal of Atmospheric Chemistry* 13, 1-32.

McKay, H., 2006. Environmental, economic, social and political drivers for increasing use of woodfuel as a renewable resource in Britain. *Biomass & Bioenergy* 30, 308-315.

Mentel, T.F., Kleist, E., Andres, S., Maso, M.D., Hohaus, T., Kiendler-Scharr, A., Rudich, Y., Springer, M., Tillmann, R., Uerlings, R., Wahner, A., Wildt, J., 2013. Secondary aerosol formation from stress-induced biogenic emissions and possible climate feedbacks. *Atmospheric Chemistry and Physics Discussions* 13, 7463-7502.

Misztal, P., 2010. Concentrations and fluxes of atmospheric biogenic volatile organic compounds by proton transfer reaction mass spectrometry, EaStCHEM School of Chemistry. University of Edinburgh, Edinburgh.

Misztal, P.K., Heal, M.R., Nemitz, E., Cape, J.N., 2012. Development of PTR-MS selectivity for structural isomers: Monoterpenes as a case study. *International Journal of Mass Spectrometry* 310, 10-19.

Misztal, P.K., Owen, S.M., Guenther, A.B., Rasmussen, R., Geron, C., Harley, P., Phillips, G.J., Ryan, A., Edwards, D.P., Hewitt, C.N., Nemitz, E., Siong, J., Heal, M.R., Cape, J.N., 2010. Large estragole fluxes from oil palms in Borneo. *Atmospheric Chemistry and Physics* 10, 4343-4358.

Naidu, S.L., Moose, S.P., Al-Shoaibi, A.K., Raines, C.A., Long, S.P., 2003. Cold tolerance of C-4 photosynthesis in *Miscanthus x giganteus*: Adaptation in amounts and sequence of C-4 photosynthetic enzymes. *Plant Physiology* 132, 1688-1697.

Olofsson, M., Ek-Olausson, B., Jensen, N.O., Langer, S., Ljungström, E., 2005. The flux of isoprene from a willow coppice plantation and the effect on local air quality. *Atmospheric Environment* 39, 2061-2070.

Owen, S.M., Hewitt, C.N., 2000. Extrapolating branch enclosure measurements to estimates of regional scale biogenic VOC fluxes in the northwestern Mediterranean basin. *Journal of Geophysical Research: Atmospheres* 105, 11573-11583.

Peters, R.J.B., Johannes, A.D.V., Duivenbode, R.V., Duyzer, J.H., Verhagen, H.L.M., 1994. The determination of terpenes in forest air. *Atmospheric Environment* 28, 2413-2419.

Pio, C.A., Nunes, T.V., Brito, S., 1993. Volatile hydrocarbon emissions from common and native species of vegetation in Portugal, in: Slanina, J., Angeletti, G., Beilke, S. (Eds.), *Proceedings on the General Assessment of Biogenic Emissions and Deposition of Nitrogen Compounds, Sulfur Compounds and Oxidants in Europe*, pp. 291-298.

Pressley, S., Lamb, B., Westberg, H., Guenther, A., Chen, J., Allwine, E., 2004. Monoterpene emissions from a Pacific Northwest old-growth forest and impact on regional biogenic VOC emission estimates. *Atmospheric Environment* 38, 3089-3098.

Räisänen, T., Ryyppö, A., Kellomäki, S., 2009. Monoterpene emission of a boreal Scots pine (*Pinus sylvestris* L.) forest. *Agricultural and Forest Meteorology* 149, 808-819.

- Rinne, H.J.I., Guenther, A.B., Warneke, C., de Gouw, J.A., Luxembourg, S.L., 2001. Disjunct eddy covariance technique for trace gas flux measurements. *Geophysical Research Letters* 28, 3139-3142.
- Rinne, J., Ruuskanen, T.M., Reissell, A., Taipale, R., Hakola, H., Kulmala, M., 2005. On-line PTR-MS measurements of atmospheric concentrations of volatile organic compounds in a European boreal forest ecosystem. *Boreal Environment Research* 10, 425–436.
- Rinne, J., Taipale, R., Markkanen, T., Ruuskanen, T.M., Hellen, H., Kajos, M.K., Vesala, T., Kulmala, M., 2007. Hydrocarbon fluxes above a Scots pine forest canopy: Measurements and modeling. *Atmospheric Chemistry and Physics* 7, 2357-2388.
- Rosenstiel, T.N., Potosnak, M.J., Griffin, K.L., Fall, R., Monson, R.K., 2003. Increased CO<sub>2</sub> uncouples growth from isoprene emission in an agriforest ecosystem. *Nature* 421, 256-259.
- Rowe, R.L., Street, N.R., Taylor, G., 2009. Identifying potential environmental impacts of large-scale deployment of dedicated bioenergy crops in the UK. *Renewable & Sustainable Energy Reviews* 13, 260-279.
- Sanadze, G.A., 2004. Biogenic isoprene - (A review). *Russian Journal of Plant Physiology* 51, 729-741.
- Saunders, S.M., Jenkin, M.E., Derwent, R.G., Pilling, M.J., 2003. Protocol for the development of the Master Chemical Mechanism, MCM v3 (Part A): tropospheric degradation of non-aromatic volatile organic compounds. *Atmospheric Chemistry and Physics* 3, 161-180.
- Schade, G.W., Goldstein, A.H., 2001. Fluxes of oxygenated volatile organic compounds from a ponderosa pine plantation. *Journal of Geophysical Research: Atmospheres* 106, 3111-3123.

Sharkey, T.D., Yeh, S.S., 2001. Isoprene emission from plants. *Annual Review of Plant Physiology and Plant Molecular Biology* 52, 407-436.

Sheppard, L.J., Crossley, A., Leith, I.D., Hargreaves, K.J., Carfrae, J.A., van Dijk, N., Cape, J.N., Sleep, D., Fowler, D., Raven, J.A., 2004. An automated wet deposition system to compare the effects of reduced and oxidised N on ombrotrophic bog species: Practical considerations. *Water, Air, & Soil Pollution: Focus* 4, 197-205.

Sheppard, L.J., Leith, I.D., Mizunuma, T., Neil Cape, J., Crossley, A., Leeson, S., Sutton, M.A., van Dijk, N., Fowler, D., 2011. Dry deposition of ammonia gas drives species change faster than wet deposition of ammonium ions: evidence from a long-term field manipulation. *Global Change Biology* 17, 3589-3607.

Snow, M.D., Bard, R.R., Olszyk, D.M., Minster, L.M., Hager, A.N., Tingey, D.T., 2003. Monoterpene levels in needles of Douglas fir exposed to elevated CO<sub>2</sub> and temperature. *Physiologia Plantarum* 117, 352-358.

Solomon, S., Qin, D., Manning, M., Alley, R.B., Berntsen, T., Bindoff, N.L., Chen, Z., Chidthaisong, A., Gregory, J.M., Hegerl, G.C., Heimann, M., Hewitson, B., Hoskins, B.J., Joos, F., Jouzel, J., Kattsov, V., Lohmann, U., Matsuno, T., Molina, M., Nicholls, N., Overpeck, J., Raga, G., Ramaswamy, V., Ren, J., Rusticucci, M., Somerville, R., Stocker, T.F., Whetton, P., Wood, R.A., Wratt, D., 2007. Technical Summary, in: Solomon, S., Qin, D., Manning, M., Chen, Z., Marquis, M., Averyt, K.B., Tignor, M., Miller, H.L. (Eds.), *Climate Change 2007: The Physical Science Basis. Contribution of Working Group I to the Fourth Assessment Report of the Intergovernmental Panel on Climate Change*, Cambridge, United Kingdom and New York, NY, USA.

Staudt, M., Lhoutellier, L., 2011. Monoterpene and sesquiterpene emissions from *Quercus coccifera* exhibit interacting responses to light and temperature. *Biogeosciences* 8, 2757-2771.

Steiner, A.H., Goldstein, A.L., 2007. Biogenic VOCs, in: Koppmann, R. (Ed.), *Volatile Organic Compounds in the Atmosphere*. Wiley-Blackwell.

Stevens, C.J., Manning, P., van den Berg, L.J.L., de Graaf, M.C.C., Wamelink, G.W.W., Boxman, A.W., Bleeker, A., Vergeer, P., Arroniz-Crespo, M., Limpens, J., Lamers, L.P.M., Bobbink, R., Dorland, E., 2011. Ecosystem responses to reduced and oxidised nitrogen inputs in European terrestrial habitats. *Environmental Pollution* 159, 665-676.

Stewart, H.E., Hewitt, C.N., Bunce, R.G.H., Steinbrecher, R., Smiatek, G., Schoenemeyer, T., 2003. A highly spatially and temporally resolved inventory for biogenic isoprene and monoterpene emissions: Model description and application to Great Britain. *Journal of Geophysical Research: Atmospheres* 108, 4644-4665.

Taipale, R., Ruuskanen, T.M., Rinne, J., 2010. Lag time determination in DEC measurements with PTR-MS. *Atmospheric Measurement Techniques* 3, 853-862.

Taipale, R., Ruuskanen, T.M., Rinne, J., Kajos, M.K., Hakola, H., Pohja, T., Kulmala, M., 2008. Technical Note: Quantitative long-term measurements of VOC concentrations by PTR-MS - measurement, calibration, and volume mixing ratio calculation methods. *Atmospheric Chemistry and Physics* 8, 6681-6698.

Tani, A., Hayward, S., Hewitt, C.N., 2003. Measurement of monoterpenes and related compounds by proton transfer reaction-mass spectrometry (PTR-MS). *International Journal of Mass Spectrometry* 223–224, 561-578.

Tiiva, P., Rinnan, R., Faubert, P., Rasanen, J., Holopainen, T., Kyro, E., Holopainen, J.K., 2007a. Isoprene emission from a subarctic peatland under enhanced UV-B radiation. *New Phytologist* 176, 346-355.

Tiiva, P., Rinnan, R., Holopainen, T., Morsky, S.K., Holopainen, J.K., 2007b. Isoprene emissions from boreal peatland microcosms; effects of elevated ozone concentration in an open field experiment. *Atmospheric Environment* 41, 3819-3828.

Tillmann, R., Hallquist, M., Jonsson, Å.M., Kiendler-Scharr, A., Saathoff, H., Iinuma, Y., Mentel, T.F., 2010. Influence of relative humidity and temperature on the production of pinonaldehyde and OH radicals from the ozonolysis of  $\alpha$ -pinene. *Atmospheric Chemistry and Physics* 10, 7057-7072.

Tsigaridis, K., Kanakidou, M., 2003. Global modelling of secondary organic aerosol in the troposphere: a sensitivity analysis. *Atmospheric Chemistry and Physics* 3, 1849-1869.

Turunen, J., Tomppo, E., Tolonen, K., Reinikainen, A., 2002. Estimating carbon accumulation rates of undrained mires in Finland - application to boreal and subarctic regions. *Holocene* 12, 69-80.

Van Den Berg, L.J.L., Dorland, E., Vergeer, P., Hart, M.A.C., Bobbink, R., Roelofs, J.G.M., 2005. Decline of acid-sensitive plant species in heathland can be attributed to ammonium toxicity in combination with low pH. *New Phytologist* 166, 551-564.

Warneke, C., Karl, T., Judmaier, H., Hansel, A., Jordan, A., Lindinger, W., Crutzen, P.J., 1999. Acetone, methanol, and other partially oxidized volatile organic emissions from dead plant matter by abiological processes: Significance for atmospheric HO<sub>x</sub> chemistry. *Global Biogeochemical Cycles* 13, 9-17.

Warneke, C., Luxembourg, S.L., de Gouw, J.A., Rinne, H.J.I., Guenther, A.B., Fall, R., 2002. Disjunct eddy covariance measurements of oxygenated volatile organic compounds fluxes from an alfalfa field before and after cutting. *Journal of Geophysical Research: Atmospheres* 107, 4067-4076.

Went, F.W., 1960. Blue hazes in the atmosphere. *Nature* 187, 641-643.

Winer, A.M., Fitz, D.R., Miller, P.R., 1983. Investigation of the role of natural hydrocarbons in photochemical smog formation in California. Statewide Air Pollution Research Center, Riverside, California, U.S.A.

Zimmerman, P.R., 1979. Determination of emission rates of hydrocarbons from indigenous species of vegetation in the Tampa/St. Petersburg Florida area. Appendix

C. Tampa Bay area photochemical oxidant study. U.S. Environmental Protection Agency, Region IV, Atlanta, Georgia.

## Appendix I: Publication

This appendix contains the peer-reviewed publication which forms the basis of Chapter 3 (a pdf version is also attached electronically):

Copeland, N., Cape, J.N., Heal, M.R., 2012. Volatile organic compound emissions from *Miscanthus* and short rotation coppice willow bioenergy crops. *Atmospheric Environment* 60, 327-335.

Accessible via ScienceDirect: <http://dx.doi.org/10.1016/j.atmosenv.2012.06.065>



## Volatile organic compound emissions from *Miscanthus* and short rotation coppice willow bioenergy crops

Nichola Copeland<sup>a,b</sup>, J. Neil Cape<sup>a</sup>, Mathew R. Heal<sup>b,\*</sup>

<sup>a</sup> Centre for Ecology & Hydrology, Bush Estate, Penicuik EH26 0QB, UK

<sup>b</sup> School of Chemistry, University of Edinburgh, West Mains Road, Edinburgh EH9 3JJ, UK

### HIGHLIGHTS

- ▶ *Miscanthus* and coppice willow are increasingly important bioenergy crops.
- ▶ Above-canopy fluxes were measured using PTR-MS and virtual disjunct eddy covariance.
- ▶ Willow isoprene emission peaked at  $\sim 1 \text{ mg m}^{-2} \text{ h}^{-1}$ ,  $\equiv 20 \text{ } \mu\text{g g}_{\text{dw}}^{-1} \text{ h}^{-1}$  standardised.
- ▶ Bioenergy crop species choice should consider their impact on regional air quality.

### ARTICLE INFO

**Article history:**  
Received 29 March 2012  
Received in revised form  
18 June 2012  
Accepted 19 June 2012

**Keywords:**  
VOC  
Isoprene  
Bioenergy  
*Miscanthus*  
Willow  
Eddy covariance

### ABSTRACT

*Miscanthus*  $\times$  *giganteus* and short rotation coppice (SRC) willow (*Salix* spp.) are increasingly important bioenergy crops. Above-canopy fluxes and mixing ratios of volatile organic compounds (VOCs) were measured in summer for the two crops at a site near Lincoln, UK, by proton transfer reaction mass spectrometry (PTR-MS) and virtual disjunct eddy covariance. The isoprene emission rate above willow peaked around midday at  $\sim 1 \text{ mg m}^{-2} \text{ h}^{-1}$ , equivalent to  $20 \text{ } \mu\text{g g}_{\text{dw}}^{-1} \text{ h}^{-1}$  normalised to  $30 \text{ } ^\circ\text{C}$  and  $1000 \text{ } \mu\text{mol m}^{-2} \text{ s}^{-1}$  PAR, much greater than for conventional arable crops. Average midday peak isoprene mixing ratio was  $\sim 1.4$  ppbv. Acetone and acetic acid also showed small positive daytime fluxes. No measurable fluxes of VOCs were detected above the *Miscanthus* canopy. Differing isoprene emission rates between different bioenergy crops, and the crops or vegetation cover they may replace, means the impact on regional air quality should be taken into consideration in bioenergy crop selection.

© 2012 Elsevier Ltd. All rights reserved.

### 1. Introduction

Bioenergy crops are those grown specifically for energy production rather than food, as a means of mitigating two problems associated with the use of traditional fossil fuels: anthropogenic climate forcing and energy security (McKay, 2006). Such crops contribute to carbon neutrality since  $\text{CO}_2$  produced during the combustion of the crop is offset by the  $\text{CO}_2$  sequestered during growth. There is also potential for long-term storage of carbon via uptake by soil through plant roots (Grogan and Matthews, 2002). Consequently, cultivation of bioenergy crops is increasing rapidly. For example, power generators in the UK are required to increase to 15.4% by 2015/16 the energy derived from renewable sources (DTI,

2005), with biomass being acknowledged as a key resource in achieving this target.

Although bioenergy crops are perceived to be carbon neutral, full life-cycle analysis needs also to take account of changes in emissions of other potent greenhouse gases such as  $\text{CH}_4$  or  $\text{N}_2\text{O}$ . Also, few studies have investigated volatile organic compound (VOC) emissions from bioenergy crops. Biogenic VOC emissions from vegetation (Steiner and Goldstein, 2007) are estimated as about 10 times greater globally than VOC emissions from anthropogenic sources (Guenther et al., 1995). The dominant BVOC is isoprene (Guenther et al., 2006), but other important compounds include oxygenated VOCs and terpenoids.

Emissions of VOCs are important for several reasons. Their rapid oxidation chemistry, particularly in the presence of  $\text{NO}_x$ , affects the oxidative capacity of the atmosphere, the generation of tropospheric ozone (Atkinson, 2000), of concern for human and plant health (Ashmore, 2005) and as a radiative forcing gas, and on formation of secondary organic particles, which likewise affect

\* Corresponding author. Tel.: +44 (0)131 6504764.  
E-mail address: [m.heal@ed.ac.uk](mailto:m.heal@ed.ac.uk) (M.R. Heal).

human health (Dockery et al., 1993) and radiative forcing (Kulmala et al., 2004).

The potential for BVOC emissions from crops to have a significant impact on atmospheric composition has been demonstrated in the tropics (Hewitt et al., 2009). The aim of this study was to determine fluxes of BVOCs for two bioenergy crops grown in the UK and elsewhere: short rotation coppice (SRC) willow (*Salix* spp.), a woody crop grown in dense plantations of multi-stemmed plants and harvested every 3 years; and *Miscanthus* × *giganteus*, a perennial grass native to Asia, of the same taxonomic group as sugarcane, sorghum and maize (Naidu et al., 2003) but more resilient to lower temperature whilst maintaining high CO<sub>2</sub> assimilation and biomass conversion efficiency. The crop grows up to 3.5 m per year (Rowe et al., 2009), and is harvested annually between January and March. The chipped and dried biomass of both crops is used to fuel biomass burners or to co-fire existing coal-fired power stations.

Fluxes from this work are compared with those for conventional UK arable crops to assess the potential impact of this land-use change on atmospheric chemistry.

## 2. Methods

### 2.1. Sampling site

The field measurements were carried out from mid July to mid August 2010 near Lincoln, UK (53° 19' N, 0° 35' W). Fig. 1 shows the layout of the site, which consisted of several fields of *Miscanthus*, willow and wheat, located within an area of predominantly flat arable fields separated by hedgerows and isolated areas of mixed deciduous woodland. Mean annual rainfall at the site was 600 mm and the soil was a fine loam, overlying Charnmouth mudstone. The nearest settlement (population: 113), which had a relatively busy through-road, was ~0.7 km to the southeast. A minor road running east–west was situated 0.3 km to the south.

The *Miscanthus* plot (~11 ha, planted in spring 2006) was surrounded by the following vegetation types: hedgerow and wheat to the north; willow to the east; deciduous trees to the west; willow

and wheat to the south. Crop height was typically 2.5 m. Sampling was carried out from 16th July to 2nd August 2010, near the NE corner of the plot, downwind of the prevailing wind direction, at an inlet height of approximately 4 m.

The willow plot (~6.5 ha, planted in 2001 with five different genotypes) was bounded as follows: a row of deciduous trees and a ploughed field to the north; *Miscanthus* to the west; mixed deciduous woodland to the south; wheat to the east. Typical canopy height was 4 m. Sampling was carried out from 5th to 13th August 2010 at an inlet height of 6.7 m on the north edge of the field. Trees were planted in pairs of rows 1.3 m apart, with 0.6 m spacing within each pair.

Flux footprints for both sampling sites were predicted using a simple parameterisation model (Kljun et al., 2004). Model results are shown in Supplementary information Fig. S1. For the *Miscanthus* measurements, the largest distance for 80% flux contribution over the range of friction velocities encountered (122 m) was within the area of the *Miscanthus* field throughout the south-westerly sector (180–270°). For the willow measurements, the largest distance for 80% flux contribution (185 m) meant there may have been some small flux contributions from outside the willow field when wind was from the west. Flux contribution was otherwise within the willow field for the whole southerly wind sector (90–270°). These sectors were used for directional filtering of data prior to deriving diurnal averages. Directionally-filtered data comprised 23% and 71% of all data for *Miscanthus* and willow, respectively.

Harvesting activities in surrounding farms during this study may have affected results, particularly during *Miscanthus* measurements, and are discussed later.

### 2.2. Proton transfer reaction mass spectrometer (PTR-MS)

BVOC mixing ratios and fluxes above both crop canopies were measured using proton transfer reaction mass spectrometry (PTR-MS) (Blake et al., 2009) coupled with virtual disjunct eddy covariance (vDEC) (Karl et al., 2002; Rinne et al., 2001). PTR-MS is a 'soft'

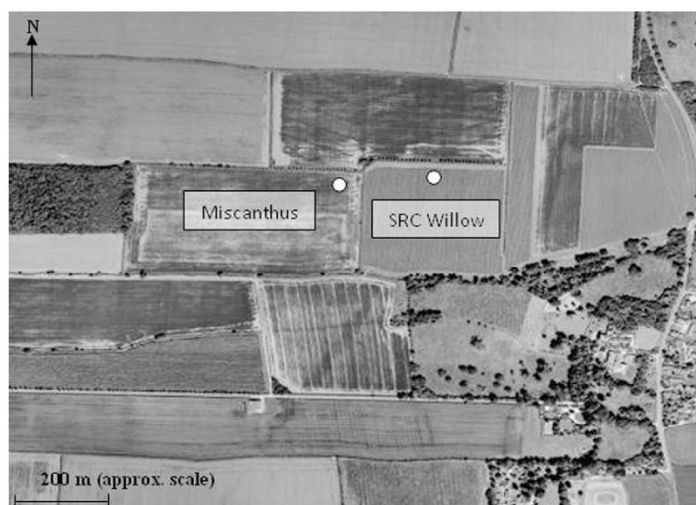


Fig. 1. Aerial view of the *Miscanthus* and willow plantations. The white dots denote the measurement locations at the NE corner of the *Miscanthus* field and the N edge of the SRC willow field. (Map attributable to: ©2001 DigitalGlobe, GeoEye, Getmapping plc, Infoterra Ltd & Bluesky, TerraMetrics. Map data ©2011 Google).

chemical ionisation method in which hydronium ions ( $\text{H}_3\text{O}^+$ ) formed in a hollow cathode ion source pass into a drift tube subject to an electric field ( $E$ ) into which the ambient air is also introduced. As most VOC molecules have a proton affinity greater than water, they react with  $\text{H}_3\text{O}^+$  ions to form protonated products, predominantly the protonated molecular ion, but also fragments or clusters. The extent of fragmentation/clustering can be controlled by tuning the  $E/N$  ratio ( $N$  is the  $\text{H}_3\text{O}^+$  ion density).

The PTR-MS used in this study (Ionicon Analytik, Innsbruck, Austria) was fitted with an extra turbopump connected to the detection chamber, and Teflon instead of Viton rings in the drift tube (Davison et al., 2009; Misztal et al., 2010). Pfeiffer turbopumps replaced the Varian equivalents. The drift tube conditions were held constant throughout (pressure 2 mbar, temperature 40 °C, voltage 572 V) to maintain an  $E/N$  ratio of  $\sim 130$  Td ( $1 \text{ Td} = 10^{-17} \text{ V cm}^2$ ).

The sampling inlet and 20 Hz sonic anemometer (WindmasterPro, Gill Instruments) were positioned above the canopy using a telescopic mast. Air was sampled at  $30 \text{ L min}^{-1}$  through a 20 m PTFE inlet line (1/4" OD, 3/16" ID) with a T-piece for sub-sampling into the PTR-MS inlet at a rate of  $100 \text{ mL min}^{-1}$ . Condensation of water vapour in the inlet line was prevented by wrapping with self-regulating heating tape (Omega, UK type SRF3-2C). Data were logged using a program written in LabVIEW (Version 8.5, National Instruments).

### 2.3. Determination of VOC mixing ratios and fluxes

The PTR-MS signal was calibrated explicitly for several VOCs using a mixed gas calibration cylinder (Apel-Riemer Environmental Inc., USA) containing 1 ppmv each of formaldehyde, methanol, acetonitrile, acetone, acetaldehyde, isoprene and 0.18 ppmv  $\alpha$ -limonene. The calibration gas was diluted with VOC-scrubbed air to produce 6 samples with concentrations of 0.5, 1.0, 10, 20, 30 and 50% of the pure calibration gas standard. A relative transmission curve was then constructed to determine empirical calibration coefficients for other VOCs under study not present in the standard (Taipale et al., 2008). Calibrations were carried out in the lab before commencement of the field campaign, and on 22nd July during the campaign. Concentrations of gases in the calibration cylinder were verified using GC-MS calibrated with its own independent standards (details given in Section 2.4).

The PTR-MS was run in multiple ion detection (MID) mode for two 25 min sampling periods per hour. During these periods only the targeted VOC ions listed in Table 1 were measured, with dwell times of 0.5 s, in addition to the primary ion  $\text{H}_3\text{O}^+$ , and water cluster ( $\text{H}_2\text{O})\text{H}_3\text{O}^+$ , which had dwell times of 0.2 s. The sensitivities (ncps ppbv $^{-1}$ ) and limits of detection (ppbv) for the target ions for the *Miscanthus* and willow campaigns are also included in Table 1. LODs were calculated as the ratio of twice the standard deviation of the background ion counts for a particular  $m/z$  throughout the campaign divided by the sensitivity (Karl et al., 2003).

The remaining 10 min per hour were used for full mass scans in the range 21–206 amu at a dwell time of 1 s per amu. For one 5 min period, ambient air was scanned to allow information about the full VOC composition to be acquired. For a further 5 min per hour, 'zero air' was scanned to determine the instrument background. Zero air was achieved by sampling ambient air through a custom-made zero-air generator comprising a glass tube packed with platinum wool and a 50:50 mixture of platinum mesh and activated charcoal heated to 200 °C. The background spectrum was subtracted in subsequent processing of data.

As the PTR-MS was run in MID mode, fewer data points were generated than required for direct eddy covariance due to the non-continuous manner in which the quadrupole mass analyser

**Table 1**  
Compounds measured during the field campaign including dwell times, sensitivities and limits of detection.

$m/z$	Contributing compound(s)	Formula	Dwell time [s]	Sensitivity [ncps ppbv $^{-1}$ ]	Limit of detection [ppbv]	
					<i>Miscanthus</i>	<i>Willow</i>
21	Water isotope	$\text{H}_2^{18}\text{O}$	0.2	–	–	–
33	Methanol	$\text{CH}_4\text{O}$	0.5	4.1	1.41	2.03
37	Water cluster	$(\text{H}_2\text{O})_2$	0.2	–	–	–
45	Acetaldehyde	$\text{C}_2\text{H}_4\text{O}$	0.5	12	0.44	0.21
59	Acetone	$\text{C}_3\text{H}_6\text{O}$	0.5	11	0.41	0.06
	Propanal					
61	Acetic acid	$\text{C}_2\text{H}_4\text{O}_2$	0.5	10	0.08	0.06
69	Isoprene	$\text{C}_5\text{H}_8$	0.5	3.5	0.13	0.12
	Furan					
	Methyl butenol fragment					
71	Methyl vinyl ketone (MVK)	$\text{C}_4\text{H}_6\text{O}$	0.5	6.2	0.06	0.07
	Methacrolein (MACR)					
73	Methyl ethyl ketone (MEK)	$\text{C}_4\text{H}_8\text{O}$	0.5	6.0	0.11	0.08

measures each  $m/z$ . The set-up resulted in 30,000 wind speed measurements and up to 441 VOC measurements in each 25 min sampling period (depending on how many VOCs were being measured). The total lag time between PTR-MS and wind speed data was determined by examining the cross-correlation between vertical wind speed and VOC mixing ratio as a function of lag time (with 15 s window). Total lag includes residence time in the sampling inlet line but also lag associated with collection and data writing of a full cycle of analysis by disjunct sampling and the response of the PTR-MS. The median of the lag times for each 5 min sub-period was used to calculate the flux in that 25 min period (Misztal, 2010). For example, the average lag-time for isoprene above the willow was 9.58 s, with a standard deviation between 25 min periods of 1.41 s. This method produced less variable lag times than those derived using the prevalent MAX method in cross-correlation function ( $\sim 72\%$  lower sd), and has been shown to be a practical alternative (Taipale et al., 2010).

Quality controls were used to filter data for periods of low friction velocity ( $u^* < 0.15 \text{ m s}^{-1}$ ), non-stationarity, large spikes in vertical wind speed or VOC concentration, and where  $< 20,000$  data points were acquired in a 25 min sampling period. Most discarded data occurred during night when turbulence was low. High frequency flux losses due to the relatively slow disjunct VOC sampling frequency (0.25 Hz, compared to 20 Hz sonic data capture) were estimated using empirical ogive analysis (Ammann et al., 2006) for each 25 min period. At least 78% of flux was captured for all individual 25 min data periods, and values were corrected accordingly. Standard rotations of the coordinate frame were applied to correct for sonic anemometer tilt for each 25 min period separately.

### 2.4. Chromatographic analysis of ambient air samples

Ambient air samples were collected for chromatographic analysis, to confirm the identity of the VOC components measured by the PTR-MS, approximately hourly from 06:53 to 16:20 on 23 September 2010 above *Miscanthus* and from 06:32 to 17:30 on 11 August 2010 above willow (at  $\sim 1 \text{ m}$  above the canopies). Sampling above *Miscanthus* was carried out at a later date because initial samples taken during the intensive campaign were lost due to GC-MS instrument failure. A mass-flow controlled Pocket Pump (210-1000 Series, SKC Inc.) was used to pump air at  $100 \text{ mL min}^{-1}$

for 15 min through stainless steel adsorbent tubes (6 mm OD) packed with 200 mg Tenax TA and 100 mg CarboTrap (Markes International Ltd., UK). Prior to sampling, packed tubes were conditioned at 300 °C for 15 min with a flow of helium.

Analyses were carried out using a Hewlett–Packard 5890/5970 GC–MS with an automated thermal desorption unit (ATD 400, Perkin Elmer) connected via a 200 °C heated transfer line. Transfer of samples from the adsorbent tubes was performed in two steps: heat to 280 °C for 5 min at 25 mL min<sup>-1</sup> to desorb samples onto a Tenax-TA cold trap at -30 °C, followed by transfer to the GC column at 300 °C for 6 min. Chromatographic separation utilised an Ultra-2 column (Agilent Technologies, 50 m × 0.2 mm ID × 0.11 μm film, 5% phenylmethyl silica) and a temperature program of 35 °C for 2 min, heat at 5 °C min<sup>-1</sup> to 160 °C, heat at 10 °C min<sup>-1</sup> to 280 °C, and hold for 5 min.

Calibration was carried out using a mixed monoterpene in methanol standard (10 ng μL<sup>-1</sup> α-pinene, β-pinene, α-phellandrene, 3-carene and limonene (Sigma Aldrich, UK)) and an isoprene in nitrogen gas standard (700 ppbv, BOC Gases, UK). Aliquots of the monoterpene standard (0, 1, 3 and 5 μL) were injected onto 4 adsorbent tubes with helium carrier gas. Tubes continued to be purged with helium for 2 min after the standard injection. Isoprene calibration tubes were prepared by slowly (over a period of about 2 min) injecting 0, 10, 30 and 50 mL of the gas standard onto 4 adsorbent tubes, while purging with helium. The limits of detection for isoprene, α-pinene and limonene were 0.16, 0.23 and 0.30 ng on column, corresponding to mixing ratios of 38, 27 and 35 pptv, respectively, for a 1.5 L sample.

## 2.5. Meteorological measurements

Photosynthetically active radiation (PAR), rainfall, temperature and relative humidity were available as part of long-term measurements at the site.

## 3. Results

### 3.1. *Miscanthus*

The time series of VOC fluxes above *Miscanthus* are shown in Fig. 2 along with  $u^*$  and sensible heat flux. Two periods of missing data 21st–22nd and 25th–27th July were due to failure of the sampling pump. Data in the first few days were relatively noisy, showing no particular diurnal trend up to 20th July. This was likely due to elevated O<sub>3</sub> impurities during transport of the instrument resulting in less reliable primary ion counts or higher LOD. Additionally, episodes of rainfall on 17th, 18th, 20th and 22nd July may have resulted in a reduction in mixing ratio of VOCs where emission is proportional to PAR.

Small net emissions of isoprene and MEK from *Miscanthus* during daytime were just discernible, most noticeable on 18th July when sensible heat flux was also at its maximum. However, in general, flux data were somewhat noisy for all VOCs measured, and mostly not significantly different from zero. The directionally-filtered diurnal averages of VOC fluxes are shown in Supplementary information Fig. S2. As described earlier, the relevant sector for the *Miscanthus* measurements was south-west (180–270°). The

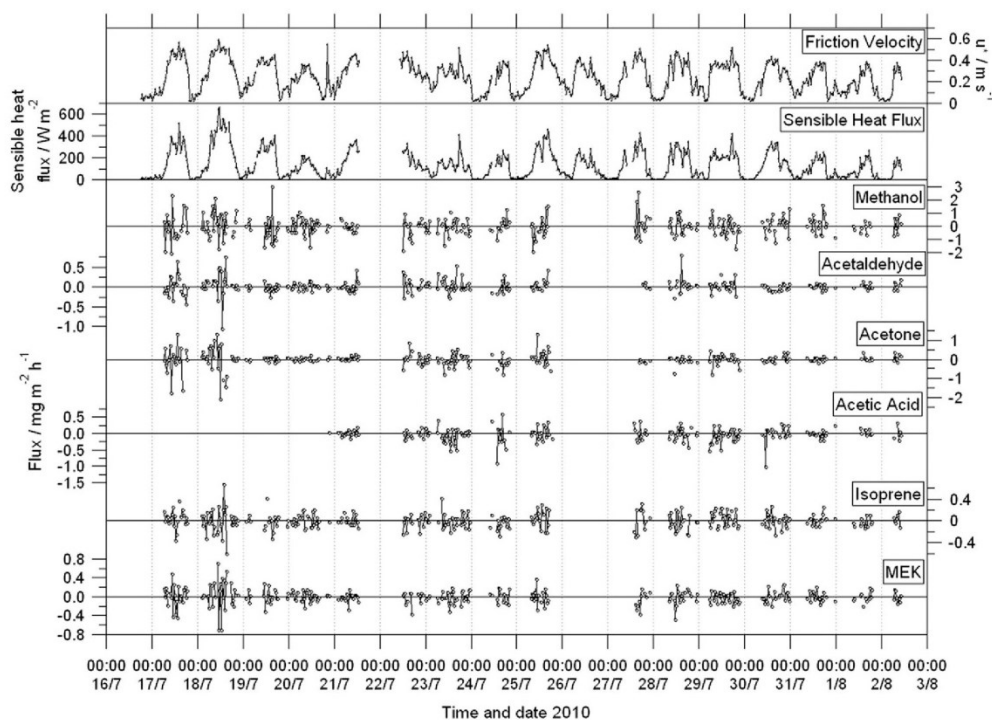


Fig. 2. Time series of VOC fluxes measured above *Miscanthus*. Dashed gridlines denote midnight. Note the variable flux scales.

mixing ratios of MVK + MACR (the first-generation oxidation products of isoprene) showed no diurnal pattern and were below LOD, so no data for these species are shown.

The time series of VOC mixing ratios above *Miscanthus* are shown in Supplementary information Fig. S3. For the period 27th July to 2nd August, mixing ratios of all measured VOCs had maxima at night except for isoprene whose mixing ratios were elevated in late afternoon. The average diurnal VOC mixing ratios above *Miscanthus* are shown in Fig. S4. Methanol, acetaldehyde, acetone, acetic acid and MEK had similar diurnal profiles in mixing ratio. All showed a minimum mixing ratio around midday. The isoprene mixing ratio peaked around midday consistent with observation of a possible small isoprene flux above *Miscanthus* (Fig. S2). No isoprene or monoterpenes were detected in the GC–MS analysis of adsorption tube sampling above the *Miscanthus* canopy.

### 3.2. Short rotation coppice willow

The time series of VOC fluxes, and  $u^*$  and sensible heat, measured above willow are shown in Fig. 3. Missing data on 10th and 12–13th August were due to failure of the mobile power supply. Data were directionally filtered to include only those from over the willow field ( $90\text{--}270^\circ$ ) before diurnally averaging (Fig. 4). Willow showed a distinct diurnal pattern of isoprene flux, peaking at  $\sim 1 \text{ mg m}^{-2} \text{ h}^{-1}$  around midday and decreasing to zero overnight, driven by the strong dependence of isoprene emissions on temperature and PAR. All other VOC measured showed positive and negative fluxes throughout the day, with no significant net positive or negative daily flux overall.

Supplementary information Fig. S5 shows the time series of VOC mixing ratios and temperature above SRC willow. The time series showed clear diurnality in mixing ratios of all VOCs measured, except for methanol. The directionally-filtered diurnal averages of mixing ratio over the willow are shown in Fig. 5.

Isoprene had a dominant maximum mixing ratio in early afternoon ( $\sim 1 \text{ ppbv}$ ), temporally coincident with the temperature profile, and low mixing ratios at night. Fig. 5 also plots the isoprene mixing ratios determined by adsorption tube sampling and GC–MS analysis. There was good agreement. Small quantities of the monoterpenes  $\alpha$ -pinene and limonene were also detected by GC–MS, but no diurnal patterns were discernable in these data.

Acetic acid, acetaldehyde and MVK + MACR also showed diurnal profiles with maxima in the afternoon and minima around 6 am, closely mirroring daily temperature variation. The amplitude of the daytime maximum of MEK mixing ratio was considerably less. Acetone exhibited low diurnal variability but with the small maximum in early morning similar to the observation of *Miscanthus*.

As isoprene oxidation is the only known source of MVK and MACR, the ratio of MVK + MACR to isoprene mixing ratios can be used to examine the degree of isoprene oxidation (Fig. 6). The [MVK + MACR]:[isoprene] ratio peaked around midnight with an average value of about 0.8 when isoprene was not being emitted and MVK + MACR were not undergoing photochemical loss or dispersion. At dawn there was a rapid decline in the ratio as the canopy responded to increasing PAR and temperature hence isoprene emissions increased, and the boundary layer depth also increased. The minimum ratio of  $\sim 0.1$  occurred for several hours around midday. The ratio rose in late afternoon as isoprene emissions declined but isoprene oxidation continued.

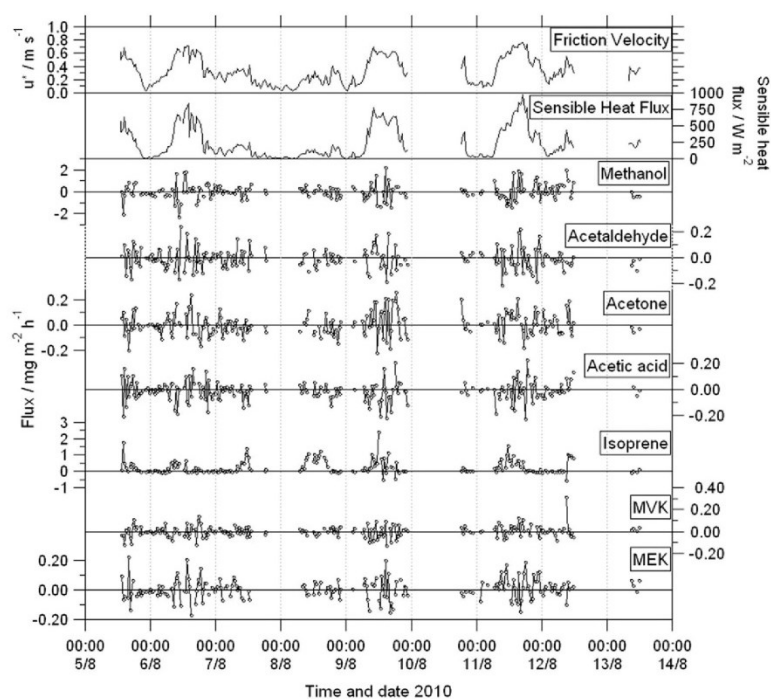


Fig. 3. Time series of VOC fluxes measured above willow canopy. Dashed gridlines denote midnight. Note the variable scales.

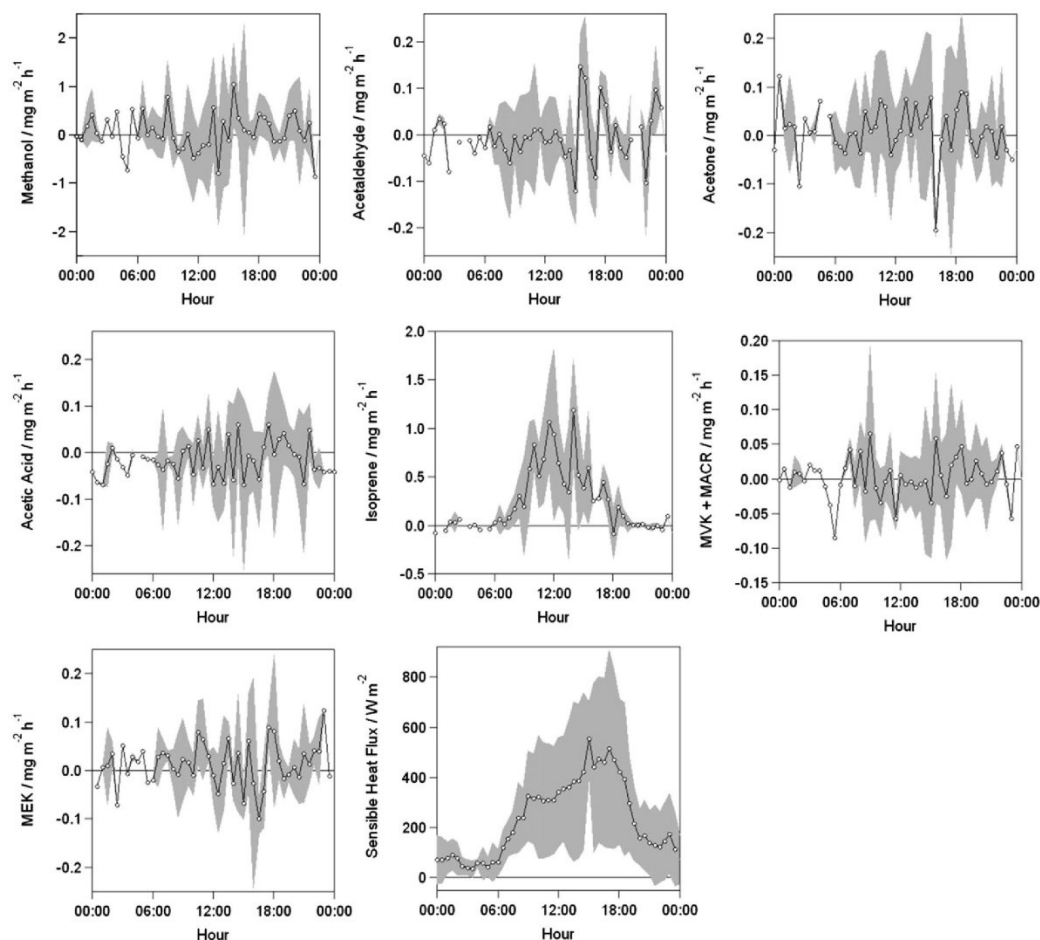


Fig. 4. Average diurnal profiles of VOC fluxes above willow, and of sensible heat flux, when wind direction was between 90 and 270° (i.e. from over the willow field). Note the variable scales. Grey areas show variability calculated as  $\pm 1$  sd of the averaged half-hourly values of all measurements.

The average measured daytime [MVK + MACR]:[isoprene] ratio of 0.24 is comparable with those from other northern latitude studies. A daytime ratio of 0.23 was measured in a rural Canadian forest clearing (Biesenthal et al., 1998), 0.12 was reported for a mixed forest in Michigan, USA (Apel et al., 2002) and 0.4–0.8 in a deciduous forest in Pennsylvania, USA (Martin et al., 1991).

### 3.3. Standardised isoprene emission

As isoprene emission from plants is strongly influenced by light and leaf temperature, the canopy-level emission,  $F$ , was recalculated as a standard emission factor ( $\epsilon$ ) normalised to a standard leaf temperature of 303 K and PAR flux of  $1000 \mu\text{mol m}^{-2} \text{s}^{-1}$ , as described by the G95 algorithm (Guenther et al., 1995),

$$\epsilon = \frac{F}{D \gamma} \quad (1)$$

where  $D$  is foliar density ( $\text{g dry weight m}^{-2}$ ) and  $\gamma$  is a non-dimensional activity adjustment factor to account for the effect of light and temperature:

$$\gamma = C_L C_T \quad (2)$$

The light dependence,  $C_L$ , is defined by

$$C_L = \frac{\alpha c_{L1} Q}{\sqrt{1 + \alpha^2 Q^2}} \quad (3)$$

where  $\alpha$  (0.0027) and  $c_{L1}$  (1.066) are empirical coefficients and  $Q$  is PAR flux ( $\mu\text{mol m}^{-2} \text{s}^{-1}$ ). The temperature dependence  $C_T$ , is defined by

$$C_T = \frac{\exp\left(\frac{c_{T1}(T - T_s)}{R T_s T}\right)}{1 + \frac{\exp(c_{T2}(T - T_M))}{R T_s T}} \quad (4)$$

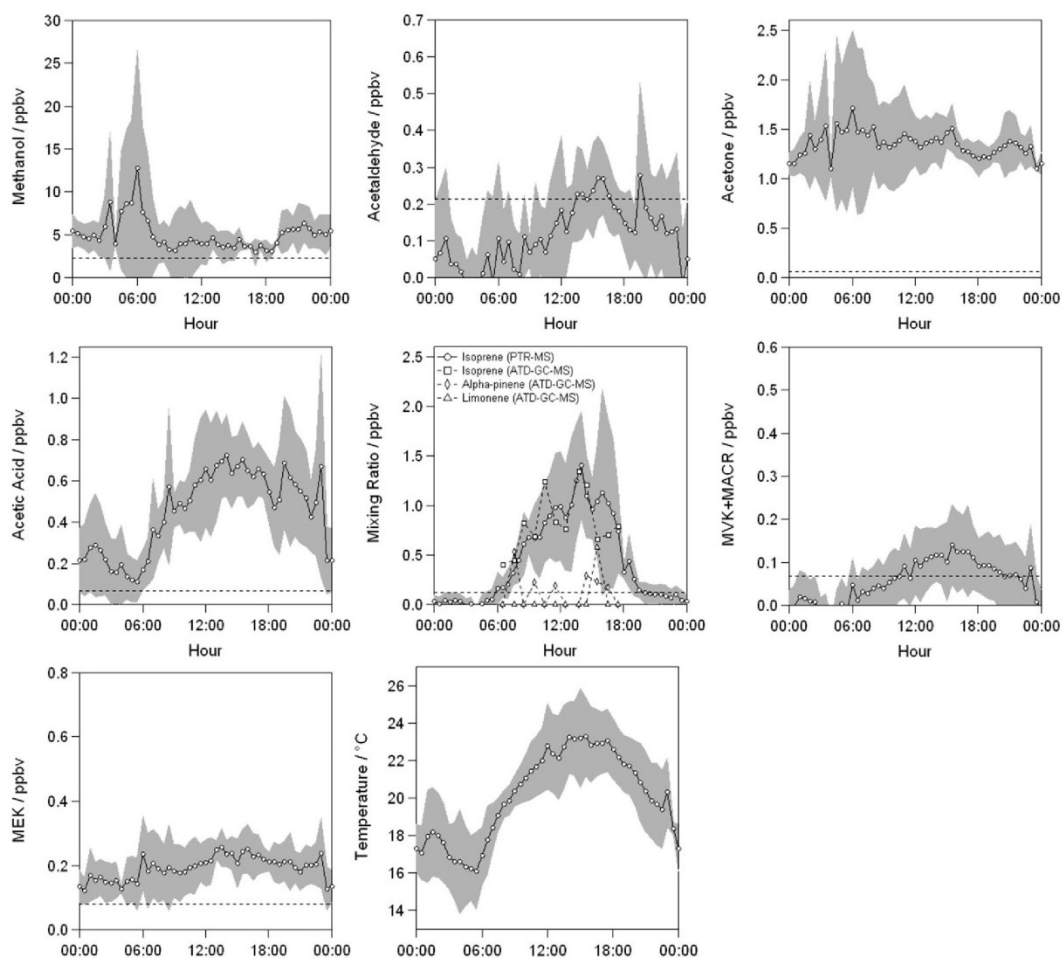


Fig. 5. Average diurnal profiles of VOC mixing ratios above willow, and of temperature, when wind direction was between 90 and 270° (i.e. from over the willow field). Note the variable scales. Dashed lines denote LOD. Grey areas represent variability calculated as  $\pm 1$  sd of the averaged half-hourly values of all measurements.

where  $T$  is leaf temperature (K),  $T_s$  is leaf temperature at standard conditions (303 K),  $R$  is the universal gas constant ( $8.314 \text{ J K}^{-1} \text{ mol}^{-1}$ ), and  $c_{T1}$  ( $95,000 \text{ J mol}^{-1}$ ),  $c_{T2}$  ( $230,000 \text{ J mol}^{-1}$ ) and  $T_M$  (314 K) are empirical coefficients.

Values of above-canopy PAR and temperature, and of isoprene flux (from Fig. 4), at hourly intervals during the willow campaign were used for the calculation of  $\gamma$  and  $F$  respectively. Foliar density  $D$  was estimated at  $150 \text{ g}_{\text{dw}} \text{ m}^{-2}$  for *Salix* spp. (Karl et al., 2009). Hourly emission factors  $\epsilon$  were then determined for isoprene from willow, and were found to have a peak value of  $25 \mu\text{g g}_{\text{dw}}^{-1} \text{ h}^{-1}$  at 10:00. A mean midday value of  $20 \mu\text{g g}_{\text{dw}}^{-1} \text{ h}^{-1}$  for  $12:00 \pm 2 \text{ h}$  was determined to allow comparison, in Table 2, with mean values from other studies.

Table 2 shows that the emission factor from this study was within the range of values derived previously for *Salix* spp. The slightly lower measurements derived in this work and in the other above-canopy study (Olofsson et al., 2005) were canopy-averaged

emissions factors which included leaves which were in shade as well as those in direct sunlight. It was therefore expected that these measurements would result in lower standard emission factors than from individual branch or leaf-level experiments.

#### 4. Discussion

In the context of SRC willow as a bioenergy crop, the significant isoprene emission factor could potentially impact local and regional air quality by affecting tropospheric ozone production and SOA formation. Conventional agricultural crops are regarded as being low emitting species. For example, wheat and oats are estimated as having isoprene emission factors in the range  $0\text{--}0.5 \mu\text{g g}_{\text{dw}}^{-1} \text{ h}^{-1}$  (Karl et al., 2009; König et al., 1995), while those for rapeseed, rye and barley are zero (Karl et al., 2009; Kesselmeier and Staudt, 1999). Replacement of conventional crops with SRC willow would therefore result in increased isoprene emission. A recent study examined

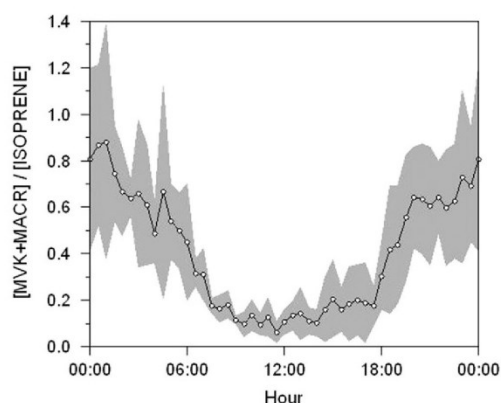


Fig. 6. Average diurnal profile of [MVK + MACR]:[isoprene] ratio above the willow canopy. Grey areas represent variability calculated as  $\pm 1$  sd of the averaged half-hourly values of all measurements.

the impact of SRC crop cultivation in Europe (Ashworth et al., 2012). It was concluded that monthly mean increases in ozone and BSOA (+1% and +5% respectively) from low level planting scenarios were significant enough to affect regional air quality and therefore warrant consideration in short term local impact assessments, as well as life cycle analysis of bioenergy crops.

At the end of 2009, total UK plantings of *Miscanthus* and SRC willow were 12,700 and 6400 ha respectively (DEFRA, 2009). A government report stated that there is potential in the UK to increase bioenergy crop cultivation substantially by a further 350,000 ha by 2020, accounting for ~6% of total UK arable land (DEFRA, 2007), with the assumption that 70% would be *Miscanthus* and SRC willow (Rowe et al., 2009). In the case of 70% being converted solely to SRC willow, then a UK-wide increase of up to  $735 \text{ t h}^{-1}$  in emissions of isoprene would result (assuming zero isoprene emissions from the land prior to conversion to willow,  $150 \text{ g}_{\text{dw}} \text{ m}^{-2}$  willow, and an isoprene standard emission rate of  $20 \text{ } \mu\text{g g}_{\text{dw}}^{-1} \text{ h}^{-1}$  determined here). The annual increase in isoprene would require calculation using PAR and temperature data across the likely planting sites in the UK, and a whole-canopy model.

Table 2  
Comparison of standardised emission rates of isoprene from willow. REA = relaxed eddy accumulation.

Species	Standard emission rate/ $\mu\text{g g}_{\text{dw}}^{-1} \text{ h}^{-1}$	Measurement type	Reference
<i>Salix</i> spp.	20	Canopy-scale, PTR-MS	This study
<i>Salix</i> spp.	28	Branch enclosure	(Owen and Hewitt, 2000)
<i>Salix alba</i>	18	Branch enclosure, lab conditions	(Pio et al., 1993)
<i>Salix alba</i>	37.2	–	(Karl et al., 2009)
<i>Salix babylonica</i>	115	–	(Winer et al., 1983)
<i>Salix caprea</i>	18.9	Branch enclosure	(Karl et al., 2009)
<i>Salix caroliniana</i>	12.5	Air-exchange branch enclosure	(Zimmerman, 1979)
<i>Salix nigra</i>	25.2	Whole plant, air-exchange chamber	(Evans et al., 1982)
<i>Salix phylicifolia</i>	32	Branch enclosure	(Hakola et al., 1998)
<i>Salix viminalis</i>	12	Canopy-scale, REA	(Olofsson et al., 2005)

The standard emission factor for isoprene from SRC willow measured in this study was  $26.5 \text{ g C ha}^{-1} \text{ h}^{-1}$ . This is an order of magnitude higher than was determined for total emission of VOCs from the biofuel crop switchgrass (Eller et al., 2011), where emissions were dominated by oxygenated VOCs and isoprene contributed less than 8%.

For *Miscanthus*, the near-zero values of flux at night were in contrast to the increase in mixing ratios of oxygenated VOCs (Figs. S3 and S4). Since reliability of the eddy covariance technique depends on friction velocity, the greater boundary layer stability at night (hence low friction velocity) resulted in unreliable night time flux measurements. It may therefore be possible that night time fluxes were non-zero. A more likely scenario is that increasing VOC mixing ratios at night were affected by sources in the wider area. Towards the start of the measurement period, several of the surrounding fields were subject to harvesting and subsequent ploughing activities, which are known to be a source of oxygenated VOCs (Karl et al., 2001). Mixing ratios of methanol, acetaldehyde and acetone were comparable to those measured in previous field experiments of crop cutting (Warneke et al., 2002). The enhanced mixing ratios towards dusk, and at night can be explained by reduced radical sink chemistry, together with accumulation within a shallower nocturnal boundary layer from reduced vertical transport and mixing, as demonstrated by the lower wind speed and  $u^*$  at night (Fig. 2). During willow measurements, atypical increases in mixing ratios of methanol, acetone and acetic acid on 8th August may also have been caused by further harvesting activity in the wider area.

## 5. Conclusions

Measurements of above-canopy fluxes and mixing ratios of VOCs revealed significant emissions of isoprene from short rotation coppice willow, with a standard emission factor of  $20 \text{ } \mu\text{g g}_{\text{dw}}^{-1} \text{ h}^{-1}$ . No significant emissions were measured from *Miscanthus*. This is the first field study of bioenergy crops in the UK and shows that a change in land use from conventional to bioenergy crops could result in increased isoprene emissions. Bioenergy crop species choice should therefore include consideration of their impact on regional air quality. Further work could include measurement of VOC emissions from *Miscanthus* and SRC willow during senescence and harvesting.

## Acknowledgements

N. Copeland acknowledges PhD studentship funding from EaStChem School of Chemistry and CEH Edinburgh. The authors thank Jonathan Wright and Frank Wilson for site access, Julia Drewer, Jon Finch and Eilidh Morrison for assistance with fieldwork set up, and Kirsti Ashworth and Catherine Hardacre for help with standard emission factors. We are also grateful to the anonymous reviewers of this paper for their helpful comments and suggestions.

## Appendix A. Supplementary information

Supplementary information associated with this article can be found, in the online version, at <http://dx.doi.org/10.1016/j.atmosenv.2012.06.065>.

## References

- Ammann, C., Brunner, A., Spirig, C., Neftel, A., 2006. Technical note: water vapour concentration and flux measurements with PTR-MS. *Atmospheric Chemistry and Physics* 6, 4643–4651.
- Apel, E.C., Riemer, D.D., Hills, A., Baugh, W., Orlando, J., Faloon, I., Tan, D., Brune, W., Lamb, B., Westberg, H., Carroll, M.A., Thornberry, T., Geron, C.D., 2002.

- Measurement and interpretation of isoprene fluxes and isoprene, methacrolein, and methyl vinyl ketone mixing ratios at the PROPHET site during the 1998 intensive. *Journal of Geophysical Research* 107, 4034.
- Ashmore, M.R., 2005. Assessing the future global impacts of ozone on vegetation. *Plant Cell and Environment* 28, 949–964.
- Ashworth, K., Folberth, G., Hewitt, C.N., Wild, O., 2012. Impacts of near-future cultivation of biofuel feedstocks on atmospheric composition and local air quality. *Atmospheric Chemistry and Physics* 12, 919–939.
- Atkinson, R., 2000. Atmospheric chemistry of VOCs and NOx. *Atmospheric Environment* 34, 2063–2101.
- Biesenthal, T.A., Bottenheim, J.W., Shepson, P.B., Li, S.M., Brickell, P.C., 1998. The chemistry of biogenic hydrocarbons at a rural site in eastern Canada. *Journal of Geophysical Research* 103, 25487–25498.
- Blake, R.S., Monks, P.S., Ellis, A.M., 2009. Proton-transfer reaction mass spectrometry. *Chemical Reviews* 109, 861–896.
- Davison, B., Taipale, R., Langford, B., Misztal, P., Fares, S., Matteucci, G., Loreto, F., Cape, J.N., Rinne, J., Hewitt, C.N., 2009. Concentrations and fluxes of biogenic volatile organic compounds above a Mediterranean Macchia ecosystem in western Italy. *Biogeosciences* 6, 1655–1670.
- DEFRA, 2007. UK Biomass Strategy. DEFRA.
- DEFRA, 2009. Experimental Statistics. Non-food Crop Areas: United Kingdom. DEFRA.
- Dockery, D.W., Pope, C.A., Xu, X.P., Spengler, J.D., Ware, J.H., Fay, M.E., Ferris, B.G., Speizer, F.E., 1993. An association between air-pollution and mortality in 6 United-States cities. *New England Journal of Medicine* 329, 1753–1759.
- DTI, 2005. Implementation Guidance for the Renewables Obligation Order 2005. DTI.
- Eller, A.S.D., Sekimoto, K., Gilman, J.B., Kuster, W.C., de Gouw, J.A., Monson, R.K., Graus, M., Crespo, E., Warneke, C., Fall, R., 2011. Volatile organic compound emissions from switchgrass cultivars used as biofuel crops. *Atmospheric Environment* 45, 3333–3337.
- Evans, R.C., Tingey, D.T., Gumpertz, M.L., Burns, W.F., 1982. Estimates of isoprene and monoterpene emission rates in plants. *Botanical Gazette* 143, 304–310.
- Grogan, P., Matthews, R., 2002. A modelling analysis of the potential for soil carbon sequestration under short rotation coppice willow bioenergy plantations. *Soil Use and Management* 18, 175–183.
- Guenther, A., Hewitt, C.N., Erickson, D., Fall, R., Geron, C., Graedel, T., Harley, P., Klinger, L., Lerdau, M., McKay, W.A., Pierce, T., Scholes, B., Steinbrecher, R., Tallamraju, R., Taylor, J., Zimmerman, P., 1995. A global model of natural volatile organic compound emissions. *Journal of Geophysical Research-Atmospheres* 100, 8873–8892.
- Guenther, A., Karl, T., Harley, P., Wiedinmyer, C., Palmer, P.I., Geron, C., 2006. Estimates of global terrestrial isoprene emissions using MEGAN (Model of Emissions of Gases and Aerosols from Nature). *Atmospheric Chemistry and Physics* 6, 3181–3210.
- Hakola, H., Rinne, J., Laurila, T., 1998. The hydrocarbon emission rates of tea-leaved willow (*Salix phylicifolia*), silver birch (*Betula pendula*) and European aspen (*Populus tremula*). *Atmospheric Environment* 32, 1825–1833.
- Hewitt, C.N., MacKenzie, A.R., Di Carlo, P., Di Marco, C.F., Dorsey, J.R., Evans, M., Fowler, D., Gallagher, M.W., Hopkins, J.R., Jones, C.E., Langford, B., Lee, J.D., Lewis, A.C., Lim, S.F., McQuaid, J., Misztal, P., Moller, S.J., Monks, P.S., Nemitz, E., Oram, D.E., Owen, S.M., Phillips, G.J., Pugh, T.A.M., Pyle, J.A., Reeves, C.E., Ryder, J., Siong, J., Skiba, U., Stewart, D.J., 2009. Nitrogen management is essential to prevent tropical oil palm plantations from causing ground-level ozone pollution. *Proceedings of the National Academy of Sciences* 106, 18447–18451.
- Karl, M., Guenther, A., Koble, R., Leip, A., Seufert, G., 2009. A new European plant-specific emission inventory of biogenic volatile organic compounds for use in atmospheric transport models. *Biogeosciences* 6, 1059–1087.
- Karl, T., Guenther, A., Jordan, A., Fall, R., Lindinger, W., 2001. Eddy covariance measurement of biogenic oxygenated VOC emissions from hay harvesting. *Atmospheric Environment* 35, 491–495.
- Karl, T., Hansel, A., Märk, T., Lindinger, W., Hoffmann, D., 2003. Trace gas monitoring at the Mauna Loa Baseline Observatory using Proton-Transfer Reaction Mass Spectrometry. *International Journal of Mass Spectrometry* 223–224, 527–538.
- Karl, T.G., Spirig, C., Rinne, J., Stroud, C., Prevost, P., Greenberg, J., Fall, R., Guenther, A., 2002. Virtual disjunct eddy covariance measurements of organic compound fluxes from a subalpine forest using proton transfer reaction mass spectrometry. *Atmospheric Chemistry and Physics* 2, 279–291.
- Kesselmeier, J., Staudt, M., 1999. Biogenic volatile organic compounds (VOC): an overview on emission, physiology and ecology. *Journal of Atmospheric Chemistry* 33, 23–88.
- Kljun, N., Calanca, P., Rotachhi, M.W., Schmid, H.P., 2004. A simple parameterisation for flux footprint predictions. *Boundary-Layer Meteorology* 112, 503–523.
- König, G., Brunda, M., Puxbaum, H., Hewitt, C.N., Duckham, S.C., Rudolph, J., 1995. Relative contribution of oxygenated hydrocarbons to the total biogenic VOC emissions of selected mid-European agricultural and natural plant-species. *Atmospheric Environment* 29, 861–874.
- Kulmala, M., Suni, T., Lehtinen, K.E.J., Dal Maso, M., Boy, M., Reissell, A., Rannik, U., Aalto, P., Keronen, P., Hakola, H., Back, J.B., Hoffmann, T., Vesala, T., Hari, P., 2004. A new feedback mechanism linking forests, aerosols, and climate. *Atmospheric Chemistry and Physics* 4, 557–562.
- Martin, R.S., Westberg, H., Allwine, E., Ashman, L., Farmer, J.C., Lamb, B., 1991. Measurement of isoprene and its atmospheric oxidation products in a central Pennsylvania deciduous forest. *Journal of Atmospheric Chemistry* 13, 1–32.
- McKay, H., 2006. Environmental, economic, social and political drivers for increasing use of woodfuel as a renewable resource in Britain. *Biomass & Bioenergy* 30, 308–315.
- Misztal, P., 2010. Concentrations and Fluxes of Atmospheric Biogenic Volatile Organic Compounds by Proton Transfer Reaction Mass Spectrometry. PhD thesis, EaStCHEM School of Chemistry, University of Edinburgh, Edinburgh.
- Misztal, P.K., Owen, S.M., Guenther, A.B., Rasmussen, R., Geron, C., Harley, P., Phillips, G.J., Ryan, A., Edwards, D.P., Hewitt, C.N., Nemitz, E., Siong, J., Heal, M.R., Cape, J.N., 2010. Large estragole fluxes from oil palms in Borneo. *Atmospheric Chemistry and Physics* 10, 4343–4358.
- Naidu, S.L., Moose, S.P., Al-Shoaibi, A.K., Raines, C.A., Long, S.P., 2003. Cold tolerance of C-4 photosynthesis in *Miscanthus × giganteus*: adaptation in amounts and sequence of C-4 photosynthetic enzymes. *Plant Physiology* 132, 1688–1697.
- Olofsson, M., Ek-Olausson, B., Jensen, N.O., Langer, S., Ljungström, E., 2005. The flux of isoprene from a willow coppice plantation and the effect on local air quality. *Atmospheric Environment* 39, 2061–2070.
- Owen, S.M., Hewitt, C.N., 2000. Extrapolating branch enclosure measurements to estimates of regional scale biogenic VOC fluxes in the northwestern Mediterranean basin. *Journal of Geophysical Research-Atmospheres* 105, 11573–11583.
- Pio, C.A., Nunes, T.V., Brito, S., 1993. Volatile hydrocarbon emissions from common and native species of vegetation in Portugal. In: Slanina, J., Angeletti, G., Beilke, S. (Eds.), *Proceedings on the General Assessment of Biogenic Emissions and Deposition of Nitrogen Compounds, Sulfur Compounds and Oxidants in Europe*, pp. 291–298.
- Rinne, H.J.I., Guenther, A.B., Warneke, C., de Gouw, J.A., Luxembourg, S.L., 2001. Disjunct eddy covariance technique for trace gas flux measurements. *Geophysical Research Letters* 28, 3139–3142.
- Rowe, R.L., Street, N.R., Taylor, G., 2009. Identifying potential environmental impacts of large-scale deployment of dedicated bioenergy crops in the UK. *Renewable & Sustainable Energy Reviews* 13, 260–279.
- Steiner, A.H., Goldstein, A.L., 2007. Biogenic VOCs. In: Koppmann, R. (Ed.), *Volatil Organic Compounds in the Atmosphere*. Wiley-Blackwell, p. 512.
- Taipale, R., Ruuskanen, T.M., Rinne, J., 2010. Lag time determination in DEC measurements with PTR-MS. *Atmospheric Measurement Techniques* 3, 853–862.
- Taipale, R., Ruuskanen, T.M., Rinne, J., Kajos, M.K., Hakola, H., Pohja, T., Kulmala, M., 2008. Technical note: quantitative long-term measurements of VOC concentrations by PTR-MS – measurement, calibration, and volume mixing ratio calculation methods. *Atmospheric Chemistry and Physics* 8, 6681–6698.
- Warneke, C., Luxembourg, S.L., de Gouw, J.A., Rinne, H.J.I., Guenther, A.B., Fall, R., 2002. Disjunct eddy covariance measurements of oxygenated volatile organic compounds fluxes from an alfalfa field before and after cutting. *Journal of Geophysical Research-Atmospheres* 107, 10.
- Winer, A.M., Fitz, D.R., Miller, P.R., 1983. Investigation of the Role of Natural Hydrocarbons in Photochemical Smog Formation in California. By the Statewide Air Pollution Research Center, Riverside, California, U.S.A.
- Zimmerman, P.R., 1979. Determination of Emission Rates of Hydrocarbons from Indigenous Species of Vegetation in the Tampa/St. Petersburg Florida Area. Appendix C. Tampa Bay Area Photochemical Oxidant Study. U.S. Environmental Protection Agency, Region IV, Atlanta, Georgia.

## Appendix II: MCM programs

The two MCM programs used to run gas-phase simulations of oxidation of  $\alpha$ -pinene and limonene (as detailed in Chapter 5) are attached electronically as text files: a-Pinene.txt and Limonene.txt

## Appendix III: Raw PTR-MS chamber data

This appendix includes raw PTR-MS data of  $\alpha$ -pinene and limonene measurements. Exponential fits of these data are shown in Chapter 5.

Figure III-A to Figure III-C show the PTR-MS data for decay of  $\alpha$ -pinene.

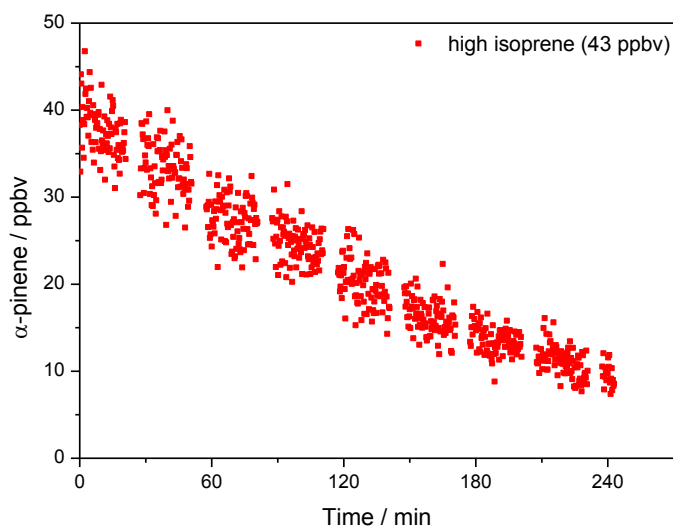


**Figure III-A** PTR-MS data showing decay of  $\alpha$ -pinene (starting mixing ratio  $\sim$ 40 ppbv) in the presence of high isoprene mixing ratio (43 ppbv).

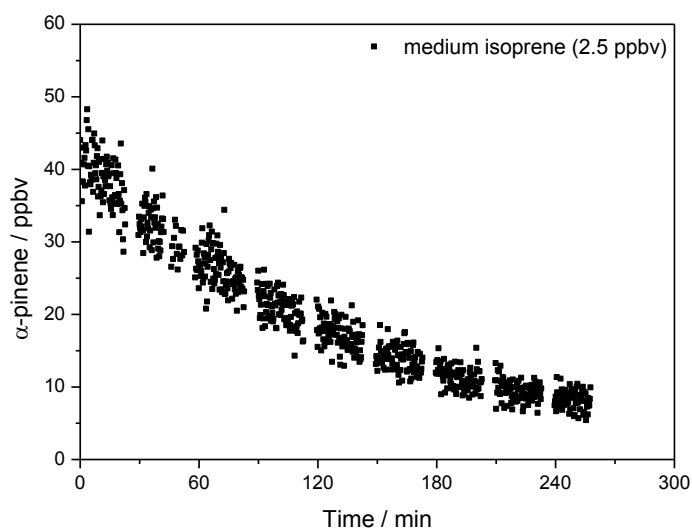


**Figure III-B** PTR-MS data showing decay of  $\alpha$ -pinene (starting mixing ratio  $\sim$ 43 ppbv) in the presence of medium isoprene mixing ratio (2.5 ppbv).

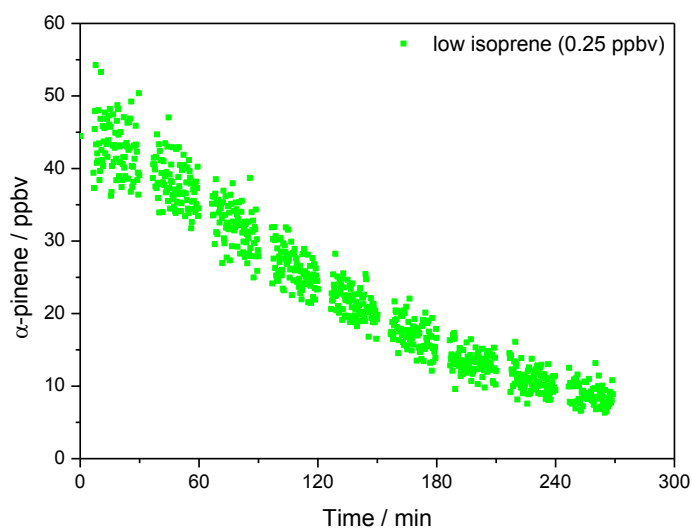


Figure III-C PTR-MS data showing decay of  $\alpha$ -pinene (starting mixing ratio  $\sim$ 45 ppbv) in the presence of low isoprene mixing ratio (0.25 ppbv).

Figure III-D to Figure III-F show the PTR-MS data for decay of limonene.

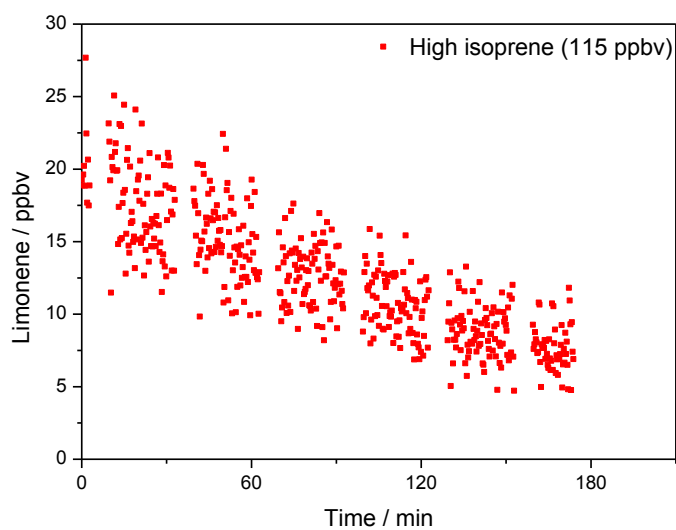
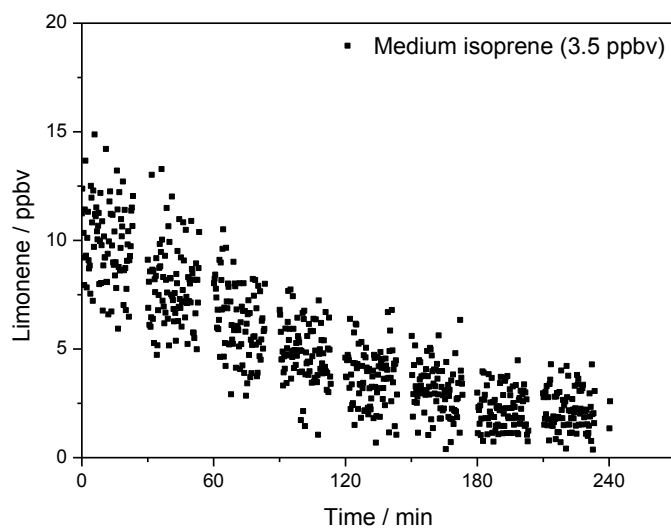
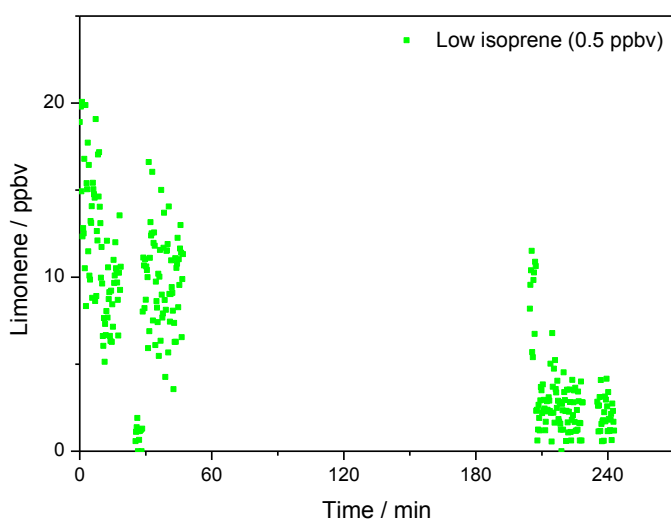


Figure III-D PTR-MS data showing decay of limonene (starting mixing ratio  $\sim$ 20 ppbv) in the presence of high isoprene mixing ratio (115 ppbv). Data beyond  $\sim$ 180 min were not acquired due to data acquisition problems with the PTR-MS.



**Figure III-E PTR-MS data showing decay of limonene (starting mixing ratio ~11 ppbv) in the presence of high isoprene mixing ratio (3.5 ppbv).**



**Figure III-F PTR-MS data showing decay of limonene (starting mixing ratio ~15 ppbv) in the presence of high isoprene mixing ratio (0.5 ppbv). Missing data between ~60 and 210 min were due to data acquisition problems with the PTR-MS.**

Figure III-G to Figure III-I show plots of the natural log of raw PTR-MS data for decay of  $\alpha$ -pinene (referred to in Figure 5-3).

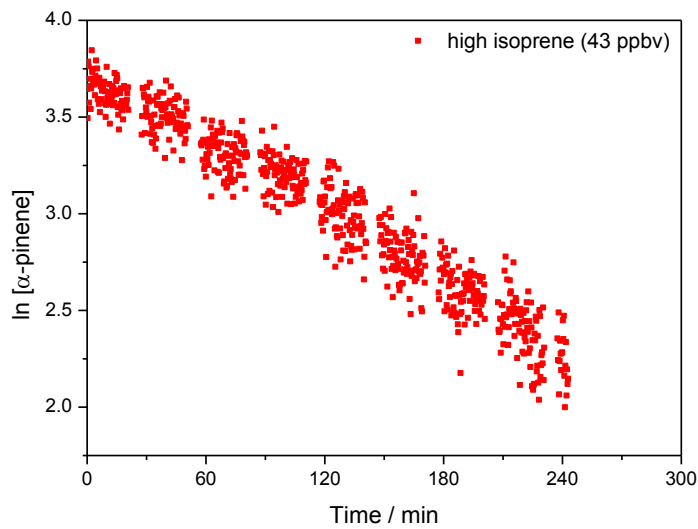


**Figure III-G Natural logarithm of  $\alpha$ -pinene mixing ratio against time in the presence of high isoprene mixing ratio (43 ppbv).**

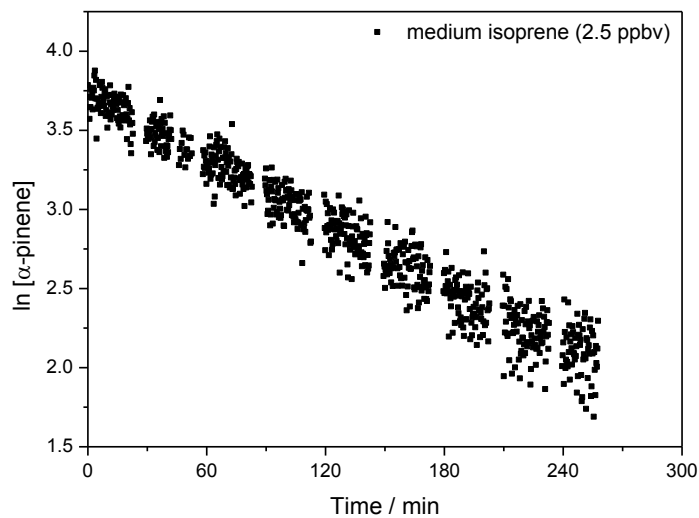


**Figure III-H Natural logarithm of  $\alpha$ -pinene mixing ratio against time in the presence of medium isoprene mixing ratio (2.5 ppbv).**

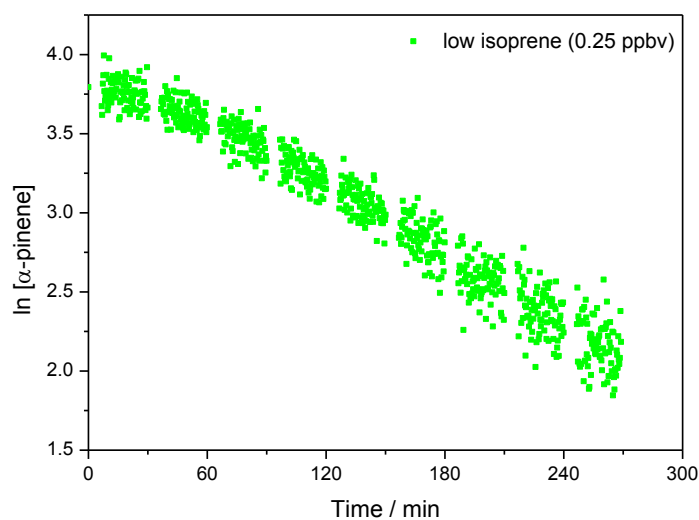


**Figure III-I** Natural logarithm of  $\alpha$ -pinene mixing ratio against time in the presence of low isoprene mixing ratio (0.25 ppbv).

Figure III-J to Figure III-L show plots of the natural log of raw PTR-MS data for decay of limonene (referred to in Figure 5-5).

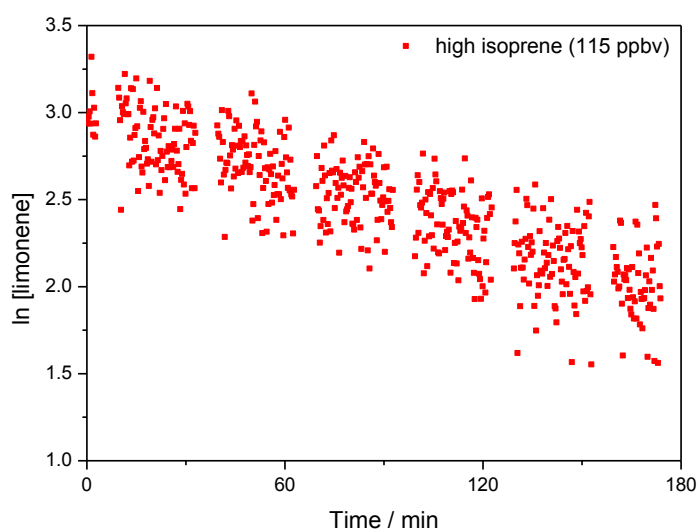


**Figure III-J** Natural logarithm of limonene mixing ratio against time in the presence of high isoprene mixing ratio (115 ppbv).

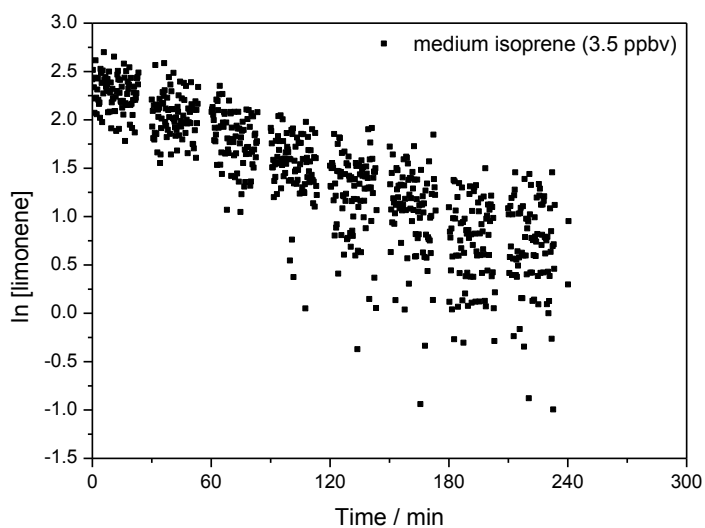


**Figure III-K** Natural logarithm of limonene mixing ratio against time in the presence of medium isoprene mixing ratio (3.5 ppbv).

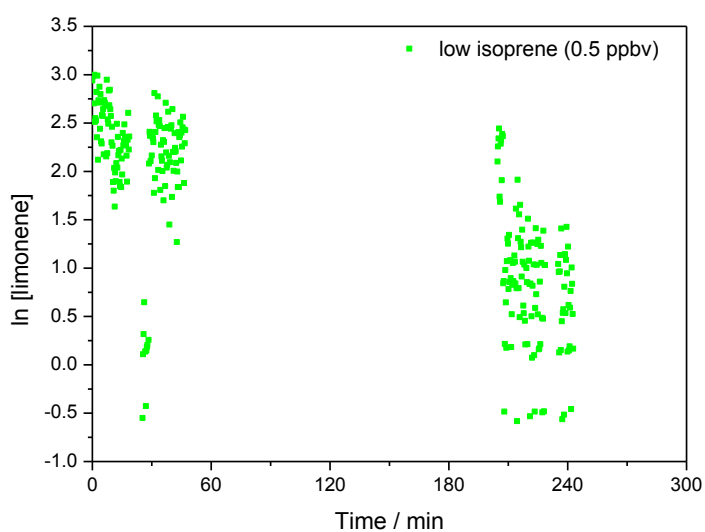


**Figure III-L** Natural logarithm of limonene mixing ratio against time in the presence of low isoprene mixing ratio (0.5 ppbv). Missing data between ~60 and 210 min were due to data acquisition problems with the PTR-MS.